ACOUSTIC TRANSDUCTION – MATERIALS AND DEVICES

Period 1 January 2000 to 31 December 2000

Annual Report

VOLUME II

OFFICE OF NAVAL RESEARCH
Contract No: N00014-96-1-1173

APPROVED FOR PUBLIC RELEASE – DISTRIBUTION UNLIMITED

Kenji Uchino

PENNSTATE

THE MATERIALS RESEARCH LABORATORY
UNIVERSITY PARK, PA

REPORT DOCUMENTATION PAGE

Form Approved
OMB No. 0704-0188

1. AGENCY USE ONLY (Leave blank)	2. REPORT DATE	3. REPORT TYPE AND DATES COVERED
	7/12/2001	ANNUAL REPORT 01/01/2000--12/31/2000

4. TITLE AND SUBTITLE
ACOUSTIC TRANSDUCTION -- MATERIALS AND DEVICES

5. FUNDING NUMBERS
ONR CONTRACT NO.
N00014-96-1-11173

6. AUTHOR(S)
Materials Research Laboratory
The Pennsylvania State University
University Park, Pa 16802

7. PERFORMING ORGANIZATION NAME(S) AND ADDRESS(ES)

8. PERFORMING ORGANIZATION REPORT NUMBER

9. SPONSORING/MONITORING AGENCY NAME(S) AND ADDRESS(ES)
Office of Naval Research
ONR 321SS
Ballston Centre Tower One
800 N. Quincy Street
Arlington, VA 2217-5660

Office of Naval Research
Regional Office Chicago
536 S. Clark Str. RM 208
Chicago IL 60605-1588

10. SPONSORING/MONITORING AGENCY REPORT NUMBER

11. SUPPLEMENTARY NOTES

12a. DISTRIBUTION/AVAILABILITY STATEMENT

12b. DISTRIBUTION CODE

13. ABSTRACT *(Maximum 200 words)*

SEE FOLLOWING PAGE

14. SUBJECT TERMS

15. NUMBER OF PAGES

16. PRICE CODE

17. SECURITY CLASSIFICATION OF REPORT	18. SECURITY CLASSIFICATION OF THIS PAGE	19. SECURITY CLASSIFICATION OF ABSTRACT	20. LIMITATION OF ABSTRACT
UNCLASSIFIED	UNCLASSIFIED	UNCLASSIFIED	

GENERAL INSTRUCTIONS FOR COMPLETING SF 298

The Report Documentation Page (RDP) is used in announcing and cataloging reports. It is important that this information be consistent with the rest of the report, particularly the cover and title page. Instructions for filling in each block of the form follow. It is important to ***stay within the lines*** to meet ***optical scanning requirements***.

Block 1. Agency Use Only *(Leave blank)*.

Block 2. Report Date. Full publication date including day, month, and year, if available (e.g. 1 Jan 88). Must cite at least the year.

Block 3. Type of Report and Dates Covered. State whether report is interim, final, etc. If applicable, enter inclusive report dates (e.g. 10 Jun 87 - 30 Jun 88).

Block 4. Title and Subtitle. A title is taken from the part of the report that provides the most meaningful and complete information. When a report is prepared in more than one volume, repeat the primary title, add volume number, and include subtitle for the specific volume. On classified documents enter the title classification in parentheses.

Block 5. Funding Numbers. To include contract and grant numbers; may include program element number(s), project number(s), task number(s), and work unit number(s). Use the following labels:

C	- Contract	PR	- Project
G	- Grant	TA	- Task
PE	- Program Element	WU	- Work Unit Accession No.

Block 6. Author(s). Name(s) of person(s) responsible for writing the report, performing the research, or credited with the content of the report. If editor or compiler, this should follow the name(s).

Block 7. Performing Organization Name(s) and Address(es). Self-explanatory.

Block 8. Performing Organization Report Number. Enter the unique alphanumeric report number(s) assigned by the organization performing the report.

Block 9. Sponsoring/Monitoring Agency Name(s) and Address(es). Self-explanatory.

Block 10. Sponsoring/Monitoring Agency Report Number. *(If known)*

Block 11. Supplementary Notes. Enter information not included elsewhere such as: Prepared in cooperation with...; Trans. of...; To be published in.... When a report is revised, include a statement whether the new report supersedes or supplements the older report.

Block 12a. Distribution/Availability Statement. Denotes public availability or limitations. Cite any availability to the public. Enter additional limitations or special markings in all capitals (e.g. NOFORN, REL, ITAR).

DOD	- See DoDD 5230.24, "Distribution Statements on Technical Documents."
DOE	- See authorities.
NASA	- See Handbook NHB 2200.2.
NTIS	- Leave blank.

Block 12b. Distribution Code.

DOD	- Leave blank.
DOE	- Enter DOE distribution categories from the Standard Distribution for Unclassified Scientific and Technical Reports.
NASA	- Leave blank.
NTIS	- Leave blank.

Block 13. Abstract. Include a brief *(Maximum 200 words)* factual summary of the most significant information contained in the report.

Block 14. Subject Terms. Keywords or phrases identifying major subjects in the report.

Block 15. Number of Pages. Enter the total number of pages.

Block 16. Price Code. Enter appropriate price code *(NTIS only)*.

Blocks 17. - 19. Security Classifications. Self-explanatory. Enter U.S. Security Classification in accordance with U.S. Security Regulations (i.e., UNCLASSIFIED). If form contains classified information, stamp classification on the top and bottom of the page.

Block 20. Limitation of Abstract. This block must be completed to assign a limitation to the abstract. Enter either UL (unlimited) or SAR (same as report). An entry in this block is necessary if the abstract is to be limited. If blank, the abstract is assumed to be unlimited.

ABSTRACT

This report describes research performed over the period 1st January 2000 to 31st December 2000 on a MURI under Office of Naval Research contract N00014-96-1-1173 on the topic "Acoustic Transduction Materials and Devices". This program brings together researchers from the Materials Research Laboratory (MRL), the Applied Research Laboratory (ARL) and the Center for Acoustics and Vibrations (CAV) at the Pennsylvania State University. As has become customary over many years, research on the program is detailed in the technical appendices of published work, and only a brief narrative description connecting these studies is given in the text.

The program combines a far reaching exploration of the basic phenomena contributing to piezoelectric and electrostrictive response with the highly applied thrusts necessary to produce the "pay-off" in new applications relevant to Navy needs. Polarization vector tilting in the ferroelectric phase of perovskite structure crystals at compositions close to a morphotropic phase boundary (MPB) was first underscored on this program some four years ago, and is now widely accepted as one mode for exploiting the large intrinsic spontaneous strain in the ferroelectric to produce exceedingly strong anhysteritic piezoelectric response and very large electric field controlled elastic strain. New evidence for the importance of both spontaneous (monoclinic) and electric field induced tilting on the properties of both single and polycrystal MPB systems is presented in this report.

The puzzling phenomena associated with relaxor ferroelectric response have long been a topic of study in MRL, where the micro-polar region model and the application of Vogel/ Fulcher to the dielectric slowing down were first applied. The current "pay-off" is in the greatly enhanced relaxor ferroelectric electrostrictive response from high electron energy irradiated polyvinylidene difluoride: triflouroethylene (PVDF: TrFE) co-polymer discussed in this report. This development opens a new field of high strain, high energy density actuators with tremendous practical applicability. Now the possibility of engineering this response by chemical manipulation in the terpolymer systems without irradiation further enhances the exciting possibilities.

In composite structures, the early promise of the flextensional cymbal type actuators is now being fully realized and programs exploring large area cymbal transducer arrays are progressing very well, both at MRL/ARL and at NRL. The connection with CAV at Penn State is particularly important in keeping the MURI faculty aware of problems endemic to water as our host medium and the effects of turbulence in flow and the need for many types of acoustic noise control.

New designs of piezoelectric transformers and motors are demanding materials with lower loss levels under continuous high driving, and important progress is reported in separating and understanding the components of this loss and in designing new doping schemes for ceramics which enhance power capability almost tenfold. New piezoelectric micro-motor designs look particularly attractive and appear to offer significant advantages over electromagnetics for very small-scale applications. Thick and thin film studies for MEMS are progressing well and offering new insights into fatigue and switching behavior in the ferroelectrics.

ACOUSTIC TRANSDUCTION – MATERIALS AND DEVICES

Period 1 January 2000 to 31 December 2000

Annual Report

VOLUME II

OFFICE OF NAVAL RESEARCH
Contract No: N00014-96-1-1173

Kenji Uchino

APPENDICES

VOLUME I

GENERAL SUMMARY PAPERS

1. Uchino, K., Encyclopedia of Vibration, Partial Charge "Electrostrictive Materials", Academic Press, London (2000). [in press]
2. Uchino, K., and Y. Ito, Encyclopedia Smart Materials, J. Harvey, Edit., Partial Charge "Smart Ceramics: Transducers, Sensors and Actuators", John Wiley & Sons, New York (2000). [in press]
3. Wennu Ma, L.E. Cross, "Observation of the flexoelectric effect in relaxor PB ($Mg_{1/3}NB_{2/3}$) O_3 ceramics", Applied Physics Letters. Volume #8 number 19 pp. 2920
4. R. Hatt and W. Cao, "Landau-Ginzburg Model for Antiferroelectric Phase Transition Based on Microscopic Symmetry", Phys. Rev. B, vol. **62**, pp. 818-823 (2000).

2.0 MATERIALS STUDIES

2.1 Polycrystal Perovskite Ceramics

5. A.S. Bhalla, R. Guo, R. Roy, "The Perovskite Structure - A Review of Its Role in Ceramic Science and Technology, "*Mat. Res. Innovat.,* **4(1),** 3-26, (2000)
6. E.F. Alberta, R. Guo, L.E. Cross, A.S. Bhalla, "Structure-Property Diagrams of Ferroic Solid Solutions. Part I: Perovskite Ferroelectrics with Morphotropic Phase Boundaries," *Ferroelectrics Review*, 3, 1, (2001)
7. B. Noheda, J.A. Gonzalo, L.E. Cross, R. Guo, S-E. Park, D.E. Cox, G. Shirane, "Tetragonal-to-Monoclinic Phase Transition in a Ferroelectric Perovskite: the Structure of $PbZr_{0.52}Ti_{0.48}O_3$, "*Phys. Rev. B,* **61(13),** 8687-8689, (2000)
8. B. Noheda, D.E. Cox, G. Shirane, R. Guo, B. Jones, L.E. Cross, "Stability of the monoclinic phase in the ferroelectric perovskite $PbZr_{(1-x)}Ti_xO_3$, "*Los Alamos Natl. Lab., Prepr. Arch., Condens. Matter,* **1-8,** arXiv:cond-mat/0006152, (2000)
9. R. Guo, L.E. Cross, S-E. Park, B. Noheda, D.E. Cox, G. Shirane, "Origin of the high piezoelectric response in $PbZr_{1-x}Ti_xO_3$," *Phys. Rev. Letters,* **84(23),** 5423-5426, (2000)
10 W. Jiang and W. Cao, "Nonlinear Elastic Properties of Lead Zirconate Titanate Ceramics", J. Appl. Phys. vol. **88**: 6684-6689 (2000).
11. Chen, Y. H., D. Viehland and K. Uchino, "Substituent Effects in 0.65Pb($Mg_{1/3}$ $Nb_{2/3}$)O_3-0.35$PbTiO_3$ Piezoelectric Ceramics" J. Electroceramics, **6**, 13-20 (2001). (First Author Supervised by Candidate).
12. W.H. Jiang and W. Cao, " Intrinsic and Coupling-induced Elastic Nonlinearity of Lanthanum-doped Lead Magnesium Niobate-Lead Titanate Electrostrictive Ceramic", Appl. Phys. Lett., vol. **77**, pp. 1387-1389 (2000).

VOLUME II

2.0 MATERIALS STUDIES

2.2 Single Crystal Systems

13. L.E. Cross, J. Fousek, " Engineering Multidomain Ferroic Samples", Ferroelectrics, 2001, Vol. 252, pp. 171-180.
14. Wada, Satoshi, Takaaki Tsurmi, Miour Osada, Masato Kakihana, Seung Eek Park, L.Eric Cross and Thomas R. Shrout. "Change of Macroscopic and Microscopic Symmetries in Relaxor PZN Single Crystal Under Bias Filed." Transactions of the Material Research Society of Japan, **25** (1). 281-284 (2000).
15. Wada, Satoshi, Takaaki Tsurmi, Miour Osada, Masato Kakihana, Seung Eek Park, L.Eric Cross and Thomas R. Shrout. "Dipolar Behavior in PZN Relaxor Single crystals under Bias Fields." Transactions of the Materials Research Society of Japan **25** (1), 281-284 (2000).
16. Belegundu, U., X. Du and K. Uchino, "Switching Current in $Pb(Zn_{1/3}Nb_{2/3})O_3$-$PbTiO_3$ Single Crystals," Symp. LL Proc., Mater. Res. Soc. Fall Mtg. '99, (LL.1.9, Boston, Nov. 29-Dec.3. 1999), Vol.**604**, 39-44 (2000).
17. Yu Lu, D.-Y. Jeong, Z. Y. Cheng, Q. M. Zhang, H. Luo, Z. Yin, and D. Viehland. Phase Transitional Behavior and Piezoelectric Properties of the orthorhombic Phase of PMN-PT Single Crystals. Appl. Phys. Lett. 78, 3109 (2001).
18. Yu Lu, Z.-Y. Cheng, E. Park, S. F. Liu and Q. M. Zhang. Linear Electro-optic Effect of $0.88Pb(Zn_{1/3}Nb_{2/3})$-$0.12PbTiO_3$ Single Crystal. Jpn. J. Appl. Phys. 39, 141-145 (2000).
19. Y. Barad, Yu Lu, Z. Y. Cheng, S. E. Park, and Q. M. Zhang. Composition, Temperature, and Crystal Orientation Dependence of Linear Electro-optic Properties of PZN-PT Single Crystals. Appl. Phys. Lett. 77, 1247-1249 (2000).
20. Y. Lu, Z.-Y. Cheng, Y. Barad, and Q. M. Zhang. Photoelastic Effects in the Tetragonal PZN-PT Single Crystals near the Morphotropic Phase Boundary. J. Appl. Phys. 89, 5075 (2001).

2.3 High Strain Polymers

21. Vivek Bharti, H. S. Xu, G. Shanthi, Q. M. Zhang, and Kuming Liang. Polarization and Structural Properties of High Energy Electron Irradiated P(VDF-TrFE) Copolymer Films. J. Appl. Phys. 87, 452-461 (2000).
22. Haisheng Xu, G. Shanthi, V. Bharti, Q. M. Zhang, and T. Ramatowski. Structural, Conformational, and Polarization Changes of P(VDF-TrFE) Copolymer Induced by High Energy Electron Irradiation. Macromolecules, 33, 4125-4131(2000).
23. Q. M. Zhang, Z. Y. Cheng, and Vivek Bharti. Relaxor Ferroelectric Behavior in High Energy Electron Irradiated P(VDF-TrFE) copolymers. Appl. Phys. A70, 307-312 (2000).
24. Vivek Bharti and Q. M. Zhang. Dielectric Study of Relaxor Ferroelectric P(VDF-TrEF) Copolymer System. Phys. Rev. B. 63, 184103 (2001).
25. Z.Y. Cheng, Vivek Bharti, T.B. Xu, Hansheng Xu, T. Mai, and Q. M. Zhang. Electrostrictive P(VDF-TrFE) Copolymers. Sensors and Actuators A-Phys. 90, 138-147 (2001)

26. Z. Y. Cheng, V. Bharti, T. Mai, T. B. Xu, Q. M. Zhang, K. Hamilton, T. Ramotowski, K. A. Wright, and R. Ting. Effect of High Energy Electron Irradiation on the Electromechanical Properties of Poly(vinylidene fluoride-trifluorethylene) 50/50 and 65/35 Copolymers. IEEE Trans. UFFC 47, 1296 (2000).
27. Vivek Bharti, Z.-Y. Cheng, T, Mai, Q. M. Zhang, T. Ramotowski, K. A. Wright. High Electromechanical Coupling Factor and Electrostrictive Strain over a Broad Frequency Range in Electrostrictive Poly(vinylidene fluoride-trifluoroethylene) Copolymer. Japn. J. Appl. Phys. 40, 672 (2001).
28. Vivek Bharti, G. Shanthi, H. Xu, Q. M. Zhang, and K. Liang. Evolution of Transitional Behavior and Structure of Electron Irradiated P(VDF-TrFE) Copolymer Films. Mater. Lett. 47, 107-111 (2001).
29. F. Xia, H. Xu, F. Fang, B. Razivi, Z. Y. Cheng, Yu Lu, Baoming Xu, and Q. M. Zhang. Thickness Dependence Behavior of Ferroelectric Switching in P(VDF-TrFE) Spin Cast Films. Appl. Phys. Lett. 78, 1122 (2001).
30. Q. M. Zhang, H. S. Xu, Fei Fang, Z.-Y. Cheng, Xia Feng, and H. You. Observation of Critical Thickness of Crystallization in Spin Cast Ferroelectric Thin Films. J. Appl. Phys. 89, 2613 (2001).
31. Shizhuo Yin, Q. M. Zhang, K.-W. Chung, R. Yang, Z. Y. Cheng, and Yu Lu. Investigation of the Electro-optic Properties of Electron-irradiated P(VDF-TrFE) Copolymer. Opt. Eng. 39, 670-672 (2000).
32. Hai-Sheng Xu, Z.-Y. Cheng, Vivek Bharti, Shexi Wang, and Q. M. Zhang. All-Polymer Electromechanical Systems Consisting of Electrostrictive Poly(vinylidene fluoride-trifluoroethylene) and Conductive Polyaniline. J. Appl. Poly. Sci. 75, 945-951 (2000).
33. H. Xu, Z.Y. Cheng, D. Olson, T. Mai, Q. M. Zhang, and G. Kavarnos. Ferroelectric and Electromechanical Properties of P(VDF-TrFE-CTFE) Terpolymer. Appl. Phys. Lett. 78, 2360 (2001).

3.0 TRANSDUCER STUDIES

3.1 Composite Structures

34. Uchino, K., "Piezoelectro Composites," Chap.5.24, Comprehensive Composite Materials, Elsevier Science, Oxford, UK (2000).
35. Tressler, J. and K. Uchino, "Piezoelectric Composite Sensors," Chap.5.22, Comprehensive Composite Materials, Elsevier Science, Oxford, UK (2000).

VOLUME III

36. Meyer, R.J. Jr., A. Dogan, C. Yoon, S. Pilgrim and R.E. Newnham, "Displacement Amplification of Electroactive Materials Using the Cymbal Flextensional Transducer," Sensors & Actuators A, vol.87, pp. 157-162 (2001).
37. Dogan, A., K. Uchino and R. E. Newnham, "Flextensional Composite Transducers: Designing, Fabrication and Application," Proc. NATO- Advanced Research Workshop: Piezoelectric Materials: Advance in Science, Technology and Applications, (Predeal, Romania, May 24-27, 1999, Kluwer Academic Publ., p.357-374 (2000).

38. Zhang, J., A.C. Hladky-Hennion, W.J. Hughes, and R.E. Newnham, "Modeling and Underwater Characterization of Cymbal Transducers and Arrays," IEEE Transactions on Ultrasonics, Ferroelectrics, and Frequency Control, vol. 48 (2), pp. 560-568 (2001).
39. Zhang, J., W. J. Hughes, R. J. Meyer Jr., K. Uchino and R. E. Newnham, "Cymbal Array: A Broad Band Sound Projector," Ultrasonics 37, 523-529 (2000).
40. Zhang, J., A.C. Hladky-Hennion, W.J. Hughes, and R.E. Newnham, " A Miniature Class V flextensional cymbal transducer with directional beam pattern: The Double-Driver," Ultrasonics, vol. 39, pp. 91-95 (2001).
41. Meyer, R.J. Jr. and R.E. Newnham, "Flextensional transducers with Shape Memory Caps for Tunable Devices," Journal of Intelligent Materials Systems and Structures, vol. 11, pp. 199-205 (2001).
42. Meyer, R.J. Jr., S. Alkoy, J. Cochran, T. Ritter, and R.E. Newnham, "Pre-focused Lead Titanate > 25 MHz Single Element Transducers from Hollow Spheres," IEEE Transactions on Ultrasonics, Ferroelectrics, and Frequency Control, vol. 48 (2), pp. 488-493 (2001).
43. Y. Bai, Z.Y. Cheng, V. Bharti, H. S. Xu, and Q. M. Zhang. High Dielectric Constant Ceramic Powder Polymer Composites. Appl. Phys. Lett. 76, 3804-3806 (2000).
44. M.R. Shen and W. Cao, "Acoustic Bandgap Formation in a Periodic Structure with Multilayer Unit Cells", J. Phys. D: Applied Physics, vol. **33**, pp. 1150-1154 (2000).
45. T.B. Xu, Z-Y. Cheng, Q. M. Zhang, R. Baughman, C. Cui, A. Zakhidov, and J. Su. Fabrication and Characterization of 3-Dimensional Periodic Ferroelectric Polymer-Silica Opal Composites and Inverse Opal. J. Appl. Phys. 88(1), 405-409 (2000).

3.2 Piezoelectric Transformers

46. Uchino, K., B. Koc, P. Laoratanakul and A. Vazquez Carazo, "Piezoelectric Transformers –New Perspective--," Proc. 3rd Asian Mtg. Ferroelectrics, D1d.1, Hong Kong, Dec. 12-15 (2000).
47. Koc, B., and K. Uchino, "Disk Type Piezoelectric Transformer with Crescent Shape Input Electrodes," Proc. NATO- Advanced Research Workshop: Piezoelectric Materials: Advance in Science, Technology and Applications, (Predeal, Romania, May 24-27, 1999, Kluwer Academic Publ., p.375-382 (2000).

3.3 High Power Level Materials

48. Uchino, K. and S. Hirose, "Loss Mechanisms in Piezoelectrics: How to Measure Different Losses Separately," IEEE UFFC Transactions, **48**, 307-321 (2001).
49. Uchino, K., and J. Zheng, Y. H. Chen, X. Du and S. Hirose, "Loss Mechanisms in Piezoelectrics and Resonance/ Antiresonance," Proc. 101st Annual Mtg. of Amer. Ceram. Soc., Symp. Electronic Ceramic Materials and Devices, (Indianapolis, April 25 – 28, 1999), p.79-100 (2000).
50. Uchino, K., J. Zheng, Y. H. Chen, X. Du, S. Hirose and S. Takahashi, "Loss Mechanisms in Piezoelectrics –Extrinsic and Intrinsic Losses--," Mater. Res. Soc. Fall Mtg. '99, (LL.1.6, Boston, Nov. 29-Dec.3, 1999), Vol. **604**, 25-31 (2000).

51. Chen, Y. H., S. Hirose, D. Viehland and K. Uchino, "Doping Effects in $Pb(Mg_{1/3}Nb_{2/3})O_3$-$PbTiO_3$ Ceramics for High Power Transduction Applications," Mater. Res. Soc. Fall Mtg. '99, (LL.5.8, Boston, Nov. 29-Dec.3, 1999), Vol. **604**, 215-220 (2000).
52. Chen, Y. H., S. Hirose, D. Viehland, S. Takahashi and K. Uchino, " Mn-Modified Pb(Mg1/3Nb2/3)O3-PbTiO3 Ceramics: Improved Mechanical Quality Factors for High-Power Transducer Applications," Jpn. J. Appl. Phys. 39, 4843-4852 (2000).
53. Gao, Y. Y. H. Chen, J. Ryu, K. Uchino and D. Viehland, " Eu and Yb Substituent Effects on the Properties of $Pb(Zr_{0.52}Ti_{0.48})O_3$-$Pb(Mn_{1/3}Sb_{2/3})O_3$ Ceramics: Development of a New High-Power Piezoelectric with Enhanced Vibrational Velocity," Jpn. J. Appl. Phys., 40, 79-85 (2001).

VOLUME IV

3.4 Fluid Structure Interactions

54. Lauchle, G. C., W. A. Kargus IV. Scaling of Turbulent Wall Pressure Fluctuations Downstream of a Rearward Facing Step. *J. Acoust. Soc. Am.* **107**: L1-L6 (2000).
55. Capone, D. E., G. C. Lauchle. Modeling the Unsteady Lift and Drag on a Finite-Length Cylinder in Cross Flow. *J. Fluids and Struct.* **14**: 799-817 (2000).
56. Gavin, J. R., G. C. Lauchle. Modeling the Space-Time Correlations in the Wake Region of a Turbulent Boundary Layer. *Proc. of the ASME Noise Control and Acoustics Division 2000*, NCA-Vol. 27, pp 227-241 (2000).
57. Gavin, J. R., G. C. Lauchle, M. L. Jonson. Prediction of Turbulence Ingestion Forces for Rotors with Arbitrary Rake and Skew. *Proc. of the ASME Noise Control and Acoustics Division 2000.* NCA-Vol. 27, pp 217-226 (2000).
58. Lauchle, G. C, D. K. McLaughlin. Review of: *Acoustics of Fluid Structure Interactions* by M. S. Howe in *Noise Control Eng. J.* **48**: 70-71 (2000).

4.0 ACTUATOR STUDIES

4.1 Materials and Designs

59. Koc, B. and K. Uchino, "Piezoelectric Ultrasonic Motors," Chap.6.34, Comprehensive Composite Materials, Elsevier Science, Oxford, UK (2000).
60. Uchino, K., "Recent Trend of Piezoelectric Actuator Developments –Material, Design and Drive Technique Related Issues--," Proc. Actuator 2000 (7th Int'l Conf. New Actuators, June 19-21, 2000), p.34-39 (2000).
61. Yao, K., K. Uchino, Y. Xu, S. Dong, and L. C. Lim, "Compact Piezoelectric Stacked Actuators for High Power Applications," IEEE Trans. UFFC, **47**, 819-825 (2000).
62. Liu, Rubin,L.e. Cross, Gareth Knowles, Bruce Bower, and Brookd Childers. " A Stackable Bonding-Free Flextensional Piezoelectirc Actuator" Journal of Electroceramics **4** (1), 201-206 92000)
63. A. E. Glazounov, Q. M. Zhang, C. Kim. Torsional Actuator Based on Mechanically Amplified Shear Piezoelectric Response. Sensors and Actuators A79, 22-30 (2000).

4.2 Photostriction

64. Poosanaas, P., K. Tonooka and K. Uchino, "Photostrictive Actuators," J. Mechatronics **10**, 467-487 (2000).
65. Uchino, K., P. Poosanaas and K. Tonooka, "Photostrictive Actuators–New Perspective-," Proc. 3rd Asian Mtg. Ferroelectrics, C3p.105, Hong Kong, Dec. 12-15 (2000).
66. Uchino, K., P. Poosanaas and K. Tonooka, "Photostrictive Actuators–New Perspective-," Proc. 5th Euroconf. Appl. Polar Dielectrics, O-43, Jurmala, Latvia, Aug. 27-30 (2000).
67. Poosanaas, P., K. Tonooka, I. R. Abothu, S. Komarneni, and K. Uchino, "Influence of Composition and Dopant on Photostriction in Lanthanum-Modified Lead Zirconate Titanate Ceramics," J. Intelligent Mater. Systems and Structures **10**, 439-445 (2000). (
68. Poosanaas, P., Dogan, A., Prasadarao, A. V., Komarneni, S. and Uchino, K., "Effect of Ceramic Processing Methods on Photostrictive Ceramics", J. Advanced Performance Mater. **6**, 57-69 (1999).

VOLUME V

4.3 High Force Actuators

69. A. E. Glazounov, Q. M. Zhang, and C. Kim. Torsional Actuator and Stepper Motor Based on Piezoelectric d_{15} Shear Response. J. Intel. Mater. Syst. & Struct. 11(6), 456-468 (2000).
70. Galante, T., J. Frank, J. Bernard, W. Chen, G.A. Lesieutre, and G.H. Koopmann, "A High-Force, High-Displacement Piezoelectric Inchworm Actuator," Journal of Intelligent Materials Systems and Structures, Vol. 10, No. 12, December, 2000, pp. 962-972.

4.4 Piezoelectric Motors

71. Koc, B. and K. Uchino, "Piezoelectric Ultrasonic Motors," Chap.6.34, Comprehensive Composite Materials, Elsevier Science, Oxford, UK (2000).
72. Uchino, K., and B. Koc, "Compact Piezoelectric Ultrasonic Motors," Proc. NATO-Advanced Research Workshop: Piezoelectric Materials: Advance in Science, Technology and Applications, (Predeal, Romania, May 24-27, 1999, Kluwer Academic Publ., p.309-320 (2000).
73. Koc, B., J. F. Tressler and K. Uchino, "A Miniature Piezoelectric Rotary Motor Using Two Orthogonal Bending Modes of a Hollow Cylinder," Proc. Actuator 2000 (7th Int'l Conf. New Actuators, June 19-21, 2000), p.242-245 (2000).
74. Koc, B., J. F. Tressler and K. Uchino, "A Miniature Piezoelectric Rotary Motor Using Two Orthogonal Bending Modes of a Hollow Cylinder," Proc. Actuator 2000 (7th Int'l Conf. New Actuators, June 19-21, 2000), p.242-245 (2000).
75. Bouchilloux, P., B. Koc and K. Uchino, "New Concept for Resonant Longitudinal-Shear Ultrasonic Motor," Symp. LL Proc., Mater. Res. Soc. Fall Mtg. '99, (LL.2.10, Boston, Nov. 29-Dec.3, 1999), Vol.**604**, 71-78 (2000).

76. Koc. B., P. Bouchilloux, and K. Uchino, "Piezoelectric Micromotor Using A Metal-Ceramic Composite Structure," IEEE Trans. Ultrasonic, Ferroelectrics, and Frequency Control **47** (4), 836-843 (2000).

4.5 Acoustic Absorbers

77. Davis, C.L. and G.A. Lesieutre, "An Actively Tuned Solid State Vibration Absorber Using Capacitive Shunting of Piezoelectric Stiffness," Journal of Sound and Vibration, Vol. 232(3), 4 May 2000, pp. 601-617.

78. Patricia L. Driesch, Hisao Iwata, Gary H. Koopmann, and Jeff Dosch. Nov. 2000. Development and evaluation of a surface acoustic intensity probe. Review of Scientific Instruments, 71 (11), pp. 1-6.

79. W. Huang. G. H. Koopmann, S. J. Sharp, and W. Chen. April 2000. Enhanced Low Frequency Transmission Loss of Lightweight Trim Panels. Journal of Intelligent Material Systems and Structures, Volume 11, No 4.

80. E.W. Constans, A.D. Belegundu, and G.H. Koopmann. 2000. Optimally Designed Shell Enclosures with Tuned Absorbers for Minimizing Sound Power. Optimization and Engineering, 1, 67-86, (an International Journal, Kluwer Publishers)

VOLUME VI

5.0 MODELING AND CHARACTERIZATION

5.1 Design and Simulation

81. K. Uchino, "Designing With Piezoelctric Devices" Internation Center for Actuators and Transducers, Materials Research Institute, The Pennsylvanis State University, University Park, PA (2000)

82. W.K. Qi, and W. Cao, "Finite Element Study on 1-D Array Transducer Design", IEEE Transaction, Ultra. Ferro. and Frequency Control, vol. **47**, pp. 949-955 (2000).

83. T.A. Ritter, K. K. Shung, W. Cao and T. R. Shrout, "Electromechanical Properties of Thin Strip Piezoelectric Vibrators at High Frequency", J. Applied Phys, vol. **88**, pp. 394-397 (2000).

84. T.A. Ritter, K. K. Shung, W. Cao and T. R. Shrout, "Electromechanical Properties of Thin Strip Piezoelectric Vibrators at High Frequency", J. Applied Phys, vol. **88**, pp. 394-397 (2000).

5.2 Thick and Thin Films

85. Kalpat, S., X. Du, I. R. Abothu, A. Akiba, H. Goto and K. Uchino, "Effect of Crystal Orientation on Dielectric Properties of Lead Zirconate Titanate Thin Films Prepared by Reactive RF-Sputtering," Jpn. J. Appl. Phys., **40**, 158-162 (2001).

86. Kalpat, S., X. Du, I. R. Abothu, A. Akiba, H. Goto, S. Trolier-McKinstry and K. Uchino, "Dielectric Properties of Highly Oriented Lead Zirconate Titanate Thin Films Prepared by Reactive RF-Sputtering," Symp. LL Proc., Mater. Res. Soc. Fall Mtg. '99, (LL.1.3, Boston, Nov. 29-Dec.3, 1999), Vol. **604**, 3-8 (2000).

87. S. Trolier-McKinstry, "Piezoelectric Films for MEMS Applications," J. Ceram. Soc. Jpn. 109 (5) S76-S79 (2001).

88. Jeong Hwan Park, Fei Xu, and Susan Trolier-McKinstry, "Dielectric and Piezoelectric Properties of Sol-Gel Derived Lead Magnesium Niobium Titanate Films with Different Textures," J. Appl. Phys. 89(1) 568 - 574 (2001).
89. Q. F. Zhou, E. Hong, R. Wolf, and S. Trolier-McKinstry, "Dielectric and Piezoelectric Properties of PZT 52/48 Thick Films with (100) and Random Crystallographic Orientation," Ferroelectric Thin Films, Vol 655 (2000).
90. L.-P. Wang, R. Wolf, Q. F. Zhou, S. Trolier-McKinstry and R. J. Davis, "Wet-etch patterning of lead zirconate titanate (PZT) thick films for microelectromechanical systems (MEMS) application," Mat. Res. Soc. Symp. Vol.657 (MEMS)

5.3 Domain Studies

91. Uchino, K., and H. Aburatani, "Field Induced Acoustic Emission in Ferroelectric Ceramics," Proc. 101st Annual Mtg. of Amer. Ceram. Soc., Symp. Electronic Ceramic Materials and Devices, SE-56, (Indianapolis, April 25 – 28, 1999), (2000).
92. J. Fousek [ab], L.E. Cross [b], "Engineering Multidomain Ferroic Samples, Dept of Physics and International Center for Piezoelectric Research, University of Technology, Liberec, 46117 Czech Republic and [b] Materials Research Laboratory, The Pennsylvania State University, University Park, PA 16802, USA. (June 2000)
93. J.H. Yin, and W. Cao, "Domain Configurations in Domain-Engineered $0.955Pb(Zn_{1/3}Nb_{2/3})O_3$-$0.045PbTiO_3$ Single Crystals", J. Appl. Phys, vol. **87**, pp. 7438-7441 (2000).
94. Rajeev Ahluwalia, "Computer Simulations of Domain Pattern Formation in Ferroelectrics", AIP Conference Proceedings Series, © 2001 American Institute of Physics, Proceedings of the 2001 Workshop on Fundamental Physics of Ferroelectrics Williamsburg, Va, 2001
95. R. Ahluwalia and W. Cao, "Influence of Dipolar Defects on Switching Behavior in Ferroelectrics", Phys. Rev. B, vol. **63**, pp. 012103 (2000)
96. Uchino, K., and H. Aburatani, "Field Induced Acoustic Emission in Ferroelectric Ceramics," Proc. 101st Annual Mtg. of Amer. Ceram. Soc., Symp. Electronic Ceramic Materials and Devices, SE-56, (Indianapolis, April 25 – 28, 1999), (2000).

MATERIALS STUDIES

Single Crystal Systems

APPENDIX 13

Ferroelectrics, 2001, Vol. 252, pp. 171-180
Reprints available directly from the publisher
Photocopying permitted by license only

Engineering Multidomain Ferroic Samples

J. FOUSEK[ab] and L. E. CROSS[b]

[a]*Dept. of Physics and International Center for Piezoelectric Research, University of Technology, Liberec, 46117 Czech Republic and* [b]*Materials Research Laboratory, The Pennsylvania State University, University Park, PA 16802, U.S.A.*

(Received June 2, 2000)

The existence of domains is essential in many practical applications of ferroics. Here we discuss devices in which a *fixed* spatial distribution of domains plays the significant role. Depending on the prevailing attributes of multidomain single crystals, three different possibilities can be distinguished. In *domain-geometry-engineered* samples the spatial distribution of domains is tuned to correspond to the k-vectors of fields propagating through the material. In *domain-average-engineered* samples the crystal is subdivided into a very large number of domains, representing a *limited* number of domain states. In *domain-wall-engineered* samples the characteristics of static walls can play an essential role in the averaged macroscopic properties. Examples illustrating these approaches are given.

Keywords: domain engineering; domain-geometry engineering; domain-average-engineering; domain-wall-engineering; multidomain ferroics; static domain pattern

1. INTRODUCTION

Practical applications of ferroics (undergoing a phase transition from the point group G to F) are of two basically different characters: those which rely on properties of single domain samples and those in which the presence of domains is essential. The latter can be categorized into

devices based on dynamical domain processes or those in which a static distribution of domains plays a significant role. Here we discuss the last mentioned case: general characteristics of multidomain samples with fixed spatial distribution of domains.

Depending on the prevailing attributes of multidomain single crystal samples, several possibilities can be distinguished. Those discussed in the following sections 2 to 4 differ in general features of the geometry of domains and it is assumed that domain walls are of negligible thickness. In the last considered case, the thickness of domain walls is finite and specimens exhibit large wall density. Aspects of preparation and properties of such samples are discussed in the section 5.

2. DOMAIN-GEOMETRY-ENGINEERED FERROIC SAMPLES

As early as in 1964, Miller[1] showed that a regular pattern consisting of 180^0 domains in $BaTiO_3$ with a period corresponding to the coherence length could substantially increase the effectiveness of optical second harmonic generation. The idea is based on two factors: a) domain states differ in the sign of nonlinear optical coefficient, b) the width of domains is tuned to the coherence length. It was Feng Duan et al. [2] who succeeded in manufacturing a periodic domain pattern in $LiNbO_3$ and proved its efficiency in nonlinear optics. More recently, S. N. Zhu et al.[3] initiated an essential progress in this field by producing a domain pattern whose geometry corresponds to a Fibonacci superlattice and which makes it possible to realize second harmonic generation for multiple wavelengths. But the significance of domain patterns with engineered geometry was proved also in acoustics. Meeks at el.[4] produced tunable acoustic systems based on spatial modulation of elastic coefficients in a periodic domain pattern in NdP_5O_{14} while Y. Y. Zhu et al.[5] succeeded in producing transducers up to 800 MHz based on spatial modulation of piezoelectric coefficients in multidomain $LiNbO_3$.

In all these applications the periodicity of domain patterns corresponds to k-vectors of propagating waves and the multidomain domain systems represent just two domain states. Up to now less than 10 ferroics have been utilized in this area, and in any of these materials the total number of domain states $\nu = |G| / |F| = 2$ (here $|G|$ and $|F|$ stand for the order of the parent and ferroic phase point groups, resp.). This is understandable since to produce a regular pattern in ferroics with $\nu > 2$ in which only two domain states are involved is not trivial.

To solve this task in particular cases experimentally is, however, possible. In fact the nature itself shows that patterns with a regular geometry of a limited number $\mu < \nu$ of domain states can be materialized. Several observations have been made of domain patterns with regular geometry, fulfilling this requirement. As an example, we refer to the Forsbergh's square-net pattern[6] shown in Fig.1, which has been repeatedly observed in $BaTiO_3$ single crystals as well as ceramic grains. It might be inspiring to examine its macroscopic properties for external fields with both $k = 0$ and $k \neq 0$, based on its symmetry characteristics.

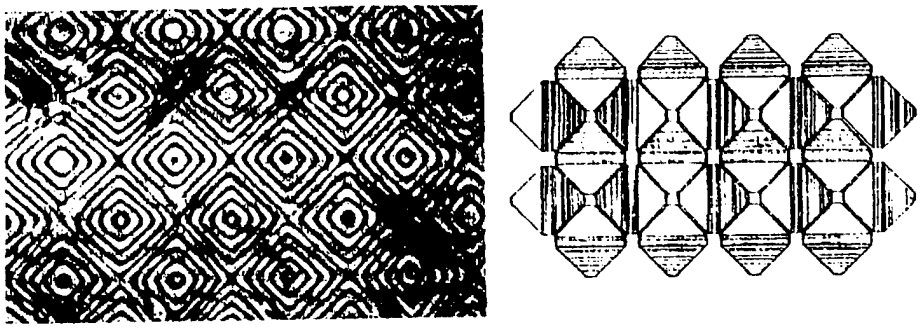

FIGURE 1 Example of a "natural" multiaxial domain-geometry engineered system: the Forsbergh's square-net pattern in tetragonal $BaTiO_3$. Left: microscopic picture; right: arrangement of tetrahedral building blocks. From Ref. [6].

Several other multiaxial threedimensional and reproducible patterns have been observed under natural conditions and there is little doubt that they could be produced artificially. To mention just one more example, we refer to the Arlt's[7] patterns α and β; till now they have been observed only in ceramic grains but very probably they could be created in crystals under properly designed external forces. Again, in order to deliberate about their properties, the symmetry analysis would be the first step to take.

Indeed, regular domain systems can offer unexpected symmetry properties. Thus, for instance, the well known Hallbach array of magnets with asymmetric distribution of magnetic field can have a simple analogy in thin ferroelectric plates containing a regular system of 90^0 domain pairs. While in the latter case, because of the existence of free charges, we do not expect pronounced external depolarizing field

effects, macroscopic properties of the array could offer new applicable aspects.

3. DOMAIN-AVERAGE-ENGINEERED FERROIC SAMPLES

In contrast to the previous cases, in *domain-average-engineered* samples of ferroic crystals the specimen is subdivided into a very large number of domains, representing just $\mu < \nu$ domain states. Such situations can be achieved by cooling samples through their phase transition temperatures under properly oriented stresses, electric fields or their combinations. The geometry of domains is irregular. The sample's response to external fields is roughly described by tensorial properties averaged over all involved domain states. Thus, e.g. for the piezoelectric response we can write in the zeroth approximation

$$\bar{\varepsilon}_{jk} = \bar{d}_{ijk}\bar{E}_i, \quad \bar{d}_{ijk} = \frac{1}{V}\sum_{\alpha=1}^{\mu} d_{ijk}^{(\alpha)} V^{(\alpha)}.$$

Here $V(\alpha)$ denotes the volume occupied by the domain state α.

In recent years, Park et al.[8,9], Yin and Cao[10] and other authors considered a case of this character to discuss piezoelectric properties of PZN-PT single crystals poled along one of the {001} directions. Assuming that the material went through the phase transition from G = $m\bar{3}m$ to F = $3m$, the poling along [100] supports the coexistence of four domain states with spontaneous polarization along the directions [111], [1 $\bar{1}$ 1], [11 $\bar{1}$] and [1 $\bar{1}$ $\bar{1}$], with equal probability. In this statement, it is assumed that the domain wall orientation aspects (e.g. mechanical compatibility) can be neglected. In fact, in samples of ferroelastic crystals strictly speaking, only one set of mechanically permissible parallel domain walls is allowed[11] while in real samples walls of various orientations coexist connected with additional elastic strains, paid by increased elastic energy.

The symmetry aspects of domain–average–engineered samples can be discussed in a general way. The task is to determine the average point symmetry H, i.e. the symmetry of the subset of domain states contained in the multidomain sample. This was addressed by Fousek et al.[12] and the procedure can be facilitated by the use of the computer programme of Schlesmann and Litvin.[13]

As an example, in Fig.2 we reproduce[12] the average symmetry groups H of six selected subsets of domain states (out of 13 leading to

different symmetries F) which arise in the phase transition specified above (here $\mu = 8$). States are represented by self-explanatory numbers and dots indicating the directions of $\mathbf{P}_S$ vectors.

Representative subset	Subset symmetry H
[1] 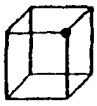	$3_{xyz}\, m_{\bar{x}y}$
[13] 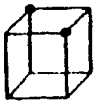	$m_{xy}\, m_{\bar{x}y}\, 2_z$
[15] 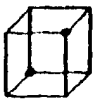	$\bar{3}_{xyz}\, m_{\bar{x}y}$
[136] 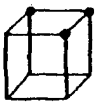	m_{xy}
[1356] 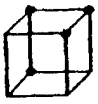	$2_{\bar{x}z}$
[1368] 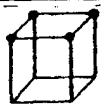	$4_z m_x m_{xy}$

FIGURE 2 Examples of subsets of domain states corresponding to the transition $m\bar{3}m - 3m$ and their symmetries.

Taking into account the distribution of polar vectors and corresponding strain tensors, one can determine which external forces should be applied in order to obtain any of the domain-average-engineered systems. The trivial example is the subset [1] produced by the electric field **E** along [111]. The subset [1368], discussed[8-10] before, will be produced by the field along [001] while the combination [15] requires the application of a uniaxial stress along [111]. The subset [13] calls for the application of both electric field along [001] and uniaxial stress along [$\bar{1}$10].

In addition to the applied fields, electrical or mechanical, there are other approaches which can eliminate particular domain states in a

given ferroic material. The stimulating example is based on chiral dopants. Keve et al.[14] showed that doping TGS with *L*-α-alanine prefers just one of the two domain states with antiparallel $\mathbf{P}_S$. Zikmund and Fousek[15,16] generalized this approach and showed that chiral substitients can reduce the number of domain states by a factor of two in a number of ferroic species.

It is understood that in the mentioned approaches we leave behind the problems of domain coexistence connected with their mechanical compatibility. It seems obvious that domain average engineering can succesfully lead to formation of crystalline systems with new desired properties in particular in crystals where the domain size is small. Crystalline systems exhibiting tweed microstructures similar to those observed in La-modified lead titanate[17] or PLZT[18] might serve as candidates for this approach.

4. PHASE- AND- DOMAIN-AVERAGE ENGINEERED FERROICS

The domain-average-engng concept can be generalized to systems in which the prescribed domain states represent two or more ferroic species. Such multiphase situations occur in PZT ceramics near the morphotropic boundary and originate[19] in concentration gradients as well as in the independent nucleations of the ferroic phases since the transition is of the 1st order. It appears that PZN-PT single crystals with a pronounced piezoelectric response contain blocks of both tetragonal and rhombohedral symmetry[20]. In the basic approximation, the piezoelectric coefficient of a properly poled sample is then described by

$$\bar{d}_{ijk} = \frac{1}{V_1}\left[\sum_{\alpha=1}^{\mu 1} d_{ijk}^{(\alpha)} V^{(\alpha)}\right] + \frac{1}{V_2}\left[\sum_{\beta=1}^{\mu 2} d_{ijk}^{(\beta)} V^{(\beta)}\right] + \\ + \Delta d_{ijk}\,(walls) + \Delta d_{ijk}\,(phase\ bndrs)$$

where μ1 and μ2 are numbers of domain states represented in the phase 1 and 2, resp., after poling. The high piezoelectric response of PZN-PT single crystals originates in the combination of intrinsic coefficients $d_{ijk}^{(\alpha)}$, $d_{ijk}^{(\beta)}$ as well as in the extrinsic contributions due to the motion of domain walls and phase boundaries. The question what role is played by any of these contributions is still to be solved.

When addressing the problem of average symmetries of phase-and-domain-average-engineered samples one can follow[21] a similar approach as mentioned above. Consider that two species coexist, namely $m\bar{3}m$ $3m$ and $m\bar{3}m$ $4mm$. It can be shown that when poling along principal directions, i.e. **E** ∥ [001] or **E** ∥ [011] or **E** ∥ [111], regions of the two species differ in the systems of $\mathbf{P}_S$ vectors but are of the same averaged symmetries $4mm$, $mm2$ or $3m$, resp.

It has to be stressed that in both domain-average enginnered and phase-and-domain-average engineered systems, electrical and mechanical compatibility conditions play, in the energy evaluations, a significant role. It is beyond the scope of this presentation to discuss these problems in detail and the subject will be addressed in another paper.

5. DOMAIN-WALL-ENGINEERING

In the last considered case, the thickness of domain walls is finite and the specimens exhibit large wall density. As before, the representation of specific walls can be influenced by external forces. In such *domain-wall-engineered* samples the characteristics of static walls can play an essential role in the averaged macroscopic properties.

It was predicted by Walker and Gooding[22] that Dauphiné domain walls in nonpolar quartz can carry a dipole moment and this was later demonstrated experimentally by Snoeck et al.[23], in the incommensurate phase of SiO_2. In fact it is easy to demonstrate this possibility for ferroelastic walls. If in the free energy function the invariant $\mu_{ijkl}(\partial\varepsilon_{ij}/\partial x_k)E_l$ is allowed by symmetry, a ferroelastic wall will carry polarization

$$P_l = \mu_{ijkl}\frac{\partial\varepsilon_{ij}}{\partial x_k}.$$

Here the μ-tensor describes the flexoelectric effect. As an example, consider the species $m\bar{3}m$ – $4/mmm$ represented by crystals of $SrTiO_3$, or $CsPbCl_3$ and the species $m\bar{3}m$ – $4mm$ describing the properties of $BaTiO_3$. In both cases, ferroelastic walls (90^0 wall in the latter case) are, by symmetry, allowed to carry polarization

$$P_x = P_z = (\mu_{1111} - \mu_{3311})\frac{\partial\varepsilon_{xx}}{\partial x};$$

this is demonstrated in Fig. 3. Symmetries of nonferroelastic domain walls from which their possible macroscopic properties can be envisaged have been discussed by Přívratská and Janovec[24].

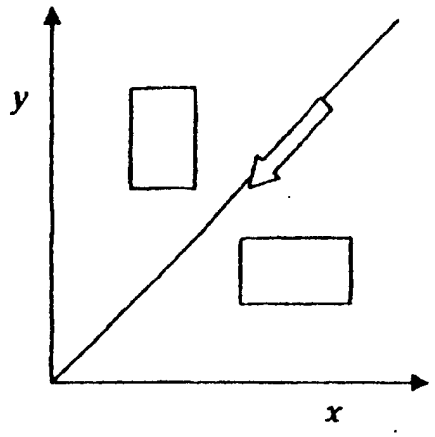

FIGURE 3 Due to flexoelectricity, domain wall separating two ferroelastic domains of species $m\bar{3}m - 4/mmm$ or $m\bar{3}m - 4mm$ can carry polarization represented by the arrow.

Should macroscopic properties of domain walls play a non-negligible role in the properties of a ferroic sample, they have to occupy a sizable volume. Realistic values of domain width and domain wall thickness are d_{domain} = 1 to 10 μm and t_w = 3 nm, resp. Suppose that the required relative volume occupied by domain walls is 10% and that there so no way how to increase the wall thickness. Then we look for methods how to reduce the average domain width to about 30 nm, i.e. how to increase the wall density 30 times or more.

It appears that there is a significant number of experimental methods which could address this problem. Here we mention in passing only some of those which might be considered. The density of defect-induced order parameter gradients could be increased at crystal growth[2]. The size of AFM-written domains[25] could be further reduced, their density increased. Attempts to freeze-in high density tweed structures[26] in some ferroelastics close above T_C or high density pattern of discommensurations in modulated phases close above the lock-in temperatures[27] appear attractive. Fixing photorefractive gratings by domains[28] in ferroelectrics with small P_S (small defect-

assisted nucleation energies to produce domains in real time) looks also promissing.

6. CONCLUSIONS

Till now, the field of domain geometry engineering has been succesfully developed and applied to ferroics representing five species of ferroelectrics and one species of ferroelastics, all with two domain states. Such specimens proved to be competitive in the field of nonlinear optics and promissing in the field of ultrasonic generation and detection. But much more complex domain systems are obtainable and have not yet been considered and investigated.

Two new areas of research appear to be very promissing. Domain- and phase-average engineered systems offer increased values of macroscopic properties, probably strengthened by domain wall and/or phase boundary induced motions. We still miss detailed data about the real structure of existing compounds like PZN-PT as well as theoretical analysis of multiple domain states compatibility, the more so for multiple phase systems. Domain-wall engineered samples with high density of walls also promise a new interesting research and application area. At present, particular systems useful in selected applications could be specified and methods to produce high density domain patterns investigated experimentally.

Acknowledgments

J.F. appreciates the support of the Ministry of Education of the Czech Republic (Project VS 96006) and the assistance of the Materials Research Laboratory, The Pennsylvania State University.

References

[1] R. C. Miller, *Phys. Rev.* **134,** A1313 (1964).
[2] D. Feng, N. B. Ming, J. F. Hong, Y. S. Yang, J. S. Zhu, Z. Yang and Y. N. Wang, *Appl. Phys. Lett.* **37,** 607 (1980).
[3] S. N. Zhu, Y. Y. Zhu, Y. Q. Qin, H. F. Wang, C. Z. Ge and N. B. Ming, *Phys. Rev. Lett.* **78,** 2752 (1997).
[4] S. W. Meeks, L. Clarke and B. A. Auld, IEEE Ultrasonics Symposium, San Francisco, CA (1985).
[5] Y. Y. Zhu, N. B. Ming, W. H. Jiang and Y. A. Shui, *Appl. Phys. Lett.* **53,** 1381 (1988).
[6] P. W. Forsbergh, Jr., *Phys. Rev.* **76,** 1187 (1949).
[7] G. Arlt and P. Sasko, *J. Appl. Phys.* **51,** 4956 (1980).
[8] Seung-Eek Park and T. R. Shrout, *J. Appl. Phys.* **82,** 1804 (1997).
[9] Seung-Eek Park, S. Wada, P. W. Rehrig, Shi-Fang Liu, L. E. Cross and T. R. Shrout, "Crystallographic Engineering in High-performance Piezoelectric Crys tals." Paper presented at SPie Smart tructures and Materials (New Port Beach, 1999).

[10] Jianhua Yin and W. Cao, *J. Appl. Phys.* **87,** 7438 (2000).
[11] J. Fousek and V. Janovec, *J. Appl. Phys.* **40,** 135 (1969).
[12] J. Fousek, D. B. Litvin and L. E. Cross, submitted.
[13] J. Schlessman and D. B. Litvin, *Acta Cryst.* **A51,** 947 (1995).
[14] E. T. Keve, K. L. Bye, P. W. Whipps and A. D. Annis, *Ferroelectrics* **3,** 39 (1971).
[15] Z. Zikmund and J. Fousek, *Ferroelectrics* **79,** 73 (1988).
[16] Z. Zikmund and J. Fousek, *phys. stat. sol. (a)* **112,** 625 (1989) and **118,** 539 (1990).
[17] G. A. Rossetti, Jr., W. Cao and C. A. Randall, *Ferroelectrics* **158,**343 (1994).
[18] C. A. Randall, G. A. Rossetti, Jr. and W. Cao, *Ferroelectrics* **150,**163 (1993).
[19] V. A. Isupov, *Ferroelectrics* **46,** 217 (1983).
[20] K. Fujishiro, R. Vlokh, Y. Uesu, Y. Yamada, J.-M. Kiat, B. Dkhil and Y. Yamashita, *Jpn. J. Appl. Phys.* **37,** 5246 (1998).
[21] J. Fousek, D. B. Litvin and L. E. Cross, to be published.
[22] M. B. Walker and R. J. Gooding, *Phys. Rev. B* **32,** 7408 (1985).
[23] E. Snoeck, P. Saint-Gregoire, V. Janovec and C. Roucau, *Ferroelectrics* **155,** 371 (1994).
[24] J. Přívratská and V. Janovec, *Ferroelectrics* **191,** 17 (1997).
[25] L. M. Eng, M. Bammerlin, Ch. Loppacher, M. Guggisberg, R. Bennewitz, R. Lüthi, E. Meyer, Th. Huser, H. Heinzelman and H.-J. Güntherodt, *Ferroelectrics* **222,** 153 (1998).
[26] A. M. Bratkovsky, E. K. H. Salje and V. Heine, *Phase Transitions* **52,** 77 (1994).
[27] V. Novotna, H. Kabelka, J. Fousek, M. Havrankova and H. Warhanek, *Phys. Rev. B* **47,** 11019 (1993).
[28] J. Fousek, M. Marvan and R. S. Cudney, *Appl. Phys. Letters* **72,** 430 (1998).

APPENDIX 14

Transactions of the Materials Research Society of Japan 25 [1] 19-24 (2000)

Change of Macroscopic and Microscopic Symmetries in Relaxor PZN Single Crystal under DC-bias Field

Satoshi Wada, Takaaki Tsurumi, Minoru Osada[1], Masato Kakihana[2], Seung-Eek Park[3], L. Eric Cross[3] and Thomas R. Shrout[3]

Department of Metallurgy & Ceramics Science, Tokyo Institute of Technology, 2-12-1 Ookayama, Meguro-ku, Tokyo 152-8552, JAPAN
Fax: 81-3-5734-2514, e-mail: swada@ceram.titech.ac.jp

[1]Institute of Physical & Chemical Research, 2-1 Hirosawa, Wako, Saitama 351-0198, JAPAN
Fax: 81-48-462-4623, e-mail: mosada@postman.riken.go.jp

[2]Materials & Structure Laboratory, Tokyo Institute of Technology, 4259 Nagatsuta-cho, Midori-ku, Yokohama 226-8502, JAPAN
Fax: 81-45-924-5309, e-mail: kakihana@rlem.titech.ac.jp

[3]Materials Research Laboratory, The Pennsylvania State University, University Park, PA 16802-4801, U.S.A.
Fax: 1-814-865-2326, e-mail: sxp37@psu.edu

Pure $Pb(Zn_{1/3}Nb_{2/3})O_3$ (PZN) single crystal is the typical relaxor ferroelectrics with an optical isotropic property. Using the PZN crystal, two kinds of symmetries were investigated by using a polarized microscope and a Raman scattering spectroscopy under DC-bias field to obtain some important informations about polar micro regions (PMR). In the relaxor state, its macroscopic symmetry on the basis of domain observation was assigned to the highest symmetry *i.e.*, *m3m*. However, DC-bias exposure to the PZN crystal with the relaxor state induced the ferroelectric domains, and finally all regions in the crystal became to ferroelectrics. This domain configuration was analyzed crystallographically, and its macroscopic symmetry was assigned to acentrosymmetric *3m*. On the other hand, no change between Raman scattering spectra in relaxor and ferroelectric states was observed. This means that their microscopic symmetries of acentrosymmetric *3m* and phonon damping states did not changed in the both states. These results revealed that for the relaxor state, the existence of the disorder system in the structure is very important.

Key word: PZN single crystal, Raman scattering, domain configuration, polar micro regions, DC-bias

1. INTRODUCTION

It was well known that PZN single crystal is the typical relaxor ferroelectrics with a maximum dielectric constant around 140°C, and has an optical isotropic property[1-5]. Many researchers have considered that PMR was the origin of the relaxor behavior with an optical isotropic state[5-9]. Therefore, PMR is the most important factor in the relaxor behavior. At present, there are some models about PMR state, *i.e.*, (i) superparaelectric model[6], (ii) dipolar and spin glass model[7], (iii) dipolar dielectric with random field model[8] and (iv) breathing model[9]. First three models were on the basis of flipping polar vector in PMR while the last model was on the basis of fixed polar vector. Therefore, it is important to understand PMR. However, the polar state in PMR has been still unclear, and moreover, a time scale and a spatial magnitude in PMR were also unknown. Previously, it has been considered that chemically ordered domains (COD) observed by TEM might be PMR, but Akbas and Devis[10-11] revealed that COD did not relate with the relaxor behavior.

Time scale t / Spatial magnitude d	Dynamic t < 1 ns	Intermediate 1 ns < t < 10 μs	Quasi-static 10 μs < t
Microscopic d < 1~2 nm	Raman Scattering Spectroscopy		Transmittance Electron Microscopy
Mesoscopic 2 nm < d < 0.5 μm	Brillouin Scattering Spectroscopy		X-ray Diffraction Spectroscopy
Macroscopic 0.5 μm < d		Microwave Dielectric Spectroscopy	Polarized Microscopy

Table I Relationship between measurement method and spatial magnitude and time scale of measured physical phenomenon[12].

Nomura *et al.*[5] reported that a DC-bias exposure on an optical isotropic PZN crystals induced a ferroelectric state with normal ferroelectric domains. This means that using DC-bias field, two states, *i.e.*, the relaxor and ferroelectric states, were controlled in PZN crystals. Therefore, if under the both states, some symmetries with various time scales and spatial magnitudes (Table I) are measured[12], it can be expected to obtain some important informations about the polar state in PMR. In this study, we focused two kinds of symmetries. One is a dynamic and local symmetry on the basis of the lattice vibration (phonon) which was measured by a Raman scattering spectroscopy. We call this symmetry a microscopic symmetry with a dynamic time scale ($t <$ 1nsec) and a microscopic spatial magnitude ($d <$ 1~2nm). The other is a statistic and macro symmetry on the basis of the domain configuration which was observed by a polarized microscope. We call this symmetry a macroscopic symmetry with a quasi-static time scale ($t > 10\mu$sec) and a macroscopic spatial magnitude ($d > 0.5\mu$m).

Our final objective is to elucidate the relaxor

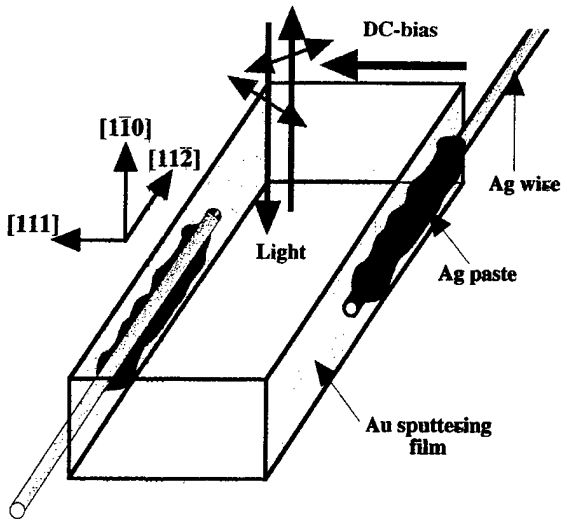

Fig. 1 A schematic diagram for *in-situ* Raman scattering measurement.

behavior in PZN crystals and its origin. In this study, we investigated about a change of the macroscopic and microscopic symmetries under DC-bias field, and discussed about PMR.

2. EXPERIMENTAL

PZN single crystals were grown by a conventional flux method using a PbO flux. Further details on the crystal growth were reported elsewhere[13]. These crystals were oriented along [111] direction using a back reflection Laue method. For *in-situ* domain observation and Raman scattering measurement under DC-bias field, samples were prepared by polishing to an optimum size of approximately 0.2x0.5x4mm^3. Their top and bottom surfaces (0.5x4mm^2) were mirror-polished, normal to an incident light. Gold electrodes were sputtered on both sides (0.2x4mm^2), and the width between electrodes was around 0.5mm along [111] direction, as shown in Fig. 1. The details were described elsewhere[14-15]. Domain configuration was always observed under crossed-nicols using a polarized microscope (Carl Zeiss, D-7082). DC-bias exposure was done along [111] direction, being normal to the incident polarized light, using a Trek 610D high-voltage DC amplifier. Raman scattering spectra under DC-bias were measured in the backward scattering geometry using a Raman scattering spectrometer with a triple monochromator (Jobin-Yvon, T64000). DC-bias exposure was done in the same way as that in domain observation. The top surface (0.5x4mm^2) was excited by unpolarized and polarized Ar ion laser with a wavelength of 514.5nm and power below 20W/cm^2. The details are described elsewhere[16].

3. RESULTS AND DISCUSSION

3.1 in-situ domain observation under DC-bias field:

In-situ domain observation was done at 25°C. Figs. 2(a)-(l) show domain configurations under various DC-bias fields from 0 to 39kV/cm. Fig. 2(a) indicates a micrograph before a DC-bias exposure. When this crystal was rotated under fixed crossed-nicols, all regions in PZN crystal were always dark, except for some surface scratch. This means that the PZN crystal before the DC-bias exposure was the relaxor state with the optical isotropic property. Therefore, its indicatrix was a perfect sphere[17], and thus its macroscopic symmetry was assigned to the highest symmetry of *m3m*.

With increasing DC-bias field, ferroelectric domains appeared near the electrodes and grew. From 15 to 21kV/cm, the coexistence of relaxor regions and ferroelectric domains was observed in Figs. 2(b)-(d). Above 27kV/cm, all regions completely became to ferroelectric regions. The domain configuration was analyzed crystallographically, and these domain walls were assigned to 109° domain walls of {100} planes[18].

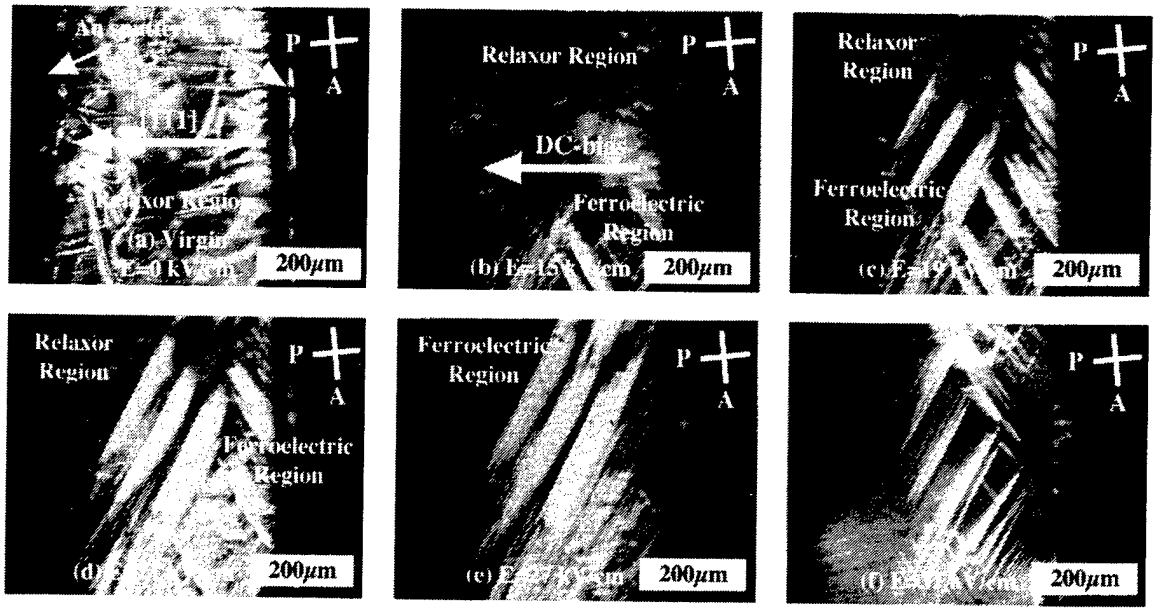

Fig. 2 Domain configuration under various DC-bias fields from 0 to 39kV/cm at 25°C.

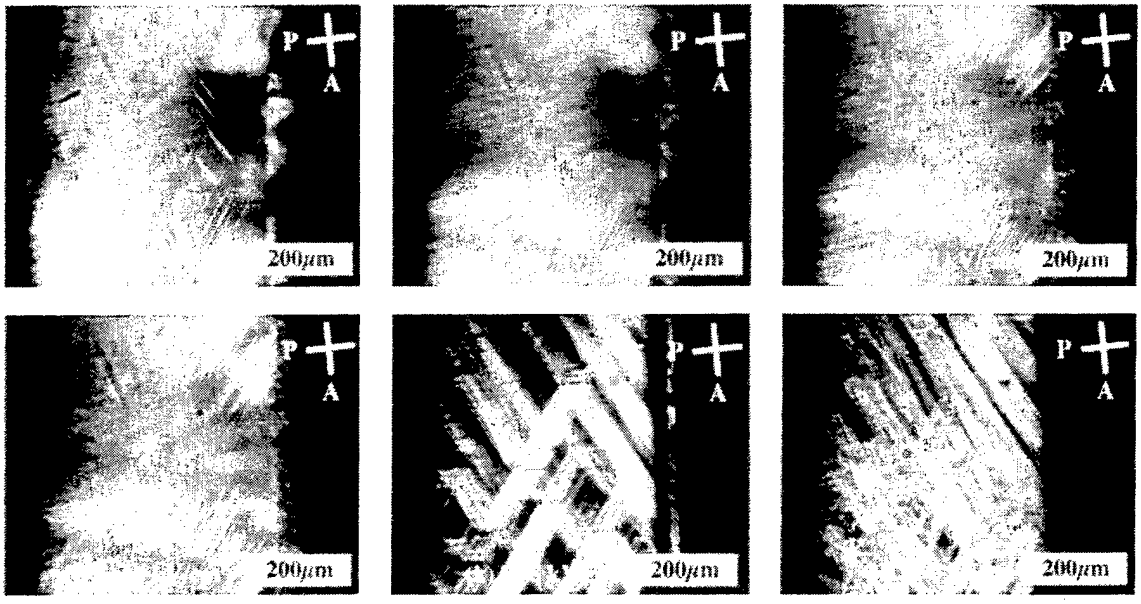

Fig. 2 Domain configuration under various DC-bias fields from 0 to 39kV/cm at 25°C. (*cont.*)

This domain configuration revealed that its macroscopic symmetry was assigned to rhombohedral symmetry *3m*. Moreover, the DC-bias exposure above 30kV/cm reduced domain wall density (Figs. 2(f)-(g)), and around 39kV/cm, most of PZN crystal became to a single domain state (Fig. 2(h)).

On the other hand, with decreasing DC-bias field, new domains appeared near the electrodes (Fig. 2(i)), and grew, as shown in Figs. 2(j)-(k). Finally a multidomain state was observed without DC-bias field (Fig. 2(l)). It should be noted that under no DC-bias field, its macroscopic symmetry after DC-bias exposure was assigned to *3m* acentric symmetry. The above result showed that the macroscopic symmetry in PZN crystal was changed from *m3m* to *3m* by the DC-bias exposure. Thus, we consider this phenomenon as a kind of phase transition induced by an electric-field. The ferroelectric state in Fig. 2(l) was completely disappeared by annealing at 250°C for 16h, and returned to the relaxor state as shown in Fig. 2(a).

3.2 in-situ Raman scattering measurement under DC-bias field:

In-situ Raman scattering measurement was done at 25°C using polarized and unpolarized lights. Through this manuscript, the scattering configuration is denoted by A(BC)$\overline{A}$, which means that the incident light polarized along "B" direction propagates along "A" direction, and the scattered light polarized along "C" direction propagates along opposite "A" direction ($\overline{A}$). In domain observation, we used "*cubic-axis*" notation system such as [111], but in Raman scattering measurement, we changed the notation system from "*cubic-axis*" notation system to "*principle-axis*" notation system. In *3m* rhombohedral crystal, [1$\overline{1}$0], [11$\overline{2}$] and [111] in "*cubic-axis*" notation system (Fig. 1) correspond to X, Y and Z in "*principle-axis*" notation system, respectively. In this study, Raman scattering measurement was done in three kinds of backward scattering geometries, *i.e.*, X(NN)$\overline{X}$, X(ZZ)$\overline{X}$ and X(ZY)$\overline{X}$ (N: unpolarized light).

Fig. 3 shows Raman scattering spectra measured in X(NN)$\overline{X}$ geometry under upward DC-bias field from 0 to 28.4kV/cm while Fig. 4 shows those measured under downward DC-bias field from 28.4 to 0.04kV/cm. In Raman spectra using unpolarized lights, all Raman-active phonon modes could be observed. PZN crystal before DC-bias exposure exhibits 12 peaks, as shown in the bottom of Fig. 3. XRD measurement using crashed PZN crystals was assigned to rhombohedral *3m* symmetry[13]. If a microscopic symmetry on the basis of phonon is *3m* symmetry, there are 14 Raman-active modes, *i.e.*, $3A_1(TO)+3A_1(LO)+4E(TO)+4E(LO)$. Thus, we regarded the microscopic symmetry of PZN crystal before DC-bias exposure as *3m* symmetry.

With increasing DC-bias field to 28.4kV/cm, the peak positions and their FWHM did not change while only intensity of some peaks changed irregularly, especially peaks around 600.9 and 784.6cm^{-1}. Now, we can not assign these Raman peaks to the corresponding phonon modes. Peak position means vibration energy and peak FWHM means damping of phonon. Thus, no change of peak position means that the microscopic symmetries before and after DC-bias exposure were the same, and no change of peak FWHM also indicates that the phonon damping states did not change by the DC-field exposure.

With decreasing DC-bias field from 28.4 to 0.04kV/cm, peak positions and their FWHM also did not change whereas only intensity of some peaks changed irregularly (Fig. 4). Therefore, the above result revealed that the microscopic symmetry of *3m* and phonon state, except for the intensity, did not change between the relaxor and the ferroelectric states.

Fig. 5 shows Raman scattering spectra measured in X(ZZ)$\overline{X}$ geometry under upward DC-bias field from 0 to 28.4kV/cm while Fig. 6 shows those measured under downward DC-bias field from 28.4 to 0.04kV/cm. If *3m* crystals is a single domain state, Raman scattering

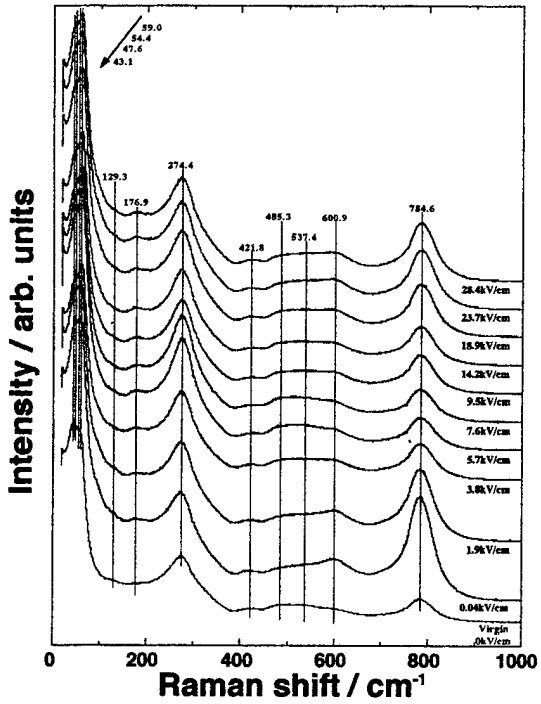

Fig. 3 Raman scattering spectra measured in X(NN)$\overline{X}$ geometry under upward DC-bias fields.

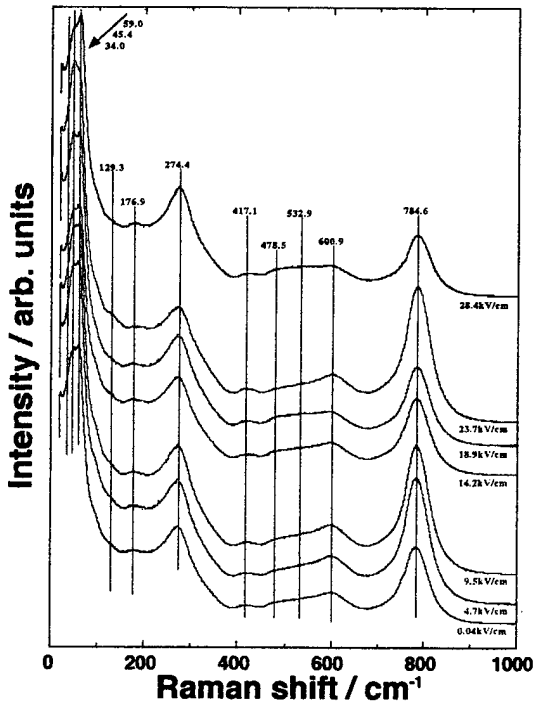

Fig. 4 Raman scattering spectra measured in X(NN)$\overline{X}$ geometry under downward DC-bias fields.

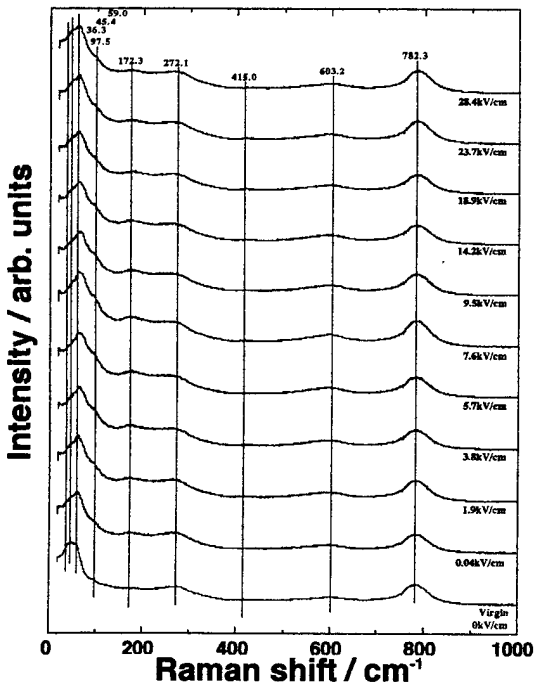

Fig. 5 Raman scattering spectra measured in X(ZZ)$\overline{X}$ geometry under upward DC-bias fields.

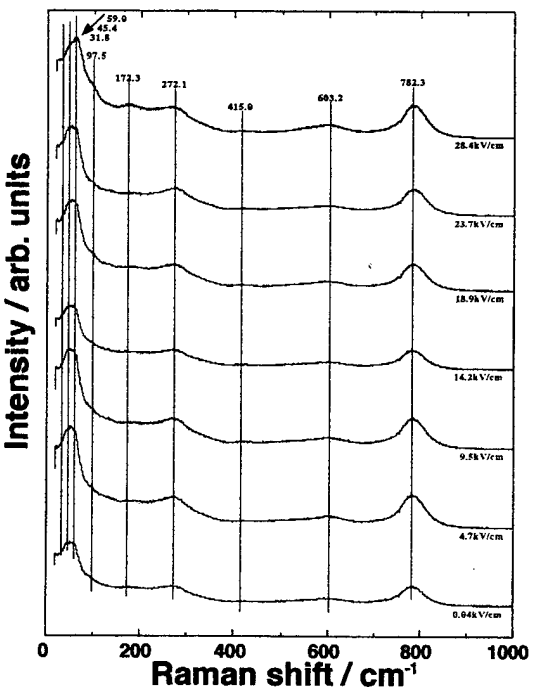

Fig. 6 Raman scattering spectra measured in X(ZZ)$\overline{X}$ geometry under downward DC-bias fields.

spectra measured in the X(ZZ)$\overline{X}$ geometry exhibit only mixed modes of A_1(TO) and A_1(LO). With increasing DC-bias field from 0 to 28.4kV/cm, no change in peak positions, their FWHM and intensity was observed (Fig. 5). Similarly, With decreasing DC-bias field from 28.4 to 0kV/cm, no change in peak positions, their FWHM and intensity was also observed (Fig. 6). A_1 modes are phonon modes vibrating along Z axis. This means that the phonon state along Z axis was not affected by DC-bias exposure. Therefore, about A_1 modes, there was no difference between the relaxor and ferroelectric states.

Fig. 7 shows Raman scattering spectra measured in X(ZY)$\overline{X}$ geometry under upward DC-bias field from 0 to 28.4kV/cm while Fig. 8 shows those measured under downward DC-bias field from 28.4 to 0.04kV/cm. If *3m* crystals is a single domain state, Raman scattering

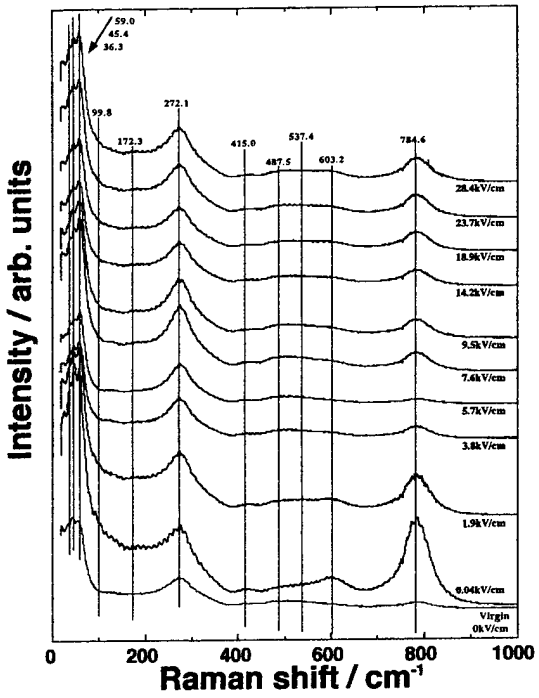

Fig. 7 Raman scattering spectra measured in X(ZY)$\overline{X}$ geometry under upward DC-bias fields.

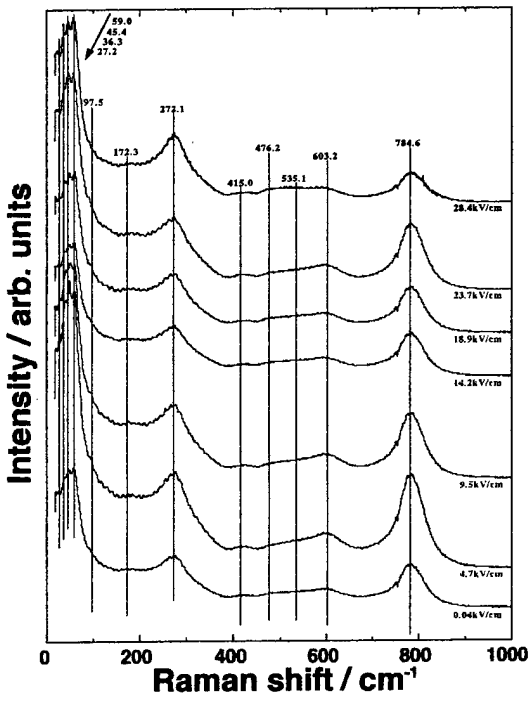

Fig. 8 Raman scattering spectra measured in X(ZY)$\overline{X}$ geometry under downward DC-bias fields.

spectra measured in the X(ZY)$\overline{X}$ geometry exhibit only mixed modes of E(TO) and E(LO). With increasing DC-bias field from 0 to 28.4kV/cm, the peak positions and their FWHM did not changed while only their intensity, especially the intensity of some peaks with higher frequencies, changed irregularly (Fig. 7). Moreover, with decreasing DC-bias field from 28.4 to 0kV/cm, the similar tendencies were observed (Fig. 8). E modes are phonon modes vibrating along X or Y axis. This result suggests that the irregular change of some peak intensity in Fig. 3 was originated from the change of peak intensity in E modes. However, all peak frequencies and their FWHM did not changed, which indicates that the microscopic symmetry and phonon damping were not affected by DC-bias exposure. At present, we can not explain the change of intensity in E modes. Perhaps, a contribution of the 109° domain wall motion to the phonon intensity by DC-bias exposure may be more significant along X or Y direction than along Z direction.

Raman scattering measurement of PZN crystals using DC-bias field revealed that its microscopic symmetry of *3m* and phonon damping did not change between the relaxor and ferroelectric states.

3.3 Change of macroscopic and microscopic symmetries by DC-bias field:

Table II shows the macroscopic and microscopic symmetries in virgin PZN crystal before DC-bias exposure. In the relaxor state with the optical isotropic property, its macroscopic symmetry was assigned to centrosymmetrical *m3m* while its microscopic symmetry was assigned to acentrosymmetrical *3m*, *i.e.*, a symmetry with a spontaneous polarization, as shown in Table II. This difference between two symmetries suggests that PZN crystal with the relaxor state had a disorder system in the structure.

On the other hand, in the PZN crystal with the ferroelectric domains, the both macroscopic and microscopic symmetries were assigned to acentrosymmetrical *3m*, *i.e.*, a symmetry with a spontaneous polarization, as shown in Table III. Thus, no difference between two symmetries indicates that in the ferroelectric state after the DC-bias exposure, there was no disorder system. Thus, this study revealed that for the relaxor state, the existence of the disorder system in the structure is an important factor. This supports the validity of some models using "flipping polar vector"[6-8] as the origin of relaxor behavior. It should be also noted that in the both states, *i.e.*, relaxor and ferroelectrics in PZN, their microscopic symmetries were assigned to same *3m*, and there was no difference between phonon

Time scale t / Spatial magnitude d	Dynamic t < 1 ns	Intermediate 1 ns < t < 10 μs	Quasi-static 10 μs < t
Microscopic d < 1~2 nm	***3m***		Transmittance Electron Microscopy
Mesoscopic 2 nm < d < 0.5 μm	Brillouin Scattering Spectroscopy		X-ray Diffraction Spectroscopy
Macroscopic 0.5 μm < d		Microwave Dielectric Spectroscopy	***m3m***

Table II Various symmetries in PZN crystals with the relaxor state before the DC-bias exposure.

Time scale t / Spatial magnitude d	Dynamic t < 1 ns	Intermediate 1 ns < t < 10 μs	Quasi-static 10 μs < t
Microscopic d < 1~2 nm	*3m*		Transmittance Electron Microscopy
Mesoscopic 2 nm < d < 0.5 μm	Brillouin Scattering Spectroscopy		X-ray Diffraction Spectroscopy
Macroscopic 0.5 μm < d		Microwave Dielectric Spectroscopy	*3m*

Table III Various symmetries in PZN crystals with the ferroelectric state after the DC-bias exposure.

damping states. In $BaTiO_3$ single-domain crystal, it was known that just above Tc of 133°C, phonon damping increased remarkably, which suggested a coupling between phonon frequency and flipping frequency of polar vector[12]. On the other hand, in PZN crystal, phonon damping was almost same between relaxor and ferroelectric states. This means that the origin of relaxor behavior is "flipping polar vector" in PMR.

Therefore, to clarify relaxor behavior, it is important to investigate other symmetries with intermediate time scale and/or mesoscopic spatial magnitude under DC-bias field. Our next strategy is to study a symmetry with dynamic time scale (t < 1nsec) and mesoscopic spatial magnitude (2nm < d < 0.5μm). This symmetry can be measured by a Brillouin scattering spectroscopy under DC-bias field. We expect that in this symmetry, some difference will be obtained between the relaxor and ferroelectric states.

4. CONCLUSION

Using pure PZN single crystal, two kinds of symmetries were measured by a polarized microscope and a Raman scattering spectroscopy under DC-bias field. In the relaxor state, its macroscopic symmetry on the basis of domain observation was assigned to the highest symmetry *m3m*. However, DC-bias exposure to PZN crystal with the relaxor state induced the ferroelectric domains. This domain configuration was analyzed crystallographically, and its macroscopic symmetry was assigned to acentrosymmetric *3m*. On the other hand, Raman scattering spectra exhibited no change under between relaxor and ferroelectric states. Thus, their microscopic symmetries of acentrosymmetric *3m* did not changed in the both states. These results revealed that for the relaxor state, the existence of the disorder system in the structure is important. Moreover, this study also suggested that it is important to investigate a mesoscopic symmetry in order to obtain valuable informations about PMR.

5. ACKNOWLEDGEMENTS

The authors thank Mrs. Lei and Mr. Liu for great help with PZN crystal growth, and also thank Dr. Newnham, Dr. Fousek, Dr. Cao and Dr. Randall of MRL, PennState university for helpful discussion about domain configuration.

References

[1]V. A. Bokov and I. E. Myl'nikova, *Soviet Phys. Solid State*, **2**, 2428-31 (1961).
[2]N. P. Khuchua, V. F. Bova and I. E. Myl'nikova, *Soviet Phys. Solid State*, **10**, 194-5 (1968).
[3]Y. Yokomizo and S. Nomura, *J. Phys. Soc. Jpn.*, **28**, Supplement, 150-2 (1970).
[4]Y. Yokomizo, T. Takahashi and S. Nomura, *J. Phys. Soc. Jpn.*, **28**, 1278-84 (1970).
[5]S. Nomura, M. Endo and F. Kojima, *Jpn. J. Appl. Phys.*, **13**, 2004-8 (1974).
[6]L. E. Cross, *Ferroelectrics*, **76**, 241-67 (1987).
[7]D. Viehland, S. J. Jang and L. E. Cross, *J. Appl. Phys.*, **68**, 2916-21 (1990).
[8]W. Kleemann, *Int. J. Mod. Phys. B*, **7**, 2469-507 (1993).
[9]A. E. Glazounov and A. K. Tagantsev, *Ferroelectrics*, **221**, 57-66 (1998).
[10]M. A. Akbas and P. K. Davies, *J. Am. Ceram. Soc.*, **80**, 2933-6 (1997).
[11]P. K. Davies and M. A. Akbas, *Ferroelectrics*, **221**, 27-36 (1998).
[12]S. Wada, T. Suzuki, M. Osada, M. Kakihana and T. Noma, *Jpn. J. Appl. Phys.*, **37**, 5385-93 (1998).
[13]S.-E. Park, M. L. Mulvihill, G. Risch and T. R. Shrout, *Jpn. J. Appl. Phys.*, **36**, 1154-8 (1997).
[14]S. Wada, S.-E. Park, L.E. Cross and T. R. Shrout, *J. Korean Phys. Soc.*, **32**, S1290-3 (1998).
[15]S. Wada, S.-E. Park, L.E. Cross and T. R. Shrout, *Ferroelectrics*, **221**, 147-55 (1999).
[16]S. Wada, S. Suzuki, T. Noma, T. Suzuki, M. Osada, M. Kakihana, S.-E. Park, L.E. Cross and T. R. Shrout, *Jpn. J. Appl. Phys.*, **38**, 5505-11 (1999).
[17]E.E. Wahlmstrom, *Optical Crystallography* (John Wiley and Sons, New York, 1979) 5th ed. Chap. 10.
[18]J. Fousek, *Czech. J. Phys.*, **B21**, 955-68 (1979).
[19]J.F. Nye, Physical Properties of Crystals (Oxford Science, Oxford, 1985) Appendix B.

APPENDIX 15

Transactions of the Materials Research Society of Japan 25 [1] 281-284 (2000)

Dipolar Behavior in PZN Relaxor Single Crystals under Bias Field

Satoshi Wada, Takaaki Tsurumi, Seung-Eek Park*, L. Eric Cross* and Thomas R. Shrout*
Department of Metallurgy & Ceramics Science, Tokyo Institute of Technology,
2-12-1 Ookayama, Meguro-ku, Tokyo 152-8552, JAPAN
Fax: 81-3-5734-2514, e-mail: swada@ceram.titech.ac.jp
*Materials Research Laboratory, The Pennsylvania State University, University Park, PA 16802-4801, U.S.A.
Fax: 1-814-865-2326, e-mail: sxp37@psu.edu

Pure $Pb(Zn_{1/3}Nb_{2/3})O_3$ (=PZN) single crystal is the typical relaxor ferroelectrics with an optical isotropic property. However, PZN crystals with defects showed a defect-induced domain configuration with very small birefringence. This birefringence decreased drastically around 120°C and this decrease suggested the change of the polar state in polar micro regions (PMR) at 120°C under a weak stress-field. Moreover, polarization and strain behaviors showed normal ferroelectric hysteresis below 120°C and double hysteresis loop above 120°C. This difference suggested that there was a transition around 120°C between relaxor states under no electric(E)-field and ferroelectric domains under a high E-field. The temperature dependence of dielectric constant in as-grown PZN crystal showed a strong frequency dependence. On the other hand, the dielectric property in the PZN crystal poled at 20°C showed no frequency dependence below 110°C while the strong frequency dependence reappeared above 110°C. The above results revealed that under bias fields such as stress and E-fields, all anomalous changes were observed around 110~120°C, while under no bias field, there was no change around 120°C. We concluded that the significant change around 110~120°C observed under bias fields was a kind of transition between flipping and frozen polar directions in PMR.
Key word: PZN single crystal, defect-induced domain, polar micro regions, relaxer behavior, bias field

1. INTRODUCTION

PZN single crystal is the typical relaxor ferroelectrics with a maximum dielectric constant around 140°C, and has an optical isotropic property[1-5]. Many researchers have considered that PMR is the origin of the relaxor behavior with an optical isotropic state[5-9]. Therefore, PMR is the most important factor in the relaxor behavior. At present, there are some models about PMR state, *i.e.*, (i) superparaelectric model[6], (ii) dipolar and spin glass model[7], (iii) dipolar dielectric with random field model[8] and (iv) breathing model[9]. First three models are on the basis of flipping polar vector in PMR, whereas the last model is on the basis of fixed polar vector. Therefore, it is important to understand PMR, but the polar state in PMR has been still unclear. Previously, it was considered that chemically ordered domains (COD) observed by TEM might be PMR, but Akbas and Devis[10-11] revealed that COD did not relate with the relaxor behavior.

Nomura *et al.* reported that a DC-bias exposure on an optical isotropic PZN crystals induced a ferroelectric state with normal ferroelectric domains[5]. However, in PZN single crystal with the inhomogeneous defect structure, a domain-like configuration with very low birefringence was observed clearly under crossed-nicols, as shown in Fig. 1[12]. This domain-like pattern was investigated crystallographically, and it was clarified that this pattern was due to the polar vector ordered by a weak stress-field originated from the physical defects[12]. We called this pattern a "defect-induced domain configuration". The study on the defect-induced domain possibly gives important information on relaxor mechanism in PZN crystals because the defect-induced domain involves the direct information on PMR.

Our final objective is to elucidate the relaxor behavior in PZN crystals and its origin. In this study, we investigated the defect-induced domain, dielectric properties, polarization and strain as a function of temperature and bias field.

2. EXPERIMENTAL

PZN single crystals were grown by a conventional flux method using a PbO flux. Further details on the crystal growth were reported elsewhere[13]. These crystals were oriented along [111] direction using a back reflection Laue method. For *in-situ* domain observation from -100°C to 200°C, thin crystals with thickness of around 50 μm and two mirror-polished (111) surfaces were prepared. Domain configuration was observed under crossed-nicols at transmittance configuration using a polarizing microscope (Carl Zeiss, D-7082). Prior to the domain observation, all crystals were annealed at 250°C for 15hr in air in order to remove ferroelastic domains. On the other hand, samples with a size around 2x2x0.2 mm^3 were prepared for the measurements of dielectric constant and polarization.

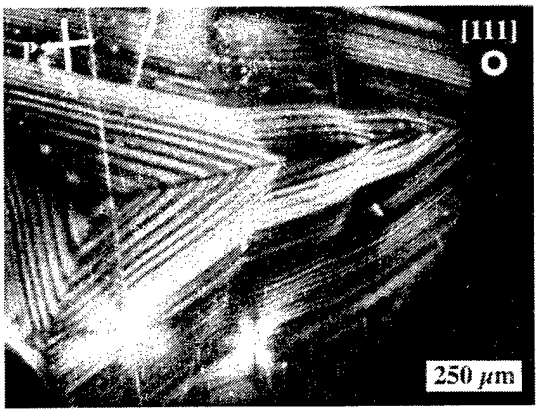

Fig. 1 Domain configuration of PZN single crystal oriented along [111].

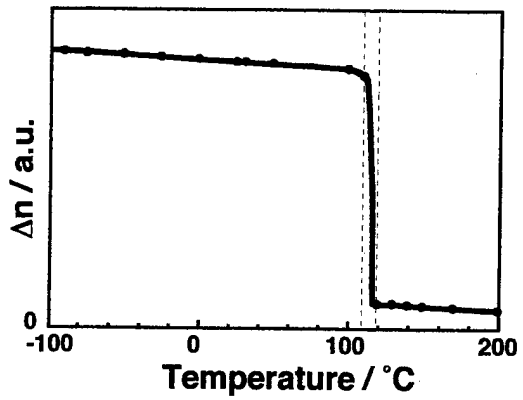

Fig. 2 Temperature dependence of birefringence Δn in the defect-induced domain.

Dielectric properties were measured using a multifrequency LCR meter (HP4274A and HP4275A) while polarization and strain were measured at 0.2Hz using a modified Sawyer-Tower circuit and a linear variable differential transducer (LVDT).

3. RESULTS AND DISCUSSION

3.1 Temperature dependence of the defect-induced domain configuration:

In-situ domain observation was done at temperatures from -100°C to 200°C. Between -100°C and 110°C, the domain configuration did not changed while its birefringence slightly increased with decreasing temperature. This slight increase of the birefringence suggests an increase of spontaneous polarization. On the other hand, a drastic decrease of the birefringence was observed between 110°C and 120°C, as shown in Fig. 2, although the domain configuration was still observed even at 200°C[12]. Pure PZN crystal has a strong frequency dependence of dielectric property. Yokomizo and Nomura[3] reported that the temperature at maximum dielectric constant (T_{max}) extrapolated to the zero frequency was estimated to be about 120°C. This temperature was corresponded to the change of birefringence in this study. Previously, we reported that the origin of the defect-induced domain was assigned to the ordered PMR, in which the polar directions in PMR were ordered by the weak stress-field, in the disordering PMR matrix with the randomly oriented polar vectors[12]. Therefore, this significant birefringence change around 120°C means the change of polar states in the ordered PMR. Crystallographically, the birefringence is proportional to the magnitude of crystal anisotropy. Thus, as the origin of the change of birefringence, the following factors would be considered, *i.e.*, (1) the change of spontaneous polarization, (2) the volume change of the ordered PMR, and (3) the change of flipping behavior in the ordered PMR.

3.2 Temperature dependence of polarization and strain:

To investigate the origin of the above drastic change of the birefringence around 120°C, both polarization and strain were measured, as shown in Figs. 3 and 4. Fig. 3(a) shows a normal ferroelectric hysteresis loop at 25°C. This is because although PZN crystal was a relaxor before E-field exposure, the poled PZN crystal changed to a normal ferroelectrics with ferroelectric domains[12]. In Figs. 3(a)-(c), with increasing temperature from 25°C to 110°C, the spontaneous polarization decreased slightly while the coercive field decreased significantly. Around 120°C, polarization curve became to a double hysteresis loop (Fig. 3(d)). The appearance of double hysteresis means that ferroelectric domains induced by E-field did not exist stably at 120°C, and disappeared easily by the removal of E-field, *i.e.*, polar directions ordered along applied E-field changed to polar directions randomly oriented between eight equivalent <111> directions without E-field. On the contrary, below 120°C, the ferroelectric domains induced by E-field existed stably despite the removal of E-field. We consider that this difference is originated from the difference of the thermal fluctuation between below and above 120°C. In other words, below 120°C, the polar directions ordered by E-field were frozen

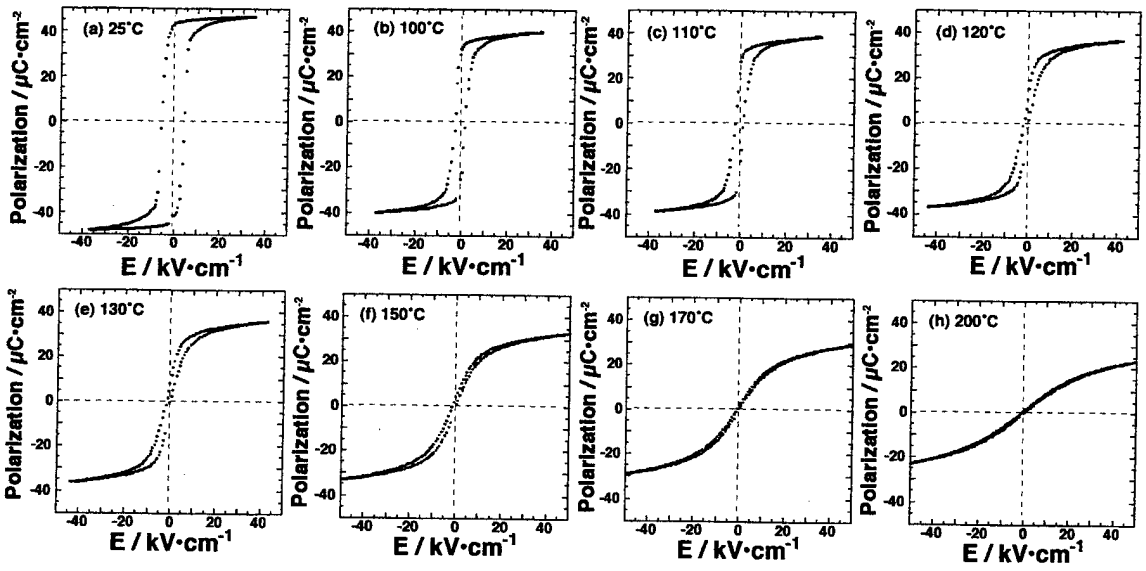

Fig. 3 Temperature dependence of polarization in PZN single crystal measured at 0.2Hz using a triangle wave function.

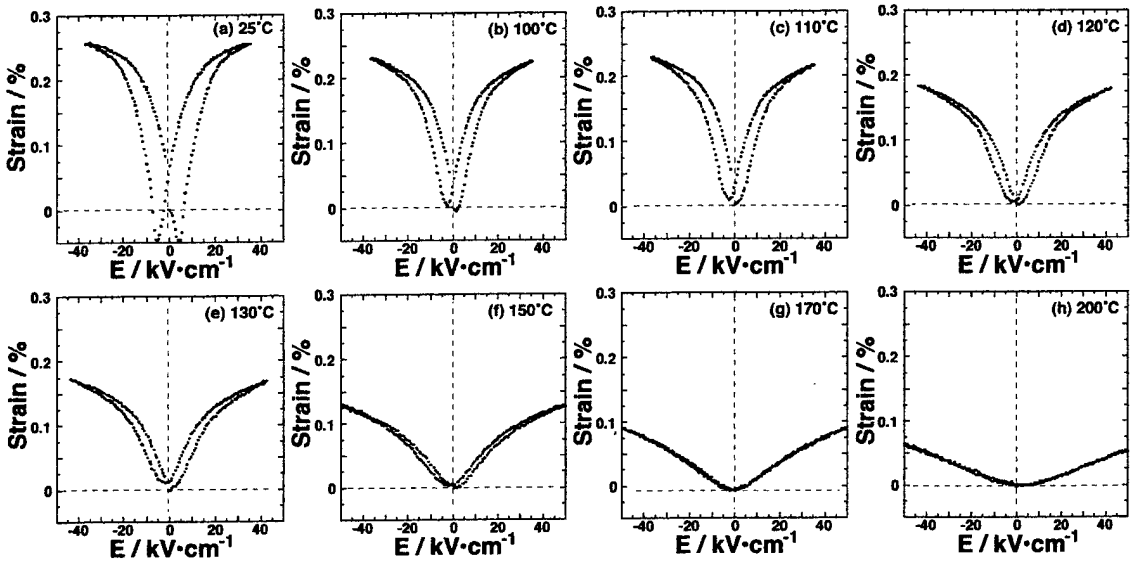

Fig. 4 Temperature dependence of strain in PZN single crystal measured at 0.2Hz using a triangle wave function.

without bias, whereas above 120°C, the polar vector ordered by E-field flipped between eight equivalent polar directions by the thermal fluctuation without E-field. This result supported the "superparaelectric model" proposed by Cross[6]. Above 170°C, hysteresis behavior disappeared completely (Fig. 3(g)), and with increasing temperature from 170°C to 200°C, "*S*" curves approached to linear. The polar state of PMR above 170°C was almost similar to that observed in pure $Pb(Mg_{1/3}Nb_{2/3})O_3$ (PMN) around room temperature[6]. These results were corresponded to *in-situ* domain observation of PZN crystals under AC-bias field reported by Mulvihill[14].

The strain behavior as a function of E-field shows almost the same behavior as that of the polarization. The strain behavior at 25°C (Fig. 4(a)) looks like normal ferroelectric one characterized by the domain reorientation. Below 110°C, hysteresis due to domain reorientation was also observed in Figs. 4(a)-(c). However, above 120°C (Figs. 4(d)-(h)), all strain curves indicated zero strain at the zero E-field. However, from 120°C to 150°C, the hysteresis behavior was observed clearly under high E-field. This observation suggests that above zero E-field, the ferroelectric domain structure was induced, and also supports the prediction from Fig. 3 that around 120°C, the ferroelectric domains were induced by electric-field. Above 170°C, no hysteresis was observed (Figs. 4(g)-(h)) and this is almost similar to the electrostrictive strain behavior[6]. This also means that there was no domain reorientation above 170°C.

The polarization and strain behaviors revealed that around 120°C, the polar vector in PMR is flipping between eight equivalent <111> directions without E-field, whereas under E-field, its polar direction is oriented along the applied E-field directions. Moreover, it should be noted that although the spontaneous polarization decreased with increasing temperature, there was no drastic decrease around 120°C in their spontaneous polarization. This means that the origin of the change of birefringence around 120°C was not assigned to the change of spontaneous polarization. The observation of the E-field induced transition between relaxor and ferroelectrics around 120°C suggests that the change of the birefringence around 120°C is originated from the change of flipping behavior of polar vector in the PMR.

3.3 Temperature dependence of dielectric properties:

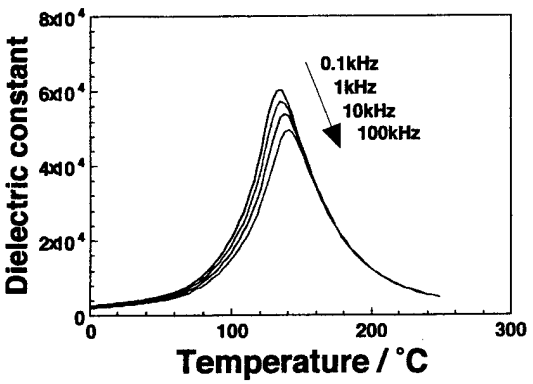

Fig. 5 Temperature dependence of dielectric constant in as-grown PZN single crystal.

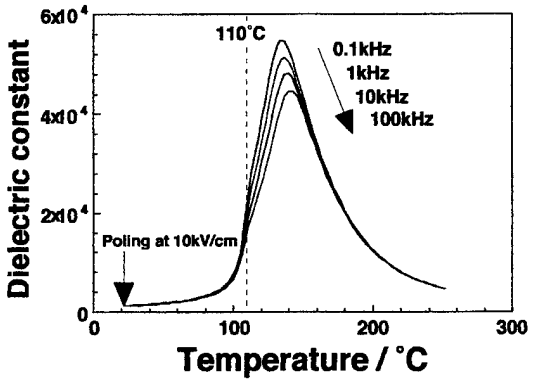

Fig. 6 Temperature dependence of dielectric constant in PZN single crystal poled at 20°C.

Fig. 5 shows temperature dependence of dielectric constant for the as-grown PZN single crystal along [111]. Dielectric constant and T_{max} measured at 100Hz was around 60000 and 134°C, respectively, and T_{max} shifted to higher temperatures with increasing frequency, whereas dielectric constant also decreased at the same way as that of T_{max}[13]. Moreover, it should be noted that the PZN crystal with the defect-induced domain exhibited almost the same dielectric properties with those in Yokomizo's isotropic PZN[3-4]. The optical isotropic PZN crystals showed no anomalous change around 120°C in dielectric properties. The difference between two PZN crystals is the existence of stress-field.

The observation of the defect-induced domain using a polarized microscope directly indicated the existence of PMR with the polar vector frozen by a weak stress-field. The temperature dependence of the birefringence showed that the polar state in PMR changed remarkably around 120°C, whereas the defect-induced domain was still remained at 200°C. On the contrary, the polarization and strain behaviors in the PZN crystal with the defect-induced domain exhibited that above 120°C, most of PMR had the flipping polar vector under no E-field, and a contribution of PMR with the frozen polar vector was not observed (Figs. 3 and 4). These results suggested that a volume fraction of PMR with the fixed polar direction was a little. Thus, the similar dielectric properties in between two kinds of PZN crystals were explained by the above reason.

Fig. 6 shows temperature dependence of dielectric constant measured using the PZN crystal poled at 20°C. Although PZN crystal was relaxor before E-field exposure, PZN crystal after E-field exposure was normal ferroelectrics with domain structure[12]. In Fig. 6, below 110°C, no frequency dependence in dielectric constants was observed, whereas above 110°C, the normal frequency dependence was observed. This indicates that around 110°C, the ferroelectric state changed to the relaxor state, and also supports that around 110~120°C, the fixed polar vector changed to the flipping polar vector.

3.4 Dipolar behavior in PZN crystals under bias field:
The temperature dependences of properties measured under stress-field (Fig. 2) and E-field (Figs. 3, 4 and 6) revealed an anomalous change around 110~120°C. Especially, under a weak stress-field, the anomalous change was the transition between the fixed polar vector and the flipping one in PMR around 120°C while under strong E-field, the anomalous changes was the transition between ferroelectric one and relaxor state around 110~120°C. On the other hand, in the optical isotropic PZN crystal without any bias field[3] and the PZN crystal with a weak stress-field (Fig. 5), there was no anomalous change around 120°C for their dielectric properties. These results suggested that a dipolar behavior under bias field is completely different from that under no bias field. In Fig. 6, below 110°C, there was no frequency dependence of dielectric constants, whereas in Fig. 5, below 110°C, the strong frequency dependence was observed. This difference may be caused by a difference of dipolar behavior, *i.e.*, the fixed polar direction under bias field and the flipping polar direction under no bias field. This means that the origin of relaxor behavior is the flipping polar direction in PMR. Ohwa *et al.*[15] measured the temperature dependence of Raman scattering using PZN crystals, and reported that Raman spectra did not change significantly from 25°C to 200°C. Wada *et al.* measured E-field dependence of Raman scattering in PZN crystals, and also reported that Raman spectra did not change in the both relaxor and ferroelectric states[16]. These results indicated that in the phonon frequency region of GHz~THz order, there is no difference between relaxor and ferroelectric states. This suggests that the flipping frequency of polar vector is much slower than phonon frequency. To clear flipping frequency for relaxor behavior, more study is required.

4. CONCLUSION

Using the PZN crystal with the defect-induced domain, its temperature dependence was investigated. As a result, its birefringence decreased significantly around 120°C and this decrease suggested the change of the polar state under a weak stress-field, *i.e.*, a transition between the fixed and flipping polar directions in PMR. Their polarization and strain behaviors also showed the transition between ferroelectric state and relaxor one around 120°C under a high E-field. In the PZN crystal poled at 20°C, its dielectric properties showed no frequency dependence of dielectric constants below 110°C and the strong frequency dependence reappeared above 110°C. These results showed that under some bias fields, the polar state in PMR changed around 120°C. We concluded that the change around 110~120°C was the transition between flipping and frozen polar directions in PMR.

5. ACKNOWLEDGEMENTS

The authors thank Mrs. Lei and Mr. Liu for great help with PZN crystal growth, and also thank Dr. Newnham, Dr. Fousek, Dr. Cao and Dr. Randall of MRL, PennState university for helpful discussion about domain configuration.

References

[1]V. A. Bokov and I. E. Myl'nikova, *Soviet Phys. Solid State*, **2**, 2428-31 (1961).
[2]N. P. Khuchua, V. F. Bova and I. E. Myl'nikova, *Soviet Phys. Solid State*, **10**, 194-5 (1968).
[3]Y. Yokomizo and S. Nomura, *J. Phys. Soc. Jpn.*, **28**, Supplement, 150-2 (1970).
[4]Y. Yokomizo, T. Takahashi and S. Nomura, *J. Phys. Soc. Jpn.*, **28**, 1278-84 (1970).
[5]S. Nomura, M. Endo and F. Kojima, *Jpn. J. Appl. Phys.*, **13**, 2004-8 (1974).
[6]L. E. Cross, *Ferroelectrics*, **76**, 241-67 (1987).
[7]D. Viehland, S. J. Jang and L. E. Cross, *J. Appl. Phys.*, **68**, 2916-21 (1990).
[8]W. Kleemann, *Int. J. Mod. Phys. B*, **7**, 2469-507 (1993).
[9]A. E. Glazounov and A. K. Tagantsev, *Ferroelectrics*, **221**, 57-66 (1998).
[10]M. A. Akbas and P. K. Davies, *J. Am. Ceram. Soc.*, **80**, 2933-6 (1997).
[11]P. K. Davies and M. A. Akbas, *Ferroelectrics*, **221**, 27-36 (1998).
[12]S. Wada, S.-E. Park, L. E. Cross and T. R. Shrout, *Trans. Mater. Res. Sci. Jpn.*, **24**, 19-22 (1999).
[13]S.-E. Park, M. L. Mulvihill, G. Risch and T. R. Shrout, *Jpn. J. Appl. Phys.*, **36**, 1154-8 (1997).
[14]M. L. Mulvihill, *A Doctor Thesis in Pennsylvania State University*, (1996) p.187-205.
[15]H. Ohwa, M. Iwata, N. Yasuda and Y. Ishibashi, *Jpn. J. Appl. Phys.*, **37**, 5410-2 (1998).
[16]S. Wada, T. Tsurumi, M. Osada, M. Kakihana, S.-E. Park, L. E. Cross and T. R. Shrout, *Trans. Mater. Res. Sci. Jpn.* (2000) in press.

(Received December 16,1999 ; Accepted January 31,2000)

APPENDIX 16

Switching Current In $Pb(Zn_{1/3}Nb_{2/3})0_3$ –$PbTiO_3$ Single Crystals

Uma Belegundu, Xiaohong Du and Kenji Uchino
International Center for Actuators Transducers
Materials Research Laboratory, Pennsylvania State University
University Park PA 16803, USA

Abstract: Switching current measurements have been carried out on relaxor ferroelectric single crystal - pure PZN, and the solid solution (1-x) $Pb(Zn_{1/3}Nb_{2/3})O_3$ - x $PbTiO_3$ with x= 0.04, 0.09, 0.10. Measurements have been done for crystallographic directions [001] and [111] for all these compositions. Switching times versus the applied field showed the following results. Pure PZN along [111] and 0.90PZN – 0.10PT along [001], and [111] showed an exponential dependence. Along [001] the PZN showed a linear fit. For solid solution single crystals- 0.96PZN -0.04PT and 0.91PZN – 0.09PT, a linear fit was obtained for the reciprocal switch times versus applied field for both the directions. If we draw a parallel picture with the reported barium titanate data, it appears that the polarization reversal is controlled by nucleation along [111]- spontaneous direction for PZN and [001], [111] for 0.90PZN – 0.10PT. The mobility of the reversed domains controls the reversal along [001] for PZN and the solid solution single crystals with rhombohedral composition along [001] and [111]. The transient current curves showed two maximum points for crystals with x = 0.04 and 0.09. This is attributed to the co-existence of the two phases in 0.96PZN -0.04PT and 0.91PZN – 0.09PT crystals.

INTRODUCTION

Measurement of switching current to study the polarization reversal phenomena[1] is well known. In this method, a series of symmetric bipolar voltage pulse which produces polarization reversal is applied to the crystal and the transient current measured across a resistor connected in series with the sample. Information on polarization reversal processes was obtained by switching current measurements for $BaTiO_3$ (BT)[2,3]. These measurements for BT showed that the total polarization reversal time depends on the applied field.

Such transient current studies have not been carried out on relaxor ferroelectric single crystals such as $Pb(Zn_{1/3}Nb_{2/3})0_3$ (PZN) and their solid solutions with $PbTiO_3$ (PT). In this paper, the experimental results of switching current measurements for PZN, PZN – PT single crystals and their dependence on crystal orientation are presented. Their switching behavior is examined in terms of the presently accepted model of domain nucleation and growth.

Single crystals of 0.91PZN- 0.09PT are known to show very high values of electromechanical coupling factor k_{33} of 92-95 % and piezoelectric constant d_{33} of 2500 pC/N[4,5]. In this system, PZN having rhombohedral symmetry is a relaxor ferroelectric material which undergoes a diffuse phase (frequency dependent) transition around 140°C. On the other hand lead titanate PT having a tetragonal symmetry is a normal ferroelectric with a sharp phase transition at 490°C. These two composition form a solid solution system with a morphotropic phase boundary (MPB) around 0.91PZN-0.09PT. It has to be mentioned that the giant values of k_{33} and d_{33} are obtained for crystals with rhombohedral composition with spontaneous polarization along [111] is poled along [001]. This direction is the spontaneous polarization direction for tetragonal crystals.

EXPERIMENTAL DETAILS

All the single crystals PZN and (1-x)PZN- xPT used for the measurements were grown the lab by the flux method. The crystal direction [001] and [111] were determined by Laue back reflection method. The crystals were then cut and polished to form rectangular plates with the desired orientation perpendicular to major faces. The thickness of all the samples varied from 0.20 mm – 0.23 mm and the area was around 4mm x 1.3mm. Sputtered gold was used as electrodes. A function synthesizer (DF –194 digital function synthesizer) in conjunction with an amplifier was used to apply rectangular pulses of one second duration to the sample. A resistor of 150 ohms was used in series with the sample and voltage across it was measured using oscilloscope for determining the switching current. A representative switching current obtained when a positive pulse is applied to the sample is shown in Fig. 1. The normal displacement current transient obtained when the second positive pulse is applied is also shown in the same figure. This

Mat. Res. Soc. Symp. Proc. Vol. 604 © 2000 Materials Research Society

displacement current is subtracted to obtain the actual switching current. The fields applied ranged from 3-36 kV/cm. The switching time is defined here as the time taken for the current to reduce from maximum to 1/10 of the maximum. The field was applied along [001] and [111] crystallographic directions. All these crystals have rhombohedral compositions. The spontaneous polarization for rhombohedral composition is along [111] and that for tetragonal is along [001] respectively.

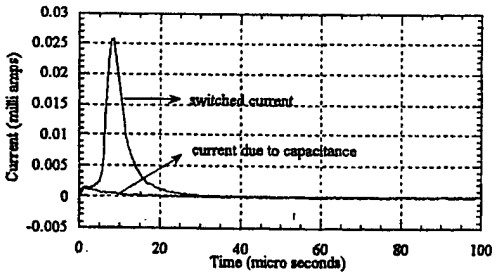

Fig.1 A representative switching and the corresponding displacement current. The two are subtracted to get the actual switching current.

RESULTS

Figure 2 shows the transient current associated with switching for PZN, 0.96PZN -0.04PT and 0.91PZN – 0.09PT single crystals. We will name them crystals A, B and C for discussion purposes. It has to be mentioned that the time scale for all the curves are not same, they vary from 2.5 millisecond (for low field) to 100 microsecond for high applied electric field. Hence no unit has been mentioned in the figure. These curves are overlapped only for comparison. However, each curve is considered separately for calculation of the switching time. Looking at this data for spontaneous polarization direction [111], the crystals B and C showed a double maximum in the switching current curve. For crystals B, having 0.04 PT at low field values (5 – 9 kV/cm) the first peak was much higher in magnitude than the second peak. As the field is increased, the second peak increases in magnitude and finally only one peak is observed. For crystals C having 0.09PT, similar variation of second peak overtaking the magnitude of the first peak was observed. However, two distinct peaks were present even at high fields. Such a behavior was not observed for pure PZN crystal with field along [111] direction. For field applied along [001] -the spontaneous polarization direction for tetragonal crystals, no such double maximum in the switching curve was observed for pure PZN (crystal A) and crystal B. The crystal C showed a double maximum at low field values. The curve corresponding to 26kV/cm for 0.91PZN – 0.09PT with field along [001] shows the field induced phase transition from rhombohedral to tetragonal.

This leads us to believe that the presence of two peaks is due to the co-existence of both rhombohedral and tetragonal phases in these crystals. It is difficult to associate a particular peak with either rhombohedral or tetragonal composition. The two parameters –the component of electric field along a crystallographic direction and the volume fraction of the second phase present may also need to be considered in explaining the presence of the double peaks. More detailed work is continuing and will be reported shortly.

The reciprocal switching time as a function of applied field is shown in Fig. 3. For pure PZN (crystal A), linear dependence was observed along [001] and exponential dependence along [111] direction. The figure shows a linear variation with different slopes at low and high field values for the crystals B, C and both the directions [111] and [001]. It appears that a linear law can describe the switching process

$$\frac{1}{t} = \frac{\mu}{d} E \qquad (1)$$

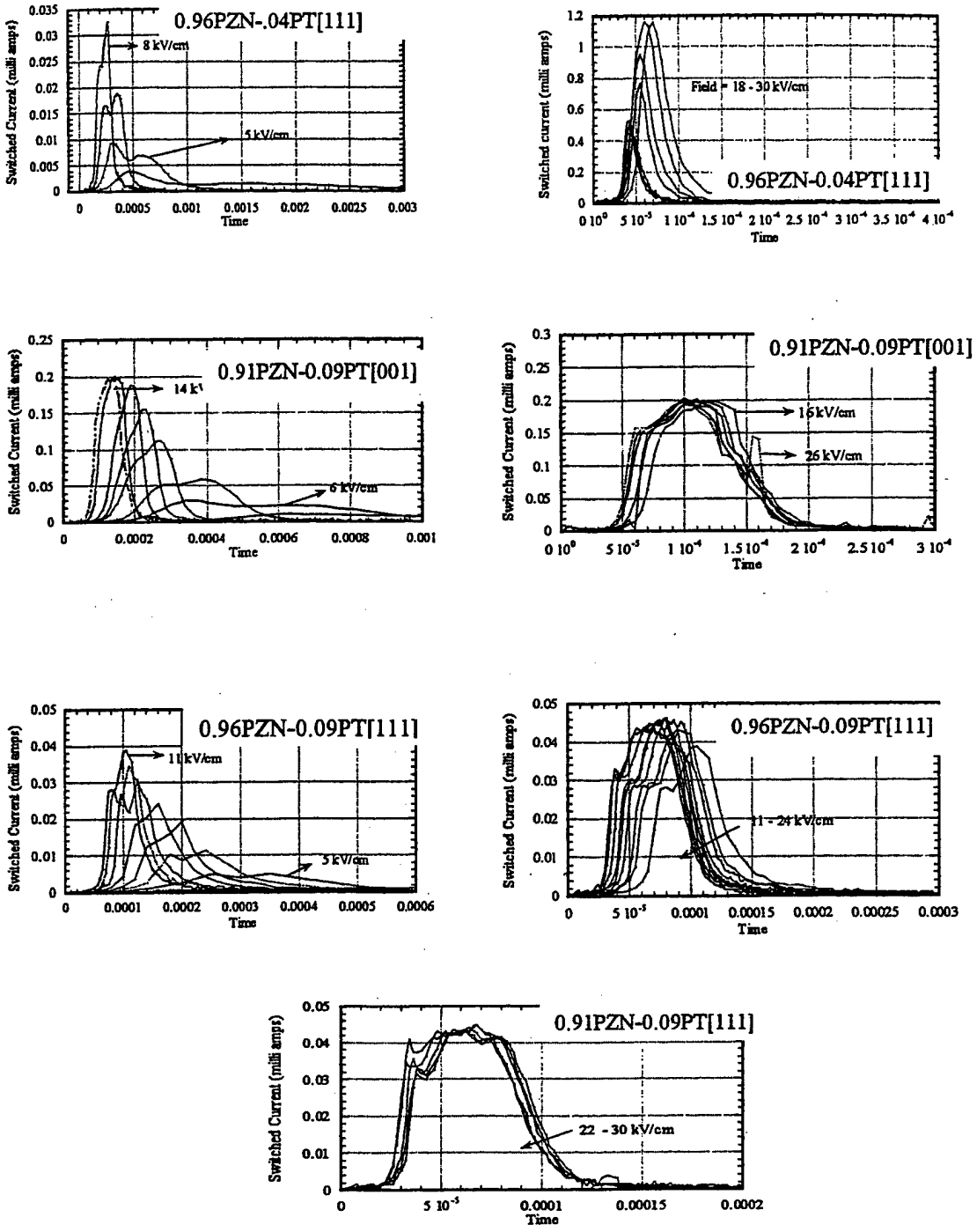

Fig.2 The switching current observed for the PZN –PT single crystals showing the double peak observed due to co-existence of both rhombohedral and tetragonal phases.

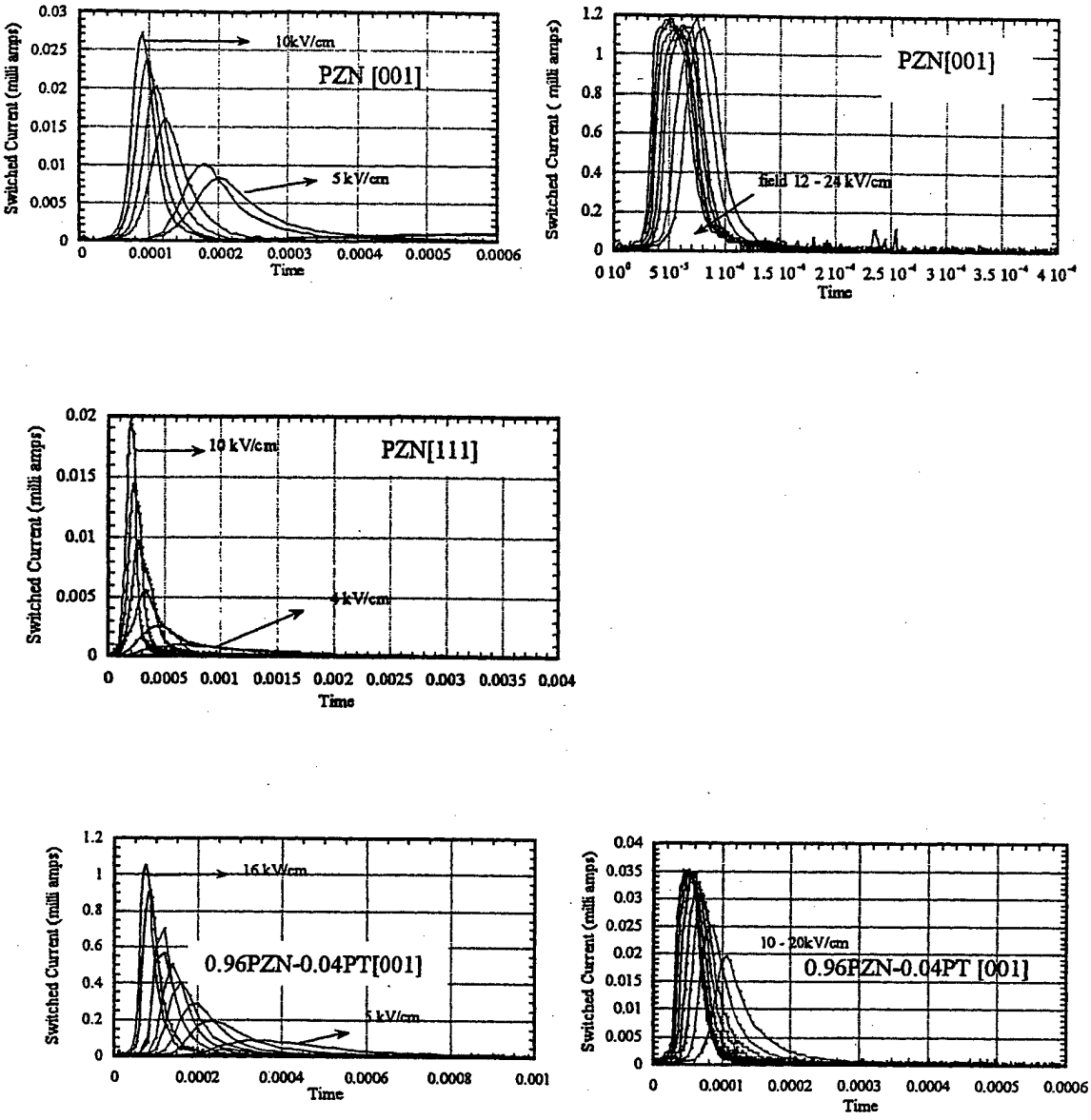

Fig. 2 The switching current observed for the PZN –PT single crystals showing the double peak observed due to co-existence of both rhombohedral and tetragonal phases.

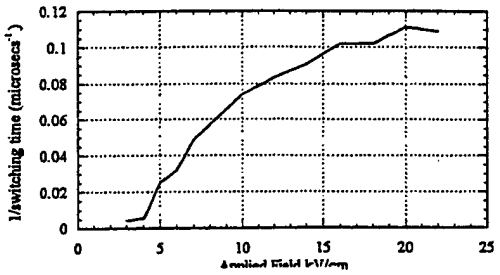

PZN [001]

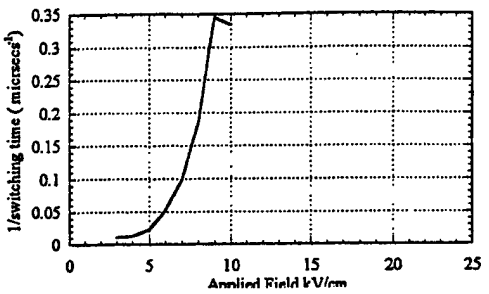

PZN [111]

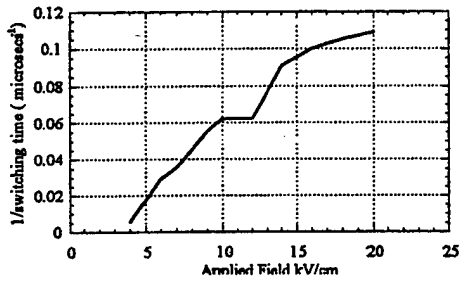

0.96PZN –0.04 PT [001]

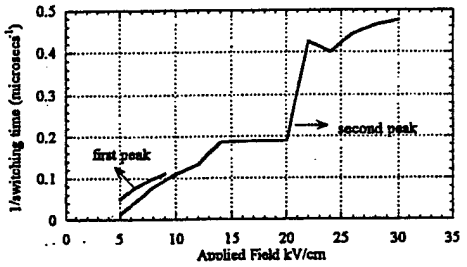

0.96PZN –0.04 PT [111]

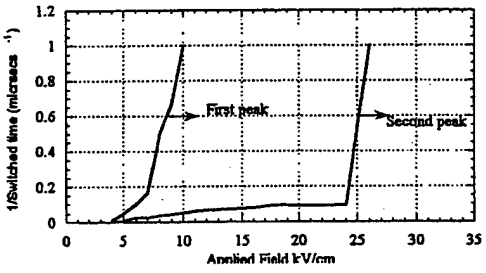

0.91PZN-0.09PT [001]

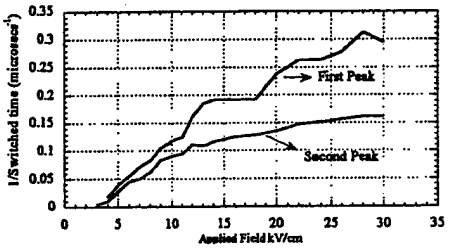

0.91PZN-0.09PT [111]

Fig.3 Dependence of inverse switching time on applied field for PZN –PT single crystals showing the linear or exponential dependence.

where t is the switching time, d the thickness of the crystal, μ is the mobility of the moving domain wall, E is the applied field. However, there is a change in the slope at a certain applied field for all the crystals. At higher fields, the curve becomes almost horizontal to field axis.

DISCUSSION

From the published data[2,3,6,7] for $BaTiO_3$ (BT), the switching current shows an exponential dependence on applied field at small field values. The dependence becomes linear as the applied field is increased. On the basis of these results, it was suggested that the polarization reversal for BT at small-applied fields is controlled by nucleation rate of the reversed domains. At higher field, the mobility of the reversed domains controls the reversal mechanism.

We now compare this with the present data for relaxor based single crystals of PZN, 0.96PZN - 0.04PT and 0.91PZN – 0.09PT. The field was applied along [001] and [111] – the spontaneous direction for rhombohedral and tetragonal compositions.

For PZN along [111] the dependence of switching time on applied field was exponential. Along [001], the dependence was linear. If we draw a parallel picture with the barium titanate data, it appears that the polarization reversal is controlled by nucleation along [111] and the mobility of the reversed domains along [001].

For solid solution single crystals 0.96PZN -0.04PT and 0.91PZN – 0.09PT, a piecewise linear fit was obtained for the reciprocal switch times versus applied field. Unlike the barium titanate, no exponential dependence was observed at small field values. Assuming the model of domain nucleation and motion, it appears that the polarization reversal in these crystals is controlled by the forward motion of the domains.

A double maximum observed in the switched current is attributed to the co-existence of the two phases in 0.96PZN -0.04PT and 0.91PZN – 0.09PT crystals. This was not observed in PZN crystal.

ACKNOWLEDGEMENT

This work is supported by Office of Naval Research through contract # N00014-91-J-4145

REFERENCES

1) F. Jona and G. Shirane, "Ferroelectric Crystals" Dover Publications Inc.p172 (1993)
2) W. J. Merz, Phys. Rev., v 95, p690 (1954)
3) R. C. Miller and A. Savage, Phys. Rev., v 112, p755 (1958)
4) J. Kuwata, K. Uchino and S. Nomura, Ferroelectrics, v 37, p579 (1981)
5) S. E. Park and T. R. Shrout, J. Mater, Res. Innovations vol.1, p20 (1997)
6) W. J. Merz, J.Appl. Phys. v 27, p938 (1956)
7) H. L. Stadler, J. Appl. Phys. v29, p1485 (1958)

APPENDIX 17

Phase transitional behavior and piezoelectric properties of the orthorhombic phase of $Pb(Mg_{1/3}Nb_{2/3})O_3$–$PbTiO_3$ single crystals

Yu Lu, D.-Y. Jeong, Z.-Y. Cheng, and Q. M. Zhang[a)]
Materials Research Laboratory, The Pennsylvania State University, University Park, Pennsylvania 16802

Hao-Su Luo and Zhi-Wen Yin
Laboratory of Functional Inorganic Materials, Shanghai Institute of Ceramics, Chinese Academy of Science, Shanghai, China

D. Viehland
Naval Seacommand, Division Newport, Newport, Rhode Island 02841

(Received 21 December 2000; accepted for publication 24 March 2001)

We report on the observation of an orthorhombic ferroelectric phase in $0.67Pb(Mg_{1/3}Nb_{2/3})O_3$ $-0.33PbTiO_3$ single crystals, whose polarization is along ⟨011⟩ direction and stability can be altered by poling conditions. We studied the piezoelectric properties on poled ⟨011⟩ crystals, in both monodomain and polydomain states, and found that the piezoelectric d_{32} coefficient, which is the piezoelectric response in perpendicular to the poling direction, is positive in both cases. Based on the phenomenological theory, we show that this is possible in a crystal with the electrostrictive coefficients $Q_{11}>Q_{44}-Q_{12}$. © *2001 American Institute of Physics.* [DOI: 10.1063/1.1372360]

We report in this letter on the phase transition behavior and piezoelectric responses of $Pb(Mg_{1/3}Nb_{2/3})O_3$–$PbTiO_3$ (PMN–PT) single crystals, for compositions close to the morphotropic phase boundary (MPB) between rhombohedral ferroelectric (FE_r) and tetragonal ferroelectric (FE_t) phases. Recent discoveries in mixed B-site cation ferroelectric perovskites have stimulated significant research activities.[1–4] In $Pb(Zn_{1/3}Nb_{2/3})O_3$–$PbTiO_3$ (PZN–PT) and PMN–PT single crystals, an electromechanical coupling factor of greater than 0.9 has been reported in the FE_r phase near the MPB for specimens poled along ⟨001⟩.[1–3] Similar enhancements in the electromechanical properties were also reported when crystals were poled at finite angles with respect to the spontaneous polarization direction, although the coupling factors of these finite miss-oriented crystals were lower (~0.8).[5–7]

Naturally, a question to ask is what is unique about the PZN–PT and PMN–PT crystalline solutions and the role of the MPB. In 0.92PZN–0.08PT crystals (which at $T=25\,°C$ is in the FE_r phase and near a MPB), recent investigations have demonstrated the presence of monoclinic domains, and orthorhombic ferroelectric (FE_o) and monoclinic ferroelectric (FE_m) states.[8–10] This opens an interesting possibility that those states, even metastable, may be regarded as intermediate states and responsible for the high piezoelectric and electromechanical responses in PZN–PT and PMN–PT single crystals near the MPB.

In $Pb(Zr_{1-x}Ti_x)O_3$, which is another related ferroelectric perovskite material, high electromechanical properties have been widely studied over many years for compositions close to the MPB between FE_r and FE_t phases.[11] Much effort has been expended in determining the mechanism responsible for these significant enhancements. Recently, a FE_m state has been reported over a very narrow composition range near MPB. In this FE_m state, the polarization was confined to the ⟨*hhk*⟩ plane, which is one of the planes that can "bridge" the tetragonal ⟨001⟩ and rhombohedral ⟨111⟩ directions.[4,12] It was suggested that this "bridging" effect, via the FE_m state, is responsible for the enhanced electromechanical properties.[12]

This investigation reports the phase transition behavior and piezoelectric responses in PMN–PT single crystals of approximate compositions of 0.67PMN–0.33PT, which are close to the MPB. Dielectric and piezoelectric methods have been used to study crystals with various poling histories. We have observed, by dielectric and optical microscopy techniques, an intermediate FE_o state whose phase stability depends upon its poling history and mechanical condition. In addition, it was observed that this monodomain FE_o does not exhibit enhanced piezoelectricity and its piezoelectricity can be described quite well by the phenomenological theory.[13,14]

Crystals were grown by the Bridgman method.[15] Various crystals were oriented along the ⟨001⟩, ⟨110⟩, and ⟨111⟩ directions. Typical specimen dimensions were $2\times2\times2\,mm^3$. Crystals were poled at room temperature, with monodomain conditions achieved in both ⟨111⟩ and ⟨110⟩ oriented crystals. Dielectric characterization (at 1 kHz) was carried out using a standard LCR meter (HP4284A) equipped with a temperature chamber (Delta 9023). Piezoelectric coefficients were measured at 1 kHz using a laser dilatometer.[16] Domain patterns were characterized by a Zeiss Axioskop cross-polarized optical microscope (100× amplification).

Figures 1(a)–1(d) show the dielectric constant and loss as functions of temperature for poled ⟨111⟩, ⟨011⟩($E_{poling}>5\,kV/cm$), ⟨011⟩($E_{poling}=4\,kV/cm$), and ⟨001⟩ oriented PMN–PT crystals, respectively. It is important to emphasize that the difference between Figs. 1(b) and 1(c) (which are both for ⟨011⟩ orientations) is only the poling field (E_{poling}). Each figure exhibited a transition at 145 °C which is the FE_t to cubic transformation,[17,18] and a second dielectric anomaly at ~80 °C. For ⟨111⟩ and ⟨011⟩($E_{poling}<4\,kV/cm$)

a)Electronic mail: qxz1@psu.edu

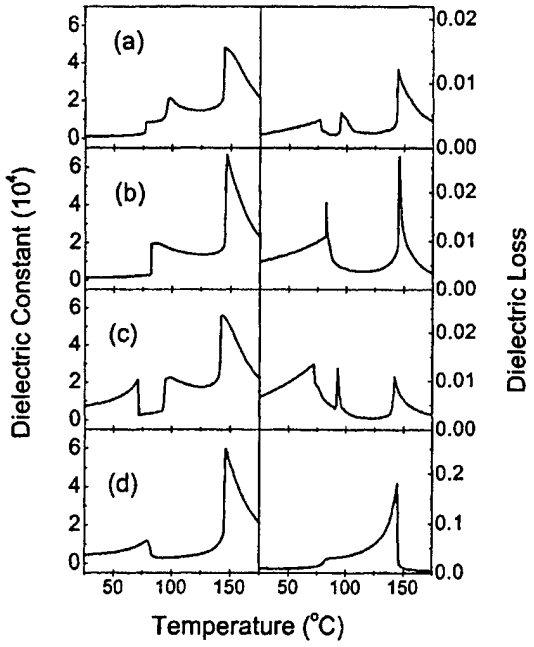

FIG. 1. The dielectric constant and dielectric loss measured at 1 kHz as functions of temperature for 0.67PMN–0.33PT single crystals (a) poled and measured along the [111] direction (monodomain rhombohedral phase); (b) poled and measured along [011] (monodomain orthorhombic phase); (c) poled along [011] direction to form ⟨111⟩ twined crystal and measured along [011]; and (d) poled and measured along [001] (polydomain crystal).

orientations, an additional third anomaly was found at ~100 °C.

For ⟨011⟩-oriented crystals poled at $E_{poling}<4$ kV/cm, optical microscopy revealed the presence of a polydomain condition with domains oriented along the ⟨111⟩, typical of that of a FE_r state. These domain orientations are schematically illustrated in Fig. 2(a). However, for $E_{poling}>5$ kV/cm, ⟨011⟩-oriented crystals were observed under cross-polarized light to be in a monodomain state with the polarization along the ⟨011⟩. This domain orientation is schematically illustrated in Fig. 2(b). It should be mentioned that even small variations in the PT content resulted in deviations from this monodomain condition and the disappearance of the FE_o state at 25 °C, demonstrating that this state only exists over a narrow composition range near the MPB. Accordingly, at room temperature most of the crystals poled along ⟨011⟩ were polydomain and FE_r.

The differences in the dielectric responses of the ⟨011⟩

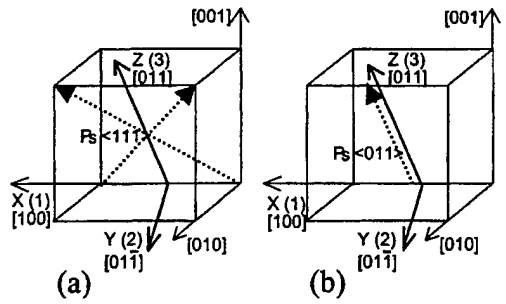

FIG. 2. Schematic drawings for [011] poled crystals in (a) twined crystals and (b) monodomain crystals. The dashed arrows indicate the remanent polarization direction and orthorhombic coordinate system used to describe the piezoelectric coefficients is also presented.

TABLE I. Piezoelectric coefficients of 0.67PMN–0.33PT single crystals poled along [011] direction at room temperature.

	d_{33} (pm/V)	d_{32} (pm/V)	d_{31} (pm/V)	$\epsilon_{33}^{(o)}/\epsilon_0$[a]
Monodomain	250	40	−220	880
Polydomain (experimental)	1780	1100	−2740	
Polydomain (calculated)	1770	980	−2760	

[a] ϵ_0 is the vacuum permittivity.

crystals due to the various poling histories can be explained on the basis of these optical microscopy observations. For $E_{poling}<4$ kV/cm [Fig. 1(c)], the FE_r state is stable at room temperature. Upon heating to ~80 °C, a transition occurs to a FE_o state. On further increase of temperature to ~100 °C, a secondary transformation to a FE_t state occurred. In contrast, for $E_{poling}>5$ kV/cm [Fig. 1(b)], a monodomain FE_o state can be induced at room temperature. Upon heating to 80 °C, a transition occurs to a FE_t state. Interestingly, the FE_o–FE_t transition temperature in the monodomain condition was significantly lower (80 °C) than in the polydomain condition (100 °C). Clearly, the phase transformational pathway is altered by whether the specimen is elastically constrained (polydomain) or free to deform (monodomain).[9]

The dielectric constant for the poled ⟨111⟩ crystals [Fig. 1(a)] exhibited a similar transition sequence as the polydomain ⟨011⟩ [Fig. 1(c)]. In both cases, the FE_r to FE_t transition proceeded through an intermediate FE_o state, with the FE_o state being present for $\sim 80<T<100$ °C. The dielectric constant for poled ⟨001⟩ crystals was shown in Fig. 1(d). Only one FE–FE transition was observed, which occurred at 80 °C. This transition temperature is close to that of the FE_o–FE_t along the ⟨011⟩ ($E_{poling}>5$ kV/cm, monodomain), and with that of the FE_r–FE_o along the ⟨111⟩ and ⟨011⟩ ($E_{poling}<4$ kV/cm, polydomain).

The results in Fig. 1 demonstrate a complex transformation sequence that is dependent upon orientation and electrical history. An intermediate FE_o state exists between the FE_r and FE_t ones, whose temperature range of existence varies, suggesting metastability. Furthermore, these results indicate that the margin of stability in the FE_r, FE_o, and FE_t states may all be sufficiently fragile that changes in orientation, electrical history, or mechanical constraints may change the free energy balance. The reason why ceramic specimens have not revealed a FE_o state in the last 20 years[17,18] may then reflect the fact that under all circumstances the polarization is elastically constrained, preventing strain accommodation.

To determine the influence of monodomain versus polydomain conditions upon the electromechanical properties of ⟨011⟩ oriented crystals, the piezoelectric coefficients (d_{33}, d_{31}, and d_{32}) were measured. The results are given in Table I. First, the values of all coefficients were much lower in the monodomain FE_o state than the polydomain FE_r one. The results were a little unusual in that $d_{32}>0$ for both the mono and polydomain conditions, and also in that $|d_{31}|>|d_{33}|$ for the polydomain condition.

In order to explain the observed piezoelectric properties in poled ⟨011⟩ crystals in both the poly and monodomain states, we derived expressions for the piezoelectric coeffi-

cients from phenomenological theory.[13,14] Along the ⟨011⟩ in the monodomain condition, the piezoelectric responses were found to be

$$d_{33}^{(o)}=\sqrt{2}(Q_{11}+Q_{12}+Q_{44})\epsilon_{33}^{(o)}P_r^{(o)},$$
$$d_{32}^{(o)}=\sqrt{2}(Q_{11}+Q_{12}-Q_{44})\epsilon_{33}^{(o)}P_r^{(o)}, \quad (1)$$
$$d_{31}^{(o)}=2\sqrt{2}Q_{12}\epsilon_{33}^{(o)}P_r^{(o)},$$

where the superscript (o) stands for properties that are referenced with respect to the coordinate system of the FE_o state (see Fig. 2), $\epsilon_{33}^{(o)}$ is the dielectric permittivity of the FE_o state, $P_r^{(o)}$ is the remanent polarization of the FE_o state (0.39 C/m^2),[9] and Q_{11}, Q_{12}, and Q_{44} are the electrostrictive coefficients (in the pseudocubic coordinates) expressed in matrix notation. For ferroelectric perovskites, it is known that $Q_{11}>0$, $Q_{44}>0$, $Q_{12}<0$, and $|Q_{11}|>2|Q_{12}|$.[13] Therefore, under the condition that $Q_{11}>Q_{44}-Q_{12}$, Eq. (1) predicts that $d_{32}^{(o)}$ is positive. Using Eq. (1) and the data in Table I, the values of the electrostrictive coefficients can be estimated: $Q_{11}=0.06\,m^4/C^2$, $Q_{12}=-0.025\,m^4/C^2$, and $Q_{44}=0.024\,m^4/C^2$, respectively.

For the ⟨011⟩-oriented FE_r polydomain state, assuming that there are [111] and $[\bar{1}11]$ domains only, the piezoelectric coefficients were derived as

$$\begin{aligned}
d_{33}^{(o)}&=\sqrt{2}/3[(Q_{11}+Q_{44})(\epsilon_{11}^{(R)}+2\epsilon_{33}^{(R)})\\
&\quad+Q_{12}(4\epsilon_{33}^{(R)}-\epsilon_{11}^{(R)})]P_r^{(R)},\\
&\approx\sqrt{2}/3(Q_{11}+Q_{44}-Q_{12})\epsilon_{11}^{(R)}P_r^{(R)},\\
d_{32}^{(o)}&=\sqrt{2}/3[(Q_{11}-Q_{44})(\epsilon_{11}^{(R)}+2\epsilon_{33}^{(R)})\\
&\quad+Q_{12}(4\epsilon_{33}^{(R)}-\epsilon_{11}^{(R)})]P_r^{(R)},\\
&\approx\sqrt{2}/3(Q_{11}-Q_{44}-Q_{12})\epsilon_{11}^{(R)}P_r^{(R)},\\
d_{31}^{(o)}&=2\sqrt{2}/3[Q_{11}(\epsilon_{33}^{(R)}-\epsilon_{11}^{(R)})+Q_{12}(2\epsilon_{33}^{(R)}+\epsilon_{11}^{(R)})]P_r^{(R)},\\
&\approx 2\sqrt{2}/3(-Q_{11}+Q_{12})\epsilon_{11}^{(R)}P_r^{(R)},
\end{aligned} \quad (2)$$

where $\epsilon_{33}^{(R)}$ and $\epsilon_{11}^{(R)}$ are the dielectric permittivity measured in the FE_r state along and perpendicular to the [111] polarization direction, respectively, and $P_r^{(R)}$ is the remanent polarization of the rhombohedral phase ($\sim$0.39 C/m^2).[9] In the second part of each relationship in Eq. (2), we have made use of the fact that $\epsilon_{11}^{(R)}\gg\epsilon_{33}^{(R)}$. The values of $d_{33}^{(o)}$, $d_{33}^{(o)}$, and $d_{33}^{(o)}$ for the FE_r polydomain condition can be estimated by placing the values of the electrostriction coefficients estimated in the proceeding paragraph into Eq. (2). These calculated values for the piezoelectric coefficients are given in Table I where $\epsilon_{11}^{(R)}/\epsilon_0=10\,000$ is used. Inspection of the data in the table reveals remarkable agreement, in particular in consideration of the use of a single crystalline single domain phenomenological approach to the properties of polydomain conditions.

This work was supported by the Office of Naval Research.

[1] J. Kuwata, K. Uchino, and S. Nomura, Jpn. J. Appl. Phys., Part 1 **21**, 1298 (1982).
[2] S. Park and T. R. Shrout, J. Appl. Phys. **82**, 1804 (1997).
[3] S. Park and T. Shrout, IEEE Trans. Ultrason. Ferroelectr. Freq. Control **44**, 1140 (1997).
[4] B. Noheda, D. E. Cox, G. Shirane, J. Gonzalo, L. Cross, and S. Park, Appl. Phys. Lett. **74**, 2059 (1999).
[5] K. Nakamura and Y. Kawamura, in *1999 IEEE Ultrasonics Symposium Proceedings*, edited by S. C. Schneider, M. Levy, and B. R. McAvoy (IEEE, New York, 1999), pp. 1013–1018.
[6] S. Park, S. Wada, L. Cross, and T. Shrout, J. Appl. Phys. **86**, 2746 (1999).
[7] X.-H. Du, J. Zheng, U. Belegundu, and K. Uchino, Appl. Phys. Lett. **72**, 2421 (1998).
[8] M. K. Durbin, J. C. Hicks, S. Park, and T. Shrout, J. Appl. Phys. **87**, 8159 (2000).
[9] D. Viehland, J. Appl. Phys. **88**, 4794 (2000).
[10] B. Noheda, D. Cox, G. Shirane, S. Park, L. E. Cross, and Z. Zhong (unpublished).
[11] B. Jaffe, W. Cook, Jr., and H. Jaffe, *Piezoelectric Ceramics* (Academic, New York, 1971), Chap. 7.
[12] R. Guo, L. Cross, S. Park, B. Noheda, D. Cox, and G. Shirane, Phys. Rev. Lett. **84**, 5423 (2000).
[13] A. F. Devonshire, Philos. Mag. **3**, 85 (1954).
[14] F. Jona and G. Shirane, *Ferroelectric Crystals* (Dover, New York, 1993), Chap. IV.
[15] Z. Yin, H. Luo, P. Wang, and G. Xu, Ferroelectrics **229**, 207 (1999).
[16] Q. M. Zhang, W. Pan, and L. Cross, J. Appl. Phys. **63**, 2492 (1988).
[17] S. W. Choi, T. Shrout, S. Jang, and A. Bhalla, Ferroelectrics **100**, 29 (1989).
[18] O. Noblanc, P. Gaucher, and G. Calvarin, J. Appl. Phys. **79**, 4291 (1996).

APPENDIX 18

Jpn. J. Appl. Phys. Vol. 39 (2000) pp. 141–145
Part 1, No. 1, January 2000

Linear Electro-optic Effect of $0.88Pb(Zn_{1/3}Nb_{2/3})O_3$–$0.12PbTiO_3$ Single Crystal

Yu LU, Zhong-Yang CHENG, Seung-Eek PARK, Shi-Fang LIU and Qiming ZHANG*
Materials Research Laboratory and Department of Electrical Engineering, The Pennsylvania State University, University Park, PA 16802, USA

(Received August 23, 1999; accepted for publication October 14, 1999)

The linear electro-optic (E-O) coefficients of poled $0.88Pb(Zn_{1/3}Nb_{2/3})O_3$–$0.12PbTiO_3$ single crystal were characterized using an automated scanning Mach-Zehnder interferometer and the senarmont compensator method at room temperature. They were obtained at a wavelength of 632.8 nm: $r_{33} = 134$ pm/V, $r_{13} = 7$ pm/V, $r_{51} = 462$ pm/V, and $r_c = 131$ pm/V respectively and the refractive indices: $n_e = 2.57$ and $n_o = 2.46$. The large r_{51} coefficient compared with r_{33} is caused by the high dielectric constant at perpendicular to the polar-axis compared with the dielectric constant along the c-axis. Comparison with the quadratic E-O coefficients measured at near and above the Curie temperature suggests that the values of the quadratic E-O coefficients measured earlier may be smaller than the intrinsic ones due to the influence of micro-polar regions. The development of an automated scanning Mach-Zehnder interferometer, which is less susceptible to the errors caused by the laser intensity fluctuation and drafting in the optical path length in the system, is also described.

KEYWORDS: ferroelectric, electro-optic, refractive index, interferometer

1. Introduction

Ferroelectric crystals, such as $LiNbO_3$ and KH_2PO_4 (KDP), are widely used in electro-optic (E-O) devices such as electro-optic modulators, electro-optic switches, and light valves.[1,2] More recently, there is an increased interest in the relaxor ferroelectric crystal $Pb(Zn_{1/3}Nb_{2/3})O_3$–$PbTiO_3$ (PZN–PT), which over a broad composition range possesses a very high electromechanical coupling factor, piezoelectric coefficients, and field induced strain response.[3–7] A uniqueness of this crystal system is that relatively high quality single crystals can be grown at compositions near the tetragonal-rhombohedral morphotropic phase boundary (MPB). It is well known that many of the material responses exhibit increased activity near a MPB.[8,9] In this paper, we report the result of the linear E-O coefficients in 0.88PZN–0.12PT single crystal, which is near the MPB on the tetragonal side.[3,5]

The E-O effect describes the change of refractive index Δn_{ij} due to the applied field:

$$\Delta n_{ij} = -\frac{1}{2} n_{ij}^3 \left(\sum_{j=1}^{3} r_{ijk} E_k + \sum_{j,k=1}^{3} R_{ijkl} E_k E_l \right) \quad (1)$$

where r_{ijk} and R_{ijkl} are linear and quadratic E-O coefficients, respectively. The quadratic coefficients for PZN–PT crystals at temperatures near and above the dielectric constant maximum have been characterized earlier, and in this paper all three non-zero linear E-O coefficients ($r_{33} = r_{333}$, $r_{13} = r_{113}$, and $r_{51} = r_{311}$) were measured for 0.88PZN–0.12PT in the ferroelectric tetragonal phase (room temperature).[10] The comparison of the two results, indicates that the coefficients measured at the high temperature phase may be affected by the relaxor ferroelectric nature of the PZN–PT system, and will be discussed in the paper. In addition, we will also report briefly a modified interferometric method for the characterization of these coefficients, which is based on the dynamic scanning concept.

*To whom correspondence should be addressed. E-mail: qxz1@psu.edu

2. Experimental

2.1 *0.88PZN–0.12PT single crystal and related E-O coefficients*

The 0.88PZN–0.12PT crystal used in this study was grown using the high temperature flux method.[5,6,11] It is known that 0.88PZN–0.12PT has a tetragonal structure at room temperature and that the spontaneous polarization is along ⟨001⟩ (c-axis) direction.[3–5] The single crystal sample was oriented along the ⟨001⟩ direction using a Laue camera, then the ⟨100⟩ faces were polished to optical quality. The sample was poled at a temperature of 230°C, which is much higher than the paraelectric to ferroelectric phase transition temperature, with an electric field of 5 kV/cm for 30 min. Then, the sample was slowly cooled down to room temperature under the electric field. It was found that poling at room temperature resulted in fractures in the sample since the domain switch induces very large strain, expansion along the poling direction. The dimension of the sample is $1.85 \times 3.85 \times 4.83$ mm^3 and the poling field was applied across the 3.85 mm thickness.

For the tetragonal symmetry, there are three non-zero E-O coefficients, i.e., r_{33}, r_{13}, and r_{51}. In this study, r_{33} and r_{13} were measured using a interferometric method, where the applied field E_3 is along the c-axis and the light passes through the sample along the ⟨100⟩ axis (a-axis),

$$\Delta n_e = -n_e^3 r_{33} E_3/2 \quad (2a)$$

$$\Delta n_o = -n_o^3 r_{13} E_3/2 \quad (2b)$$

where n_o and n_e denote the refractive index perpendicular and parallel to the c-axis, respectively. In the r_{33} measurement, the polarization direction of the laser beam is along the c-axis and in measuring r_{13}, the polarization direction is perpendicular to the c-axis.

For the PZN–PT crystal studied, the E_3 field will also induce a change in the sample thickness along the path of the laser beam due to the piezoelectric effect,[12]

$$\Delta l_1 = d_{31} E_3 l_1$$

where l_1 is the thickness of the crystal along the beam path and d_{31} is the piezoelectric coefficient. Hence, the total measured optical path length change in the interferometric method

is $\Delta n_i \cdot l_1 + (n_i - 1) \cdot \Delta l_1$.

The E-O coefficient $r_{51}(\Delta(1/n_{31}^2) = \Delta(1/n_5^2) = r_{51}E_1)$ was measured by the Senarmont compensator method, where the applied field E_1 is along the $\langle 010 \rangle$ axis perpendicular to both the c-axis and the light propagation direction.[13] The polarization direction of the laser beam is canted 45° with respect to the c-axis. In the r_{51} measurement, there is no correction due to the piezoelectric effect.

Using the Senarmont compensator method, the E-O coefficient r_c, which is defined as $r_c = r_{33} - n_o^3 r_{13}/n_e^3$ and determines the half-wave voltage of the material, was also measured.[13,14]

2.2 *Operation principle of scanning Mach-Zehnder interferometer for E-O coefficient measurement*

Shown in Fig. 1 is a typical Mach-Zehnder interferometer.[15] The interference pattern at the detection point depends on the optic path length difference ($\Phi = 2\pi(n_R l_R - n_S l_S)/\lambda$, where n and l are the refractive indices and the path lengths respectively, R and S in subscript expresses the reference and signal arms, respectively) between the signal and reference beams,

$$I = I_1 + I_2 + 2\sqrt{I_1 I_2}\cos(\Phi) = \frac{1}{2}(I_{max} + I_{min}) + \frac{1}{2}(I_{max} - I_{min})\cos(\Phi) \quad (3)$$

where $I_{max} = (\sqrt{I_1} + \sqrt{I_2})^2$ and $I_{min} = (\sqrt{I_1} - \sqrt{I_2})^2$ are the maximum and minimum intensities of interference fringes, respectively, and I_1 and I_2 are the light intensities of signal beam and reference beam, respectively. From eq. (3), one can find that when Φ has a small change ($\Delta\Phi$) around $\Phi_0 = (m + 1/2)\pi$, $m = 0, \pm 1, \ldots$, $\cos(\Phi_0 + \Delta\Phi) \approx \pm\Delta\Phi$, and the $\pm$ signs depend on the value of m, and

$$\Delta I = I - \frac{1}{2}(I_{max} + I_{min}) = \pm\frac{1}{2}(I_{max} - I_{min})\Delta\Phi. \quad (4)$$

Hence, by stabilizing the system at Φ_0 (working point), the change of interference intensity will depend linearly on the change of the optic path length. When this change is measured by a photo-detector, eq. (4) can be converted into the voltage form as:

$$\Delta\Phi = \frac{v_{out}}{(V_{max} - V_{min})/2} = \frac{v_{out}}{V_{p\text{-}p}/2}. \quad (5)$$

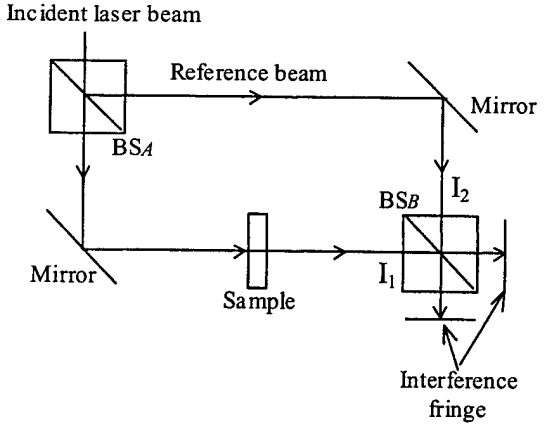

Fig. 1. Schematic drawing of a typical Mach-Zehnder interferometer.

Where v_{out} corresponds to ΔI, V_{max} and V_{min} correspond to I_{max} and I_{min} respectively and $\Delta\Phi = 2\pi\Delta(nl)/\lambda$. For E-O or piezoelectric coefficient measurement under an ac electric field of frequency (f_0), a lock-in amplifier can be used to measure v_{out} which yields a high sensitivity of the system in resolving the change in $\Delta\Phi$.

However, in developing a computer controlled experimental set-up to measure the change in the optic path length (and hence $\Delta\Phi$), we found that the approach of stabilizing the system near the working point (by using a feedback loop to control the path length of the reference arm) is not convenient. The change in the incident light intensity and other factors such as air turbulence in the system and the variation of the light absorption in the sample due to thermal and electric field can cause shift in the working point light intensity.[16] As a result, the stabilized experimental point will be no longer at Φ_0. Further more, those changes will also result in changes in I_{max} and I_{min}, causing errors in the experimental results on $\Delta(nl)$.

If instead of stabilizing the system at any specific point, an optic translation stage is used to drive a slow change in the path length l_R of the reference arm, Φ will be changed continuously. As a result, the interference intensity will change with time, from which I_{max} and I_{min} can be measured readily. If an AC electric field with a frequency f_0 is applied to a sample which causes a small change (much smaller than the wave length) in the optic path length in the signal arm, the change in the phase Φ will be $\Phi_{ref} + \Delta\Phi$. The resulting signal will be:

$$I = \frac{1}{2}(I_{max} + I_{min}) + \frac{1}{2}(I_{max} - I_{min})\cos(\Phi_{ref} + \Delta\Phi) \quad (6)$$

where Φ_{ref} describes the drifting in the phase caused by the optic path length change of the reference arm and also in the signal arm due to slow drifting, and $\Delta\Phi$ is the phase change caused by the sample due to the applied AC electric field. Since $\Delta\Phi$ is very small, one can get

$$I = \left(\frac{1}{2}(I_{max} + I_{min}) + \frac{1}{2}(I_{max} - I_{min})\cos\Phi_{ref}\right) - \left(\frac{1}{2}(I_{max} - I_{min})\sin\Phi_{ref}\right)\Delta\Phi. \quad (7)$$

Therefore, when $\Phi_{ref} = (m + 1/2)\pi$, eq. (7) is reduced to eq. (4). When $\Phi_{ref} = m\pi$, the second term on the right hand side of the equation is zero and the first term yields I_{max} and I_{min}. Thus, $V_{p\text{-}p}/2$ can be obtained. Hence, in one scanning period of the reference beam, all the quantities in eq. (5) can be determined and yield $\Delta\Phi$. Clearly, even if v_{out}, V_{max} and V_{min} may vary due to various noise sources, the corresponding variation in $\Delta\Phi$ which is the ratio between them [eq. (5)] will be much smaller. This has been verified experimentally. In addition, the data accuracy can be improved further by averaging $\Delta\Phi$ thus obtained over long time period.

Based on these considerations, a Mach-Zehnder interferometer with the reference arm scanned was developed to measure E-O or piezoelectric coefficients (as schematically shown in Fig. 2). In this scanning Mach-Zehnder interferometer, the reference mirror is driven by a servo-transducer made of piezoelectric material. In experiments for E-O or piezoelectric measurement, f_0 typically runs from 100 Hz to 100 kHz, and the corresponding scan frequency may be varied from 0.003 Hz to 3 Hz to satisfy the condition that the scanning fre-

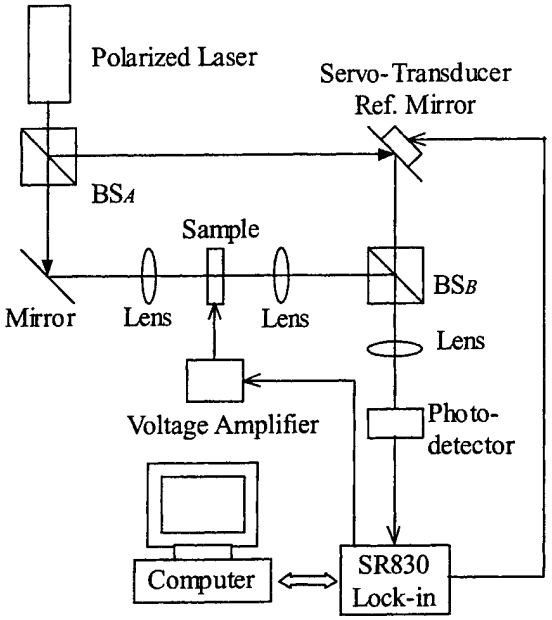

Fig. 2. Schematic drawing of the setup of the automated scanning Mach-Zehnder interferometer developed for E-O measurement.

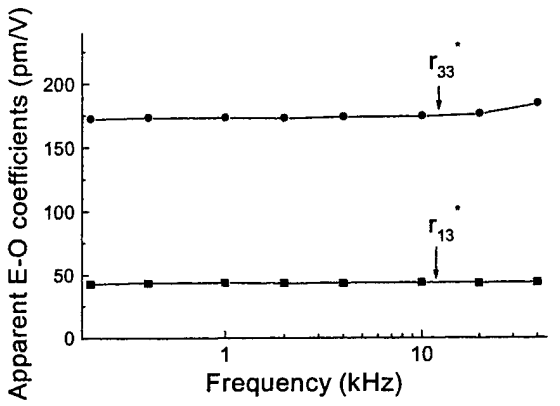

Fig. 3. Apparent E-O coefficients (r_{33}^* and r_{13}^*) measured at different frequencies for 0.88PZN–0.12PT single crystal at room temperature.

quency is much lower than the signal frequency. Both the AC and DC components of the photo-detector output are transmitted to a digital lock-in amplifier (SRS SR830). A computer is used to control the system and acquire the data from the SR830 through a GPIB cable. The system can be controlled easily by the computer over a long time period. The computer software was programmed using LabView 4.1.

3. Experiment Results and Discussion

3.1 Experimental results

For the 0.88PZN–0.12PT single crystal used in this experiment, no data of the refractive index at room temperature were available. Hence, the first step is to measure these indices. Although the refractive index can be measured by the minimum deviation method, the sample needs to be made into a wedge shape.[14,15] In order to measure the E-O coefficients, the sample has to be reshaped to a rectangular parallelepiped. Because of the relatively small size sample, instead, Brewster's angle method was used in which only one reflection surface is required.[14,15] Hence the sample used in the refractive index measurement can also be used directly in E-O measurement.

Brewster's angle (θ_B) is the incident angle at which the reflection intensity is zero for polarized light with the polarization direction parallel to the incident plane. The relationship between the refractive index and θ_B is: $n = \tan\theta_B$. By changing the orientation of the crystal with respect to the linearly polarized incident laser beam, both n_o and n_e can be determined. The obtained θ_B for the PZN–PT crystal are 68.75° and 67.84°, yielding $n_o = 2.57 \pm 0.01$ and $n_e = 2.46 \pm 0.01$ at 632.8 nm wavelength for the sample at room temperature.

To facilitate the discussion, apparent E-O coefficients r_{13}^* and r_{33}^* are introduced here to denote the coefficients obtained directly from $\Delta\Phi$ without the correction of the piezoelectric effect,

$$\Delta(n_e l) = \frac{\lambda}{2\pi}\Delta\Phi = r_{33}^* n_e^3 l E_3/2$$

or

$$\Delta(n_o l) = \frac{\lambda}{2\pi}\Delta\Phi = -r_{13}^* n_o^3 l E_3/2$$

The apparent E-O coefficients r_{13}^* and r_{33}^* are measured separately for the sample under a stress free condition. For a piezoelectric material, it is well known that there are serious resonance frequencies at which the electric field induced strain can no longer be described by the linear piezoelectric equation.[12] This certainly imposes frequency windows in which the E-O coefficient can be measured reliably. In addition, any mechanical resonance in the sample holding system can also cause error in the measurement. In this study, the frequency window used is from 200 Hz to 40 kHz, well below the first (lowest) resonance frequency (f_r) which is at several hundreds kHz. To ensure the weak field condition in the measurement, the applied field is about 15 V/cm which is also well below the room temperature coercive field of about 5 kV/cm.

The results for r_{13}^* and r_{33}^* are shown in Fig. 3. In the frequency range measured, there is no large change of the E-O coefficients with frequency and the average values of r_{13}^* and r_{33}^* are 44±1 pm/V and 173±4 pm/V, respectively. A mechanical resonance due to the sample holding system was observed at frequencies above 40 kHz, which affects the data acquired near 40 kHz.

To subtract the piezoelectric effect, the piezoelectric d_{31} coefficient was measured using a single beam laser interferometer: $d_{31} = -210 \pm 10$ pm/V. From $r_{33} = r_{33}^* + 2(n_e - 1)d_{31}/n_e^3$ and $r_{13} = r_{13}^* + 2(n_o - 1)d_{31}/n_o^3$, the E-O coefficients r_{33} and r_{13} are obtained: $r_{33} = 134 \pm 5$ pm/V and $r_{13} = 7 \pm 2$ pm/V at 632.8 nm wavelength for 0.88PZN–0.12PT at room temperature.

One of the concerns in the single crystal PZN–PT is the imperfect poling which results in residual domains in the sample. This will affect the measured E-O coefficients. In order to check this, the E-O coefficients under high DC bias field were measured. In the experiment, an oil chamber was built so that the sample can be immersed in an insulation oil which prevents electric breakdown through air when the sample is subject to a high DC voltage. Shown in Fig. 4 are the apparent E-O coefficients r_{13}^* and r_{33}^* measured at 1 kHz as a func-

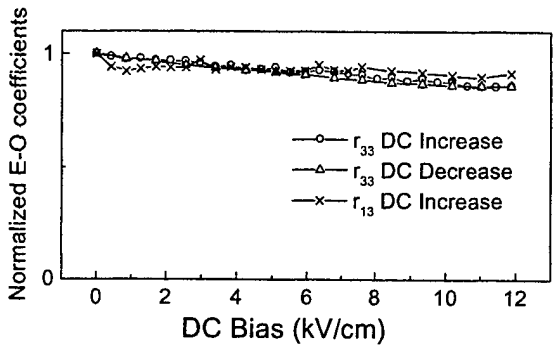

Fig. 4. The E-O coefficients as a function of the DC electric bias field for 0.88PZN–0.12PT single crystal at room temperature.

tion of a DC bias field which is applied parallel to the original poling direction up to 15 kV/cm, much higher than the room temperature coercive field. Apparently, the measured coefficients do not show much change with a DC bias field (except a small decrease which is expected) and as the bias field is reduced to zero, the E-O coefficients return to their original values. The results indicate that the sample used in this study was properly poled.

The r_{51} coefficient measured by the senarmont compensator method is $r_{51} = 462$ pm/V which is much larger than r_{33} and in the frequency range measured, (below 40 kHz), r_{51} does not show much change with frequency.

Using the senarmont compensator method, the E-O coefficient r_c was also characterized. The coefficient measured direct from the experiment data is the apparent coefficient r_c^* which is

$$r_c^* = r_{33}^* - \frac{n_o^3}{n_e^3} r_{13}^* = r_c + \frac{2(n_e - n_o)}{n_e^3} d_{31}. \tag{8}$$

Because the difference between n_e and n_o is very small, the piezoelectric effect [the second term on the right hand side of eq. (8)] has much less effect on r_c compared with r_{13} and r_{33}. The measured value of r_c^* for the sample under stress free condition used above is 128 pm/V. The corresponding coefficient after the correction of the piezoelectric effect is $r_c = 131$ pm/V.

From measured values of n_e, n_o, r_{13} and r_{33}, the E-O coefficient r_c can also be deduced from $r_c = r_{33} - n_o^3 r_{13}/n_e^3$. From the measured results of n_e, n_o, r_{13}^* and r_{33}^*, the calculated r_c^* is 124 pm/V, which is very close to 128 pm/V measured directly using the Senarmont compensator method.

A qualitative aging experiment was also performed on the E-O coefficients and it was found that even the poled sample was used for various other measurements, the E-O coefficients were nearly the same when measured after 3 months. Therefore the optical coefficients reported here are the stable material properties of 0.88PZN–0.12PT single crystal.

3.2 *Discussion*

At this point, it is interesting to compare the results obtained here with those reported earlier. For example, the quadratic E-O coefficients $g_{11} - g_{12}$ and g_{44} were measured by Nomura *et al.* [$\Delta n_{ij} = -(1/2) n_{ij}^3 \sum_{k,l=1}^{3} g_{ijkl} P_k P_l$, where P_k is the polarization component along the k-direction].[10] Since in ferroelectric single crystals, the linear E-O effect can be regarded as a polarization biased quadratic E-O effect,[17] the relationships between the linear E-O coefficients and the quadratic E-O coefficients are:

$$r_{33} - r_{13} = 2K_{33}\varepsilon_0 P_s (g_{11} - g_{12}) \tag{9a}$$

$$r_{51} = K_{11}\varepsilon_0 P_s g_{44} \tag{9b}$$

where $g_{11} = g_{1111}$, $g_{12} = g_{1122}$, and $g_{44} = 2g_{2323}$, K_{33} and K_{11} are the dielectric constant along the c-axis and a-axis, respectively, P_s is the spontaneous polarization, and $\varepsilon_0 = 8.85 \times 10^{-12}$ F/m is the vacuum permittivity.

For the crystal investigated here, at room temperature the dielectric constant was measured to be: $K_{33} = 710$ and $K_{11} = 7630$. From the data of ref. 10, $g_{11} - g_{12} = 0.013\,\mathrm{m^4/C^2}$ and $g_{44} = 0.009\,\mathrm{m^4/C^2}$. Hence, the ratio of $(r_{33} - r_{13})/r_{51}$ is equal to $2K_{33}(g_{11} - g_{12})/K_{11}g_{44} = 0.269$ using the dielectric constant measured here and the g coefficients of ref. 10. Using the value of the r coefficients measured here yields the ratio of $(r_{33} - r_{13})/r_{51} = 0.275$. The agreement between the values obtained using two sets of data is surprisingly good.

The results from the two sets of data can also be compared directly if the spontaneous polarization P_s is known. From the room temperature polarization hysteresis loop, P_s is extrapolated: $P_s = 40\,\mu\mathrm{C/cm^2}$. Substituting P_s and other data to the right hand sides of eq. (9) yields $r_{33} - r_{13} = 65.3$ pm/V and $r_{51} = 243$ pm/V. The results show that the linear E-O coefficients deduced from the quadratic E-O coefficients measured at temperatures near and above the dielectric constant maximum are about half of the values of the corresponding coefficients measured directly at poled samples (127 pm/V and 462 pm/V, respectively). In other words, either P_s and/or the g coefficients used in eq. (9) are smaller than the intrinsic values. Although one cannot rule out that the intrinsic P_s value for the crystal studied may be higher than 40 μC/cm^2, the difference will not be large enough to account for the discrepancy observed here.

In studies of the relaxor ferroelectric $Pb(Mg_{1/3}Nb_{2/3})O_3$–$PbTiO_3$ system, it was found that the electrostrictive coefficients measured at near and above the dielectric constant maximum are much smaller than the intrinsic values.[18,19] This is caused by the fact that in a relaxor ferroelectric system, the response of the local polar regions under external electric field includes the orientation of the polar regions and the motion of the interface between the non-polar area and the polar region.[20] All these responses contribute to the polarization, but do not totally contribute to the strain responses.[19] PZN–PT is also a typical relaxor ferroelectric system when the PT content is less than 10% and the evolution from a relaxor ferroelectric to a normal ferroelectric is a gradual process covering a broad composition range.[4,21] For the composition studied here, it is still quite close to the MPB and hence will possesses many features resembling a relaxor ferroelectric. For example, if there is a 180° local polar region reorientation, it will not cause a large change in the quadratic E-O coefficient in spite of the fact that there is a large polarization change. On the other hand, this response will influence $g_{11} - g_{12}$ and g_{44} in a similar way which will not affect the ratio between them as observed here. (The ratio of $(r_{33} - r_{13})/r_{51}$ measured here is the same as the ratio of $2K_{33}(g_{11} - g_{12})/K_{11}g_{44}$ deduced from the g-coefficients). Thus, the observed discrepancy be-

Table I. Properties characterized in this study for 0.88PZN–0.12PT single crystal.

$n_o = 2.57$, $n_e = 2.46$, $r_{33} = 134\,\text{pm/V}$, $r_{13} = 7\,\text{pm/V}$, $r_c = 131\,\text{pm/V}$, $r_{51} = 462\,\text{pm/V}$ (all measured at 633 nm wavelength), $d_{31} = -210\,\text{pm/V}$, $K_{33} = 710$, $K_{11} = 7630$, $P_s = 40\,\mu\text{C/cm}^2$

tween the measured linear E-O coefficients and the calculated ones from the quadratic E-O coefficients is reasonable. That is, when the measurement is performed at near the dielectric constant maximum where there is a strong contribution of the polarization responses from the local polar regions, the response of the local polar regions in relaxor systems will make the measured quadratic E-O coefficients deviating from their intrinsic values. By applying a high external field to remove this mesoscopic polarization inhomogeneity in the material, one may be able to obtain the intrinsic coefficients as observed in PMN–PT system.[19,22]

In Table I, the material properties characterized in this study are summarized.

4. Summary and Acknowledgement

Using the newly developed automated scanning Mach-Zehnder interferometer and the Senarmont compensator method, the linear E-O coefficients of 0.88PZN–0.12PT single crystal were measured at room temperature. It is found that the coefficients measured using the interferometer method and the Senarmont compensator method are in excellent accord. It is also found that the ratio of $(r_{33} - r_{13})/r_{51}$ measured here is also in very good accord with that deduced from the quadratic E-O coefficients measured earlier. However, in comparing the absolute values of the linear E-O coefficients measured here with that deduced from the quadratic E-O coefficients, it was found that the quadratic coefficients measured earlier at temperatures near the dielectric constant maximum may be substantially smaller than the intrinsic values of these coefficients due to the existence of mesoscopic polar regions and their different contributions to the polarization response and E-O response.

This work was supported by the Office of Naval Research under Contract No: N00014-98-1-0527.

1) M. E. Lines and A. M. Glass: *Principles and Applications of Ferroelectrics and Related Materials* (Clarendon Press, Oxford 1977).
2) L. J. Pinson: *Electro-optics* (John Wiley & Sons, New York, 1985).
3) J. Kuwata, K. Uchino and S. Nomura: Jpn. J. Appl. Phys. **21** (1982) 1298.
4) J. Kuwata, K. Uchino and S. Nomura: Ferroelectrics **37** (1981) 579.
5) S.-E. Park and T. Shrout: J. Appl. Phys. **82** (1997) 1804.
6) S.-F. Liu, S.-E. Park, T. R. Shrout and L. E. Cross: J. Appl. Phys. **85** (1999) 2810.
7) S.-E. Park and T. R. Shrout: Mater. Res. Innov. **1** (1997) 20.
8) B. Jaffe, W. R. Cook and H. Jaffe: *Piezoelectric Ceramics* (Academic Press, New York, 1971).
9) T. Mitsui and S. Nomura: *Ferroelectric and Related Materials* (Springer-Verlag, Berlin, 1981).
10) S. Nomura, H. Arima and F. Kojima: Jpn. J. Appl. Phys. **12** (1973) 531.
11) S.-F. Liu: unpublished.
12) IEEE Standard Board: An American National Standard, IEEE Standard on Piezoelectricity, ANSI/IEEE Std. **176** (1987).
13) A. R. Johnson and J. M. Weingart: J. Opt. Soc. Am. **55** (1965) 828.
14) D. McHenry: Dr. Thesis, Solid State Science, The Pennsylvania State University (1992).
15) F. W. Sears: *Optics* (Addison-Wesley, Cambridge, 1956).
16) T. Kwaaitaal, B. J. Luymes and G. A. Pijll: J. Phys. D **13** (1980) 1005.
17) F. Jona and G. Shirane: *Ferroelectric Crystals* (Dover, New York 1993).
18) J. Zhao, A. Glazonove, Q. M. Zhang and B. Toby: Appl. Phys. Lett. **72** (1998) 1048.
19) Q. M. Zhang and J. Zhao: Appl. Phys. Lett. **71** (1997) 1649.
20) Z.-Y. Cheng, R. S. Katiyar, X. Yao and A. S. Bhalla: Phys. Rev. B **57** (1998) 8166.
21) A. Halliyal, U. Kumar, R. E. Newnham and L. E. Cross: J. Am. Ceram. Soc. **70** (1987) 119.
22) J. Zhao: Dr. Thesis, Solid State Science, The Pennsylvania State University (1998).

APPENDIX 19

Composition, temperature, and crystal orientation dependence of the linear electro-optic properties of $Pb(Zn_{1/3}Nb_{2/3})O_3-PbTiO_3$ single crystals

Y. Barad, Yu Lu, Z.-Y. Cheng,[a] S.-E. Park, and Q. M. Zhang
Materials Research Laboratory, The Pennsylvania State University, University Park, Pennsylvania 16802

(Received 1 May 2000; accepted for publication 3 July 2000)

The linear electro-optic (EO) coefficients of $Pb(Zn_{1/3}Nb_{2/3})O_3-PbTiO_3$ single crystals over a broad composition range were investigated at temperatures from −20 to 80 °C. The orientation effect on the EO coefficients was also examined. For crystals poled in the ⟨001⟩ direction, a large r_{33} was observed near the morphotropic phase boundary (MPB). More importantly, r_{33} was found to be independent of temperature for the crystals on the tetragonal side of the MPB. In contrast, r_{13} was nearly zero for all compositions examined at all the temperatures. The large r_{33} near the MPB and the observed crystal orientation effect of the EO coefficients were also analyzed. © *2000 American Institute of Physics.* [S0003-6951(00)02735-2]

Ferroelectric crystals with high electro-optical (EO) coefficients are highly desirable for use in devices for optical communications and other commercial applications.[1,2] The search for a class of materials with high EO coefficients will allow for smaller size devices and lower operating voltage. A good candidate as such a substance is $Pb(Zn_{1/3}Nb_{2/3})O_3-PbTiO_3$ (PZN–PT) single crystals, which were found recently to possess both very high piezoelectric coefficients and electric-field-induced strains by working with different crystal orientations.[3–6] A unique feature to this crystal system is that relatively high-quality single crystals can be grown at compositions close to the tetragonal–rhombohedral morphotropic phase boundary (MPB) and a high EO response is expected at near the MPB.[7] In the following, we report on the results of a recent investigation of the linear EO coefficients of PZN–PT single crystals over a broad composition range (i.e., PZN–PT with 0%, 4.5%, 8%, 10%, and 12% PT), especially near the MPB, and in a temperature range of −20 to 80 °C [below the ferroelectric–paraelectric (FE–PE) transition temperature].

The crystals used in this work were grown by means of a high-temperature flux technique using high-purity (>99.9%) powders of Pb_3O_4, ZnO, Nb_2O_5, and TiO_2.[4,5] The single-crystal samples were orientated along the spontaneous polarization direction using a Laue camera. The crystals were then poled to ensure a single-domain configuration. The poling process was performed at a temperature about 50 °C higher than the FE–PE phase transition and then slowly cooled down to room temperature under the field. The poled samples were carefully polished to an optical grade, without affecting the crystal polarization. The poling direction was ⟨111⟩ for crystals on the rhombohedral side of the MPB (PZN–PT with 0%, 4.5%, and 8% PT) and ⟨001⟩ for crystals on the tetragonal side of the MPB (PZN–PT with 10% and 12% PT), respectively. To study the crystal orientation effect, the EO coefficients were also characterized for 0.92PZN–0.08PT poled in the ⟨001⟩ direction.

The EO effect describes the change (Δn_{ij}) in the refractive index due to an applied electric field (E_k). For poled ferroelectric crystals, we have[1,7]

$$\Delta n_{ij} = -\frac{1}{2} n_{ij}^3 \sum_{k=1}^{3} r_{ijk} E_k, \tag{1}$$

where r_{ijk} and n_{ij} are the linear EO coefficient and refractive index, respectively. In this work, the EO coefficients, r_{13} ($=r_{113}$) and r_{33}($=r_{333}$), were measured at a wavelength of 623.8 nm using a computer-controlled scanning Mach–Zender interferometer similar to the one reported in Ref. 7. For the work described here, the optical setup was upgraded to allow for varying temperature among the crystals measured. A precise feedback-controlled temperature stage was designed and built to fit into the optical setup. This apparatus can operate in a temperature range of −20–80 °C at a precision of less than 0.1 °C.

For the PZN–PT single crystals, applying an electric field contributes in two ways to the change in the optical path length (the principal parameter directly measured by the interferometer). The first is the change in optical index due to the EO effect; second is the change (Δl) in sample thickness along the optical path due to the piezoelectric effect ($\Delta l/l = d_{31}E_3$, where d_{31} and l are the transverse piezoelectric coefficient and the sample thickness along the optical path direction). In order to determine the real values of the EO coefficients, the contribution of the piezoelectric effect to the apparent EO coefficient r_{ij}^* was measured. The correction was made using the relation.[7]

$$r_{ij} = r_{ij}^* + \frac{2(n_i - 1)}{n_i^3} d_{31}, \tag{2}$$

where $ij = 33$ and 13, n_i is n_e when correcting for the value of r_{33}, and n_0 when the correction is made for the value of r_{13}.[7]

A summary of the EO coefficients measured at room temperature for the five investigated compositions is presented in Table I. Both the apparent and corrected EO coefficients are listed, along with the measured piezoelectric coefficient d_{31}. The results in Table I reveal several interesting features. First, compared with r_{33}, r_{13} is nearly zero. This is

[a]Electronic mail: zxc7@psu.edu

TABLE I. EO coefficients (r_{33} and r_{13}) of PZN–PT single crystal at room temperature. Here, r_{33}^* and r_{13}^* are the apparent values, d_{31} is the piezoelectric coefficient, and r_{33} and r_{13} are the real values.

Composition	Poling direction	r_{33}^* (pm/V)	r_{13}^* (pm/V)	$-d_{31}$ (pC/N)	r_{33} (pm/V)	r_{13} (pm/V)
PZN	⟨111⟩	77	8	10	75	6
0.955PZN–0.045PT	⟨111⟩	81	9	15	78	6
0.92PZN–0.08PT	⟨111⟩	105	24	42	97	16
0.92PZT–0.08PT	⟨001⟩	655	220	1070	450	15
0.9PZN–0.1PT	⟨001⟩	224	42	247	177	~0
0.88PZN–0.12PT	⟨001⟩	173	44	210	134	7

true for crystals in both the rhombohedral and tetragonal phases. Second, large r_{33} is observed for compositions near the MPB (see, also, Fig. 1). Third, for the same composition (e.g., 0.92PZN–0.08PT), the r_{33} coefficient of the crystal poled in the ⟨001⟩ direction is much higher than that of the crystal poled in the ⟨111⟩ direction.

For crystals in the tetragonal phase, the measured linear EO coefficients can be related to the polarization-related quadratic EO coefficients g_{11} and g_{12}, which can be determined at the prototype cubic phase at temperatures above the FE–PE transition temperature [$\Delta n_{ij} = -(1/2) n_{ij}^3 \times \Sigma_{k,l=1}^{3} g_{ijkl} P_k P_l$, where P_k is the polarization component in the k direction], as follows:[8,9]

$$r_{33} = 2K_{33}\epsilon_0 P_s g_{11} \quad \text{and} \quad r_{13} = 2K_{33}\epsilon_0 P_s g_{12}, \tag{3}$$

where $g_{11} = g_{1111}$ and $g_{12} = g_{1122}$, and P_s and K_{33} are the spontaneous polarization and dielectric constant, respectively, in the ⟨001⟩ direction. ϵ_0 is the vacuum permittivity ($=8.85\times10^{-12}$ F/m). Therefore, the observation of a near-zero r_{13} in comparison to r_{33} implies a near-zero g_{12} in comparison to g_{11} or $g_{11} - g_{12} \approx g_{11}$.

For crystals in the rhombohedral phase, the measured r_{33} and r_{13} can be also linked to g_{ij} in the prototype cubic phase:[8,9]

$$\begin{aligned} r_{33} &= (2/3)K_{33}\epsilon_0 P_s (g_{11} + 2g_{12} + 2g_{44}), \\ r_{13} &= (2/3)K_{33}\epsilon_0 P_s (g_{11} + 2g_{12} - 2g_{44}). \end{aligned} \tag{4}$$

Using $g_{11} - g_{12} = 0.013\ \mathrm{m^4/C^2}$ and $g_{44} = 0.009\ \mathrm{m^4/C^2}$ as acquired by Nomura, Arima, and Kojima for PZN–PT at compositions near the MPB, and the fact that g_{12} is near zero,[10] Eq. (4) shows that the r_{13} is very small, which is consistent with experimental results. A large r_{33} and a near-zero r_{13} indicate that the applied electric field in the spontaneous polarization direction does not affect the overall electronic polarization of the unit cell in the directions perpendicular to it. Furthermore, the near-zero g_{12} implies that the refractive index in these directions will not change with P_s as the temperature is varied, even when it passes the FE–PE transition.

It should be noted that in Eq. (4), P_s and K_{33} are the spontaneous polarization and dielectric constant, respectively, in ⟨111⟩ direction, which differs from those used in Eq. (3). Using Eqs. (3) and (4), one can directly compare the EO coefficients for the crystals in the rhombohedral and tetragonal phases since the g_{ij} value changes little at the two

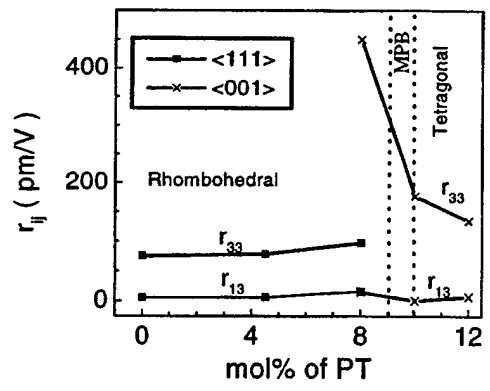

FIG. 1. EO coefficients at room temperature vs compositions for PZN–PT single crystals.

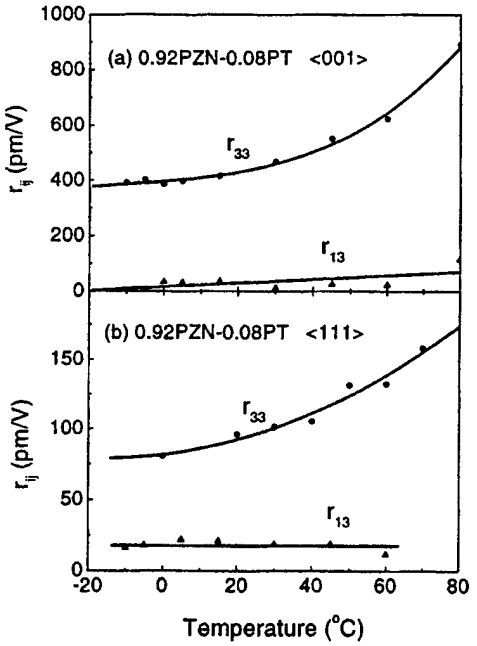

FIG. 2. Temperature dependence of EO coefficients for 0.92PZN–0.08PT single crystal poled in different directions: (a) ⟨001⟩ and (b) ⟨111⟩.

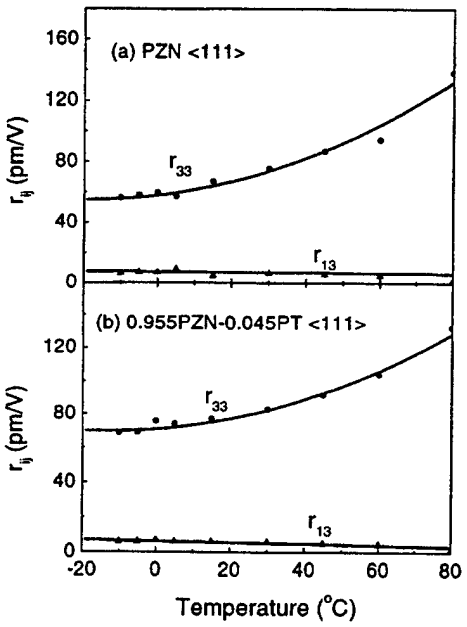

FIG. 3. Temperature dependence of EO coefficients for PZN and 0.955PZN–0.045PT single crystals poled in the ⟨111⟩ direction.

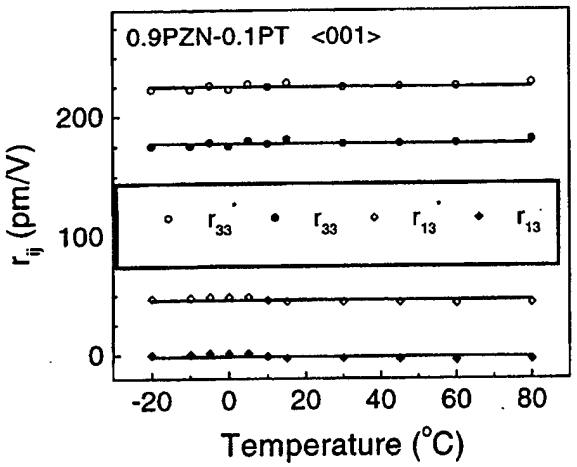

FIG. 4. Temperature dependence of EO coefficients for 0.9PZN–0.1PT single crystal poled in the ⟨001⟩ direction.

sides of the MPB. For 0.92PZN–0.08PT, the EO coefficients were measured for crystals poled along both the ⟨111⟩ and the ⟨001⟩ directions. Both the dielectric constant and P_s were also acquired for the corresponding crystals. For the crystal poled in the ⟨111⟩ direction, P_s and K_{33} in ⟨111⟩ are 0.45 C/m^2 and 807, respectively, while for the crystal poled in ⟨001⟩ direction, P_s and K_{33} are 0.32 C/m^2 and 3800, respectively. Using these values and Eqs. (3) and (4), the ratio of r_{33} between the tetragonal crystal and the rhombohedral crystal is about 4.2, while the experimentally measured ratio is 4.6. The two ratios are quite close to each other, indicating that the EO coefficients were from the responses of single-domain crystals in both cases. Also, the result suggests that K_{33} for both ⟨001⟩ and ⟨111⟩ poled 0.92PZN–0.08PT should stem mostly from the single-domain crystal. In that the quadratic EO coefficient g_{ij} exhibits no anomalous changes in compositions across the MPB, Eqs. (3) and (4) suggest that the large linear EO response observed here near the MPB is due to the large dielectric constant of the material at that region.

It should be also mentioned that direct comparison of the measured r_{33} with that from either Eq. (3) or (4) shows that the measured value is much larger than that deduced from the equations. For example, for 0.92PZN–0.08PT crystal poled in the ⟨001⟩ and ⟨111⟩ directions, the calculated r_{33} using Eqs. (3) and (4) is about 280 and 66 pm/V, respectively, while the measured r_{33} is 450 and 97 pm/V, respectively. As discussed in an early publication,[7] the discrepancy could stem from the fact that the measured g_{ij} using the EO effect at temperatures above the FE–PE transition may be smaller than the real single-crystal value. This is due to the relaxor nature of the material, in which resides local polarization regions even at temperatures higher than the FE–PE transition temperature.[11–13] Both the orientation and breathing of the polar regions contribute to the dielectric behavior (polarization) of the materials,[14,15] but do not contribute totally to the refractive-index change.[7] For example, a 180° local polar region reorientation, which leads to a large polarization change, will not cause a large change in the optic index.

We now discuss the temperature dependence of these EO coefficients. Figure 2 shows the EO coefficient r_{ij} as a function of temperature for 0.92PZN–0.08PT poled in the ⟨001⟩ and ⟨111⟩ directions, respectively, which reveals that r_{ij} changes with temperature. This temperature-dependence behavior was also observed for other compositions on the rhombohedral side of the MPB (see Fig. 3). In contrast, for the two compositions on the tetragonal side of the MPB, the EO coefficient is nearly independent of temperature, as shown in Fig. 4, where both the apparent and real EO coefficients are displayed. Since g_{11} should be nearly temperature independent, Eq. (3) implies that the value of the dielectric constant times spontaneous polarization ($K_{33}P_s$) should be nearly independent of temperature. Indeed, the directly measured P_s and K_{33} of the crystal with temperature confirm this effect.

In summary, a large r_{33} coefficient was observed for PZN–PT single crystals near the MPB. In addition, the coefficient is independent of temperature for the tetragonal phase crystal in the experimental temperature range of −20–80 °C. In comparison to r_{33}, r_{13} is nearly zero for all compositions investigated. These features are very attractive for device applications. It was also found that r_{33} for the tetragonal phase is much higher than that for the rhombohedral phase. Detailed analysis indicates that this increase is caused largely by the high dielectric constant.

This work was supported by ONR under Grant No. N00014-98-1-0527.

[1] M. E. Lines and A. M. Glass, *Principles and Applications of Ferroelectrics and Related Materials* (Oxford University Press, New York, 1977), Chap. 16.4.
[2] F. T. S. Yu and S. Jutamulia, *Optical Signal Processing, Computer, and Neural Network* (Wiley, New York, 1992).
[3] J. Kuwata, K. Uchino, and S. Nomura, Ferroelectrics **37**, 579 (1981).
[4] S.-E. Park and T. Shrout, J. Appl. Phys. **82**, 1804 (1997).
[5] S.-F. Liu, S.-E. Park, T. Shrout, and L. E. Cross, J. Appl. Phys. **85**, 2810 (1999).
[6] S. Nomura; T. Takahashi, and Y. Yokomizo, J. Phys. Soc. Jpn. **27**, 262 (1969).
[7] Y. Lu, Z.-Y. Cheng, S.-E. Park, S.-F. Liu, and Q. Zhang, Jpn. J. Appl. Phys., Part 1 **39**, 141 (2000).
[8] M. DiDomenico and S. H. Wemple, J. Appl. Phys. **40**, 720 (1969).
[9] S. H. Wemple, M. DiDomenico, and I. Camlibeel, Appl. Phys. Lett. **12**, 209 (1968).
[10] S. Nomura, H. Arima, and F. Kojima, Jpn. J. Appl. Phys. **12**, 531 (1973).
[11] G. Burns and B. A. Scott, Solid State Commun. **13**, 423 (1973).
[12] G. Burn and F. H. Dacol, Phys. Rev. B **30**, 4012 (1980).
[13] G. Burn and F. H. Dacol, Ferroelectrics **104**, 25 (1990).
[14] Z.-Y. Cheng, R. S. Katiyar, X. Yao, and A. S. Bhalla, Phys. Rev. B **57**, 8166 (1998).
[15] Q. M. Zhang and J. Zhao, Appl. Phys. Lett. **71**, 1649 (1997).

APPENDIX 20

Photoelastic effects in tetragonal $Pb(Zn_{1/3}Nb_{2/3})O_3$–$PbTiO_3$ single crystals near the morphotropic phase boundary

Y. Lu,[a] Z.-Y. Cheng, Y. Barad, and Q. M. Zhang
Materials Research Laboratory and Electrical Engineering Department, Pennsylvania State University, University Park, Pennsylvania 16802

(Received 15 January 2001; accepted for publication 15 February 2001)

In order to explore the photoelastic effects of the ferroelectric single crystal $Pb(Zn_{1/3}Nb_{2/3})O_3$–$PbTiO_3$ (PZN–PT), the piezo-optical coefficients π were characterized for 0.9PZN–0.1PT and 0.88PZN–0.12PT under uniaxial stress using an interferometer method. The results show that the crystal exhibits very large π values (for example, π_{33} can reach 19.8 $\times 10^{-12}$ m^2/N), indicating that this material is a good candidate for stress sensors and acousto-optic modulators. © *2001 American Institute of Physics.* [DOI: 10.1063/1.1363684]

I. INTRODUCTION

The phenomenon of photoelastic behavior in crystals is attractive for many applications, such as stress sensors and light modulators.[1,2] In order to improve the performance of these devices, new materials with a large photoelastic effect are highly desirable. Recently, there has been an increased interest in $Pb(Zn_{1/3}Nb_{2/3})O_3$–$PbTiO_3$ (PZN–PT) single crystals because the crystals exhibit very large piezoelectric constants, high electromechanical coupling factors, and massive electro-optic effects.[3–6] The unique feature of these materials is that high quality single crystals can be grown at compositions close to the tetragonal–rombohedral morphotropic phase boundary (MPB), where very large ferroelastic coupling is expected for this class of crystals because of a large lattice constant change between the two morphotropic phases.[7,8] In general, materials with large ferroelastic responses may also have high photoelastic effects. Especially, for materials near MPB, the large lattice parameter changes with composition will result in large changes in the refractive index. Equivalently, the stress induced phase transition (shift of the MPB with stress) will also bring additional and large refractive index changes, which enhances the overall photoelastic effects. Therefore, it is interesting to investigate the photoelastic effect of PZN–PT single crystals near MPB.

PZN–PT single crystals are the solid solutions of lead zinc niobate and lead titanate and the crystals used here were grown by a high temperature flux method.[4] Among them, 0.9PZN–0.1PT was chosen since this composition is close to MPB in the tetragonal side at room temperature, and 0.88PZN–0.12PT was also measured for comparison.[7] The sample was poled along its spontaneous polarization direction (⟨001⟩ direction) to form a single domain state, then carefully polished to optical grade as described in Ref. 5. The typical specimen dimension is $3\times3\times3$ mm^3.

[a]Electronic mail: YXL27@PSU.EDU

II. PHOTOELASTIC EFFECT AND ITS MEASUREMENT

Photoelastic effect describes the change of the refractive index as a result of mechanical stress. Under an applied stress T_{kl}, the change of refractive index n_{ij} is given by[2]

$$\Delta B_{ij}=\Delta\left(\frac{1}{n_{ij}^2}\right)=\pi_{ijkl}T_{kl}, \tag{1}$$

where B_{ij} is the optical dielectric impermeability, which is equal to $1/n_{ij}^2$; π_{ijkl} is the piezo-optical coefficient (i, j, k, and $l=1-3$). In this work, the piezo-optical coefficients, $\pi_{13}(=\pi_{1133})$, $\pi_{33}(=\pi_{3333})$, $\pi_{11}(=\pi_{1111})$, and π_{31} $(=\pi_{3311})$ were characterized at room temperature at a wavelength of 623.8 nm utilizing uniaxial stress measurements. As schematically shown in Fig. 1, by applying the compressional stress along the three axis (T_{33}) which is along the sample poling direction, the piezo-optical coefficient π_{33} can be obtained from the change of the extraordinary refractive index n_e; and π_{13} can be determined from the change of the ordinary refractive index n_0.

To generate the required uniaxial stress on the crystal, a special setup was carefully designed. In this setup, a piezoelectric actuator (Thorlabs Inc., AE0505D08) was used to generate a dynamic force by applying an ac electric driving voltage to the actuator, and the stress was measured using a high performance load cell (Omegadyne Inc., LC302-25). The refractive index change was measured at a wavelength of 623.8 nm using a computer-controlled scanning Mach–Zender interferometer, as schematically shown in Fig. 2, similar to the one reported in the Ref. 5. Since the dynamic force was used in the experiment, a lock-in amplifier was used to detect the modulated interference output signal at the frequency of the applied stress, which significantly improves the sensitivity of the measurement. Therefore, the stress applied to the sample can be very small ($\geqslant$1 kPa was used, which is actually limited by the resolution of the load cell) eliminating the possibility of stress depoling the crystal, especially when applying the compressional stress along the poling direction. For the setup designed here, the frequency of the dynamic force can be varied from 1 to 100 Hz and the results reported were obtained at 10 Hz.

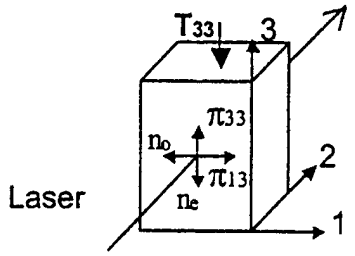

FIG. 1. Schematic drawing for the measurement of π_{33} and π_{13} where the uniaxial stress is applied along the three axis. The laser light propagation direction and the light polarization direction for the measurement of π_{33} and π_{13} are indicated.

TABLE I. Piezo-optical coefficients of single crystal PZN–PT at room temperature ($\times 10^{-12}$ m^2/N).

0.9PZN–0.1PT		0.88PZN–0.12PT	
π_{33}^E	19.8	π_{33}^E	18.2
π_{13}^E	−1.6	π_{13}^E	−0.9
π_{11}^E	2.3	π_{11}^E	0.8
π_{31}^E	−10.4	π_{31}^E	−9.3
π_{33}^D	6.2	π_{33}^D	6.0
π_{13}^D	−2.5	π_{13}^D	0.2
π_{11}^D	2.4	π_{11}^D	1.3
π_{31}^D	−4.6	π_{31}^D	−3.9

It should be mentioned that, in this interferometer technique, the directly measured optical path length change is the result of two effects, i.e., the change in the refractive index (piezo-optical effect) and the change in the sample dimension (elastic deformation of the sample due to stress). In order to extract the refractive index change due to the piezo-optical effect, the sample dimensional change along the optical path under the same applied stress was measured using a double beam interferometer method.[9] After this correction, the piezo-optical coefficient π can be obtained.

III. EXPERIMENTAL RESULTS AND DISCUSSION

For piezoelectrics, there are two types of the π coefficients, i.e., π^E and π^D, due to the different electric boundary conditions of the sample in the measurement. Because of the piezoelectric effect, a voltage will be generated under the applied stress if the measurement is carried out in an open circuit condition (constant electric displacement, D) and in this case, π^D is measured. On the other hand, if the measurement is carried out in the short circuit condition (constant electric field, E), where the sample surfaces at the positive and negative polarization directions are electroded and the two electroded surfaces are connected (shorted), π^E is measured. As will be shown later, the difference between π^E and π^D is determined by the electro-optical and piezoelectric effects. That is, the stress-generated electric field on the sample in the open circuit condition also results in a change of refractive index through the electro-optic effect. In this investigation, the piezo-optical coefficients π_{11}, π_{31}, π_{13}, and π_{33} under both the constant electric field and the constant electric displacement conditions were measured. Table I summarizes the final results for 0.9PZN–0.1PT and 0.88PZN–0.12PT single crystals.

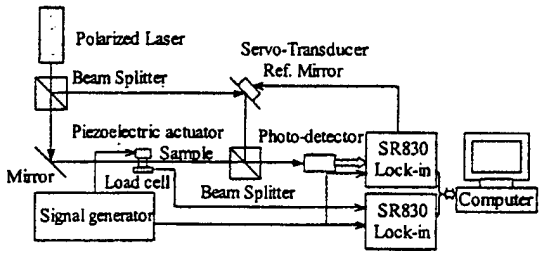

FIG. 2. Schematic drawing of the computer-controlled scanning Mach–Zender interferometer for piezo-optical measurement.

To provide an understanding of the measured results, a phenomenological treatment will be used to link the change of optical properties of the crystals to the applied stress, electric field, as well as the remanent polarization.[10] From the symmetry consideration, the change of the optical impermeability for the PZN–PT single crystals can be written as

$$\Delta B_{ij} = \pi^0_{ijkl} T_{kl} + g_{ijmn} P_m P_n + f_{ijklmn} T_{kl} P_m P_n, \tag{2}$$

where π^0_{ijkl} is the piezo-optical coefficient of the prototype phase (cubic for PZN–PT single crystals studied here) where $P_m = 0$, P_m is the polarization component along the m axis, g_{ijmn} is quadratic polarization-optic (PO) constant, and f_{ijklmn} is the first order cross term between T and P. In Eq. (2), all the higher order terms have been omitted. Based on the results in this study, we find the three terms in Eq. (2) are on the same order of magnitude. To simplify the formula, a matrix notation will be used in following derivations (i.e., $11 \rightarrow 1$, $22 \rightarrow 2$, $33 \rightarrow 3$).[11]

For the uniaxial stress used here, only T_1 or T_3 is the nonzero stress component. In the prototype cubic phase where the spontaneous polarization is zero,

$$\begin{aligned} \Delta B_1 &= \pi^0_{11} T_1 + \pi^0_{13} T_3, \\ \Delta B_3 &= \pi^0_{31} T_1 + \pi^0_{33} T_3. \end{aligned} \tag{3}$$

For the prototype cubic phase, $B_1 = B_3$, T_1 and T_3 are interchangeable, and hence the piezo-optical coefficients $\pi^0_{33} = \pi^0_{11}$, and $\pi^0_{31} = \pi^0_{13}$, respectively.

In the ferroelectric tetragonal phase where the total polarization is P_3,

$$\begin{aligned} \Delta B_1 &= \pi^0_{11} T_1 + \pi^0_{13} T_3 + g_{13} P_3^2 + f_{113} T_1 P_3^2 + f_{133} T_3 P_3^2, \\ \Delta B_3 &= \pi^0_{13} T_1 + \pi^0_{11} T_3 + g_{33} P_3^2 + f_{313} T_1 P_3^2 + f_{333} T_3 P_3^2. \end{aligned} \tag{4}$$

In order to obtain the expressions for the piezo-optical coefficients in the tetragonal phase, the total polarization, which includes the spontaneous polarization P_s and the induced polarization due to the external field, should be calculated. Under the constant electric field condition (constant E), the total polarization P_3 can be derived from the piezoelectric constitutive equation as $P_3 = P_s + d_{31} T_1 + d_{33} T_3$, where d_{31} and d_{33} are the piezoelectric constants of the crystal.[11] Substituting P_3 into Eq. (4) yields

TABLE II. Electro-optic coefficients (r_{ij}), piezoelectric constants (d_{ij}), and dielectric constant (K_3) in PZN–PT single crystals.

Composition	d_{31} (pC/N)	d_{33} (pC/N)	r_{33} (pm/V)	r_{13} (pm/V)	K_3
0.9PZN–0.1PT	−247	770	177	0	1000
0.88PZN–0.12PT	−210	610	134	7	800

$$\begin{aligned}\Delta B_1 &= g_{13}P_s^2+(\pi_{11}^0+2g_{13}P_sd_{31}+f_{113}P_s^2)T_1\\ &\quad+(\pi_{13}^0+2g_{13}P_sd_{33}+f_{133}P_s^2)T_3,\\ \Delta B_3 &= g_{33}P_s^2+(\pi_{13}^0+2g_{33}P_sd_{31}+f_{313}P_s^2)T_1\\ &\quad+(\pi_{11}^0+2g_{33}P_sd_{33}+f_{333}P_s^2)T_3.\end{aligned}\tag{5}$$

The first term in Eq. (5) represents the spontaneous birefringence by the PO effect due to the spontaneous polarization in the ferroelectric phase. The second and third terms are the refractive index changes as a consequence of the applied stress under constant electric field, which are photoelastic effects. Hence, the piezo-optical coefficients π^E can be expressed as

$$\begin{aligned}\pi_{11}^E&=\pi_{11}^0+2g_{13}P_sd_{31}+f_{113}P_s^2,\\ \pi_{13}^E&=\pi_{13}^0+2g_{13}P_sd_{33}+f_{133}P_s^2,\\ \pi_{31}^E&=\pi_{13}^0+2g_{33}P_sd_{31}+f_{313}P_s^2,\\ \pi_{33}^E&=\pi_{11}^0+2g_{33}P_sd_{33}+f_{333}P_s^2.\end{aligned}\tag{6}$$

Under the constant electric displacement condition (constant D), the total polarization P_3 equals $P_s+d_{31}T_1/K_3+d_{33}T_3/K_3$, where K_3 is the relative permittivity.[11] So, the piezo-optical coefficient π^D can also be derived as

$$\begin{aligned}\pi_{11}^D&=\pi_{11}^0+2g_{13}P_sd_{31}/K_3+f_{113}P_s^2\approx\pi_{11}^0+f_{113}P_s^2,\\ \pi_{13}^D&=\pi_{13}^0+2g_{13}P_sd_{33}/K_3+f_{133}P_s^2\approx\pi_{13}^0+f_{133}P_s^2,\\ \pi_{31}^D&=\pi_{13}^0+2g_{33}P_sd_{31}/K_3+f_{313}P_s^2\approx\pi_{13}^0+f_{313}P_s^2,\\ \pi_{33}^D&=\pi_{11}^0+2g_{33}P_sd_{33}/K_3+f_{333}P_s^2\approx\pi_{11}^0+f_{333}P_s^2.\end{aligned}\tag{7}$$

Since for material studied here K_3 is around 1000, the approximation in Eq. (7) is reasonable.

In the ferroelectric tetragonal phase the linear electro-optic effect is related to the quadratic PO effect, as $r_{13}=2g_{13}\epsilon_3P_s$ and $r_{33}=2g_{33}\epsilon_3P_s$, where r_{13} and r_{33} are the linear electro-optic coefficients, and ϵ_3 are the dielectric permittivity of the crystal.[5] Therefore, Eq. (6) can be rewritten as

$$\begin{aligned}\pi_{11}^E&=\pi_{11}^0+r_{13}d_{31}/\epsilon_3+f_{113}P_s^2,\\ \pi_{13}^E&=\pi_{13}^0+r_{13}d_{33}/\epsilon_3+f_{133}P_s^2,\\ \pi_{31}^E&=\pi_{13}^0+r_{33}d_{31}/\epsilon_3+f_{313}P_s^2,\\ \pi_{33}^E&=\pi_{11}^0+r_{33}d_{33}/\epsilon_3+f_{333}P_s^2,\end{aligned}\tag{8}$$

and Eq. (7) as,

$$\begin{aligned}\pi_{11}^E&=\pi_{11}^D+r_{13}d_{31}/\epsilon_3,\\ \pi_{13}^E&=\pi_{13}^D+r_{13}d_{33}/\epsilon_3,\\ \pi_{31}^E&=\pi_{31}^D+r_{33}d_{31}/\epsilon_3,\\ \pi_{33}^E&=\pi_{33}^D+r_{33}d_{33}/\epsilon_3.\end{aligned}\tag{9}$$

Equation (9) shows that the difference between the π^E and π^D is caused by the combination of both piezoelectric and electro-optic effects. If either the piezoelectric or electro-optic effects are equal to zero, then π^E should be equal to π^D. By knowing the relevant coefficients, this difference can also be directly calculated from Eq. (9). Making use of the electro-optic coefficients measured in Ref. 5, the piezoelectric coefficients and dielectric constants measured here that are listed in Table II,[5,6] the differences $\pi_{ij}^E-\pi_{ij}^D$ are evaluated. As shown in Table III, the calculated differences match quite well with the measured ones.

From the measured results, some of the coefficients in Eq. (2) can be estimated. The quadratic PO coefficients g_{ijmn} have been discussed in Ref. 5 and from Eq. (7), one can get,

$$\begin{aligned}\pi_{33}^D-\pi_{11}^D&\approx(f_{333}-f_{113})P_s^2,\\ \pi_{13}^D-\pi_{31}^D&\approx(f_{133}-f_{313})P_s^2.\end{aligned}\tag{10}$$

Using the values in Table I from 0.9PZN–0.1PT and $P_s=0.4\,\mathrm{C/m^2}$, $f_{333}-f_{113}=24\times10^{-12}\,\mathrm{m^6/NC^2}$ and $f_{133}-f_{313}=13\times10^{-12}\,\mathrm{m^6/NC^2}$ are obtained.

It should also be pointed out that the coefficients in Eq. (2) should remain nearly constant as the PZN–PT crystal composition changes from 0.9PZN–0.1PT to 0.88PZN–0.12PT. As a result, Eq. (7) reveals that the piezo-optical coefficients π^D should not change with composition for the two compositions investigated. Indeed, π_{33}^D measured from the two compositions are nearly the same. The observed difference in other π^D is caused by the experiment error, where except π_{33}, the correction term due to the stress induced sample dimension change is the same as or even larger than the term from the stress induced refractive change. The

TABLE III. Difference of A–O coefficients between constant E and constant D conditions ($\times10^{-12}\,\mathrm{m^2/N}$).

0.9PZN–0.1PT	$\pi_{33}^E-\pi_{33}^D$	$\pi_{13}^E-\pi_{13}^D$	$\pi_{11}^E-\pi_{11}^D$	$\pi_{31}^E-\pi_{31}^D$
Calculated	15.4	0	0	−4.9
Measured	13.6	0.9	−0.1	−5.8
0.88PZN–0.12PT	$\pi_{33}^E-\pi_{33}^D$	$\pi_{13}^E-\pi_{13}^D$	$\pi_{11}^E-\pi_{11}^D$	$\pi_{31}^E-\pi_{31}^D$
Calculated	11.5	0.6	−0.2	−4.0
Measured	12.2	−1.1	−0.5	−5.4

larger value of π_{33}^E for 0.9PZN–0.1PT in comparison with 0.88PZN–0.12PT is the MPB effect as discussed in the Introduction.

It is also interesting to compare the piezo-optical coefficients for PZN–PT crystals investigated here with the currently widely used acousto-optic material TeO_2, which has $\pi_{11} = -19.19 \times 10^{-12}\,m^2/N$ and $\pi_{12} = 19.85 \times 10^{-12}\,m^2/N$.[12] Apparently, 0.9PZN–0.1PT single crystal has a comparable photoelastic effect. In addition, this material has relatively large elastic compliance which results in a lower sound velocity (~2400 m/s).[13] Therefore, the figure of merit for an acousto-optic device will also be large.[2]

IV. CONCLUSIONS

The photoelastic effect of 0.9PZN–0.1PT single crystals was characterized under uniaxial stress using an interferometer method. The piezo-optical coefficients π_{33}, π_{31}, π_{11}, and π_{13} under both constant electric field and constant electric displacement conditions were measured. It was found that the piezo-optical coefficient π_{33}^E is $19.8 \times 10^{-12}\,m^2/N$, which is very large in comparison with currently known photoelastic materials. Therefore, the crystal is a very good candidate for stress sensors and other acousto-optic devices. In particular, since this material also possesses a very large electro-optic effect[5,6] and piezoelectric effect,[3,4,7] the combination of these three effects make it very attractive and more flexible in producing high performance multifunctional devices.

ACKNOWLEDGMENTS

The authors wish to thank Drs. S.-E. Park, T. Shrout, and S.-F. Liu for supplying the PZN–PT single crystals used in this study. This work was supported by the Office of Naval Research.

[1] J. A. Bucaro, H. D. Dardy, and E. F. Carome, Appl. Opt. **16**, 1761 (1977).
[2] T. S. Narasimhamurty, *Photoelastic and Electro-Optic Properties of Crystals* (Plenum, New York, 1981).
[3] S.-E. Park and T. R. Shrout, J. Appl. Phys. **82**, 1804 (1997).
[4] S.-F. Liu, S.-E. Park, T. R. Shrout, and L. E. Cross, J. Appl. Phys. **85**, 2810 (1999).
[5] Y. Lu, Z.-Y. Cheng, S.-E. Park, S.-F. Liu, and Q. M. Zhang, Jpn. J. Appl. Phys., Part 1 **39**, 141 (2000).
[6] Y. Barad, Y. Lu, Z.-Y. Cheng, S.-E. Park, and Q. M. Zhang, Appl. Phys. Lett. **77**, 1247 (2000).
[7] J. Kuwata, K. Uchino, and S. Nomura, Ferroelectrics **37**, 579 (1981).
[8] O. Noblanc, P. Gaucher, and G. Calvarin, J. Appl. Phys. **79**, 4291 (1996).
[9] Q. M. Zhang, S. J. Jang, and L. E. Cross, J. Appl. Phys. **65**, 2807 (1989).
[10] P. Bernasconi, M. Zgonik, and P. Günter, J. Appl. Phys. **78**, 2651 (1995).
[11] J. F. Nye, *Physical Properties of Crystals: Their Representation by Tensors and Matrices* (Oxford University Press, New York, 1985).
[12] N. Uchida and Y. Ohmachi, J. Appl. Phys. **40**, 4692 (1969).
[13] S. Saitoh, T. Kobayashi, K. Harada, S. Shimanuki, and Y. Yamashita, IEEE Trans. Ultrason. Ferroelectr. Freq. Control **45**, 1071 (1998).

MATERIALS STUDIES

High Strain Polymers

APPENDIX 21

Polarization and structural properties of high-energy electron irradiated poly(vinylidene fluoride-trifluoroethylene) copolymer films

Vivek Bharti,[a] H. S. Xu, G. Shanthi, and Q. M. Zhang
Materials Research Laboratory, The Pennsylvania State University, University Park, Pennsylvania 16802

Kuming Liang
ATL Echo Ultrasound, Reedsville, Pennsylvania 17084

(Received 2 June 1999; accepted for publication 29 September 1999)

The effect of high-energy electron irradiation on structural and polarization properties of 50/50 mol% copolymer of poly(vinylidene fluoride-trifluoroethylene) was investigated for both mechanically stretched and unstretched films. Although stretching can significantly enhance the polarization and dielectric responses in unirradiated films, it was observed that this enhancement was not significant in irradiated films. In addition, the polarization in both types of films after irradiation can be described quite well by a logarithmic mixing law of composites, which consist of crystallites embedded in an amorphous matrix with nearly the same fitting parameters. On the other hand, the enhancement of the mechanical properties from stretching persists after the irradiation, and the elastic modulus along the stretching direction remains high after irradiation in comparison with unstretched films. It was found that the dielectric dispersion in both types of films after irradiation fits well to the Vogel–Fulcher law. It was also observed that the crystallinity decreases and the crosslinking coefficient increases continuously with dose. However, there was no direct one to one type relationship between the crystallinity and the crosslinking coefficient. Although stretching can reduce the rate of crosslinking, the reduction of crystallinity with dose for stretched and unstretched films does not show a marked difference. © *2000 American Institute of Physics.* [S0021-8979(00)08501-7]

I. INTRODUCTION

Since the discovery of ferroelectricity in the vinylidene fluoride-trifluoroethylene copolymers P(VDF-TrFE), extensive research has been carried out to understand the ferroelectric behavior, to enhance the electromechanical properties, and to establish structure-property relationship.[1–4] It is well known that the electromechanical properties are highly dependent upon the structural parameters such as molecular orientation, crystallinity, and the state of polarization.[4–6] Various methods such as high temperature annealing,[7] stretching, and high electric field poling[8–10] have been employed to introduce high degree of crystallinity and perfect alignment of dipoles in polymer films.

We have shown recently that under proper electron irradiation treatment, P(VDF-TrFE) copolymers can exhibit massive electrostrictive strain with high elastic energy density.[11,12] It was also observed that a piezoelectric state can be induced in this copolymer under a dc electric bias field with a piezoelectric constant approaching those of the current piezoceramic materials.[13] In addition, the irradiation treatment was found to convert the polymer from a normal ferroelectric to a relaxor ferroelectric exhibiting a broad dielectric relaxation peak following Vogel–Fulcher law,[14] as observed in the inorganic ferroelectric relaxors like lead magnesium niobate (PMN).[15,16] These distinct features make this material very attractive for a broad range of applications such as transducers, actuators, and sensors,[17,18] and also for the fundamental study of ferroelectric systems with frozen-in defects and frustrations.[16]

It was observed that the electromechanical properties of irradiated copolymers depend crucially on the processing conditions both prior and during the irradiation. For example, by mechanically stretching the copolymer films prior to the irradiation, the electric field induced strain and electromechanical coupling coefficient can become much higher along the stretching direction in comparison to the thickness direction or unstretched films. Furthermore, the changes in the phase transition properties with irradiation doses can also be affected markedly by stretching.[13] These findings raise the questions of what are the structural reasons behind the observed phenomena, and how the field induced strain and other electromechanical properties can be improved further.

For the P(VDF-TrFE) copolymers, it is well known that depending upon the molar content ratios of VDF (x) and TrFE ($1-x$) and on crystallization conditions, the copolymer can crystallize into polar (β phase) and nonpolar (α phase).[19] The ferroelectric β phase consists of the polar packing of zigzag chains, while the α phase is constructed with an arrangement of antiparallel $TGTG'$ chains. For copolymers containing a VDF content of less than about 85%, the ferroelectric-paraelectric (F–P) transition lies below their melting temperature. At temperatures higher than the transition temperature (Curie temperature), the β phase is converted into a paraelectric phase with a random mixture of TG, TG', and $TTTG$ conformations.

[a]Electronic mail: vxb5@psu.edu

The effect of high-energy radiation such as gamma rays and electron beams on polymeric material has been intensively studied over the past several decades.[20–22] It was found that the γ irradiation improves the piezoelectric retention characteristics in uniaxially stretched and poled PVDF films.[23] It was observed that under very specific electron irradiation conditions, the P(VDF-TrFE) copolymer undergoes a solid phase transformation from the ferroelectric phase to a structure similar to the paraelectric phase.[24] Marked changes in the dielectric and mechanical properties in irradiated copolymers were also observed.[25,26] At high electron doses, P(VDF-TrFE) loses all crystallinity and becomes an amorphous polymer.[24] Although these studies provide useful results regarding changes in the crystalline phase and morphology of the VDF based polymers, no attempt has been made to investigate the changes in the ferroelectric response, and to link the structural changes to the changes in functional properties which are of most interest from both applied and fundamental points of view.

In this article, we will examine the evolution in the ferroelectric behavior of P(VDF-TrFE) copolymer with irradiation, and link them to the chemical and morphological changes in the copolymer due to irradiation. It is of great interest to understand the structural reasons for the appearance of relaxor ferroelectric behavior and directions for the further improvement of electro-mechanical properties in the irradiated copolymers. The composition chosen for this study is P(VDF-TrFE), 50/50 mol % copolymer. It was shown that among the compositions available to us and investigated earlier (50/50, 65/35, and 70/30 mol %), it is the only composition that can be converted to the relaxor ferroelectric by 2.55 MeV energy electrons in both stretched and unstretched films. One of the objectives here is to investigate the differences between unstretched and stretched films in various properties pertinent to the relaxor ferroelectric behavior and electromechanical responses in irradiated films. In parallel with the measurement of polarization hysteresis and dielectric properties, wide angle x-ray diffraction, thermal property measurement (differential scanning calorimeter, DSC data), crosslinking coefficient, and elastic modulus were also used to characterize the structural and morphological changes in the irradiated copolymer.

II. EXPERIMENT

The P(VDF-TrFE) 50/50 mol % copolymer powder was supplied by Solvay and Cie, Bruxelles, Belgium, and the copolymer has a mean molecular weight of 200 000. The films were prepared by pressing the copolymer powder between aluminum foil at 215 °C and then cooled down to room temperature, either by quenching the sandwich in ice water or by slow cooling. The stretched films were prepared by uniaxially stretching the quenched films up to five times of their initial length at 25 °C. In order to improve the crystallinity, the stretched films were annealed under the clamped condition in a vacuum oven at 140 °C for 16 h. The electron irradiation was carried out in a nitrogen atmosphere with 2.55 MeV electrons at 95 °C with different irradiation doses, ranging from 40 to 100 Mrad. The film thickness ranged from 25 to 30 μm.

The samples used for dielectric constant and polarization hysteresis measurement were sputtered with gold electrodes on both surfaces. The polarization hysteresis loops were measured using the Sawyer–Tower technique. An external electric field was applied in the form of triangular waveform with a frequency of 10 Hz and an amplitude of 160 MV/m. The dielectric measurements were carried out using a dielectric analyzer (TA instrument, Model No. 2870) in a frequency range from 30 Hz to 100 kHz and in a temperature interval of −60 to 120 °C. The DSC measurements were taken using a differential scanning calorimeter (TA instrument, Model No. 2010) at a scanning rate of 10 °C/min under a nitrogen atmosphere. The x-ray patterns were taken at room temperature (20 °C) using a Scintag diffractrometer (model PAD-V) with Ni filtered Cu $K\alpha$ radiation. The elastic modulus of the films was measured along the film direction (perpendicular to the film thickness) using a Dynamic Mechanical Analyzer (TA instruments, Model No. 2890) in a temperature range from −60 to 90 °C at 10 Hz frequency.

The measurement on the crosslinking factor was performed by measuring the gel content of irradiated films using the American standard test method (D2765-95) by placing the samples inside a Soxhlet Extractor and extracting with the methyl ethyl ketone at its boiling point for 12 h. After measuring the gel content, these films were kept in dimethyl foramide solution for ten days at room temperature in order to reach their equilibrium degree of swelling. The average molecular weight between crosslinks (M_c), which is the representative of the crosslinking density was calculated using the following equations:

$$M_c=\frac{-\rho_2 V_1 \phi_2^{1/3}}{\ln(1-\phi_2)+\phi_2+\chi_1\phi_2^2}, \tag{1}$$

where ρ_2 is the density of the polymer before swelling, V_1 is the molar volume of solvent, χ_1 is the polymer-solvent interaction parameter, and ϕ_2 is the volume fraction of the polymer which is defined as

$$\phi_2=\frac{W_2/\rho_2}{W_1/\rho_1+W_2/\rho_2}, \tag{2}$$

where W_1 and W_2 are the weights of the polymer and solvent, and ρ_1 and ρ_2 are the densities of the polymer and solvent, respectively.[27]

III. EXPERIMENTAL RESULTS AND DISCUSSION

A. Polarization responses, x-ray, DSC, and crosslinking coefficient measurements on irradiated copolymers

1. Polarization responses

Figures 1(a) and 1(b) compare the polarization hysteresis loops measured at room temperature, for unstretched and stretched films, as a function of irradiation dose. As can be seen, for unirradiated films, the polarization level of the stretched film is much higher in comparison to the unstretched films although it will be shown later that there is

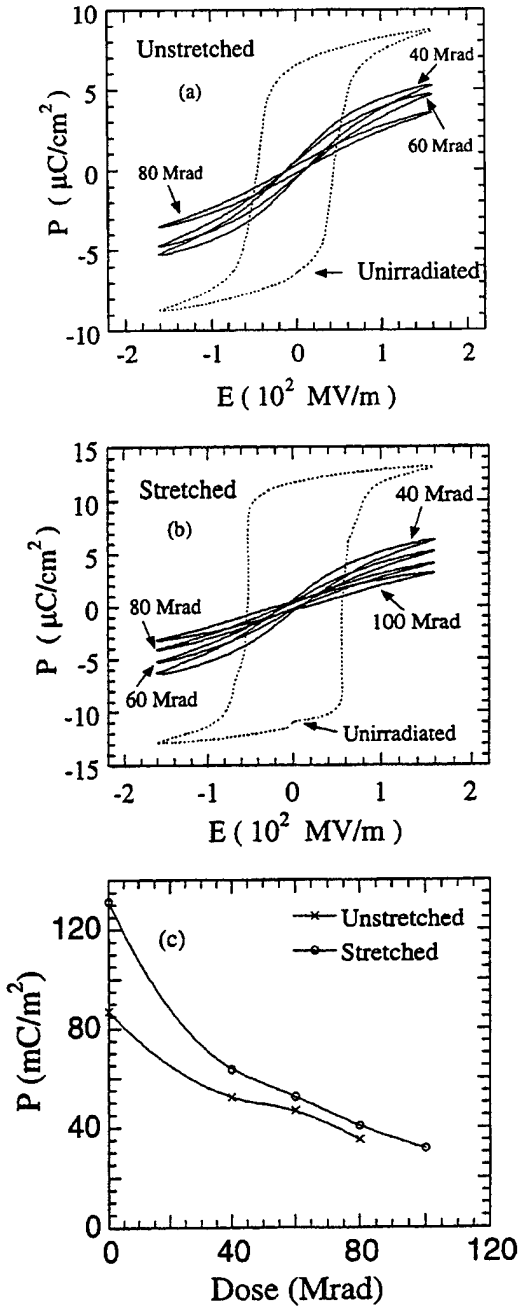

FIG. 1. Change in the polarization hysteresis loops measured for (a) unstretched, and (b) stretched, P(VDF-TrFE) 50/50 mol % copolymer films, unirradiated and irradiated at 95 °C with different doses. (c) Variation of polarization (P) induced under the 160 MV/m electric field [obtained from (a) and (b)] with the irradiation dose.

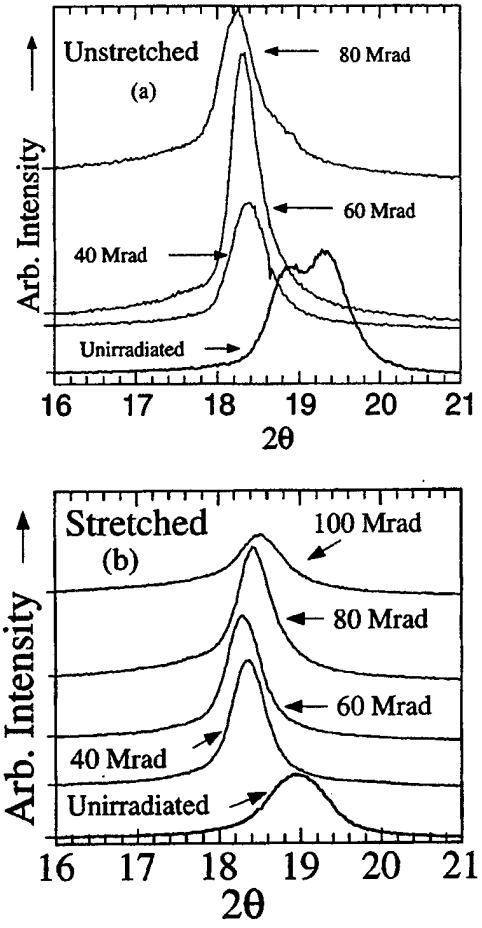

FIG. 2. X-ray diffraction pattern of (a) unstretched, and (b) stretched, P(VDF-TrFE) 50/50 mol % copolymer films irradiated with different doses at 95 °C.

not a large difference in the crystallinity between the two groups of samples. The result agrees with earlier studies and it arise due to a higher degree of crystalline orientation in the stretched films than in unstretched ones.[28]

After irradiation, the polarization hysteresis is reduced markedly for both unstretched and stretched films. The change of the field induced polarization P under 160 MV/m field as a function of dose is summarized in Fig. 1(c). For irradiated films, it can be seen clearly that there is not a large difference in the induced polarization level between the stretched and unstretched ones after 40 Mrad irradiation. This is in sharp contrast with the unirradiated films where the stretched film exhibits a substantially higher polarization compared with the unstretched one. These results show that the enhancement of the polarization due to alignment of crystallites induced by stretching is nearly eliminated as a consequence of the irradiation. On the other hand, both DMA data (Figs. 9 and 10) and electric field induced strain data[13] show that the irradiation does not change the chain orientation markedly in stretched samples, at least in the range of 40 and 60 Mrad doses. Therefore, the large reduction of the polarization in stretched films due to irradiation suggests that the irradiation randomizes the crystallite orientation in directions perpendicular to the chain stretching direction.

2. X-ray results

Figures 2(a) and 2(b) present x-ray patterns of (200) and (110) reflections obtained from unstretched and stretched films irradiated under different doses. As expected, the unirradiated unstretched films exhibit two peaks at 4.72 and 4.59 Å (2θ=18.79° and 19.28°). The peak at 4.72 Å is from the hexagonal packing of 3/1-helical chains generated by TG and TG' defects, which are due to the presence of domain patterns and the second is due to similarly packed trans-

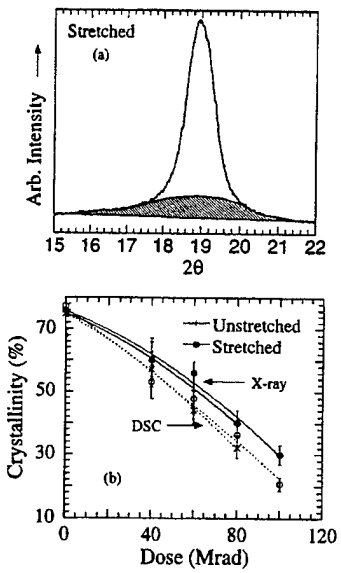

FIG. 3. (a) X-ray scan from unirradiated, stretched P(VDF-TrFE) 50/50 mol % copolymer films used to illustrate the calculation of crystallinity. The amorphous and crystalline regions were separated by fitting the Lorentzian function and are represented by shaded and nonshaded area respectively. (b) Change in the crystallinity with the irradiation dose calculated from x-ray [Figs. 2(a) and 2(b)] and DSC [Figs. 4(a) and 4(b)]. The symbols here are the data points and lines are drawn to guide points.

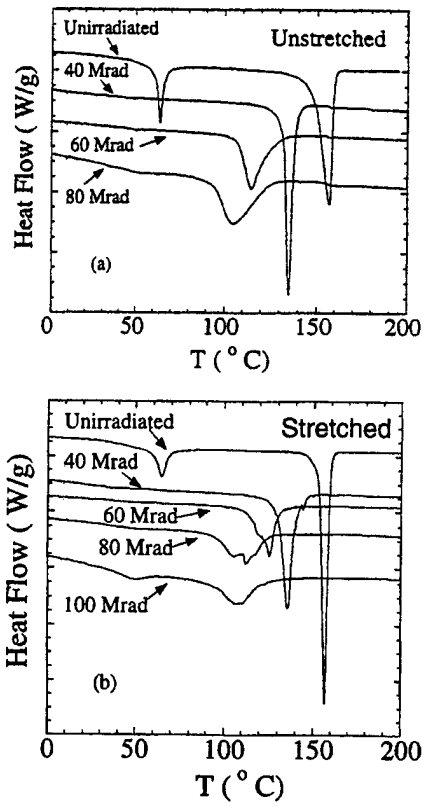

FIG. 4. DSC thermogram of (a) unstretched, and (b) stretched, P(VDF-TrFE) 50/50 mol % copolymer unirradiated, and irradiated with different doses at 95 °C.

planar chains.[19,29] However, the stretched films show only one broad peak at 4.68 Å spacing and therefore, it indicates that the stretching not only eliminates the chain segments containing 3/1 helical conformation, but also packs more closely the chain segments that already are in the trans-planar conformation.[30] The similar effect can also be observed by poling the unstretched films.[30] The broadening of the x-ray peak, in unirradiated films after stretching [Fig. 2(b)], suggests that in addition to reduction in the crystallite sizes, stretching also induces additional domain boundaries parallel to the polymer chains. This results in a reduction in the size of the coherent x-ray diffraction region for the (200) and (110) reflections.

After 40 Mrad of irradiation, only one peak is observed at a lower angle for both the unstretched and stretched films and thus clearly indicates the expansion of the lattice due to the introduction of defects in the crystalline phase during the irradiation. This is responsible for the observed change in the polarization hysteresis from a typical normal ferroelectric hysteresis loop to a slim polarization loop. After 60 Mrad irradiation, the peak appears at 4.84 Å for both unstretched and stretched films. The corresponding lattice spacing is close to the paraelectric phase as determined from x-ray data taken above the Curie temperature for unirradiated copolymer films and therefore, indicate the conversion of ferroelectric to a paraelectric-like phase at this dose.[30] It should be pointed out that, although macroscopically (from x-ray diffraction), the phase after irradiation is paraelectric like, the observed broad dielectric constant peak with Vogel–Fulcher dielectric dispersion behavior suggests that the phase resembles a relaxor ferroelectric with local polar regions (polar glass system).[11] The x-ray peaks become relatively more intense after 60 Mrad irradiation for unstretched films and after 80 Mrad irradiation for stretched films in comparison to the unirradiated films and the films irradiated with lower doses. The increase in the coherence length of x-ray diffraction is due to the disappearance of the macroscopic ferroelectric ordering.

Interestingly, at higher doses the x-ray peak moves back to higher angle and concomitantly the peak broadens, indicating the reduction of the crystallite size. The cause for the contraction in the lattice spacing between polymer chains is unclear. It might be related to the nature of the defects induced during the irradiation, which depend on the boundary conditions of the crystalline-amorphous interface and crystallite size. At high irradiation doses, the crystallite size becomes quite small and the shape of the x-ray peak becomes Lorentz type suggesting that the crystallite-amorphous interface is also quite diffused. In addition, peak area analysis, as shown in Fig. 3(a), indicates that at doses of 80 Mrad or higher, the crystallinity of the copolymer has been reduced to less than half as compared with the unirradiated films [Fig. 3(b)].

3. DSC results

In order to further quantify the change in the transitional behavior in irradiated samples, a DSC measurement was conducted on these samples. As expected, the thermal properties of the copolymer undergo a significant change after irradiation. Figures 4(a) and 4(b) summarize the DSC results obtained from unstretched and stretched copolymer films, re-

spectively. Being ferroelectric in nature, before irradiation both unstretched and stretched films exhibit two peaks. The peak at 63 °C is due to ferroelectric to paraelectric (F–P) transition, while the peak at 157 °C is due to the melting of crystals.[31] For unirradiated films, the crystal melting peak for stretched films is sharper and more intense than unstretched films and thus, reflects a higher crystalline ordering for stretched films. After the irradiation, the temperature and the enthalpy of the melting peak decrease continuously with the irradiation dose for both unstretched and stretched films. Assuming that the enthalpy of the melting is directly proportional to the crystallinity in the sample, the change of crystallinity with dose can be deduced[32,33] and is presented in Fig. 3(b). Clearly, the change of crystallinity with the dose acquired from the x-ray data, is consistent with that from the DSC data, although the DSC data yield a slightly lower crystallinity.

It is well known that the morphology of P(VDF-TrFE) copolymers is that of crystallites embedded in an amorphous matrix, which is analogous to a composite structure.[4] It is interesting to compare the results obtained here on the polarization and crystallinity (approximately the volume fraction of the crystallites in the polymer). Figure 5(a) presents the polarization P induced by 160 MV/m field as a function of crystallinity, which is taken from the averaged value of the DSC and x-ray data. Apparently, the initial drops of the crystallinity at low dose range (40 Mrad) causes a large reduction in the polarization in both stretched and unstretched films. As has been pointed out, the initial precipitant decrease of the polarization in the stretched films is also partly caused by the reduction in the crystallite orientation in the irradiation process. Therefore, if the crystallinity of the polymer under 40 Mrad dose can be raised, due to the high ratio of the polarization/crystallinity for the copolymer studied here at this particular dose the polarization level can be improved markedly, especially in stretched films.

For a composite system, there are many relationships describing the dependence of the dielectric properties of a composite with the properties of constituents. It was found that the logarithmic law of mixing of composites can fit most of the experimental data well,[19]

$$\log P = \nu_c \log P_c + (1-\nu_c)\log P_a, \tag{3}$$

where P is the total polarization, P_c and P_a are the averaged polarizations of the crystallites and amorphous regions, respectively, and ν_c is the crystallinity. The fitting of the data in Fig. 5(a) is shown in figure 5(b) where for the stretched films the data point from the unirradiated stretched film is not included because of its high crystallite orientation effect. Clearly, Eq. (3) fits the data quite well for both stretched and unstretched films. Surprisingly, the slopes of the curves from the two sets of data are nearly the same, indicating that P_c/P_a is nearly the same for both stretched and unstrectched films. The parameters obtained in the fitting are, $P_c = 144.5\,\mathrm{mC/m^2}$ and $P_a = 15.5\,\mathrm{mC/m^2}$ for unstretched films, while for stretched films, $P_c = 151.6\,\mathrm{mC/m^2}$ and $P_a = 18.4\,\mathrm{mC/m^2}$. The fact that P_c from irradiated stretched films is only about 5% higher than that in unstretched films confirms that stretching does not have a marked effect on the polarization level in irradiated films.

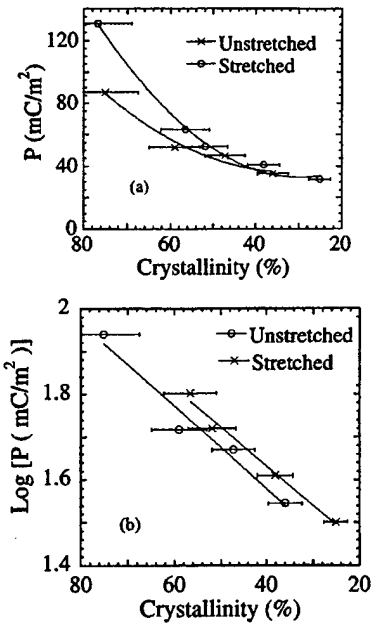

FIG. 5. (a) Change in polarization (P) induced by 160 MV/m electric field with the averaged value of crystallinity obtained from the x-ray and DSC data [Fig. 3(b)]. (b) Fitting of the logarithmic law for unstretched and stretched P(VDF-TrFE) 50/50 mol % copolymer films after 40 Mrad irradiation at 95 °C. The solid line is the fitting and points are the experimental data obtained from (a).

In addition to the reduction of the crystallinity, the DSC peak associated with melting of crystals also broadens with doses. This indicates the presence of broad distribution in crystallite sizes and crystal ordering in irradiated films, which is due to the lattice defects and crosslinking in the copolymer.

In contrast to the DSC peak of the melting process for unirradiated films, the peak of F–P transition for the unstretched film is sharper with a higher transition enthalpy in comparison with the stretched film. This shows that the stretching process does introduce defects in the crystalline region, which have a much stronger effect on the polar ordering, but have a minimum effect on the crystalline ordering.

Consistent with the polarization data where there is very weak hysteresis for film irradiated with 40 Mrad dose, the DSC data show that the F–P phase transition peak almost disappears upon 40 Mrad irradiation for both stretched and unstretched films. Interestingly, a broad DSC peak reappears at temperatures near the original F–P transition peak position of unirradiated films when the dose is increased to 80 Mrad and beyond. This is consistent with the x-ray data where at high doses the x-ray peak moves back to higher angle. The finding here indicates that the structural defects introduced by irradiation in the crystalline region depends on the crystallite size and also the boundary conditions at the crystalline-amorphous interface.

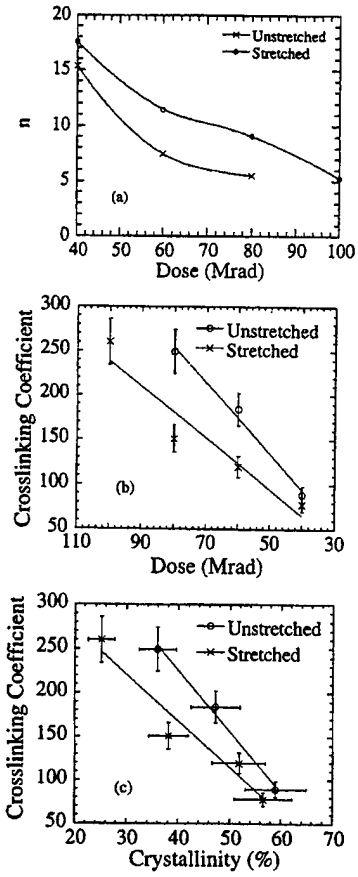

FIG. 6. (a) Variation in the number of repeating units (n) between two crosslinks for unstretched and stretched P(VDF-TrFE) 50/50 mol % copolymer films irradiated with different doses at 95 °C. (b) Change in the crosslinking coefficient with (b) doses and (c) averaged value of crystallinity obtained from the x-ray and DSC data [Fig. 3(b)], for unstretched and stretched P(VDF-TrFE) 50/50 mol % copolymer films irradiated at 95 °C. The solid lines are drawn to guide eyes.

4. Crosslinking coefficient measurements results

Crosslinking coefficient (or crosslinking density) was measured to provide information on the effect of crosslinking on the properties investigated here. Figure 6(a) presents the change in the number of repeating units (n) between two crosslink points along the chain in unit of $-CH_2-CF_2-CHF-CF_2-$as a function of dose for both stretched and unstretched films. The lower the value of n corresponds to the greater value of the crosslinking density. Clearly, with the same dose, the crosslinking density is much lower in the stretched films compared with unstretched films. In Fig. 6(b), the crosslinking coefficient, which is the number of crosslink per chain, is presented as a function of irradiation dose. For both unstretched and stretched films, the crosslinking coefficient increases with dose. The rate of the increase in the crosslinking coefficient for the stretched films at doses below 80 Mrad is a much lower than for the unstretched films. This indicates that the chain orientation introduced by stretching reduces the rate of crosslinking in the irradiation process. However, at doses from 80 to 100 Mrad, the rate of the crosslinking coefficient with dose for stretched films becomes higher than that for unstretched films. As has been shown, irradiation randomizes the orientation (crystallites and polymer chains) induced by stretching, at high dosages the local chain orientation in stretched films may not be very much different from that in unstretched films.

Presented in Fig. 6(c) is the crosslinking coefficient as a function of crystallinity for the two sets of samples investigated. For both unstretched and stretched films, the crosslinking coefficient increases in proportion to the decrease in the crystallinity. Furthermore, even with the same crystallinity, the crosslinking coefficient of unstretched films is higher than that in stretched films. In other words, the reduction of the crystallinity in the copolymer under irradiation is not directly controlled by the crosslinking density, but it is expected that the crosslinking process has a significant role here in the conversion from the crystalline to amorphous phase.

The influence of crosslinking density on the ferroelectric behavior and polar ordering in the crystalline region is not clear. From the data presented, it seems that as far as the field induced polarization is concerned, the effect of crosslinking density is not significant and direct. However, the crosslinking density should have a direct effect on the crystallite size, which may affect the polar response in the copolymer when the size of crystallites becomes small.

B. Dielectric and mechanical responses and relaxations

1. Dielectric responses

To further elucidate the change in the ferroelectric related properties in the irradiated films, the weak field dielectric constant was measured on irradiated films as a function of irradiation dose. Figures 7(a) and 7(b) show the temperature dependence of the dielectric constant at 1 kHz for the films irradiated for different doses. Before irradiation, the dielectric constant for stretched films is higher than that of unstretched films, which is consistent with the polarization result and arises due to the higher dipolar orientation in the stretched films. After the irradiation, the dielectric peak of both unstretched and stretched films shifts towards a lower temperature in comparison to respective unirradiated film and therefore, increases the room temperature dielectric constant remarkably. In addition, the dielectric peak after irradiation becomes broader and exhibits a strong frequency dispersion [Fig. 8(a)]. As shown in Figs. 8(b) and 8(c) for both stretched and unstretched irradiated films, the dispersion follows Vogel–Fulcher law, an empirical law which holds for the systems undergoing freezing below certain temperature, T_f, such as glassy and relaxor ferroelectric materials,[15]

$$f=f_0 \exp\left[\frac{-U}{k(T-T_f)}\right], \tag{4}$$

where T is the dielectric constant peak temperature, f is the corresponding frequency, and k is the Boltzmann constant. The fitting parameters obtained are summarized in Table I. If we regard that the Vogel–Fulcher law describes a thermally activated process with the activation energy approaching to infinity at T_f, Eq. (4) can be rewritten as, $f=f_0 \times \exp(-\alpha/kT)$, where for the polarization freezing process, $\alpha=UT/(T-T_f)$ which leads to Vogel–Fulcher law. Hence, U is directly related to the activation energy α.[15] The param-

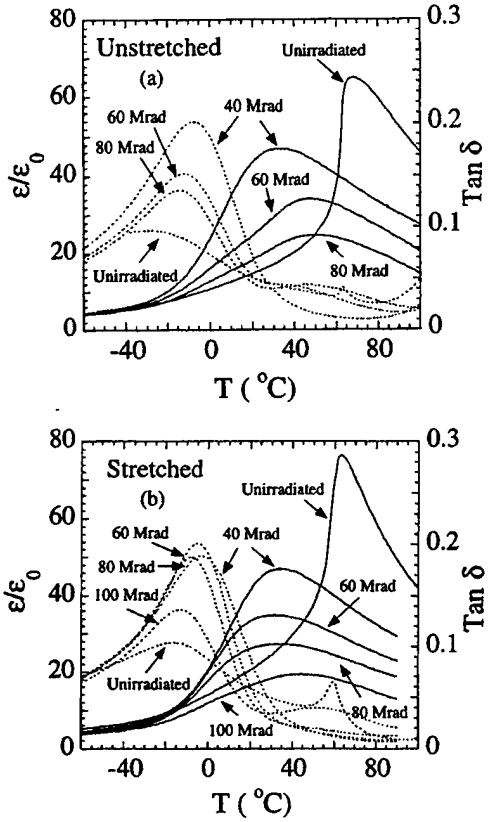

FIG. 7. Change in the dielectric constant (solid lines) and tangent loss (broken lines) measured at 1 kHz frequency as a function of temperature for P(VDF-TrFE) 50/50 mol % (a) unstretched, and (b) stretched films irradiated at 95 °C with different doses.

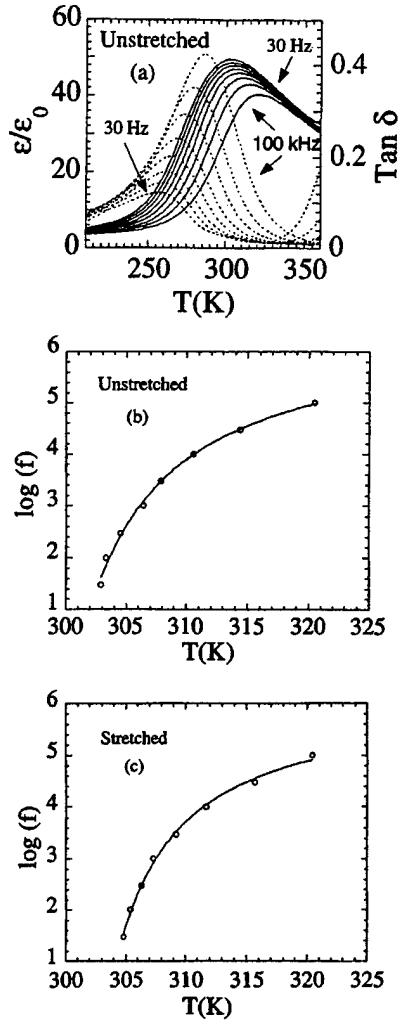

FIG. 8. (a) Dielectric constant (solid lines) and dielectric loss (broken lines) as a function of temperature for unstretched P(VDF-TrFE) 50/50 mol % copolymer films after 40 Mrad irradiation at 95 °C. The measuring frequencies (from top to bottom for dielectric constant and from bottom to top for dielectric loss) 30 Hz, 100 Hz, 300 Hz, 1 kHz, 3 kHz, 10 kHz, 30 kHz, and 100 kHz. Fitting of Vogel–Fulcher law for (b) unstretched, and (c) stretched P(VDF-TrFE) 50/50 mol % copolymer films after 40 Mrad irradiation at 95 °C. The solid line is the fitting and the circles are the experimental data.

eter U for unstretched films and stretched films shows quite different values and it is higher in unstretched films than that in the corresponding stretched films. In addition, as the dose increases, U decreases monotonically.

Therefore, both the polarization and dielectric constant data suggest that the irradiation destroys the ferroelectric ordering and breaks the macro-polar domains into micropolar regions. The observed V–F type relaxation suggests that these local polar regions couple to each other and this coupling becomes stronger with the decreasing temperature. The decrease of U with the dose indicates the reduction in the polar-region size with irradiation. The observed upward shifting of T_f at high dosage suggests that the average polar ordering in these regions increases, which is consistent with the x-ray and DSC data presented.

2. Elastic responses

For electromechanical transduction applications, mechanical properties are of great importance. They also provide valuable information on the structural and relaxation processes in the material. Presented in Figs. 9 and 10 are the elastic modulus of unstretched and stretched films respec-

TABLE I. Fitting parameters of the V–F law for P(VDF-TrFE) 50/50 mol % irradiated copolymer.

	Unstretched films			Stretched films		
Dose	Crystallinity	$U(10^{-3}$ eV)	T_f(K)	Crystallinity	$U(10^{-3}$ eV)	T_f(K)
40	0.59	3.6	294.5	0.57	2.4	298.8
60	0.47	2.0	314	0.52	1.2	299.3
80	0.36	1.62	310	0.38	0.55	304
100				0.25	0.47	316

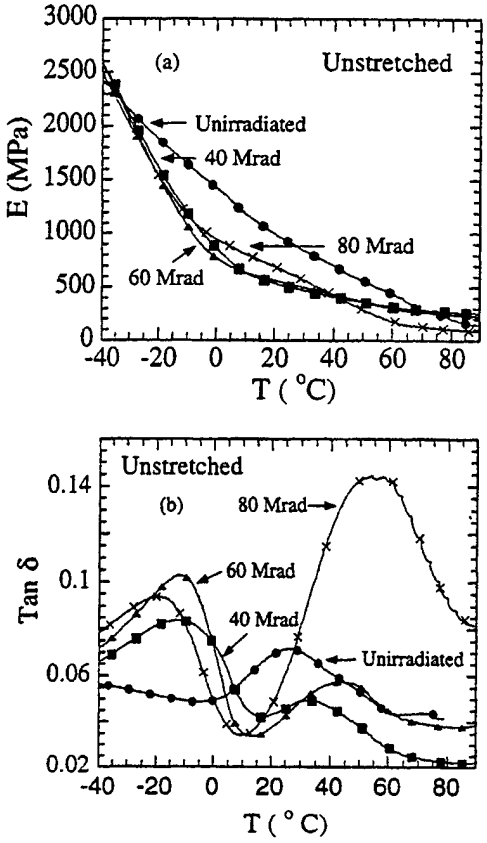

FIG. 9. Change in the (a) elastic modulus and (b) mechanical loss as a function of temperature for unstretched P(VDF-TrFE) 50/50 mol % copolymer, unirradiated, and irradiated at 95 °C with different irradiation doses.

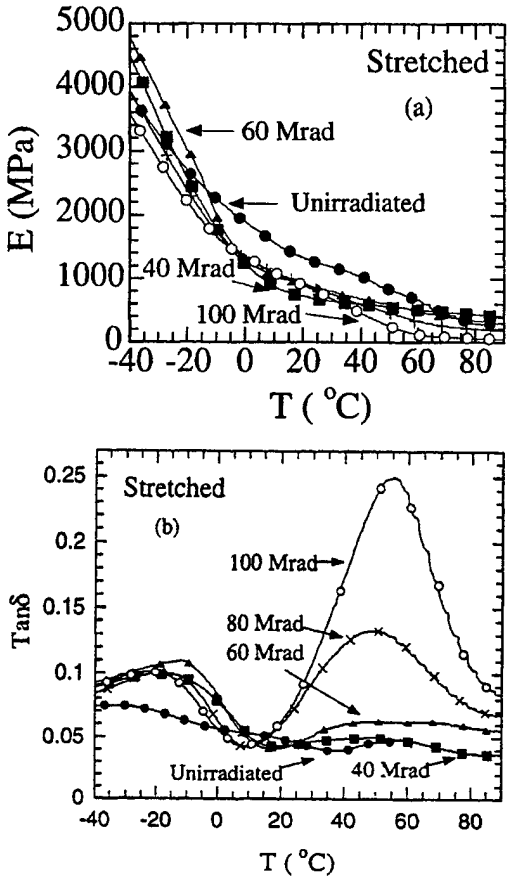

FIG. 10. Change in the (a) elastic modulus and (b) mechanical loss as a function of temperature for stretched P(VDF-TrFE) 50/50 mol % copolymer, unirradiated, and irradiated at 95 °C with different irradiation doses.

tively. For stretched films, only the modulus along the stretching direction is shown. As expected, stretched films [Fig. 10(a)] exhibit higher elastic modulus in the stretching direction in comparison to the unstretched films [Fig. 9(a)], which is due to the alignment of chains. After the irradiation, the elastic modulus is found to decrease with the irradiation dose in most of the temperature region. However, at low temperatures (below the glass transition, about −30 °C), due to the crosslinking, the irradiated films exhibit higher modulus than unirradiated films. It is also interesting to note that for unstretched films irradiated with 40 and 60 Mrad and for stretched films irradiated with 40 Mrad dose, at temperatures above 10 and to 90 °C, which is the upper temperature range measured, the elastic modulus shows a very weak temperature dependence compared with unirradiated films. Above these doses, the films exhibit an increased room temperature modulus, presumably due to increased crosslinking density. The modulus decreases with temperature with a noticeable relaxation step at temperatures near 40 °C. In addition, after the irradiation, the elastic modulus of stretched films along the stretching direction remains higher compared with unstretched films (except at 100 Mrad).

We now discuss the relaxation processes in the films studied where the data from both the mechanical and dielectric losses will be used. In P(VDF-TrFE) copolymers, it is known that several relaxations exist, which depend on the molecular relaxations in amorphous, crystalline, and at the crystal-amorphous interfaces.[34] Dielectric responses are from those relaxations in which motions of dipoles are involved, while the motions related to mechanical relaxations can be due to the non-polar processes. Therefore, as shown in an earlier study, the loss peak from the mechanical data may not be at the same temperature and frequency position as that from the dielectric data.[35]

In the temperature range studied, the mechanical tangent loss exhibits two relaxation peaks. Before irradiation two weak peaks around −40 °C (β) and 30 °C (α) are observed in unstretched films, which have been attributed in earlier studies to the molecular relaxation in amorphous and crystalline regions and/or crystalline amorphous interface boundaries [Fig. 9(b)]. While for unirradiated stretched films, these peaks are much weaker [Fig. 10(b)] due to the alignment of polymer chains. These mechanical relaxation peaks may be compared with the dielectric loss peaks [Figs. 7(a) and 7(b)]. A broad dielectric loss peak can be seen at temperatures near −30 °C and a weak sharp peak at near 65 °C for unstretched films. For stretched films, a broad dielectric loss peak is at about −20 °C and a relatively sharp loss peak at 60 °C. We believe that the sharp peak seen in the dielectric loss is associated with the F–P transition, which is not detected in the mechanical loss data and is also different from the high temperature broad relaxation seen in the mechanical loss data.

For irradiated films, the observed low temperature mechanical loss peak is mainly due to the glass transition in the polymer while the dielectric loss peak seems to be dominated by the frozen process of the polar regions, which diminishes in size as the dose increases (or the crystallinity decreases). The contribution of the glass transition to the dielectric loss is much weaker compared to the frozen process of the polar regions. On the other hand, the frozen process of the polar regions does not have a marked effect on the elastic properties, which is analogous to the DSC results.

The high temperature mechanical loss peak (at >30 °C) does not show much increase for both stretched and unstretched films at doses of 40 and 60 Mrad [Fig. 9(b) and 10(b)] compared with unirradiated films. A large increase of loss peak is seen for films irradiated at 80 and 100 Mrad. In contrast, the dielectric loss peak for this relaxation is very weak. These results suggest that the relaxation process associated with this peak (α) is mainly due to the motions involving large chain segments. Therefore, at high doses with increased crosslinking density and diminishing crystallinity, a strong mechanical relaxation will occur resulting in a drop of the elastic modulus with a temperature, as observed near 40 °C for unstretched films irradiated with 80 Mrad dose, and stretched films irradiated with 80 and 100 Mrad doses, and corresponding strong mechanical loss peaks.

IV. SUMMARY

The experimental results presented can be summarized as the following:

(1) The high-energy electron irradiation converts the polarization loop of the copolymer studied from the one with large hysteresis to a slim loop. The dielectric dispersion in the irradiated samples can be described well by the V–F law for both stretched and unstretched samples.

(2) Although in unirradiated samples, the polarization level and dielectric constant can be substantially increased by stretching but for irradiated films at doses above 40 Mrad, the induced polarization level does not show a large difference between stretched and unstretched films.

(3) In both stretched and unstretched samples, the dependence of the induced polarization P on crystallinity ν_c can be described quite well by the logarithmic law of two component composites, indicating that the morphology of the irradiated copolymer consists of micropolar regions embedded in an amorphous matrix. The results also indicate that because of the high ratio of $\Delta P/\Delta \nu_c$ at the low dose region, an increase in the crystallinity will result in a large increase in P.

(4) Although the irradiation nearly eliminates the enhanced polarization and dielectric response induced by stretching, the elastic modulus of stretched films remains higher compared with unstretched ones after the irradiation (at least for doses below 80 Mrad, indicating the difference in the molecular segment motions to the mechanical and electric responses. Similar differences between the electric and mechanical responses are also observed for the molecular relaxation processes in the copolymer.

(5) For unirradiated films, stretching improves the crystalline ordering while reduces the ferroelectric ordering as suggested by the DSC and x-ray data.

(6) Stretching can have a marked effect in reducing the crosslinking rate in the irradiation process and correspondingly, the crosslinking density of stretched samples is lower than that of unstretched samples. On the other hand, the crystallinity of stretched samples is nearly the same as that of unstretched films at the same irradiation dose. The reduction of crystallinity with irradiation does not have a direct link to the crosslinking process.

Therefore, during irradiation the changes in the structure and phase transition properties are mainly controlled by the two processes: one is the introduction of polarization defects which is responsible for the conversion from a normal ferroelectric to a relaxor ferroelectric phase and the other is the amorphization of the copolymer, which reduces the overall polar responses in the material. How to reduce the rate of the second process is crucial in order to further improve the electromechanical responses in the copolymer.

ACKNOWLEDGMENTS

The authors wish to thank Z-Y. Cheng, R. Ting, and T. Ramontowski for stimulating discussions. This work was supported by the Office of Naval Research through Grant No. N00014-97-1-0900 and the National Science Foundation through Grant No. ECS-9710459.

[1] T. Furukawa, Adv. Colloid Interface Sci. **71-72**, 183 (1997).
[2] K. Tashiro and M. Kobayashi, Phase Transit. **18**, 213 (1989).
[3] A. J. Lovinger, G. E. Johnson, H. E. Bair, and E. W. Anderson, J. Appl. Phys. **56**, 2412 (1984).
[4] T. T. Wang, J. M. Herbert, and A. M. Glass, *The Application of Ferroelectric Polymers* (Blackie, Chapman and Hall, New York, 1988).
[5] H. Ohigashi, K. Omote, and T. Gomyo, Appl. Phys. Lett. **66**, 3281 (1995).
[6] K. Omote, H. Ohigashi, and K. Koga, J. Appl. Phys. **81**, 2760 (1997).
[7] J. S. Green, B. L. Farmer, and J. F. Rabolt, J. Appl. Phys. **60**, 2690 (1986).
[8] H. Ohigashi and K. Koga, Jpn. J. Appl. Phys., Part 2 **21**, L455 (1982).
[9] M. A. Marcus, IEEE Trans. Electr. Insul. **EI-21**, 519 (1986).
[10] V. Bharti, T. Kaura, and R. Nath, IEEE Trans. Dielectr. Electr. Insul. **2**, 1106 (1995).
[11] Q. M. Zhang, V. Bharti, and X. Zhao, Science **280**, 2101 (1998).
[12] V. Bharti, X-Z Zhao, and Q. M. Zhang, Mater. Res. Innovat. **2**, 57 (1998).
[13] Z-Y Cheng, T.-B. Xu, V. Bharti, S. Wang, and Q. M. Zhang, Appl. Phys. Lett. **74**, 1901 (1999).
[14] H. Vogel, Z. Phys. **22**, 645 (1921); G. S. Fulcher, J. Am. Ceram. Soc. **8**, 339 (1925).
[15] D. Viehland, S. J. Jang, and L. E. Cross, J. Appl. Phys. **68**, 2916 (1990).
[16] L. E. Cross, Ferroelectrics **151**, 305 (1994).
[17] L. E. Cross, Jpn. J. Appl. Phys., Part 1 **34**, 2525 (1995).
[18] K. Uchino, *Piezoelectric Actuators and Ultrasonic Motors* (Kluwer, Dordrecht, 1996).
[19] H. S. Nalwa, *Ferroelectric Polymers* (Dekker, New York, 1995), Chaps. 2 and 11.
[20] B. J. Lyons, Radiat. Phys. Chem. **45**, 159 (1995).
[21] A. Chapiro, *Radiation Chemistry of Polymeric Systems* (Interscience, New York, 1962).
[22] A. Charlesby, *Atomic Radiation and Polymers* (Pergamon, London, 1960).
[23] T. T. Wang, Ferroelectrics **41**, 213 (1982).
[24] A. J. Lovinger, Macromolecules **18**, 910 (1985).
[25] B. Daudin, M. Dubus, and J. F. Legrand, J. Appl. Phys. **62**, 994 (1987).
[26] F. Macchi, B. Daudin, J. Hillairet, J. Lauzier, J. B. N'goma, J. Y. Cavaille, and J. F. Legrand, Nucl. Instrum. Methods Phys. Res. B **46**, 334 (1990).
[27] E. A. Collins, J. Bares, and F. W. Billmeyer, Jr., *Experiments in Polymer Science* (Wiley, New York, 1973).

[28] V. Bharti, T. Kaura, and R. Nath, IEEE Trans. Dielectr. Electr. Insul. **4**, 738 (1997).
[29] K. Tashiro, K. Takano, M. Kobayashi, Y. Chatani, and H. Tadokoro, Ferroelectrics **57**, 297 (1984).
[30] A. J. Lovinger, T. Furukawa, G. T. Davis, and M. G. Broadhurst, Polymer **24**, 1233 (1983).
[31] T. Yamada, T. Ueda, and T. Kitayama, J. Appl. Phys. **52**, 948 (1981).
[32] T. Yagi, Polym. J. (Tokyo) **12**, 9 (1980).
[33] K. Nakagawa and Y. Ishida, J. Polym. Sci., Polym. Phys. Ed. **11**, 2143 (1973).
[34] T. Yagi, M. Tatemato, and J. Sako, Polym. J. (Tokyo) **12**, 209 (1980).
[35] Q. M. Zhang, J. Su, C. H. Kim, R. Ting, and R. Capps, J. Appl. Phys. **81**, 2770 (1997).

APPENDIX 22

Structural, Conformational, and Polarization Changes of Poly(vinylidene fluoride−trifluoroethylene) Copolymer Induced by High-Energy Electron Irradiation

Haisheng Xu,* G. Shanthi, V. Bharti, and Q. M. Zhang

Materials Research Laboratory, The Pennsylvania State University, University Park, Pennsylvania 16802

T. Ramotowski

Naval Undersea Warfare Center, Newport, Rhode Island 02841

Received November 22, 1999

ABSTRACT: Structural and molecular conformation changes of high-energy electron-irradiated poly(vinylidene fluoride−trifluoroethylene) 50/50 copolymer have been investigated by means of FT-IR spectroscopy, X-ray diffraction, and cross-linking density measurement and are compared with the change of polarization hysteresis loops with dose. Although in general the irradiation reduces the macroscopic polar ordering, which leads to the eventual disappearance of the remanent polarization in the copolymer at room temperature, the change in the mesoscopic structure and molecular conformation with dose is not monotonic. In the intermediate dose range, there is a reversal of the change of local ordering with dose, as revealed by the decrease of the fraction of the TG conformation in the copolymer and contraction of the lattice in directions perpendicular to the polymer chain with dose, which could be caused by the high cross-linking density due to irradiation. In addition, for irradiated polymers at doses above 30 Mrad, no transition behavior with temperature is observed in the FT-IR spectra, consistent with the early experimental results that the ferroelectric−paraelectric transition has been eliminated by irradiation.

I. Introduction

Poly(vinylidene fluoride) (PVDF) and its copolymers with trifluoroethylene (P(VDF−TrFE)) have attracted a great deal of attention because of their relatively high dielectric constant and piezoelectric response compared with those of other known polymers.[1] In the past several decades, the structures of PVDF homopolymer and P(VDF−TrFE) copolymers have been studied widely using analytical tools such as X-ray diffraction, infrared and Raman spectroscopy, and the nuclear magnetic resonance method.[2−12] From these studies, it has been established that depending on the crystallization conditions, such as crystallization temperature, casting solvent, mechanical stress, external electric field, etc., these polymers can crystallize into at least four types of crystal forms: named forms I(β), II(α), III(γ), and IV (polar form II, IIp, or δ). It has also been established that there exist three basic chain conformations: all-trans planar zigzag (TTTT), trans−gauche−trans−gauche′ (TGTG′), and TTTGTTTG′ in these crystalline phases. Among these crystalline forms, the β-phase (or form I), which has all-trans chains packed with their dipoles pointing in the same direction, is the most interesting and important one because it exhibits a strong ferroelectric behavior. When cooled from the melt, PVDF homopolymer will crystallize into the antipolar α-phase, in which the molecules are in a distorted TGTG′ conformation. By mechanically drawing the polymer, the α-phase can be converted into the β-phase, which is accompanied by a large change of molecular conformation. On the other hand, for copolymers with VDF between 50 and 85 mol %, the β-phase will form directly from the melt. One interesting feature for the copolymers in this composition range is the ferroelectric−paraelectric (F−P) transition at a temperature below the melting temperature of the polymer.[10,13] Above the F−P transition temperature, the polymer loses its polarization before melting (forming a paraelectric phase). One of the most characteristic features of this transition is a large change of conformation of polymer chains between the trans and gauche forms. Such conformational changes also cause large changes of physical properties of the polymer.

Recently, we reported that high-energy electron-irradiated P(VDF−TrFE) copolymers exhibit exceptionally high electrostrictive response,[14] which will have a great impact on electromechanical transducer, sensor, and actuator applications.[15,16] Obviously, these large response behaviors in the irradiated copolymers should originate from a P(VDF−TrFE) copolymer structure, which is quite different from that before the irradiation. It is also interesting to examine what other changes are taking place during the irradiation. In the present paper, we investigate the structural and conformational changes of the irradiated P(VDF−TrFE) 50/50 copolymer at different doses utilizing FT-IR spectroscopy and X-ray diffraction. In addition, the cross-linking density was also measured as a function of the electron dose. For comparison, polarization hysteresis loops were also recorded for the copolymer in the corresponding dose range.

II. Experimental Section

The samples used in the present study are P(VDF−TrFE) copolymers with 50 mol % VDF content, supplied by Solvay and Cie, Belgium, and the weight-average molecular weight of the polymer is about 200 000. Samples of various thicknesses were prepared for different measurements using the solution cast method. For the polarization hysteresis loop and X-ray measurements, the typical sample thicknesses were in the range between 20 and 30 μm. For FT-IR spectroscopy

10.1021/ma9919561 CCC: $19.00
Published on Web 04/22/2000

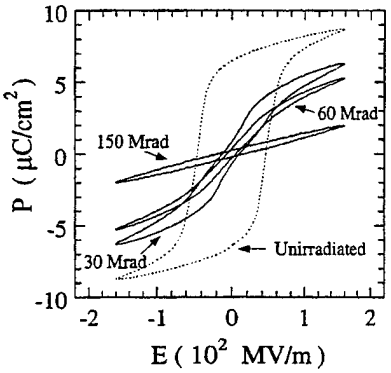

Figure 1. Polarization hysteresis loops of P(VDF–TrFE) 50/50 copolymer after different irradiation doses. The irradiation was carried out at 120 °C with 2.55 MeV electrons.

measurement, the sample thickness was 7 μm. The films were annealed at 140 °C for 4 h under vacuum and then cooled slowly to room temperature. The irradiation was carried out at 120 °C under a nitrogen atmosphere using electrons of 2.55 MeV energy with different doses.

The polarization hysteresis loops were measured using a Sawyer–Tower technique. The FT-IR spectra were obtained using a BIO-RAD WIN Fourier transform IR spectrophotometers in the wavenumber range 4000–400 cm^{-1}. The high-temperature FTIR spectra were measured using a high-temperature optical cell. The X-ray patterns were measured on a Scintag diffractometer (model PAD-V) with Ni-filtered Cu Kα radiation. The samples for polarization hysteresis measurement were sputtered with gold electrodes on both surfaces.

The measurement of the cross-linking factor was performed by measuring the gel content of each sample using the American standard test method (ASTM D2765-95) by placing the sample inside a Soxhlet extractor and extracting with methyl ethyl ketone at its boiling point for 12 h. After measuring the gel content, these films were kept in dimethylformamide solution for 10 days at room temperature to reach their equilibrium degree of swelling. The average molecular weight between cross-links (M_c) is calculated using the following equation

$$M_c = \frac{-\rho_2 V_1 \phi_2^{1/3}}{\ln(1-\phi_2) + \phi_2 + \chi_1 \phi_2^2} \quad (1)$$

where V_1 is the molar volume of the solvent, χ_1 is the polymer–solvent interaction parameter, and ϕ_2 is the volume fraction of the polymer in the swelling:

$$\phi_2 = \frac{W_2/\rho_2}{W_1/\rho_1 + W_2/\rho_2} \quad (2)$$

where W_1 and W_2 are the weight of the polymer and solvent and ρ_1 and ρ_2 are the density of polymer and solvent, respectively.

III. Results and Discussion

3.1. Structural and Conformational Changes with Irradiation. To illustrate the effect of the high-energy electron irradiation on the ferroelectric behavior of the copolymer, the polarization hysteresis loops of the polymer films under different irradiation doses were measured at room temperature, and the results are presented in Figure 1. The unirradiated film exhibits a well-defined near square polarization hysteresis loop with a large remanent polarization ($P_r \sim 7\ \mu$C/cm^2). The data in Figure 1 reveal two features due to irradiation: the reduction of the polarization hysteresis and also the reduction of the polarization level. At very high dosage (150 Mrad), the polymer exhibits a linear dielectric behavior, indicating nearly a total loss of coupling among the dipoles in the polymer chains.

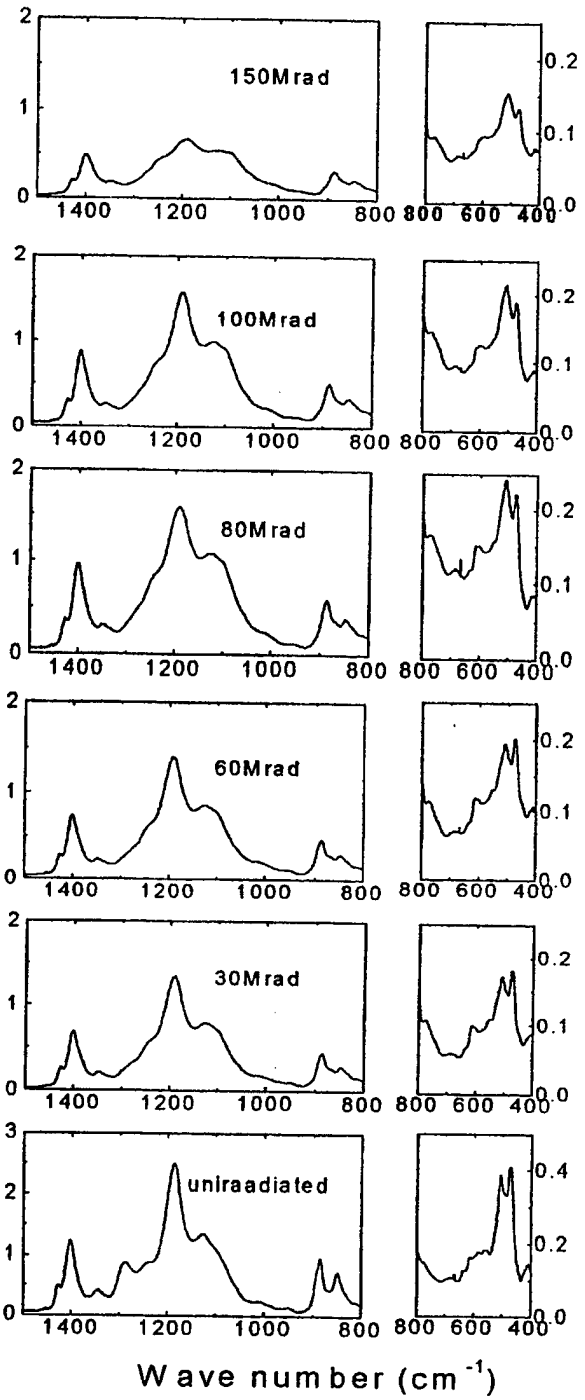

Figure 2. FTIR spectra of P(VDF–TrFE) copolymer films at different doses in wavenumber range 1500–400 cm^{-1}.

Figure 2 presents the FT-IR spectra in the wavenumber range between 1500 and 400 cm^{-1} for the P(VDF–TrFE) 50/50 copolymer in the dose range corresponding to the data in Figure 1. Before the irradiation, the spectrum is characterized by a strong absorbance peak at 1288 cm^{-1}, from the long trans sequence ($T_{m\geq 4}$) of the ferroelectric β-phase. Weak absorbance peaks corresponding to the TG (at 614 cm^{-1}) and T_3G (510 cm^{-1}) conformations are also present in the spectrum of

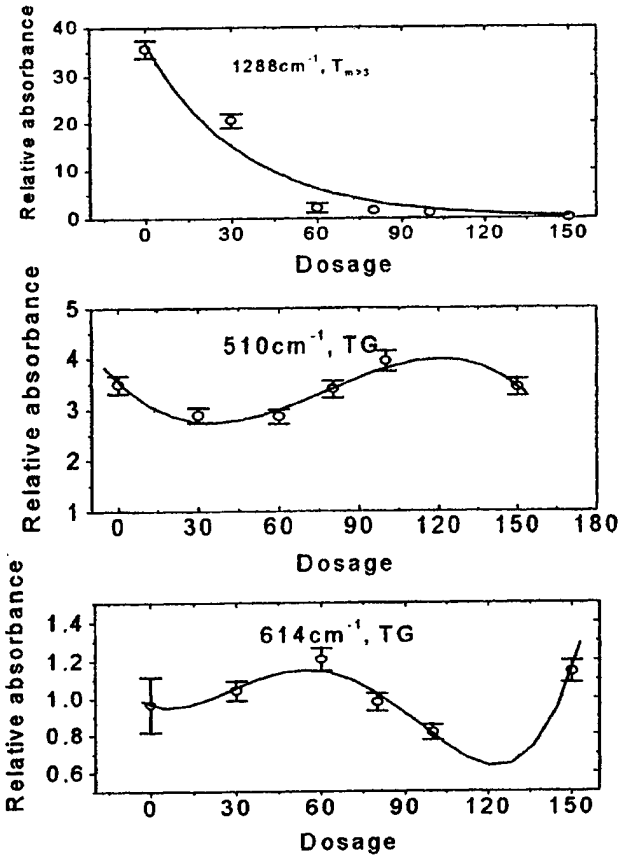

Figure 3. Dose dependence of infrared absorbances of the trans and gauche bands from P(VDF–TrFE) 50/50 copolymer films irradiated at 120 °C with 2.55 MeV electrons. The experimental data points are shown, and solid lines are drawn to guide the eye.

unirradiated copolymer, which are consistent with early experiment results and presumably due to the existence of the domain structure as has been suggested from the early X-ray diffraction and FT-IR data.[2,4] Although there are several peaks for each type of chain conformation, these three, i.e., 1288 cm^{-1} ($T_{m>4}$), 614 cm^{-1} (TG), and 510 cm^{-1} (T_3G), were chosen for the following analysis because these are all from the vibrations of the CF_2 group.[17]

Presented in Figure 3 is the dependence of the relative absorbance of these bands on the irradiation doses, deduced from the data in Figure 2. Each individual component of the bands has been fitted and separated from others by assuming a Lorentzian function peak shape. In the measurement, the samples for different doses have small variations in thickness. Moreover, the absorbance of even the same type of chain conformation may be different due to different cross-linking densities at different irradiation doses. To correct these factors, an internal standard should be used to compare the relative absorbance of different conformational sequences. The absorbance at 3022 cm^{-1} is the asymmetric stretching vibration of the C–H bond,[18] and as it is almost proportional to the thickness of the sample and does not depend on the state of the sample, it was used as an internal standard here. The data in Figure 3 are the relative absorbance after this correction.

The data in Figure 3 show that after irradiation the absorbance intensity of the all-trans peak decreases precipitously. At doses higher than 100 Mrad, this peak

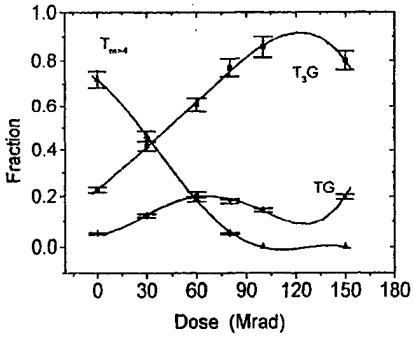

Figure 4. Fraction of trans and gauche conformations as a function of the dose for P(VDF–TrFE) 50/50 copolymer irradiated at 120 °C with 2.55 MeV electrons. The experimental data points are shown, and solid lines are drawn to guide the eye.

essentially disappears. Concomitantly, the absorbance peak corresponding to TG sequence increases with irradiation dose, and at doses beyond 60 Mrad, it shows irregular changes with dose. For the peak at 510 cm^{-1} for T_3G sequences, the absorbance does not show a monotonic change with dose, and irregular change is also observed at doses beyond 60 Mrad.

To quantify these changes with doses, we adopted the method used by Osaki et al.[18] to calculate the fraction of each chain sequence in the polymer from the infrared spectrum. Because three chain sequences are present, the fraction of each chain sequence is

$$F_i = \frac{A_i}{A_{\mathrm{I}} + A_{\mathrm{II}} + A_{\mathrm{III}}} \tag{3}$$

where i = I, II, and III, A_{I}, A_{II}, and A_{III} are the absorbances of crystal forms I, II, and III, i.e, with all-trans ($T_{m>4}$), T_3G, and TG sequences, respectively; and F_i is the fraction of chain sequence i. The result is presented in Figure 4.

The results in Figure 4 indicate that the change of the fraction of chain sequence with dose can be divided into three regions: below 60 Mrad, 60–100 Mrad, and above 100 Mrad. At doses below 60 Mrad, the fraction of all-trans sequences corresponding to macroscopic polarization drops rapidly with doses, while both TG and T_3G sequences increase. This is very similar to the observed macroscopic transformation of the ferroelectric to a nonpolar (paraelectric-like) phase of the copolymer with increased irradiation dose.[14,20,21] At 30 Mrad, the FT-IR data show that there are still relatively large regions of all-trans conformation in the polymer. Consistent with these observations, the polarization hysteresis data in Figure 1 show the presence of the polarization hysteresis and remanent polarization. At 60 Mrad, the fraction of the all-trans conformation drops to below 0.1, and correspondingly, the polarization loop has become very slim at this dose. At doses between 60 and 100 Mrad, the rate of decrease of the all-trans conformation with dose becomes lower, and more interestingly, the fraction of TG conformation exhibits a drop with dosage, suggesting a recovering of the local polar ordering in the copolymer with dose. At doses above 100 Mrad, the fraction of all-trans conformation becomes zero, and the fraction of the TG conformation increases again, due to the disappearance of the macroscopic crystal phase in the polymer at high doses, which will be discussed later.

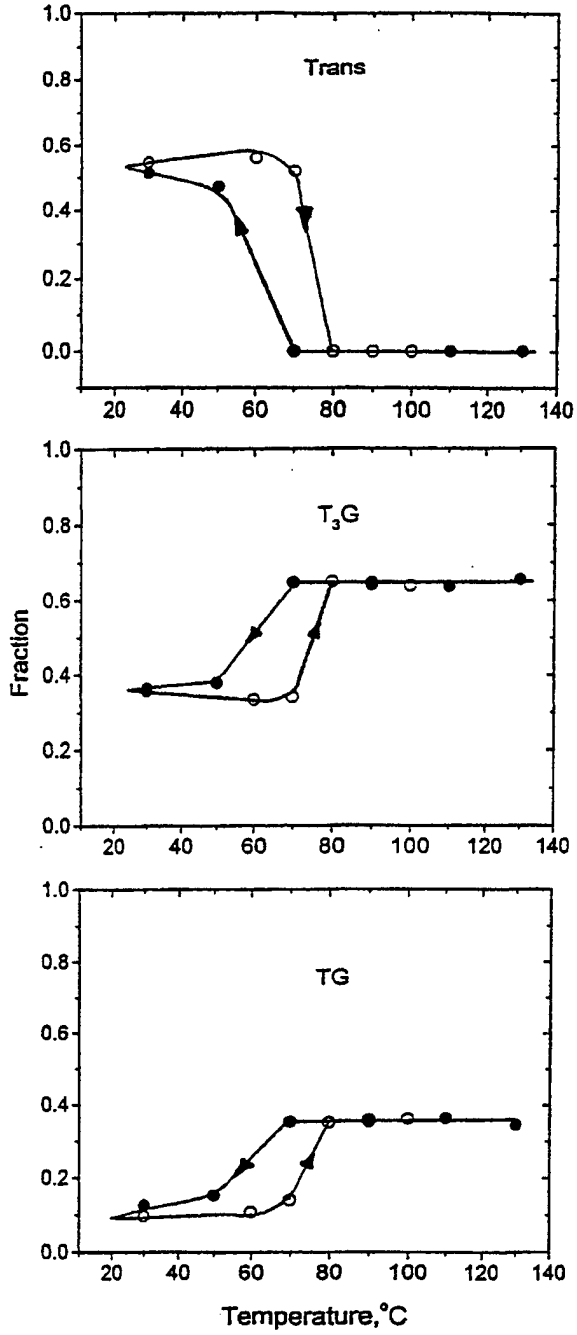

Figure 5. Fraction of trans and gauche conformations as a function of temperature for unirradiated P(VDF–TrFE) 50/50 copolymer. The data show a clear phase transition at temperatures near 70 °C. The experimental data points are shown. The solid lines are drawn to guide the eye, and arrows indicate the heating or cooling of the experiment.

Two more experiments were carried out in order to further elucidate the observed behavior. The FT-IR spectrum was measured for the unirradiated 50/50 copolymer as a function of temperature where a phase transformation from a macroscopically polar phase (ferroelectric β-phase) to a nonpolar phase the (paraelectric phase) occurs at the F–P transition temperature. X-ray diffraction data were also taken from irradiated copolymer samples as a function of dose. Presented in Figure 5 is the fraction of the three chain conformations in the unirradiated copolymer as a function of temperature (calculated using eq 3). The data reveal a clear

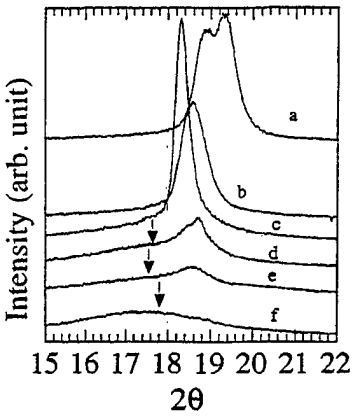

Figure 6. X-ray diffraction data at angles near the (200, 110) reflections of unirradiated film. The data were taken for films with different doses (in Mrad): a, 0; b, 30; c, 60; d, 80; e, 100; f, 150. The arrows indicate the center of a broad diffraction peak.

transition between the ferroelectric and paraelectric phase as signified by a large increase of the TG fraction (from near zero in the ferroelectric phase), a moderate increase of the T_3G fraction, and a drop to zero in the all-trans conformation. This result indicates that the phenomenon observed in the irradiated copolymer in the doses from 60 to 100 Mrad is not related to the macroscopic change from a polar to a nonpolar phase.

X-ray data taken at room temperature from the irradiated copolymer are presented in Figure 6. The data show the evolution of the (200, 110) reflection of the original ferroelectric phase with dose. For the unirradiated P(VDF–TrFE) 50/50 copolymer, a two-peak structure at θ angle near (200, 110) reflection has been observed by many early X-ray studies.[2,10] This two-peak structure is attributed to the presence of a mixture of disordered trans and $^1/_3$- helical conformations in the crystalline phase.[10] For irradiated samples, in analogy to the FT-IR data, the X-ray data also show three dose regions. Below 60 Mrad, the X-ray peak moves to a lower angle, indicating an expansion of the lattice perpendicular to the chain direction, and sharpens, due to the disappearance of the macroscopic polarization and hence the domain structure. Upon 60 Mrad irradiation, a peak appears at 4.84 Å, which is close to the lattice spacing of the paraelectric phase of unirradiated copolymer determined from X-ray data above the Curie temperature and consistent with early experimet results.[2,20,21] These results are consistent with the FT-IR data and the polarization data, showing the disappearance of the macroscopic polarization in the copolymer due to the irradiation. Interestingly, at doses higher than 60 Mrad, the X-ray peak moves back toward a higher angle, indicating a contraction of the lattice spacing in the directions perpendicular to the chain, and concomitantly the peak broadens, suggesting the reduction of the crystallite size due to the irradiation. The contraction of the lattice perpendicular to the polymer chain is consistent with the FT-IR observation, where in this dose range the fraction of TG sequence decreases with dose. TG sequences cause larger lattice spacing perpendicular to the chain compared with T_3G and all-trans sequences.[22] At 150 Mrad, the X-ray peak becomes very broad and moves to $2\theta = 17.6°$, indicating that no long-range crystalline ordering exists and the copolymer is nearly amorphous. This is consistent with the early experimental results.[20,23] The crystallinity can be esti-

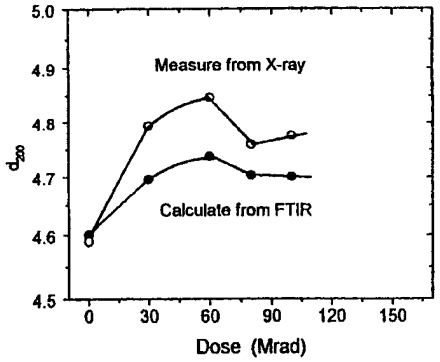

Figure 7. Lattice spacing d_{200} as a function of irradiation dose for 50/50 films irradiated at 120 °C. The open circles are taken from the fitting of X-ray data, and dots are calculated from the FT-IR data. Solid lines are drawn to guide the eye.

mated from the area of crystalline and amorphous diffraction peak. The results indicate that the crystallinity decreases with the dose. At doses of 60 Mrad or higher the crystallinity of the copolymer has been reduced to less than half as compared with the case of the unirradiated films.[23]

The change of d_{200} spacing with dose from the X-ray data is shown in Figure 7. In addition, the lattice spacing can also be estimated from the FT-IR results if the irradiated P(VDF–TrFE) copolymer is regarded as composed of TTTT, TGTG′, and T_3GT_3G' conformations with each conformation having its own lattice spacing. Tashiro et al. calculated the d_{200} for these three different conformations: 4.425, 4.82, and 4.79 Å, respectively.[22] Combining this with the fraction of three different conformations obtained from the FT-IR results, the d_{200} value of the P(VDF–TrFE) film irradiated at different doses is calculated, and the results are also presented in Figure 7. As can be seen from the data, the two results are consistent with each other although the d_{200} value from the X-ray diffraction data is higher than those from the FT-IR data except for the unirradiated film. The reason for this might be that in the calculation we assumed that the d_{200} spacing for each conformation does not change with dose, while in reality lattice deformation should exist after irradiation.

Therefore, both FT-IR and X-ray data indicate that the reduction in the crystallite size (there is a large reduction in the crystallite size after 60 Mrad irradiation) and other changes (as will be discussed later in the paper) in the copolymer due to irradiation favor the T_3G conformation compared with TG (paraelectric phase).

Figure 8 shows the temperature dependence of T_3G and TG conformations derived from FT-IR spectra measured at different temperatures for the irradiated copolymer with a dose of 60 Mrad. As expected, no transition behavior is observed (in contrast to the data in Figure 5 for unirradiated samples where a transitional change in the molecular conformations was observed), indicating that indeed the macroscopic polarization in the normal ferroelectric β-phase has been destroyed.

3.2. Chemical Changes Due to Irradiation. In addition to the conformation changes, FT-IR data also reveal other changes in the copolymer due to irradiation. In Figure 9, the FT-IR spectra in the wavenumber range between 4000 and 1600 cm^{-1} are presented where the data from samples before and after irradiation are compared. In general, irradiation of polymers may lead

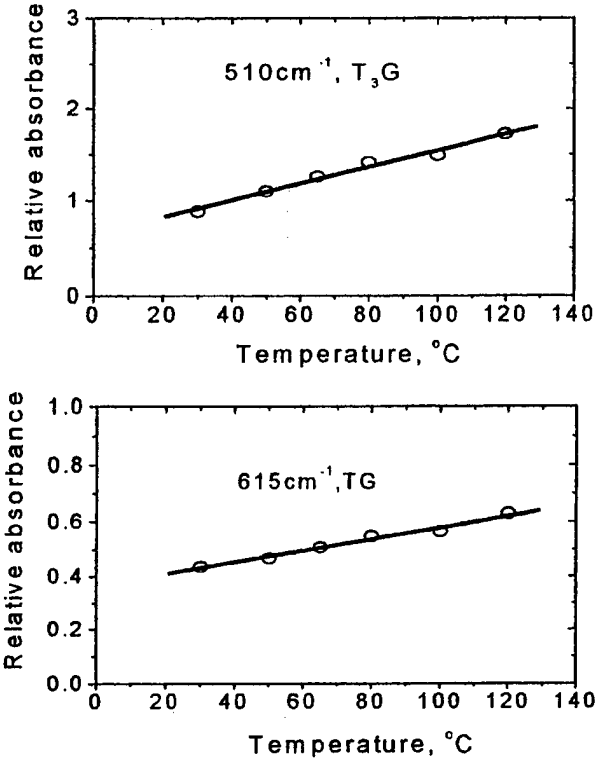

Figure 8. Relative absorbance of TG and T_3G conformations as a function of temperature for 50/50 copolymer irradiated at 120 °C with 60 Mrad dose. The open circles are the data, and solid lines are drawn to guide the eye.

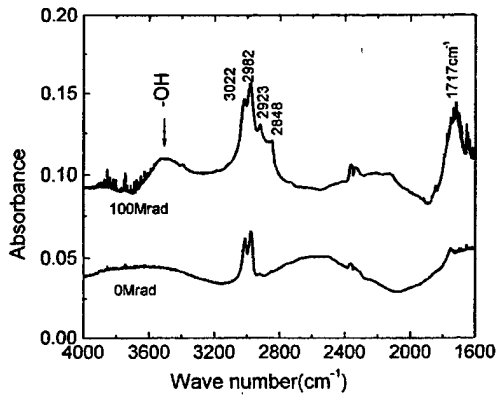

Figure 9. FT-IR spectra of irradiated P(VDF–TrFE) copolymer film (100 Mrad) compared with unirradiated film in wavenumber range 4000–1600 cm^{-1}.

to the formation of radical or ionic species due to heterolytic or homolytic bond scission reactions. These reactions will produce the following changes in the polymer:[24] (a) chain scission or cross-linking and the resulting changes in average molecular weight and (b) the formation of oxidative degradation products such as hydrofluoric acid, carboxylic acid, alcohol, and hyproperoxide groups if traces of oxygen are present during or after irradiation processing.

For the copolymer studied here, it is observed that after irradiation an absorbance peak appears at 1717 cm^{-1}, which could be assigned to the double bond structure of –CH=CF–[24] as well as a carboxyl group (–C=O–). However, the appearance of a broad peak between 3200 and 3600 cm^{-1}, the typical absorbance frequency of hydroxyl (–OH) group, for samples after

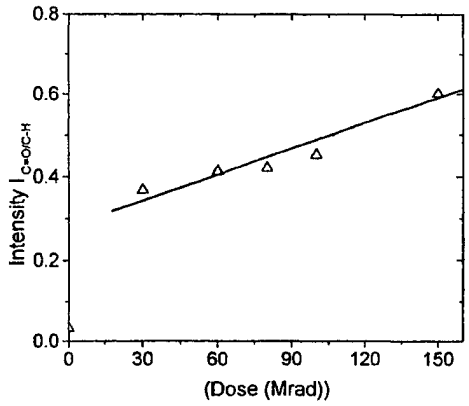

Figure 10. Intensity of FT-IR bands of carboxyl group of P(VDF–TrFE) 50/50 copolymer film irradiated under nitrogen atmosphere as a function of radiation dosage (C–H, 3022 cm^{-1}; C=O, 1717 cm^{-1}). The solid line is drawn to guide the eye.

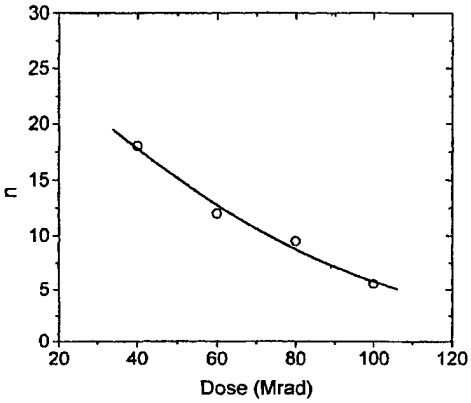

Figure 11. Number of repeating unit $(-CH_2CF_2CHFCF_2-)$ n between two cross-links for P(VDF–TrFE) 50/50 copolymer film irradiated at different doses. The solid line is drawn to guide the eye.

irradiation seems to be more consistent with the interpretation that the peak at 1717 cm^{-1} is from a carboxyl group. The formation of a terminal carboxylic acid group in the irradiated samples could be caused by the presence of trace oxygen in the samples or in the irradiation chamber. Even though the irradiation chamber has a nitrogen circulation, a small amount of oxygen might still exist in the chamber. The change of the content of carboxylated groups with dose is summarized in Figure 10, which shows that the infrared absorption intensity of carboxylated groups (quotient of absorption peak of the C=O stretching vibration and nonspecific C–H) increases with doses linearly. However, in the dose range investigated, the content of carboxylated groups is still quite small in the polymer. As will be demonstrated in the following, irradiation-induced cross-linking seems to be the dominant chemical change in the copolymer investigated here.

Cross-linking density was measured for the irradiated copolymers, and the data are presented in Figure 11, where the change in the number of repeating units (n) between two cross-linking points along the chain in the unit of $-CH_2CF_2CHFCF_2-$ is plotted versus the irradiation dose. Although P(VDF–TrFE) is a random copolymer, $-CH_2CF_2CHFCF_2-$ is taken here as a repeating unit for the sake of convenience in the presentation. The cross-linking density is inversely proportional to n (or M_c). The result in Figure 11 demonstrates that the copolymer at doses higher than 60 Mrad is highly cross-linked. The result confirms that cross-linking is the dominant chemical change during high-energy electron irradiation.

IV. Summary

The changes in the crystalline structure, molecular conformation, and other possible chemical reactions in the P(VDF–TrFE) 50/50 copolymer due to high-energy electron irradiation were investigated in terms of FT-IR, X-ray diffraction, and cross-linking density measurements. The irradiation-induced structural and conformational changes are not monotonic. For the copolymer studied here (irradiated at 120 °C), the irradiation-induced changes can be divided into three regions. Below 60 Mrad, FT-IR and X-ray data indicate that the irradiation causes a continuous reduction of the macroscopic polarization in the polymer, and this can be compared directly with the evolution of the polarization hysteresis loop with dose (from the square polarization loop to slim loop). However, for doses between 60 and 100 Mrad, the rate of decrease of the all-trans conformation with dose becomes much slower, and the fraction of TG sequence, which is related to the randomization of the polarization in the copolymer, actually shows a decrease with dose. X-ray data in the same dose range also show a contraction of the lattice spacing perpendicular to the chain. This anomalous process could be caused by a high cross-linking density in the copolymer which would favor chain conformations that have smaller lattice spacings between chains, such as the T_3G sequences. At higher doses (~150 Mrad), the irradiation leads to a near amorphous phase in the copolymer, which exhibits a linear dielectric response in the polarization hysteresis data.

The experimental results also indicate that, in addition to the changes in the crystalline phase, there is a continuous reduction of the crystallinity in the copolymer with dose due to the increased cross-linking density, which leads to the eventual disappearance of the macroscopic crystalline ordering in the copolymer which is consistent with the early experimental observations.[20,21]

Acknowledgment. This work was supported by the Office of Naval Research under Grants N00014-98-1-0254 and N00014-97–1–0667 and the National Science Foundation under Grant ECS-9710459. The authors thank Dr. A. J. Lovinger for the careful reading of the manuscript and suggestions regarding the interpretation of the experiment data presented.

References and Notes

(1) Kawai, H. *Jpn. J. Appl. Phys.* **1969**, *8*, 975.
(2) Tashiro, K.; Takano, K.; Kobayashi, M.; Chatani, Y.; Tadokoro, H. *Ferroelectrics* **1984**, *57*, 297.
(3) Lovinger, A. J. *Science* **1983**, *220*, 1115.
(4) Tashiro, K.; Takano, K.; Kobayashi, M.; Chatani, Y.; Tadokoro, H. *Polymer* **1984**, *25*, 195.
(5) Lovinger, A. J.; Davis, G. T.; Furukawa, T.; Broadhurst, M. G. *Macromolecules* **1982**, *15*, 324.
(6) Davis, G. T.; Furukawa, T.; Lovinger, A. J.; Broadhurst, M. G. *Macromolecules* **1982**, *15*, 324.
(7) Tashiro, K.; Kobayashi, M. *Polymer* **1988**, *29*, 426.
(8) Tashiro, K.; Kaito, H.; Kobayashi, M. *Polymer* **1992**, *33*, 2915.
(9) Tashiro, K.; Tanaka, R.; Ushitora, K.; Kobayashi, M. *Ferroelectrics* **1995**, *171*, 145.
(10) Lovinger, A. J.; Furukawa, T.; Davis, G. T.; Broadhurst, M. G. *Polymer* **1983**, *24*, 1225.

(11) Lovinger, A. J.; Davis, D. D.; Cais, R. E.; Kometani, J. M. *Polymer* **1987**, *28*, 619.
(12) Ishii, F.; Odajima, A.; Ohigashi, H. *Polym. J.* **1983**, *15*, 875.
(13) Yagi, T.; Tatemoto, M.; Sako, J. *Polym. J.* **1980**, *12*, 209.
(14) Zhang, Q. M.; Bharti, V.; Zhao, X. *Science* **1998**, *280*, 2101.
(15) Wang, T. T.; Herbert, J. M.; Glass, A. M. *The Application of Ferroelectric Polymers*, Blackie Chapman and Hall: New York, 1988.
(16) Galletti, P. M.; De Rossi, D. E.; De Reggi, A. S. *Medical Applications of Piezoelectric Polymers*; Gordon and Breach Science Publishers: New York, 1988.
(17) Reynolds, N. M.; Kim, K. J.; Chang, C.; Hsu, S. L. *Macromolecules* **1989**, *22*, 1092.
(18) Kobayashi, K.; Tashiro, K.; Tadokoro, H. *Macromolecules* **1975**, *8*, 158.
(19) Osaki, S.; Ishida, Y. *J. Polym. Sci., Polym. Phys.* **1975**, *13*, 1071.
(20) Lovinger, A. J. *Macromolecules* **1985**, *18*, 910.
(21) Macchi, F.; Daudin, B.; Legrand, J. F. *Nucl. Inst. Methods Phys. Res.* **1990**, *B46*, 324.
(22) Tashiro, K.; Kobayashi, M.; Tadokoro, M. *Macromolecules* **1981**, *14*, 1757.
(23) Bharti, V.; Xu, H. S.; Shanthi, G.; Zhang, Q. M.; Liang, K. *J. Appl. Phys.* **2000**, *87*, 452.
(24) Clegg, D. W.; Collyer, A. A. *Irradiation Effects on Polymer*; Elsevier: London, 1991.
(25) Kuhn, K. J.; Hahn, B.; Percec, V.; Urban, M. W. *Appl. Spectrosc.* **1987**, *41*, 843.

MA9919561

APPENDIX 23

Appl. Phys. A 70, 307–312 (2000) / Digital Object Identifier (DOI) 10.1007/s003390000451

Applied Physics A
Materials
Science & Processing

Relaxor ferroelectric behavior in high-energy electron-irradiated poly(vinylidene fluoride-trifluoroethylene) copolymers

Q.M. Zhang, Z.-Y. Cheng, V. Bharti

Materials Research Laboratory, The Pennsylvania State University, University Park, PA 16802, USA
(Fax: +1-814/863-7846, E-mail: qxz1@psu.edu; zxc7@psu.edu; vxb5@psu.edu)

Received: 13 August 1999/Accepted: 24 November 1999/Published online: 23 February 2000 –

Abstract. This paper presents experimental results showing that in a certain composition range and under a proper electron-irradiation treatment, a normal ferroelectric poly(vinylidene fluoride-trifluoroethylene) copolymer can be converted into a material exhibiting many typical features of relaxor ferroelectrics, suggesting that this is a new class of relaxor ferroelectric material. Furthermore, the irradiated copolymer can generate giant electrostriction ($\approx 5\%$) with a high elastic energy density. The X-ray diffraction results obtained from the irradiated copolymer under electric field, indicate that the observed polarization and strain responses are mainly due to the local phase transformation from a nonpolar phase to a polar phase.

PACS: 77.80.-e; 77.65.Bn; 77.84.Jd

Relaxor ferroelectrics have attracted a great deal of attention in the past several decades [1, 2]. On the fundamental science side, because the interactions responsible for the relaxor ferroelectric (RFE) phenomena are on the mesoscopic scale, it is still a challenge to develop an understanding of the many interesting and peculiar features displayed by this class of materials [3–6]. On the application side, this class of materials offers a high dielectric constant and high electrostriction, which are attractive for a broad range of devices [6–8]. It is interesting to note that although the RFE phenomenon has been observed in ceramic materials for nearly four decades, there is no direct experimental observation of a RFE phenomenon in polymer systems. Recently, we observed that poly(vinylidene fluoride-trifluoroethylene) (P(VDF-TrFE)) copolymer under proper high-energy electron-irradiation treatments can exhibit many features resembling a RFE [9]. In this paper, we will present the experimental results related to these observations. In addition, we will show that the relaxor ferroelectric P(VDF-TrFE) copolymer can generate massive electrostrictive strain, on the order of 5% with a high elastic energy density. X-ray diffraction data will also be presented to demonstrate that the polarization response in this new class of relaxor material is mainly from the local phase switching, which is also responsible for the giant electrostriction in the material.

P(VDF-TrFE) copolymer, in the compositions with VDF content > 50 mol %, exhibits characteristics of a normal ferroelectric [10]. In the composition range between about 50 mol % and 85 mol % VDF, a ferroelectric to paraelectric (F P) transition has been observed. For copolymers with VDF content higher than 85 mol %, the ferroelectric phase is directly transformed to a melt as the temperature is increased. It is assumed that the F P transition is preempted by the melting transition [10, 11]. It has been observed that as the VDF content decreases, the F P transition evolves from first order VDF content > 60 mol %) to a continuous one (VDF content < 60 mol %) [10, 12]. This is understandable since TrFE dilutes the dipole density and weakens the ferroelectricity in the polymer. As a consequence, in the irradiation experiment, it was found that with increased VDF content in the copolymer, it becomes harder to convert a normal ferroelectric P(VDF-TrFE) to a RFE. That is, the dose needed to complete this conversion becomes higher for copolymers with higher VDF content. Furthermore, using the electron sources available to us (electron energies at 1 MeV, 1.2 MeV, and 2.55 MeV), the copolymer can not be converted to a relaxor when the VDF content is higher than 70 mol %. Therefore, the experimental results presented are those from copolymers of P(VDF-TrFE) 50/50, 65/35, and 68/32.

It is interesting to point out that there are many analogies between the irradiated P(VDF-TrFE) copolymers and the La-doped $Pb(Zr_xTi_{1-x})O_3$ (PLZT) ceramics in the transformation from a normal ferroelectric to a RFE. In irradiated P(VDF-TrFE) copolymer, it is the defect structures introduced by irradiation that transform the normal ferroelectric P(VDF-TrFE) into a RFE. Whereas in PLZT ceramics, it is the defect structures introduced by La that convert the normal ferroelectric PZT into a relaxor [13]. The aforementioned phenomenon in the irradiated P(VDF-TrFE) copolymers are also very similar to what has been observed in PLZT ceramics where the amount of La required in the transformation and the ease of the conversion of PZT into a RFE also depends strongly on the PZT composition [14].

1 Experimental

The P(VDF-TrFE) copolymer powders with a mean molecular weight of 200 000 were purchased from Solvay and Cie, Brussels, Belgium. Two approaches were used here to prepare the copolymer films: melt press and solution cast. In the melt-press process, the P(VDF-TrFE) copolymer powders were pressed between two pieces of aluminum foil at temperatures between 215 °C and 225 °C. The films were then either slowly cooled down to room temperature, resulting in a high crystallinity, or quenched in ice-cold water, to keep the crystallinity of the film low. In the solution-cast method, the copolymer was dissolved in dimethyl formanide (DMF), and then the solution was cast on a flat glass plate and dried in an oven at 70 °C. Two types of films were used in this investigation: stretched and unstretched. In unstretched films, the films were annealed at 140 °C for a time period between 12 to 14 h to improve the crystallinity. In stretched films, films made from solution cast or quenched from melt press were uniaxially stretched by a factor of 5 at a temperature between 25 °C and 50 °C. Afterwards, these films were also annealed at 140 °C for 12 to 14 h to increase the crystallinity. The thickness of both the stretched and unstretched films was in the range from 15 to 30 μm. The irradiation was carried out in a nitrogen or argon atmosphere at different temperatures from room temperature to 120 °C. Three electron energies were used in the irradiation: 1 MeV, 1.2 MeV, and 2.55 MeV.

Gold sputtered films were used for the characterization of the dielectric properties, polarization, and electric-field-induced strain behavior of the films. The dielectric constant of the films was measured either by a dielectric analyzer (TA instruments, model No. 2970) or by a LCR meter (HP 4194). The polarization hysteresis loop was measured by a computer controlled automatic system based on the Sawyer–Tower circuit. The pyroelectric coefficient of P(VDF-TrFE) 50/50 copolymer was measured using the Byer–Roundy technique. The samples were first poled by applying a dc field of 50 MV/m at 80 °C and then slowly cooled down to 50 °C under field. The pyroelectric current was measured at a heating rate of 2 °C/min using a HP 4140B Picoammeter. The longitudinal strain, the strain response along the thickness direction, was characterized by a strain sensor based on the piezoelectric bimorph sensor, which was designed specifically for the polymer film strain measurements [15]. The X-ray pattern was taken at room temperature (20 °C) using a Scintag diffractrometer (model PAD-V) with Ni-filtered Cu K_α radiation.

2 Experimental results

2.1 *Relaxor ferroelectric behavior in irradiated copolymers*

Figure 1 presents a comparison of the polarization hysteresis loop of P(VDF-TrFE) 50/50 copolymer before and after irradiation measured at room temperature (1 Hz). The irradiation was performed at 120 °C with a 40-Mrad dose of 2.55-MeV electrons. Before the irradiation, the polymer film exhibits a well-defined square polarization hysteresis loop with a coercive field at 45 MV/m and a remanent polarization of 64 mC/m^2. In contrast, the film after irradiation shows a slim polarization loop.

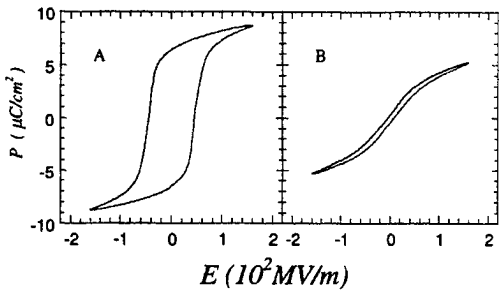

Fig. 1a,b. The polarization hysteresis loops of P(VDF-TrFE) 50/50 copolymer measured at room temperature: **a** before irradiation, **b** after irradiation with 40 Mrad at 120 °C of 2.55-MeV electrons

The slim polarization loop suggests that the polymer after irradiation may resemble a RFE observed in ceramic systems. To determine whether P(VDF-TrFE) copolymer after irradiation is a simple dielectric or a ferroelectric with RFE, the polarization hysteresis loop was measured at lower temperatures. As presented in Fig. 2, the polarization hysteresis gradually increases with reduced temperature. In order to characterize the temperature dependence of the remanent polarization P_r, the pyroelectric coefficient was measured before and after the irradiation. Before irradiation, a sharp drop of the remanent polarization P_r with temperature is seen around 70 °C the F P transition temperature (Fig. 3), but after irradiation, the change of P_r with temperature is more gradual, analogous to what has been observed in inorganic materials exhibiting RFE behavior. In addition, the derivative of P_r of irradiated sample with temperature exhibits two broad peaks, the one near 23 °C is related to the glass transition and the one near 32 °C coincides closely with the freezing temperature determined from the dielectric constant data ($T_f = 34$ °C) as will be discussed in the next paragraph.

The dielectric constant of the irradiated copolymer was characterized as a function of temperature at different frequencies. Figure 4 shows that the irradiated P(VDF-TrFE) 50/50 copolymer exhibits a broad dielectric peak (T_m) around room temperature, which is below the F P transition temperature (about 70 °C) observed in unirradiated samples. However, unlike the dielectric constant peak associated with

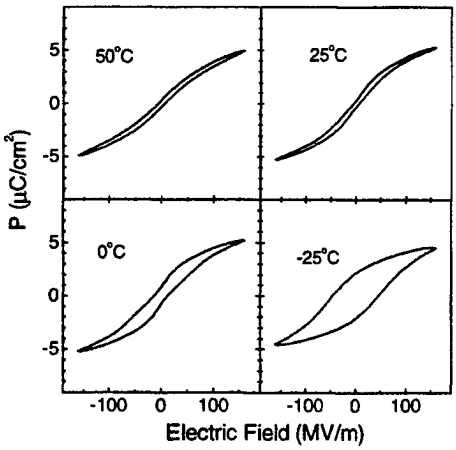

Fig. 2. Polarization hysteresis loops of P(VDF-TrFE) 50/50 copolymer (irradiated at 120 °C with 40 Mrad of 2.55-MeV electrons) measured at different temperatures. At lower temperatures the loops show the gradual increase of the remanent polarization and hysteresis

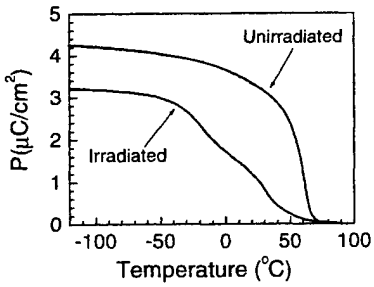

Fig. 3. Remanent polarization P_r as a function of temperature before (*dashed line*) and after (*solid line*) irradiation for P(VDF-TrFE) 50/50 copolymer irradiated at 120 °C with 40 Mrad of 2.55-MeV electrons

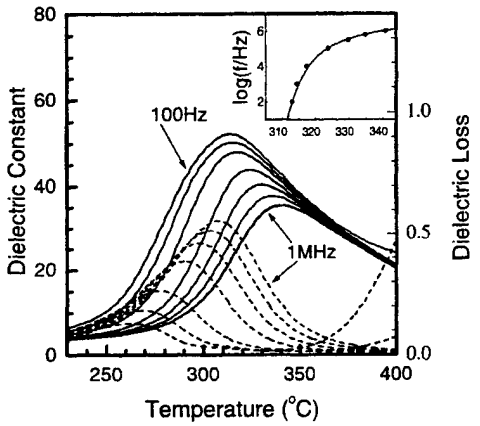

Fig. 4. The dielectric constant and dielectric loss as a function of temperature for P(VDF-TrFE) 50/50 copolymer irradiated at 120 °C with 40 Mrad of 2.55-MeV electrons. The frequency is (from top to bottom for the dielectric constant and from bottom to top for the dielectric loss) 100 Hz, 1 kHz, 10 kHz, 100 kHz, 300 kHz, 600 kHz, and 1 MHz. The *inset* shows the fitting of the V–F law, where the *solid line* is the fit and the *dots* are the data. The *horizontal axis* in the *insert* is temperature in Kelvin

the F P transition, the data in Fig. 4 show that T_m shifts progressively toward a higher temperature with frequency, another feature common to all RFE. In addition, as shown in the insert of Fig. 4, the dispersion of T_m with frequency (f) can be modeled quite well with the Vogel–Folcher (V–F) law

$$f = f_0 \exp\left(\frac{U}{k(T_m \quad T_f)}\right), \tag{1}$$

a relation observed in many relaxor ferroelectric systems and spin glass systems [4, 16–18], where U is a constant related to the activation energy, k is the Boltzmann constant, and T_f is the freezing temperature. The fitting of the data yields $f_0 = 9.6$ MHz, $U = 6.4 \times 10^{-3}$ eV (or expressed as $U = kT_0$ and $T_0 = 74.3$ K) and $T_f = 307$ K (= 34 °C). The value T_f obtained here is nearly the same as that obtained from the pyroelectric coefficient data, again a feature resembling that observed in ceramic systems with RFE. These observations suggest that the irradiated copolymer is a new class of RFE, relaxor ferroelectric polymer.

Similar results were also obtained for the irradiated copolymer 65/35 and 68/32 and the polarization and dielectric constant are presented in Figs. 5 and 6. In analyzing the dielectric data, it was found that the parameters in the V–F law can vary over a wide range with sample treatment conditions, especially the electron energy used in the irradiation.

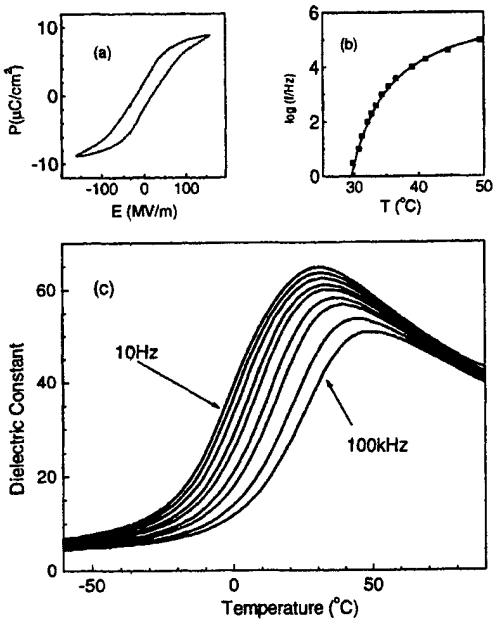

Fig. 5. **a** The polarization hysteresis loop measured at room temperature, **b** the fitting of the V–F law, and **c** the dielectric constant as a function of temperature measured at different frequencies (10 Hz, 30 Hz, 100 Hz, 400 Hz, 1 kHz, 4 kHz, 10 kHz, 40 kHz, and 100 kHz), for the copolymer 65/35 stretched (5×) irradiated at 105 °C with 70 Mrad of 2.55-MeV electrons. The parameters for the V–F law from the fit are $f_0 = 5.34$ MHz, $T_f = 297.5$ K, and $U = 5.3 \times 10^{-3}$ eV

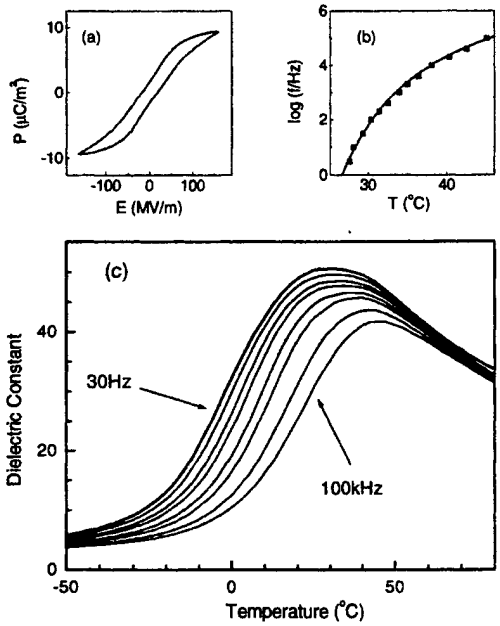

Fig. 6. **a** The polarization hysteresis loop measured at room temperature, **b** the fitting of the V–F law, and **c** the dielectric constant as a function of temperature measured at different frequencies (30 Hz, 100 Hz, 1 kHz, 4 kHz, 10 kHz, 40 kHz, and 100 kHz) for the copolymer 68/32 irradiated at 105 °C with 70 Mrad of 1-MeV electrons. The parameters for the V–F law from the fit are $f_0 = 1.47$ GHz, $T_f = 286.1$ K, and $U = 2.1 \times 10^{-2}$ eV

For example, as shown in Fig. 6, f_0 and U for the copolymer 68/32 irradiated with 1-MeV electrons are 1.47×10^9 Hz and 2.1×10^{-2} eV, respectively, much higher than those obtained in the copolymers irradiated with 2.55-MeV electrons. The observed large changes of f_0 and U for samples

treated under different conditions could be caused by the changes in the average polar cluster size and the pinning of local polar regions by defects such as crosslinking in the polymer. This is an interesting area to be investigated further.

It should be mentioned that in addition to converting the normal ferroelectric phase in the crystalline region into relaxor ferroelectric, the high-energy electron irradiation also reduces the crystallinity and causes crosslinking in the polymer [19–21]. As a result of the reduction of crystallinity, the peak dielectric constant gradually decreases with dosage at high electron doses and at very high electron doses where the crystallinity is nearly zero, the broad dielectric constant peak also nearly disappears. This results demonstrate that the observed high peak dielectric constant and dielectric dispersion are mainly from the crystalline phase.

2.2 *Field-induced strain responses and electrostriction in the irradiated copolymers*

Presented in Fig. 7a is the field-induced longitudinal strain measured at 30 °C for the copolymer 68/32 irradiated with 1-MeV electrons. As shown in the figure, the strain under a field of 146 MV/m can reach 5% (for most of the polymers, the longitudinal strain is negative), which is significantly higher than most known ferroelectric materials. This high electrostrictive strain response plus the relatively high elastic modulus ($Y \approx 0.4$ to 0.5 GPa) yield a high elastic energy density, $\frac{1}{2}YS_m^2 = 0.5\,\mathrm{J/cm^3}$, again much higher than those obtained in most known ferroelectric materials. The field-induced strain under a constant field as a function of temperature for this copolymer is summarized in Fig. 7b and the data show that the strain remains at a high value over a relatively broad temperature range.

The charge-related electrostrictive coefficient Q_{33} is calculated directly from the strain and polarization data for this irradiated copolymer, $S = QP^2$, where S is the strain and P is the polarization. It is found that Q_{33} at 30 °C is about $7\,\mathrm{C^2/m^4}$, which is higher than that calculated from the single-crystal data [22–25]. Similar behavior is also observed in other irradiated copolymers where the electrostrictive coefficient Q deduced from the experimental data varies over a wide range for the samples treated at different conditions, and can be much higher than the values calculated from the single-crystal data [26, 27]. Although this phenomenon seems puzzling, it is simply caused by the semicrystalline morphology of P(VDF-TrFE) copolymer. To some extent, a P(VDF-TrFE) copolymer can be regarded as a composite with crystallites embedded in an amorphous matrix [28]. As a result, the measured electrostrictive coefficient is an effective coefficient from this composite and can be much higher than that from the crystalline phase.

To illustrate this, the hydrostatic electrostrictive coefficient Q_h is taken here as an example. For a composite, the total volume strain is the summation of the crystalline region and amorphous region and the electrostrictive coefficients at the two constituents are Q_{hC} for the crystalline and Q_{hA} for the amorphous. For irradiated P(VDF-TrFE) copolymer, it was found that the total polarization measured can be related to the polarization in the crystalline phase P_C and amorphous P_A by the logarithmic law of mixing as observed in many diphasic 0 3 composites [20],

$$\log(P) = v_c \log(P_C) + v_a \log(P_A)\,, \tag{2}$$

where v_a and v_c are the volume fraction of the amorphous and crystalline phases, respectively. Assuming the volume change of the sample equals the sum of volume changes of both amorphous and crystal areas, using the definition of the electrostrictive coefficient $Q(S_v = Q_h P^2$, where S_v is the volume strain), it can be derived that the measured Q_h from a copolymer is

$$Q_h = Q_{hC}\,(v_c n^{2(1\ v_c)} + \frac{Q_{hA}}{Q_{hC}} \frac{1\ \ v_c}{n^{2v_c}})\,, \tag{3}$$

where $n = P_C/P_A$ [27]. Based on the fitting of the experimental data using (2), it is found that n is in the range between 7.5 to 9.5. In addition, in a pyroelectric study of PVDF, it was also found that the ratio n between the polarization in crystal area and polarization in amorphous is about 7.5 [27, 29]. Using this n values, it is easy to see from (3) that Q_h is

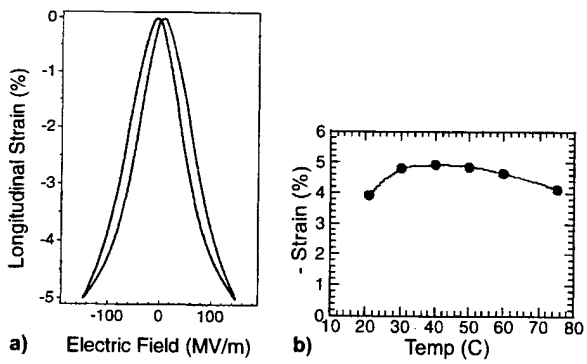

Fig. 7. **a** Field-induced strain measured at 1 Hz as a function of applied field measured at 30 °C and **b** the amplitude of the induced strain under a constant field as a function of temperature for the copolymer 68/32 irradiated at 105 °C with 70 Mrad of 1-MeV electrons

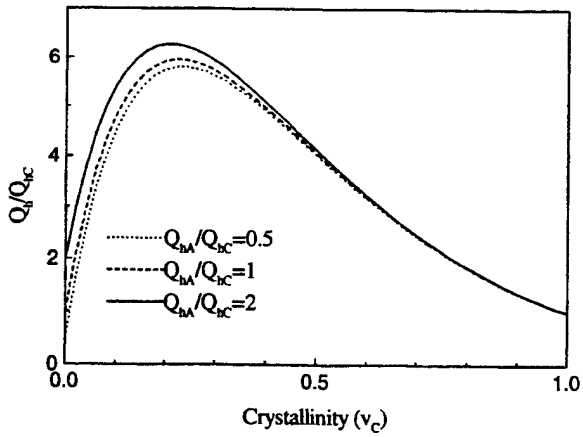

Fig. 8. The ratio of Q_h/Q_{hC} deduced from (3) as a function of crystallinity v_c where $n = 8$ is used. The *three curves* correspond to $Q_{hA}/Q_{hC} = 0.5$, 1, and 2, respectively. In most of the cases, $Q_h/Q_{hC} > 1$

larger than Q_{hC} (as illustrated in Fig. 8, in which $n = 8$ was used).

2.3 *X-ray study of the change of the lattice structure with applied electric field*

For the copolymers, X-ray data reveal that under electron irradiation, the X-ray peak intensity from the normal ferroelectric phase subsides while new peaks at positions near the corresponding paraelectric phase appear [20, 21, 30]. Therefore, the irradiated copolymer is in a non-polar phase macroscopically, analogous to that in the ceramic RFE [1]. To further understand the changes in the irradiated copolymers under electric field , X-ray diffraction data for irradiated copolymers was also obtained under electric field for series of samples.

Shown in Fig. 9 is the data taken from the copolymer 68/32 irradiated with 1-MeV electrons (Fig. 7 for the strain data). Because of the limitation of the instrument, the maximum field that can be applied to the samples is about 100 MV/m. Before the field is applied, the peak at $2\theta = 18.58°$ is close to the paraelectric (200, 110) peak position for this copolymer (non-polar phase peak) and for this sample, a shoulder at $2\theta = 19.34°$ is observed, which can be from the residual small ferroelectric region. Under a field of 63 MV/m, a large drop can be observed in the peak intensity for the non-polar phase peak and concomitantly, a broad peak appears at $2\theta = 19.36°$, close to the (200, 110) reflection of the ferroelectric phase in the unirradiated sample ($\approx 19.5°$) [29]. As the field is increased to 92.6 MV/m, the intensity of the high-angle peak (polar phase peak) is further increased compared with the non-polar phase peak. Meanwhile, the peak position of the polar phase also shows a slight increase with field and under 92.6 MV/m field, the peak is at $2\theta = 19.48°$. Therefore, the data reveal that the changes induced in the copolymer by external electric fields are a local phase transformation process.

In a RFE material, the polarization can be from the reorientation of the polar vector and/or the local phase transformation from a non-polar to a polar phase [6, 31]. In the case when the volume content of the local polar regions is low and the temperature of the system is not far above T_f, it is expected that the local phase transformation will play a major role. In the other case, the polar region reorientation may become important in the polarization response. For the irradiated copolymers studied here, the X-ray results indicate that at the field range studied, the observed polarization and strain response is indeed mainly from the local phase transformation from a non-polar phase to a polar phase.

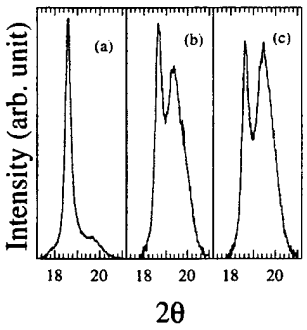

Fig. 9. X-ray diffraction patterns measured under different applied electric fields: (a) $E = 0$; (b) $E = 63$ MV/m; and (c) $E = 92.6$ MV/m for the copolymer 68/32 irradiated at 105 °C with 70 Mrad of 1-MeV electrons

3 Summary

This paper presents experimental evidence suggesting that the irradiated P(VDF-TrFE) copolymer is a new class of relaxor ferroelectric material. We also showed that the irradiated copolymer can generate a giant electrostriction ($\approx 5\%$) with a high elastic energy density. Due to the semicrystalline morphology, we showed that the experimentally determined electrostriction coefficients can be higher than those from the single-crystalline region. X-ray data measured under different dc electric fields reveal that there is an electric-field-induced local phase transformation from a non-polar to a polar phase, which is responsible for the observed polarization and strain behaviors in the irradiated copolymers. Taking all these data together, suggests that the high-energy electron irradiation breaks the macro-polar domains in the normal ferroelectric P(VDF-TrFE) copolymer into local nano-polar regions and external fields induce local phase transformation between non-polar and polar phase, which results in a slim polarization loop. This local phase transformation, coupled with a large lattice strain associated with this phase change, generates the giant electrostriction as observed.

Acknowledgements. The authors thank Ms. G. Shanthi in carrying out X-ray measurements. This work was supported by the National Science Foundation under Grant No. ECS-9710459 and Office of Naval Research under Grant No. N00014-97-1-0900.

References

1. L.E. Cross: Ferroelectrics **76**, 241 (1987)
2. H. Chen: Proc. Williamsburg Workshop on Ferroelectrics (Ferroelectrics Vol. 106 1998)
3. G. Smolenski, A. Agranovska: Sov. Phys. Solid State **1**, 1429 (1960)
4. D. Viehland, et al.: J. Appl. Phys. **68**, 1926 (1990)
5. V. Westphal, W. Kleeman, M.D. Glinchuk: Phys. Rev. Lett. **68**, 847 (1992)
6. Z.-Y. Cheng, R.S. Katiyar, X. Yao, A.S. Bhalla: Phys. Rev. B **57**, 8166 (1998)
7. K. Uchino, S. Nomura, L.E. Cross, R.E. Newnham, S.J. Jang: J. Mater. Sci. **16**, 569 (1981)
8. S.-E. Park, T. Shrout: J. Appl. Phys. **82**, 1804 (1997)
9. Q.M. Zhang, V. Bharti, X. Zhao: Science **280**, 2101 (1998)
10. T. Furukawa: Phase Trans. **18**, 143 (1989)
11. F.J. Balta, A.G. Arche, T.A. Ezquerra, C.S. Cruz, F. Batallan, B. Frick, E.L. Cabarcos: Prog. Polym. Sci. **18**, 1 (1993)
12. T. Furukawa, G.E. Johnson: J. Appl. Phys. **52**, 940 (1981)
13. G.H. Haertling: Ferroelectrics **75**, 25 (1987)
14. A.H. Meitzler, H.M. O'Bryan Jr.: Proc. IEEE **61**, 959 (1973)
15. J. Su, P. Moses, Q.M. Zhang: Rev. Sci. Instrum. **69**, 2480 (1998)
16. H. Vogel: Z. Phys. **22**, 645 (1921); G.S. Fulcher: J. Am. Ceram. Soc. **8**, 339 (1925)
17. A.K. Tagantsev: Phys. Rev. Lett. **72**, 1100 (1994)
18. J. Mattsson, T. Jonsson, P. Nordblad, H. ArAruga, A. Ito: Phys. Rev. Lett. **74**, 4305 (1995)
19. V. Bharti, X. Zhao, Q.M. Zhang, T. Romotowski, F. Tito, R. Ting: Mater. Res. Innovat. **2**, 57 (1998)
20. V. Bharti, H.S. Xu, G. Shanthi, Q.M. Zhang, K. Liang: J. Appl. Phys. **87**, 452 (2000)
21. J.K. Kruger, M. Prechtl, J.C. Wittmann, S. Meyer, J.F. Legrand, G.D. Asseza: J. Polym. Sci., Part B: Polym. Phys. **31**, 505 (1993)
22. T. Furukawa, N. Seo: Jpn. J. Appl. Phys., Part 1 **29**, 675 (1990)

23. H. Ohigashi, K. Omote, T. Gomyo: Appl. Phys. Lett. **66**, 3281 (1996)
24. K. Omote, H. Ohigashi, K. Koga: J. Appl. Phys. **81**, 2760 (1997)
25. In [22], it was found that the electrostriction is the origin of the piezoelectricity in P(VDF TrFE) copolymer and that Q_{33} is $2.1 \sim 2.5\,C^2/m^4$ for P(VDF-TrFE) 78/22, 65/35, and 52/48 copolymers with high crystallinity. In [23, 24], the single-crystal P(VDF-TrFE) 75/25 copolymer was studied. The piezoelectric coefficient ($d_{33} = 38$ pm/V), dielectric constant ($\varepsilon' \approx 4$), and remanent polarization ($P_r = 115\,mC/m^2$) were reported at the temperature of 295 K. Based on the relationship: $d_{33} = 2Q_{33}\varepsilon'\varepsilon_0 P_r$, one can get that Q_{33} is about $4.7\,C^2/m^4$
26. Z.-Y. Cheng, T.-B. Xu, V. Bharti, S. Wang, Q.M. Zhang: Appl. Phys. Lett. **74**, 1901 (1999)
27. Z.-Y. Zheng, V. Bharti, T. Mai, T.-B. Xu, Q.M. Zhang, K. Hamilton, T. Ramotowski, K.A. Wright, R. Ting: IEEE Trans. Ultrason., Ferroelectr. Freq. Cont., **47** (2000)
28. A.J. Lovinger: Science **220**, 1115 (1983)
29. D. Rollik, S. Bauer, R. Gerhard-Multhaupt: J. Appl. Phys. **85**, 3282 (1999)
30. F. Macchi, B. Daudin, J.F. Legrand: Nucl. Instrum. Methods Phys. Res., Sect. B **46**, 324 (1990)
31. Q.M. Zhang, J. Zhao: Appl. Phys. Lett. **71**, 1649 (1997)

APPENDIX 24

Dielectric study of the relaxor ferroelectric poly(vinylidene fluoride-trifluoroethylene) copolymer system

Vivek Bharti* and Q. M. Zhang
Materials Research Laboratory, The Pennsylvania State University, University Park, Pennsylvania 16802
(Received 12 June 2000; revised manuscript received 22 September 2000; published 18 April 2001)

The high-energy electron irradiated poly(vinylidene fluoride-trifluoroethylene), P(VDF-TrFE), copolymer exhibits many features resembling the relaxor ferroelectric behavior. In polymer systems, there are local dipolar motions at the monomer or unit cell scale, which manifest themselves as various relaxation processes. In this paper we investigate the relationship between the relaxor ferroelectric behavior, especially, Vogel-Fulcher (V-F) behavior and these local dipolar relaxation processes in irradiated P(VDF-TrFE) 65/35-mol % copolymer. In order to cover the change in polarization dynamics of the copolymer system, the dielectric behavior of copolymer is measured over a broad frequency (0.01 Hz–10 MHz) and temperature (−40 to 80 °C) range. The results indicate that there is an increased coupling among the local dipolar motions with reduced temperature in the crystalline region. On the other hand, the randomness introduced in the irradiation prevents the formation of a polar phase, on both the macroscale and the microscale, in the polymer. The observed relaxor behavior is a consequence of the competition of these two effects. The results further show that the V-F process of the irradiated copolymer system is different from the glass transition, which occurs in the amorphous phase of the copolymer.

DOI: 10.1103/PhysRevB.63.184103 PACS number(s): 77.84.Jd, 77.22.Gm, 77.80.Bh, 77.90.+k

I. INTRODUCTION

Relaxor ferroelectric material is a special class of ferroelectric materials that exhibits a diffused (broad) dielectric peak and that the dielectric maximum (T_m) is found to shift towards higher temperature with frequency and follows the Vogel-Fulcher (V-F) law.[1–4] Macroscopically, the dielectric constant peak does not correspond to a ferroelectric transition and under zero electric field, the material remains in a macroscopically nonpolar phase even at a temperature far below the dielectric constant peak temperature.[1,2] On the other hand, a macroscopic polar phase can be induced at a temperature below T_m where the polarization hysteresis loop can be observed. Over the past several decades, there has been a great deal of effort devoted to elucidate the fundamental mechanisms and microscopic and mesoscopic processes responsible for this peculiar phenomenon.[1–6]

Recently, we reported that poly(vinylidene fluoride-trifluoroethylene) P(VDF-TrFE) copolymers after high-energy electrons irradiation show many features resembling those observed in relaxor ferroelectric systems.[7–9] It is also interesting to note that all the relaxor ferroelectric phenomenon reported earlier was observed in inorganic systems. Here the relaxor ferroelectric behavior was observed in a polymer system, the system in which polarization response is directly from local dipolar motions.

The phase diagram of P(VDF-TrFE) copolymer system is shown in Fig. 1, where for composition range with VDF content between 50 and 85 mol %, a ferroelectric-paraelectric (F-P) transition is observed below their melting temperature.[10–14] The molecular conformation of these copolymers in the ferroelectric phase consists of the all trans planar zigzag chains while above the Curie temperature, this conformation changes to random sequences of trans and gauche bonds, resulting in a nonpolar phase (paraelectric phase).[10–13] Presented in Fig. 2 is the dielectric data as a function of temperature for unirradiated P(VDF-TrFE) 65/35-mol % copolymer measured as the sample is heated from −40 to 120 °C. The two dielectric relaxation processes (peaks) are observed in this temperature range. The peak at 105 °C, which is related to the α-relaxation process, appears to be due to the transition in crystalline region from all-trans ferroelectric phase to distorted trans-gauche paraelectric phase.[11,12] Early studies have shown that the α-relaxation process is associated with the local dipolar motions in the crystalline region.[11,12,15] Due to semicrystalline morphology of copolymer, the broad dielectric-loss peak at a temperature near −20 °C is from the glass transition in the amorphous region, i.e., from a glassy state to rubbery state and known as β-relaxation process.[12,15] However, for the β-relaxation process the real part of the dielectric constant does not show any significant anomality indicating that the molecular motions associated with this process is only weakly polar in nature.

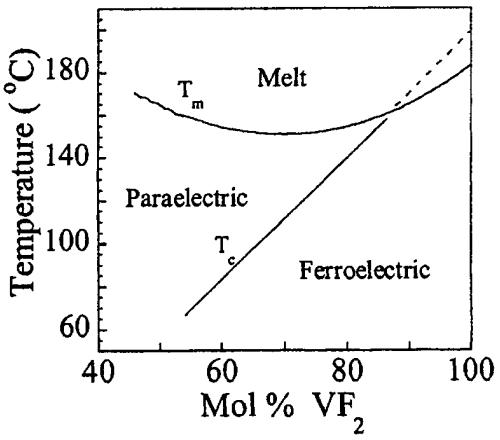

FIG. 1. The phase diagram for VDF/TrFe copolymer system. T_c denotes the F-P transition and T_m is the melting transition.

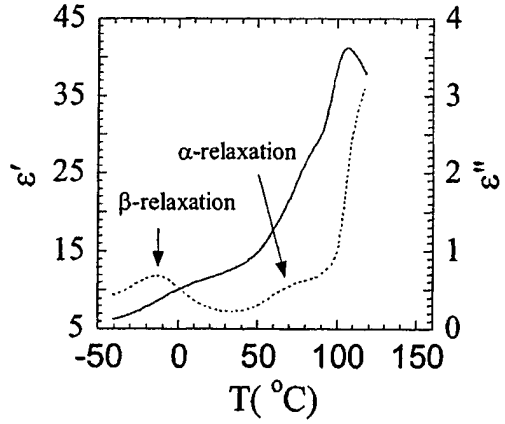

FIG. 2. The dielectric constant (solid line: real part and broken line: imaginary part) measured at 1 kHz as a function of temperature for the nonirradiated stretched film of P(VDF-TrFE) 65/35 mol % copolymer.

In this paper, we investigate the change in these relaxation processes as a consequence of high-energy electron irradiation. We will examine the relationship between these local relaxation processes, which occur at the monomer or unit cell scale and sensitive to changes in the local environment and conformation of the polymer chain, and the relaxor ferroelectric behavior, which could involve system response in the mesoscopic scale, observed in these copolymers. Hence, through this investigation, we can gain a microscopic and mesoscopic-scale understanding on the relaxor ferroelectric behavior in this class of material.

II. EXPERIMENT

P(VDF-TrFE) 65/35-mol % copolymer, supplied by Solvay and Cie, Bruxelles, was chosen for this study because the copolymer films of this composition, after having been mechanically stretched and high-energy electron irradiated, display relaxor ferroelectric behavior. The *N,N*-dimethyl formamide solvent was used to cast unstretched films. The stretched films of thickness ~25–30 μm were prepared by uniaxially stretching the solution cast films by five times the original length. In order to improve the crystallinity, these films were annealed at 140 °C for 16 h. The electron irradiation was carried out in a nitrogen atmosphere with 2.55-MeV electrons at 95 °C for several irradiation doses ranging from 40 to 100 Mrad where the copolymer exhibits relaxor ferroelectric behavior.

The temperature and frequency dependence of the dielectric constant was carried out using dielectric analyzers (DEA 2970, TA instrument) in the frequency range from 0.01 Hz to 100 kHz and impedance analyzer (HP4274A) from 1 kHz to 10 MHz. The samples were first heated up to 100 °C and then the dielectric measurements were performed for the cooling cycle in the temperature interval of 100 to −40 °C. Although a large thermal hysteresis, i.e., the difference in the dielectric constant and dielectric peak temperature between the heating and cooling cycles, was observed for nonirradiated copolymer films, for all the irradiated copolymer films

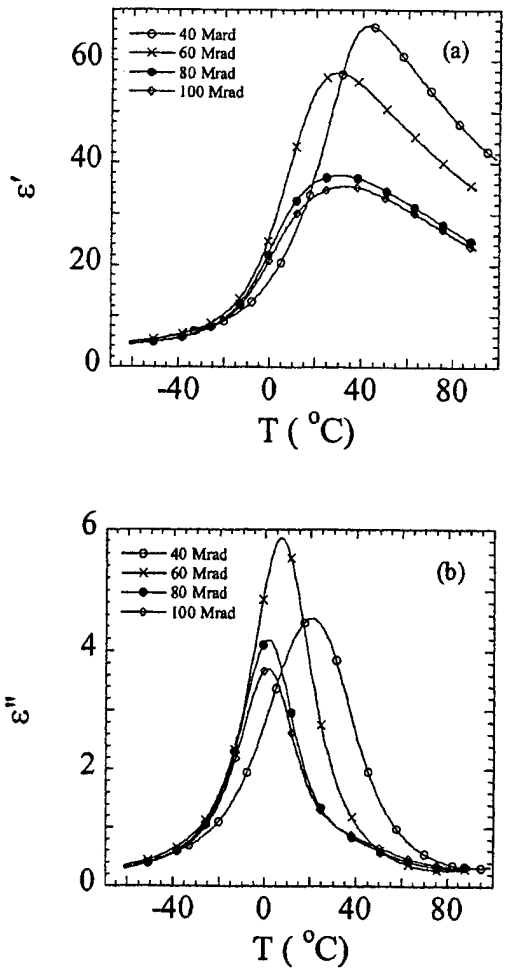

FIG. 3. The change in dielectric constant (a) real part, (b) imaginary part measured at 1 kHz as a function of temperature for P(VDF-TrFE) 65/35-mol % copolymer stretched films, irradiated at 95 °C with different irradiation doses.

there is little thermal hysteresis observed in the dielectric data. To avoid the moisture that could affect the low-frequency dielectric-loss data, all these measurements were performed in a nitrogen environment. Copolymer films used for these measurements were sputtered with gold electrodes on both surfaces.

III. RESULTS AND DISCUSSION

Figure 3 illustrates the dielectric constant data measured at 1 kHz for the copolymer films irradiated with different doses. All these copolymers exhibit a broad dielectric constant peak around room temperature, which is below the F-P transition temperature of the nonirradiated film. As has been shown in early studies, the broad dielectric peak observed here is not linked to any macroscopic structural changes in the copolymer system when there is no external high electric field.[8,16] In contrast to nonirradiated copolymer, where the peak of the real and imaginary part of the dielectric constant at the F-P transition appears at nearly the same temperature and also does not change with frequency, the imaginary di-

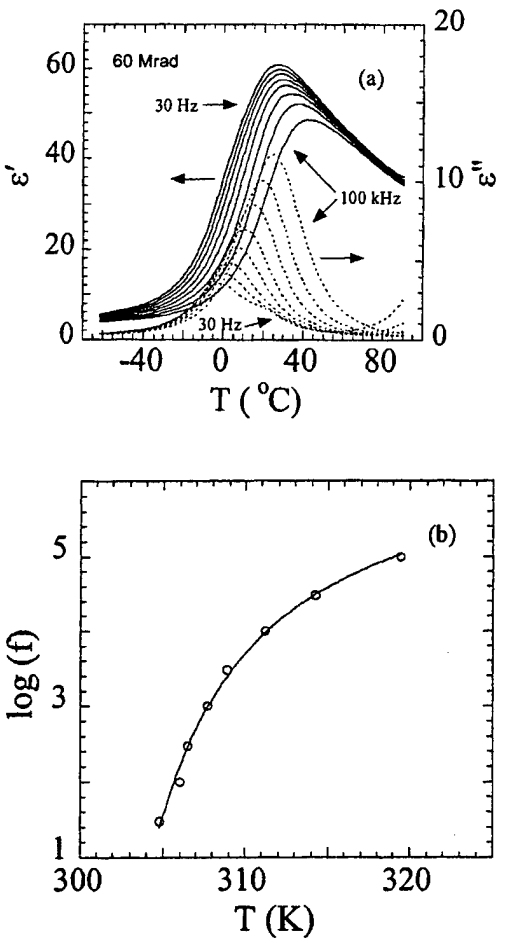

FIG. 4. (a) The dielectric constant (solid lines: real part; broken lines: imaginary part) as a function of temperature measured at different frequencies (30 Hz, 100 Hz, 300 Hz, 1 kHz, 3 kHz, 10 kHz, 30 kHz; and 100 kHz) for P(VDF-TrFE) 65/35-mol % copolymer stretched films, irradiated at 95 °C with 60-Mrad dose, and (b) fitting of V-F law for the data presented in (a), where the circles are the data points (peak of the real part of the dielectric constant) and solid line is the fitting.

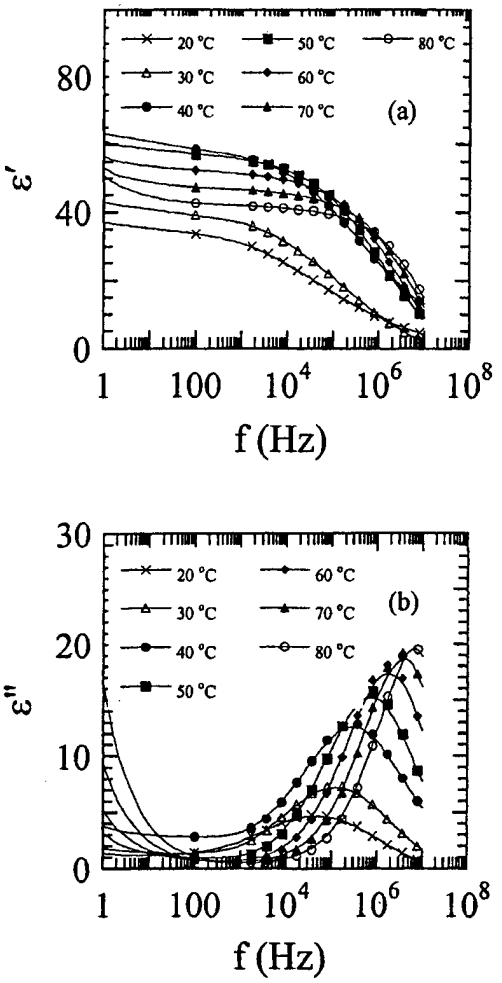

FIG. 5. The frequency dependence of the dielectric constant (a) real part and (b) imaginary part measured at temperature range between 20 and 80 °C for the P(VDF-TrFE) 65/35-mol % copolymer films irradiated with 40-Mrad dose. Solid curves are the data, and the symbols indicate the measuring temperatures.

electric constant peak of the irradiated copolymer is markedly below the peak of the real part of the dielectric constant [Fig. 4(a) for the copolymer irradiated with 60 Mrad], and the relationship between the peak temperature T_m (of the real part of the dielectric constant) and measuring frequency f can be well fitted with V-F law[17] as shown in Fig. 4(b):

$$f = f_0 \exp\left[\frac{-U}{k(T_m - T_f)}\right], \tag{1}$$

where k is the Boltzman constant, T_f has been regarded as a freezing temperature for a polar glass system and U is a constant (activation energy).[2,4] As has been observed from early studies, T_f in the irradiated copolymer coincides with the depolarization temperature, which is a temperature where the poled copolymer loses its remanent polarization as the temperature is raised.[8]

We now turn to the discussion of the dielectric relaxation processes in the irradiated copolymers. Presented in Figs. 5(a) and 5(b) are the dielectric dispersion data from the α relaxation for the irradiated copolymer film (40-Mrad dose) at temperatures around T_f of Eq. (1). The data for all nonirradiated and irradiated copolymers studied, are fitted with the modified Cole-Cole equation:[15]

$$\varepsilon(\omega) = \varepsilon(\infty) + \frac{\Delta\varepsilon}{1 + (i\omega\tau)^{\delta}}, \tag{2}$$

where $\varepsilon = \varepsilon' - j\varepsilon''$, $\Delta\varepsilon$ is the dielectric relaxation strength, τ is the average relaxation time, and δ is the parameter describing the distribution of the relaxation time in the system. When δ is equal to 1, the relaxation is monodispersive. A decrease in δ value from 1 indicates the broad distribution of relaxation times in the system.[15]

The peak of ε'' of Eq. (2) is at $\omega\tau = 1$ and fitting of the data yields τ. To facilitate the fitting to obtain $\Delta\varepsilon$ and δ, Eq. (2) is converted to

$$\left(\varepsilon' - \frac{\Delta\varepsilon}{2}\right)^2 + \left(\varepsilon'' + \frac{\Delta\varepsilon}{2}\cot(\delta\pi/2)\right)^2 = \left(\frac{\Delta\varepsilon}{2}\csc(\delta\pi/2)\right)^2,$$

which represents a circle with center at $(\Delta\varepsilon/2, -(\Delta\varepsilon/2)\cot(\delta\pi/2))$ and radius of $(\Delta\varepsilon/2)\csc(\delta\pi/2)$. The fitting results of the α-relaxation process are summarized in Fig. 6. One of the salient features of the results is that the dielectric relaxation strength $\Delta\varepsilon$ exhibits a broad peak at temperatures near the corresponding T_f for all the irradiated copolymers studied, while on the other hand, there is no anomalous change in the relaxation time with temperature [Figs. 6(a) and 6(b)]. In addition, δ decreases as the temperature is reduced, suggesting a broadening of the relaxation time distribution with reduced temperature. Figure 6(a) also reveals that T_f initially decreases with increased irradiation dose, which reflects the decrease of the polar ordering with dosage. However, T_f for the copolymers irradiated with 80-Mrad and 100-Mrad electrons is higher than that with 60-Mrad dose. This behavior is a result of the increased crosslinking density with dosage.[16] As shown in an early study, at doses higher than 60 Mrad, the increased crosslinking density leads to the reduction of the interchain spacing, which favors a less random conformation and hence, raises T_f slightly.[16]

For the comparison, the dielectric relaxation data for the α-relaxation process of nonirradiated copolymer films were measured at several temperatures (as the copolymer was heated from low to high temperature). $\Delta\varepsilon$ and τ are also fitted and plotted in Fig. 6, where anomalous changes in both $\Delta\varepsilon$ and τ are observed at the temperature of F-P transition.[12,13] In the nonirradiated copolymer, the peak in the dielectric relaxation strength $\Delta\varepsilon$ is due to the increased long-range coupling between the chain segment motions in the crystalline region with reduced temperature, which leads to the transformation to the low-temperature polar phase.[12] Because of this phase transition, there is also a change in the relaxation time, due to the change in the chain conformation between the all-trans conformation in the ferroelectric phase and the random trans-gauche conformation in the paraelectric phase. The local chain-segment motions are a thermally activated process and hence are described by the Arrhenius law,[15] $\tau = \tau_0 \exp(A/kT)$. In the nonirradiated copolymer, it is expected that the activation energy A at temperatures below the F-P transition is different from that above the transition, reflecting the change in the molecular conformation due to the transition.[18,19]

In analogy to the nonirradiated copolymer, the observed peak in $\Delta\varepsilon$ for the α-relaxation process near T_f suggests an increased coupling among the local dipoles with reduced temperature. On the other hand, there is no transformation to a polar phase, both on the macroscopic scale and the microscopic scale, when the temperature is lowered to below T_f as indicated by the data of the relaxation time τ, which is sensitive to the local phase and conformation changes. Combining these two results suggests that the defects introduced by the irradiation, such as crosslinkings and formation of side groups, prevent the development of the macroscopic polar ordering in the crystalline region. Because of the random trans-gauche conformation in the irradiated copolymer in all

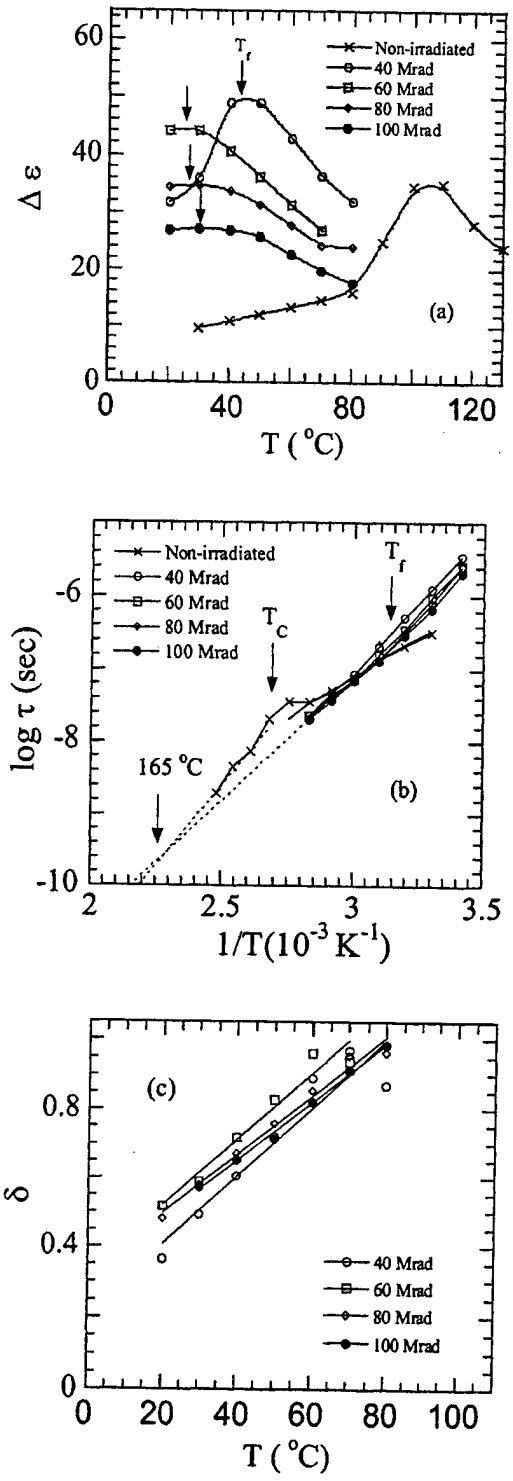

FIG. 6. The change of parameters obtained from the fitting of Eq. (2) as a function of temperature. (a) Dielectric relaxation strength $\Delta\varepsilon$ with temperature, (b) logarithms of the relaxation times τ as a function of $1/T$: the dashed lines are the extrapolation showing that at the melting temperature (165 °C), τ is the same for the nonirradiated and irradiated copolymers, (c) δ with temperature. In the figure, the corresponding T_f of the V-F law is also indicated. Data points are shown and solid curves are drawn to guide the eye.

TABLE I. Activation energy calculated from Arrhenius law [Fig. 6(a)].

Irradiation dose	Activation energy (A) calculated from Arrhenius fitting (eV)
Nonirradiated	0.19
40 Mrad	0.32
60 Mrad	0.31
80 Mrad	0.30
100 Mrad	0.29

the temperature range studied here, the activation energy of the α-process in the irradiated copolymer is higher than that of the nonirradiated copolymer in the ferroelectric phase as shown in Fig. 6(b). The activation energy A obtained from the slope of the Fig. 6(b) is summarized in Table I. For all the irradiated copolymers, the activation energy is about 0.3 eV and for nonirradiated copolymer, it is about 0.19 eV.

At this point, it is interesting to compare the results here with the dielectric behavior of a Debye relaxation system with a broad relaxation spectrum $g(\tau,T)$ and also with those of $Pb(Mg_{1/3}Nb_{2/3})O_3$ (PMN), the best-known relaxor ferroelectric system in inorganic systems. For such a system, the dielectric constant can be represented as a superposition of Debye relaxors with a relaxation distribution $g(\tau,T)$,[3,15]

$$\varepsilon^*(T)=\varepsilon_0(T)\int_0^\infty \frac{d(\ln\tau)}{(1-j\omega\tau)}g(\tau,T), \tag{3}$$

which yields the real and imaginary part of dielectric constant:

$$\varepsilon'(\omega,T)=\varepsilon_0(T)\int_0^\infty \frac{d(\ln\tau)}{1+(\omega\tau)^2}g(\tau,T), \tag{4a}$$

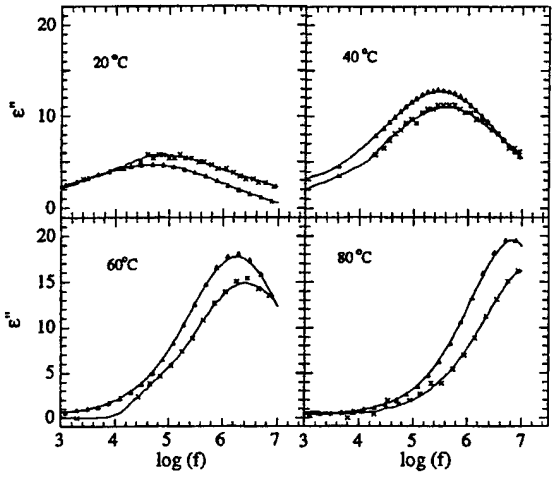

FIG. 7. Comparison of the calculated (cross) and measured (triangle) values of imaginary part of the dielectric constant of the copolymer films irradiated with 40-Mrad dose. Solid lines are drawn to guide the eye.

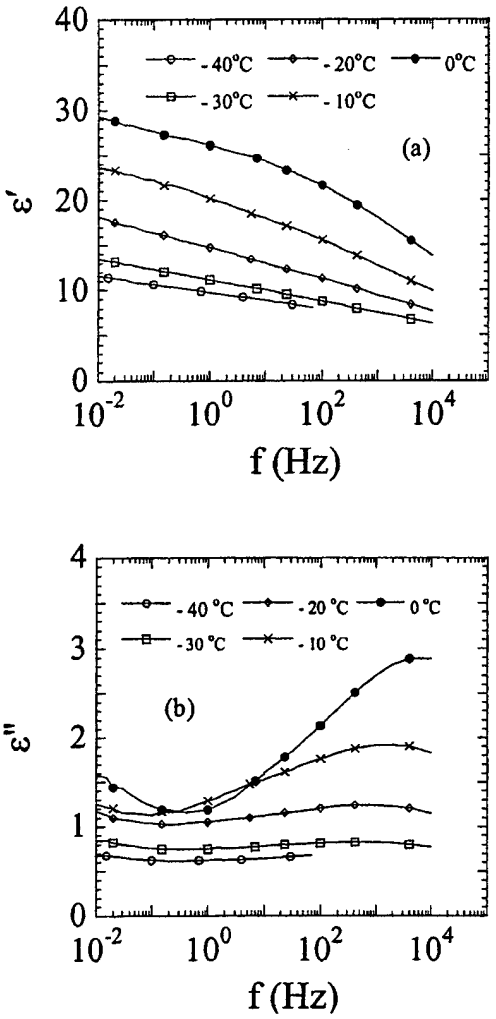

FIG. 8. The frequency dependence (low frequencies) of the (a) dielectric constant, and (b) dielectric loss measured at temperatures between −30 and 0 °C for the P(VDF-TrFE) 65/35-mol % copolymer films irradiated with 40-Mrad dose. Solid lines are the data, and the symbols indicate the temperatures.

$$\varepsilon''(\omega,T)=\varepsilon_0(T)\int_0^\infty \frac{d(\omega\tau)}{(1+\omega^2\tau^2)}g(\tau,T). \tag{4b}$$

In the limit of broad spectrum, the relation between the real and imaginary part of dielectric constant can also be described as[20]

$$\varepsilon''(\omega)=-(\pi/2)\frac{\partial\varepsilon'(\omega)}{\partial(\ln\omega)}. \tag{5}$$

Figure 7 is a comparison of the directly measured ε'' with that evaluated using Eq. (5), which shows a good agreement between the two sets of data, indicating a broad relaxation distribution in the system. Similar behavior has also been observed in PMN system,[3] hence showing the close resemblance in the broad relaxation time distribution between the two systems.

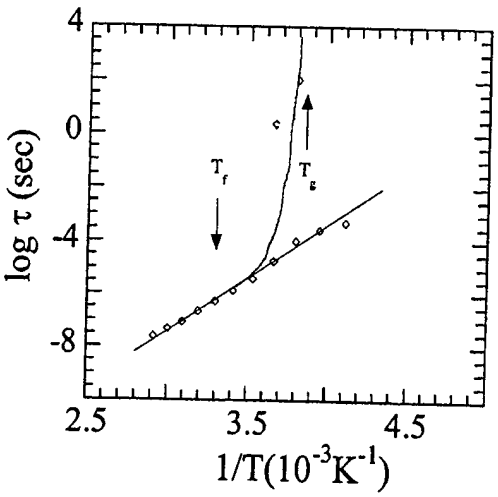

FIG. 9. The change of logarithms of relaxation time τ obtained from Cole-Cole fitting from the data in Figs. 5 and 8 with temperature for P(VDF-TrFE) 65/35-mol % copolymer films irradiated with 40-Mrad dose. Solid curves are drawn to guide the eye.

The β-relaxation process, which is attributed to the micro-Brownian motion of noncrystalline segments, is also characterized.[12,15] Presented in Fig. 8 is the frequency dependence of the real and imaginary part of the dielectric constant (ε' and ε'') measured in the frequency region from 0.01 Hz to 10 kHz and in the temperature range of -40 to 20 °C of the copolymer films irradiated with 40-Mrad dose. All the dispersion curves can be well fitted with Cole-Cole function with two relaxation processes. As shown in Fig. 9, where the change in $\log(\tau)$ obtained from fitting were plotted against $1/T$, there are two types of relaxation dispersion comprising the low-temperature dielectric data that have different temperature dependency, one is WLF-type (Williams, Landel, and Ferry), appears due to the glass transition in the amorphous region, where the relaxation time drastically increases approaching T_g, and another is Arrhenius-type due to the local dipolar motions in the crystalline region.[11,12] It is clear here that the V-F relaxation process that appears at temperature far above T_g, is a separate process and does not bear any correlation with the glassy nature of the copolymer system that appears below glass transition temperature (T_g).

IV. SUMMARY

By examining the relationship between the relaxor ferroelectric behavior, and especially, the V-F behavior and local dipolar responses in the irradiated copolymers, we show the following:

There is an increased coupling among the local dipoles in the crystalline region as the temperature is reduced. However, due to the randomness of the defect structure introduced in the irradiation process, there is no anomalous change in the relaxation time of the α-process at temperatures near T_f. This plus the high activation energy of the Arrhenius-type activation process indicate that the irradiated copolymer system remains in a nonpolar phase and there is no local polar region developed as the temperature is reduced. Those competing effects plus the broad relaxation time distribution could be responsible for the observed relaxor ferroelectric behavior in the irradiated P(VDF-TrFE) copolymer.

ACKNOWLEDGMENTS

The authors wish to thank D. Viehland and Z.-Y. Cheng for stimulating discussions and G. Shanthi for carrying out some analysis. This work was supported by the National Science Foundation under Grant No. ECS-9710459 and Office of Naval Research under Grant No. N00014-97-1-0900.

*Present address: 3M Center, Bldg. No. 201-01W-28, St. Paul, MN 55144.

[1] L. E. Cross, Ferroelectrics **151**, 305 (1994).
[2] D. Viehland, S. J. Jang, L. E. Cross, and M. Wuttig, J. Appl. Phys. **68**, 2916 (1990).
[3] E. V. Colla, E. Yu Koroleva, N. M. Okuneva, and S. B. Vakhrushev, J. Phys.: Condens. Matter **4**, 3671 (1992).
[4] A. E. Glazounov and A. K. Tagantsev, Appl. Phys. Lett. **73**, 856 (1998).
[5] Q. M. Zhang and J. Zhao, Appl. Phys. Lett. **71**, 1649 (1997).
[6] H. You and Q. M. Zhang, Phys. Rev. Lett. **79**, 3950 (1997).
[7] Q. M. Zhang, V. Bharti, and X. Zhao, Science **280**, 2101 (1998).
[8] V. Bharti, X. Zhao, and Q. M. Zhang, Mater. Res. Innovations **2**, 57 (1998).
[9] V. Bharti, H. S. Xu, and Q. M. Zhang, J. Appl. Phys. **87**, 452 (2000).
[10] H. S. Nalwa, *Ferroelectric Polymers* (Dekker, New York, 1995), Chap. 2.
[11] T. Furukawa, Phase Transit. **18**, 143 (1989).
[12] T. Furukawa, Y. Tajitsu, and X. Zhang, Ferroelectrics **135**, 401 (1992).
[13] A. J. Lovinger, T. Furukawa, G. T. Davis, and M. G. Broadhurst, Polymer **24**, 1225 (1983).
[14] T. Yagi, M. Tatemoto, and J. Sako, Polym. J. (Tokyo) **12**, 209 (1980).
[15] N. G. McCrum, B. E. Read, and G. Williams, *Anelastic and Dielectric Effects in Polymeric Solids* (Dover, New York, 1991), Chap. 4.
[16] Haisheng Xu, G. Shanthi, V. Bharti, Q. M. Zhang, and T. Ramatowski, Macromolecules **33**, 4125 (2000).
[17] H. Vogel, Z. Phys. **22**, 645 (1921); G. S. Fulcher, J. Am. Ceram. Soc. **8**, 339 (1925).
[18] T. Yamada, T. Mizutani, M. Ieda, J. Phys. D **15**, 289 (1982).
[19] N. Koizumi, N. Haikawa, and H. Habuka, Ferroelectrics **57**, 99 (1984).
[20] L. Lindgren, P. Svedlindh, and O. J. Beckman, J. Magn. Magn. Mater. **25**, 33 (1981).

APPENDIX 25

ELSEVIER

Sensors and Actuators A 90 (2001) 138–147

SENSORS AND ACTUATORS A PHYSICAL

www.elsevier.nl/locate/sna

Electrostrictive poly(vinylidene fluoride-trifluoroethylene) copolymers

Z.-Y. Cheng*, V. Bharti, T.-B. Xu, Haisheng Xu, T. Mai, Q.M. Zhang

Laboratory of Materials Research, Department of Electrical Engineering, The Pennsylvania State University, University Park, PA 16802, USA

Received 9 June 2000; received in revised form 9 January 2001; accepted 16 January 2001

Abstract

High energy electron (1.0–2.55 MeV) irradiation was used to modify the phase transitional behavior of poly(vinylidene fluoride-trifluoroethylene) (P(VDF-TrFE)) copolymers in an attempt to significantly improve the electromechanical properties of the copolymers. It is found that the copolymers under a proper irradiation treatment exhibit very little room temperature polarization hysteresis and very large electrostrictive strain (the longitudinal strain of −5% can be achieved). Because of the large anisotropy in the strain responses along and perpendicular to the polymer chain, the transverse strain can be tuned over a broad range by varying the film stretching condition. For unstretched films, the magnitude of transverse strain is approximately about/less than 1/3 of that of the longitudinal strain, and for stretched films, the transverse strain along the stretching direction is comparable to the longitudinal strain. In addition to the high strain response, the irradiated copolymers also possess high elastic energy density and mechanical load capability as indicated by the relatively high elastic modulus of the copolymer and the high strain response of the transverse strain even under 40 MPa tensile stress. The high strain and high elastic modulus of the irradiated copolymer also result in an improved electromechanical coupling factor where the transverse coupling factor of 0.45 has been observed. The frequency dependence of the strain response was also characterized up to near 100 kHz and the results show that the high electromechanical response can be maintained to high frequencies. Several unimorph actuators were fabricated using the modified copolymer and the test results demonstrate high performance of the devices due to the high strain and high load capability of the material. © 2001 Published by Elsevier Science B.V.

Keywords: Actuator; Electrostriction; P(VDF-TrFE); Phase transformation; Irradiation

1. Introduction

Electroactive polymers (EAP), which change shape as an electric field is applied, can be used in many areas, such as artificial muscles and organs, smart materials for vibration and noise control, electromechanical actuators and sensors for robots, acoustic transducers used for underwater navigation and medical imaging, and fluid pumps and valves [1–10]. The function of the EAP in these applications is to perform energy conversion between the electrical and mechanical forms. Compared with piezoceramic and magnetostrictive actuator materials, polymers have many advantages, such as flexibility, easy processing, light weight, and low cost. Polymeric materials can also withstand a large dimensional change (strain) without fatigue and are quite robust. On the other hand, the traditional piezoelectric EAPs suffer low strain, low elastic energy density, and low electromechanical conversion efficiency, which limit their applications in comparison with the piezoelectric ceramics [1,2]. Hence, one of the challenges in the development and utilization of EAPs for a wide range of applications is how to significantly increase and improve the electromechanical responses so that to achieve high strain capability, high elastic power density, and high electromechanical conversion efficiency. In recent years, there has been a great deal of effort put forth to explore different new approaches to improve the performance of existing polymers and/or to develop high performance polymers [3,6,11–13]. The recent work on high energy electron irradiated poly(vinylidene fluoride-trifluoroethylene) (P(VDF-TrFE)) copolymer, which exhibits very high electrostrictive strain with high elastic modulus and high load capability [11,14–16], is one of the advances made in this field.

In order to provide understanding on the basic mechanism underlying the high electrostrictive responses in irradiated P(VDF-TrFE) copolymers, in this paper, we will first review briefly several unique features associated with ferroelectric–paraelectric (F–P) phase transition, which can be made use of in developing high performance EAPs. Then, the electromechanical responses of this newly developed polymer will

* Corresponding author. Tel.: +1-814-865-0146; fax: +1-814-863-7846.
E-mail address: zxc7@psu.edu (Z.-Y. Cheng).

0924-4247/01/$ – see front matter
PII: S0924-4247(01)00496-4

be presented including the strain responses, electromechanical coupling factor, load capability, and frequency dependence behavior of the strain response. To demonstrate the performance of this class of material, several unimorph actuators were fabricated and test results will also be discussed.

2. Ferroelectric–paraelectric phase transformation in P(VDF-TrFE) copolymers

In this section, we will review several unique phenomena associated with F–P phase transformation, especially in P(VDF-TrFE) copolymers. In many polymeric materials, it is well known that there are large strain changes associated with transformation from one phase to another. For P(VDF-TrFE) copolymers, large lattice strains have been detected when the copolymer goes from the low-temperature (LT) ferroelectric phase to the high-temperature (HT) paraelectric phase. Presented in Fig. 1 is the X-ray data on the lattice strain along the polymer chain direction ((0 0 1) reflection) and perpendicular to the chain ((2 0 0, 1 1 0) reflections) for the copolymer of 65/35 mol% [17]. As revealed by the data, for this copolymer there is a lattice strain of −10 and 7% in the crystalline phase along and perpendicular to the polymer chain, respectively, as the copolymer goes through the phase transition. Therefore, for a highly aligned copolymer with a high crystallinity (>50% crystallinity), these strains can be translated to large macroscopic strains. Indeed, a thermal strain of more than 6% has been observed on a 65/35 copolymer when going through the phase transition [18]. In addition, for a ferroelectric polymer, the phase transformation can be controlled by an external field (both electric and mechanical), and hence, it is expected that a high field induced strain can be achieved in P(VDF-TrFE) copolymer by exploiting the lattice strain at F–P transformation.

Another interesting feature associated with the F–P transition is that there is a possibility of a very large electromechanical coupling factor ($k \sim 1$) being obtained near a first order F–P transition temperature. As shown by an earlier study based on phenomenological theory, in a ferroelectric single crystal at temperatures above the transition where a polar-state can be induced by external dc bias fields, the coupling factor can approach 1 (near 100% energy conversion efficiency) [19]. That result is presented in Fig. 2 where the parameters used for the phenomenological formula are those from the ferroelectric $BaTiO_3$ single crystal, a typical ferroelectric material. This is a general result for the first order F–P phase transformation in spite of the fact that the curves in Fig. 2 are from the parameters of $BaTiO_3$. For P(VDF-TrFE) copolymers, it has been shown that at compositions with VDF content >60%, the F–P transition is first order in nature [20]. The temperature range in which the electric field can induce the phase transition from non-polar to polar phases depends strongly on the material. For most of the inorganic ferroelectrics, this temperature range is relatively narrow. For instance, the range is about 8°C for $BaTiO_3$ (as approximately measured by the temperature range between F–P transition and critical temperature) [21]. For P(VDF-TrFE) copolymers, it has been found that this temperature range is relatively large as reported by a recent study on Langmuir–Blodgett film of P(VDF-TrFE) 70/30 mol%, where this temperature range is observed to be more than 50°C [22].

All these results indicate that one may be able to improve the electromechanical response of P(VDF-TrFE) copolymer significantly by operating the polymer near the F–P transition. However, there are several issues associated with the first order F–P transition in P(VDF-TrFE) copolymer that have to be addressed. As has been shown in the phase diagram (Fig. 3), F–P transition in all P(VDF-TrFE) compositions occurs at temperatures higher than room temperature and the transition is relatively sharp (over a relatively narrow temperature range). In addition, large hysteresis has been observed for the copolymers at the first order F–P transition, which is a basic feature for this type of transition. A large hysteresis is not desirable for practical applications.

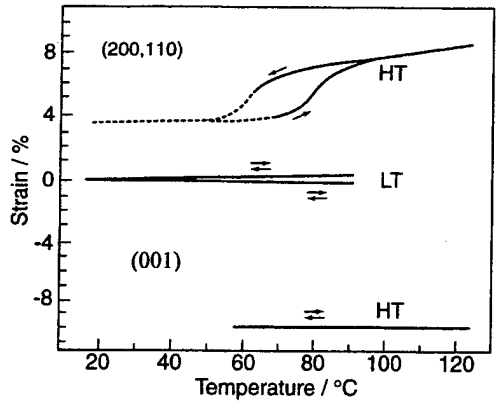

Fig. 1. Lattice strains along (0 0 1) and (2 0 0, 1 1 0), respectively, obtained from X-ray data for P(VDF-TrFE) 65/35 mol% copolymer.

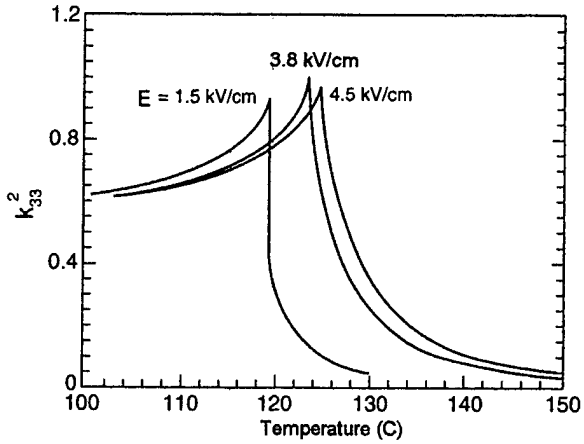

Fig. 2. Electromechanical coupling factor (k_{33}) as a function of temperature for a material with a first order F–P phase transition under different dc bias fields (E). The results are calculated based on Landau–Devonshire theory using the parameter obtained on $BaTiO_3$.

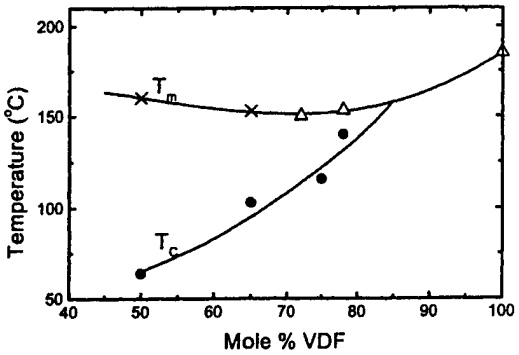

Fig. 3. Phase diagram of P(VDF-TrFE) copolymer. Where T_m and T_c are the melting temperature and F–P phase transition temperatures, respectively.

Therefore, to make use of the unique opportunities near the first order F–P transition in P(VDF-TrFE) copolymer systems, the copolymer should be modified as to broaden the phase transition region, move it to room temperature, and minimize the hysteresis.

3. Electromechanical properties of high energy electron irradiated P(VDF-TrFE) copolymer

In polymeric materials, high energy electron irradiation has been widely used to modify polymer properties. In P(VDF-TrFE) copolymers, Lovinger found that by using high energy electron irradiation, the ferroelectric phase at room temperature can be converted into a macroscopically paraelectric like phase [23]. Subsequent studies by Odajima et al. and Daudin et al. also found that a sharp dielectric constant peak from the F–P transition can be broadened markedly and moved to near room temperature [24,25]. Inspired by these early results, we carried out investigations on the electromechanical response of high energy electron irradiated P(VDF-TrFE) copolymers and the results show that indeed, the polarization hysteresis can be eliminated and copolymer with very high electrostrictive responses can be achieved.

3.1. Experimental

The P(VDF-TrFE) copolymer powders with a weight averaged mean molecular weight of 200,000 were purchased from Solvay and Cie, Bruxelles, Belgium. Two types of films are used in this investigation, stretched and unstretched films. In unstretched films, the films prepared were annealed at 140°C for a time period between 12–14 h to improve the crystallinity. In stretched films, films made from solution cast or quenched from melt press were uniaxially stretched up to five times at a temperature between 25 and 50°C. Afterwards, these films were also annealed at 140°C for 12–14 h to increase the crystallinity. The irradiation was carried out at nitrogen or argon atmosphere at different temperatures from room temperature to 120°C. Three electron energies were used in the irradiation: 1, 1.2, and 2.55 MeV. It was found that among the electron energies used, the irradiation with lower electron energy yields better electromechanical performance in the copolymers.

The elastic modulus of films was measured using a dynamic mechanical analyzer (TA Instrument, DMA model 2980). Gold electrodes with a thickness of about 40 nm were sputtered on both surfaces of the film for the electric and electromechanical characterizations. The field induced longitudinal strain was measured using a bimorph-based set-up [26]. The transverse strain was acquired using a newly developed set-up specially designed for flexible films [27]. An optical interferometer was applied to characterize the longitudinal strain response at high frequencies. An HP 4194A impedance analyzer was used to characterize the resonance behavior of the films under dc electric bias field.

Copolymers in the composition range with VDF content between 50 and 80 mol% were chosen for the investigation. In the experiment, it was found that there are two competing factors affecting the selection of the copolymers. On one hand, for copolymers in this composition range, the ferroelectricity becomes stronger with the VDF content as indicated by higher F–P transition temperature and increased coercive field for copolymers with higher VDF content. As a result, it becomes progressively more difficult to eliminate the polarization hysteresis and generate electrostrictive strain using the irradiation approach here for copolymers with high VDF content. In fact, for copolymers with VDF content higher than 70 mol%, it becomes very difficult to convert the copolymer into an electrostrictive material with small hysteresis at room temperature using the high energy electron irradiation [28]. On the other hand, the lattice strains associated F–P transition increase with the VDF content, implying a high induced strain response for copolymers with high VDF content [29]. As a compromise, therefore, in this paper, we focus on P(VDF-TrFE) copolymers with 65/35 and 68/32 mol% ratio.

Presented in Fig. 4 are polarization loops measured at room temperature at 10 Hz for 65/35 unstretched copolymer film before and after irradiation. For the unirradiated film, a typical polarization hysteresis loop was observed due to the high nucleation barrier when switching polarization from

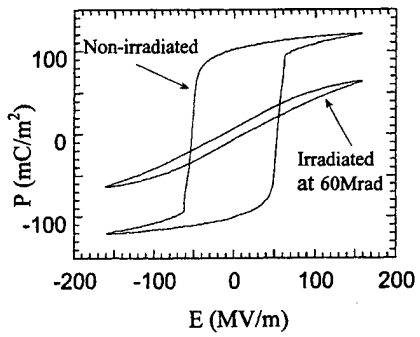

Fig. 4. Polarization loop for P(VDF-TrFE) 65/35 mol% film before and after irradiation.

the coherent macroscopic polar domains. After irradiation with 60 Mrad dose at 120°C, the polarization hysteresis is significantly reduced and the loop becomes quite slim due to the breaking up of macroscopic coherent polar domains to microscopic polar regions. The results indicate that the high energy irradiation is quite effective in eliminating the polarization hysteresis in these polymers.

3.2. Electrostrictive strains and electromechanical coupling factors at low frequency

Longitudinal strain (S_3), which is the thickness change of the film induced by applied electric fields, was characterized for films exhibiting slim polarization loops. Presented in Fig. 5(a) is the longitudinal strain measured for 65/35 mol% copolymers irradiated with 2.55 MeV electron at two irradiation temperatures and doses, where the external electric field is at 1 Hz while the strain was measured at 2 Hz because of electrostrictive nature of the strain response. In this paper, the frequency cited is that of the external electric field. The data indicate that there is no significant difference in S_3 between stretched and unstretched films. Shown in Fig. 5(b) is S_3 for unstretched 68/32 mol% copolymer film irradiated at 105°C with 70 Mrad dose of 1.0 MeV electrons. Apparently, a longitudinal strain $S_3 \approx -5\%$ can be induced by an electric field of 150 MV/m in the film. The temperature dependence of the strain response for 68/32 irradiated copolymer film (Fig. 5(b)) is summarized in Fig. 5(c), which shows that at a temperature range up to 80°C, the field induced strain can remain nearly constant.

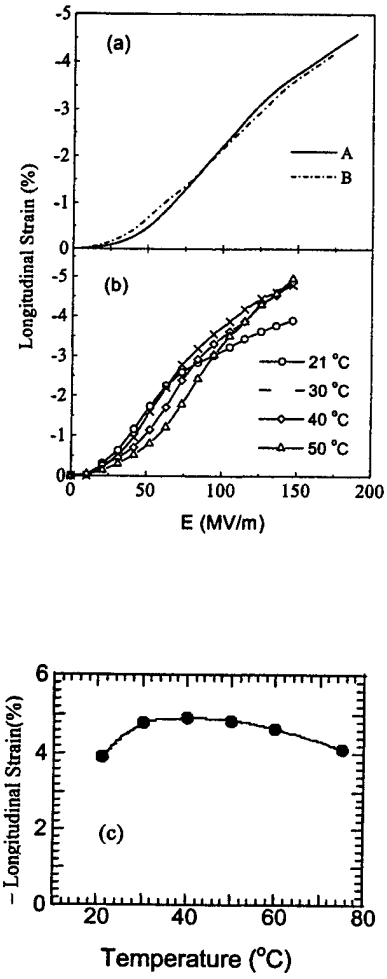

Fig. 5. Amplitude of the longitudinal strain as a function of the amplitude of the electric field at 1 Hz: (a) strain measured at room temperature for the 65/35 mol% copolymer films irradiated with 2.55 MeV electrons. Curves A and B correspond to the stretched film irradiated at 120°C with 80 Mrad dose and unstretched film irradiated at RT with 100 Mrad dose, respectively; (b) strain measured at different temperatures, which are indicated in figure, for unstretched 68/32 mol% copolymer film irradiated at 105°C with 70 Mrad dose of 1.0 MeV electrons; and (c) the temperature dependence of the longitudinal strain amplitude for the film shown in (b) under a constant electric field of 150 MV/m.

It should be mentioned that the doses used for the data in Fig. 5 are the optimum doses required to produce the slim polarization loop and high electrostrictive strain in these polymer films. Lowering the dosage will result in a large hysteresis and increasing the dosage will cause a significant reduction of the electrostrictive strain in the films.

In P(VDF-TrFE) copolymers, there exists large anisotropy in the strain responses along and perpendicular to the chain direction. Therefore, the transverse strain, which is associated with the length change of the film under an electric field, of the irradiated copolymers can be tuned over a large range by varying the film processing condition [15]. For unstretched films, the transverse strain is relatively small (approximately +1% level at ~100 MV/m) and in most of the films examined, the amplitude ratio between the transverse strain and longitudinal strain is less than 0.33. This feature is attractive for devices utilizing the longitudinal strain, such as ultrasonic transducers in the thickness mode, and actuators and sensors making use of the longitudinal electromechanical responses of the material. For example, a very weak transverse electromechanical response in comparison with the longitudinal one can significantly reduce the influence of the lateral modes on the thickness resonance and improve the performance of the thickness transducer.

On the other hand, for stretched films, a large transverse strain (S_1) along the stretching direction can be achieved as shown in Fig. 6, where the transverse strain about +3.5% is observed in the irradiated copolymer under an electric field of 110 MV/m. It is also found that for stretched films, the amplitude of the transverse strain along the stretching direction can be comparable with that of the longitudinal strain, while amplitude of the transverse strain in direction perpendicular to the stretching direction (S_2) is much small (approximately −1% at 100 MV/m).

It is interesting to note that for P(VDF-TrFE) copolymers, the strain along the thickness direction (parallel to the electric field) is always negative regardless the sample processing condition. That is, the thickness is reduced as the field or polarization is raised. In fact, this is a general feature for a system in which polarization response

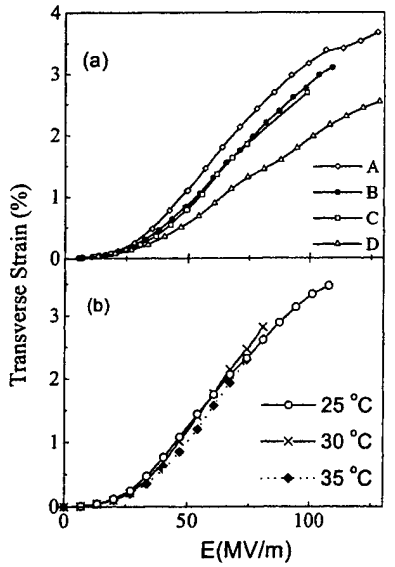

Fig. 6. Amplitude of the transverse strain along stretching direction as a function of amplitude of the electric field at 1 Hz for stretched samples: (a) curves A, B, C, and D correspond to the strain measured at room temperature for copolymer films under different irradiation conditions, A: 68/32 mol% film irradiated at 100°C with 65 Mrad doses of 1.2 MeV electrons, B: 65/35 mol% film irradiated at 105°C with 70 Mrad dose of 1.0 MeV electrons, C: 65/35 mol% film irradiated at 95°C with 60 Mrad dose of 2.55 MeV, and D: 65/35 mol% film irradiated at 77°C with 80 Mrad dose of 2.55 MeV; (b) strain measured at different temperatures, which are indicated in figure, for stretched 68/32 mol% copolymer film irradiated at 100°C with 70 Mrad dose of 1.2 MeV electrons.

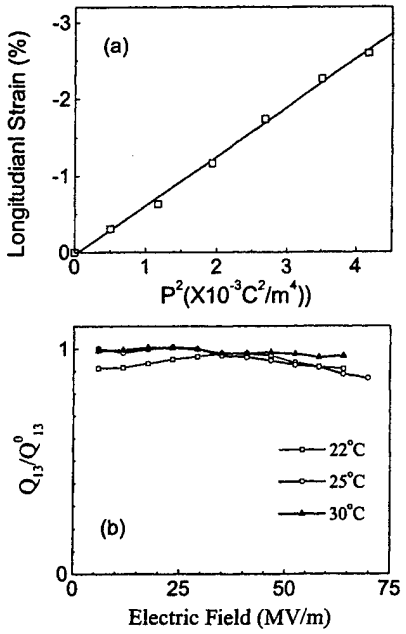

Fig. 7. (a) Longitudinal strain measured at room temperature vs. P^2 for unstretched 68/32 mol% copolymer film irradiated at 105°C with 70 Mrad dose of 1.0 MeV electrons, where P is the polarization; (b) electrostrictive coefficient Q_{13} vs. electrical field amplitude measured at 22, 25, and 30°C for stretched 65/35 film irradiated at 95°C with 60 Mrad dose of 2.5 MeV electrons, where Q_{13}^0 is the weak field Q_{13} (measured at about 10 MV/m and 30°C).

originates from the dipolar interaction and, therefore, is true for all the polymeric piezoelectric and electrostrictive responses [30,31]. For the strains perpendicular to the applied field direction, the sign of the strain will depend on the sample processing conditions. For an anisotropic sample, such as stretched films examined here, the electric induced strain along the stretching direction, which is perpendicular to the applied field, is positive, while in the direction perpendicular to both stretching and applied field directions, the strain is negative. For unstretched samples which are isotropic in the plane perpendicular to the applied field, the strain component in the plane is an average of the strains along the chain (positive) and perpendicular to the chain (negative) and is in general positive.

From the data of the longitudinal and transverse strain responses, the volume strain can be determined, which is about 1/3 of the longitudinal strain. That is, the volume of the film decreases with applying electric fields and the volume strain can reach −1% under a field of 100 MV/m, which is relatively large compared with other electroactive materials, such as polyurethane, silicone, and piezoelectric ceramics. The large volume strain induced by external electric fields in the irradiated copolymer indicates that the copolymer should have a high response when used for hydrostatic applications. This large volume strain originates from the local electric field induced phase transformation, which is a unique feature of this class of material and has been confirmed directly in a recent X-ray experiment [32].

By plotting the field induced strain versus the square of induced polarization, it is found that the strain is almost linearly dependent on P^2 as shown in Fig. 7(a), confirming that the strain response is electrostrictive in nature. The charge related electrostrictive coefficients (Q_{ij}) can be obtained

$$S_3 = Q_{33}P^2 \text{ and } S_1 = Q_{13}P^2 \quad (1)$$

The Q_{33} is found to be in the range from −4 to −12 m^4/C^2, depending on the irradiation condition. On the other hand, since the dielectric constant of the irradiated copolymer is strongly non-linear, the relationship between the strain and applied electric field E_3 is not well defined. Although the relationship of

$$S_3 = M_{33}E_3^2 \text{ and } S_1 = M_{13}E_3^2 \quad (2)$$

are often used in the literature to approximate the strain responses of ferroelectric-based electrostrictive materials, the field related electrostrictive coefficient M_{ij} will change with the applied field amplitude.

We now discuss the electromechanical coupling factors for the irradiated copolymers, which are directly related to the energy conversion efficiency of the material, and hence, are important parameters for most of electromechanical applications. For electrostrictive materials, the

electromechanical coupling factor (k_{ij}) has been derived by Hom et al. based on the consideration of electric and mechanical energies generated in the material under external field [33]

$$k_{3i}^2 = \frac{kS_i^2}{s_{ii}^D[P_E \ln((P_S+P_E)/(P_S-P_E))+P_S \ln(1-(P_E/P_S)^2)]} \quad (3)$$

where $i = 1$ or 3, corresponding to the transverse or longitudinal direction (for example, k_{31}, is the transverse coupling factor) and s_{ii}^D the elastic compliance under constant polarization, S_i and P_E are the strain and polarization responses, respectively, for the material under an electric field of E. The coupling factor depends on E, the electric field level. In Eq. (3), it is assumed that the polarization–field (P–E) relationship follows approximately [33]

$$|P_E| = P_S \tanh(k|E|) \quad (4)$$

where P_S is the saturation polarization and k a constant. It is found that Eq. (4) describes the P–E relationship of the irradiated copolymers studied here quite well [14].

The elastic modulus for the films examined here are shown in Fig. 8. Using the data in Figs. 5b, 6b and 8, along with the polarization data, the coupling factors, k_{33} for the unstretched sample and k_{31} for the stretched sample along the drawing direction, are evaluated and presented in Fig. 9. At near room temperature and under 80 MV/m electric field, k_{33} can reach more than 0.3, which is comparable to that obtained in single crystal P(VDF-TrFE) copolymer [13]. More importantly, the data also shows that a coupling factor k_{31} of 0.45 can be obtained, which is much higher than those in unirradiated P(VDF-TrFE) copolymers and even higher than k_{31} from most piezoceramics [34]. Since the energy conversion efficiency is proportional to the square of the coupling factor, this improvement is significant. In many applications, such as micro-electromechanical-systems (MEMS), electrical power generation from ocean waves, and artificial muscles, it is the transverse strain that is often used and a high transverse coupling factor, therefore, is highly desirable.

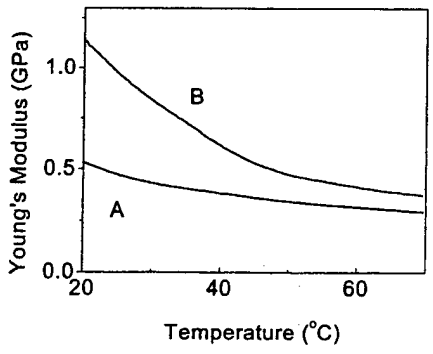

Fig. 8. Young's modulus at 1 Hz as a function of temperature for irradiated P(VDF-TrFE) copolymer films. Curve A is the modulus of unstretched 68/32 mol% irradiated at 105°C with 70 Mrad dose of 1.0 MeV electrons, and curve B is the modulus along stretching direction of stretched 68/32 mol% irradiated at 100°C with 70 Mrad dose of 1.2 MeV electrons.

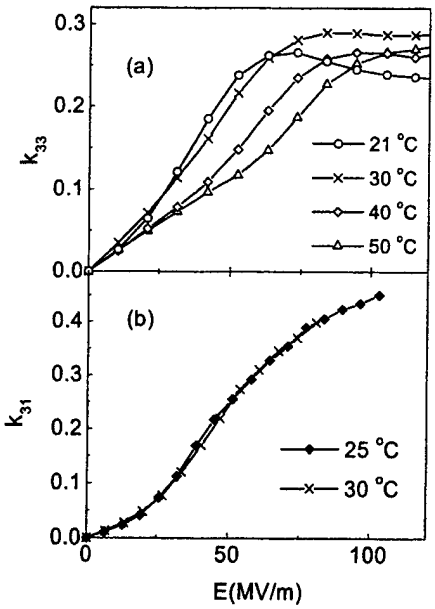

Fig. 9. Electromechanical coupling factor as a function of the electric field: (a) k_{33} for unstretched P(VDF-TrFE) 68/32 mol% film irradiated at 105°C with 70 Mrad dose of 1.0 MeV electrons; (b) k_{31} for stretched P(VDF-TrFE) 68/32 mol% film irradiated at 100°C with 70 Mrad dose of 1.2 MeV electrons.

3.3. High frequency strain response and electromechanical resonance behavior

The irradiated copolymer exhibits relaxor ferroelectric behavior which shows a strong dielectric dispersion at near room temperature [11]. Therefore, it is expected that there will also be frequency dispersion of the field induced strain since the electrostrictive strain is closely related to the polarization response in the material, i.e. Eqs. (1) and (2). To characterize the electromechanical responses at high frequencies, we carried out two experiments. One is to perform the field induced strain measurements directly to high frequencies. The other is to measure the electromechanical resonance, which occurs at frequencies higher than 30 kHz when the copolymers are under dc bias fields (for an electrostrictive copolymer, a dc bias field is required to induce an effective piezoelectric state) and from which the electromechanical coupling factor can be obtained.

The frequency dependence of the longitudinal strain (in reduced unit) for 68/32 unstretched film is shown in Fig. 10. The measuring field used here is limited to below 30 MV/m due to the limitation of the power supply. Although the strain response decreases with frequency as one would expect, this reduction is not severe. Over a four-decade frequency change, i.e. from 1 Hz to 10 kHz, the reduction of the strain at near room temperature is less than half and at higher temperatures, the strain level can remain nearly constant in this frequency range. The results demonstrate that the

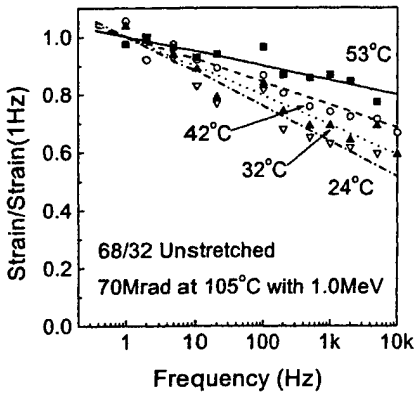

Fig. 10. Frequency dependence of longitudinal strain response for unstretched 68/32 mol% copolymer under 20 MV/m field. The film was irradiated at 105°C with 70 Mrad of 1.0 MeV electrons.

material studied here can produce high strain at high frequencies. The results here are also consistent with the dielectric data where at temperatures higher than the broad dielectric peak (>40°C), the dielectric dispersion becomes quite small. In fact, since the charge related electrostrictive coefficient Q is nearly independent of frequency and weakly dependent on temperature, Eq. (1) indicates that the frequency dependence of high field polarization (and dielectric) response can be used to predict the frequency dependence of the strain response, which provides a more convenient means to estimate the strain response at high frequencies.

The electromechanical resonance behavior was characterized for copolymers under different dc bias fields and the results are presented in Fig. 11(a) where the ac signal used is 1 V_{rms}. In Fig. 11(a), the data were taken from stretched 68/32 film and the resonance occurred along the stretching direction. A very clear resonance (electromechanical behavior) was observed. For the data in Fig. 11(a), the elastic compliance (s_{11}) and related coupling factor (k_{31}) along the stretching direction can be derived from [35]

$$\frac{1}{s_{11}^{E}} = 4\rho f_s l \tag{5}$$

$$\frac{k_{31}^2}{1-k_{31}^2} = \frac{\pi f_p}{2 f_s}\tan\left(\frac{\pi}{2}\frac{\Delta f}{f_s}\right) \tag{6}$$

where, s_{11}^{E} (Young's modulus $Y = 1/s_{11}^{E}$) is the elastic compliance along the stretching direction, ρ the density, the l the length along the resonance direction, f_p and f_s are the parallel and series resonance frequencies, and $\Delta f = f_p - f_s$. The Young's modulus along the stretching direction, thus, obtained is shown in Fig. 11(b). The comparison of the data here with that in Fig. 8 indicates that the Young's modulus increases significantly at high frequencies (3 GPa at 35 kHz as compared with 1 GPa at 1 Hz). The data also reveal that the modulus increases with dc bias field, which is associated with the reduced entropy in the copolymer under dc bias

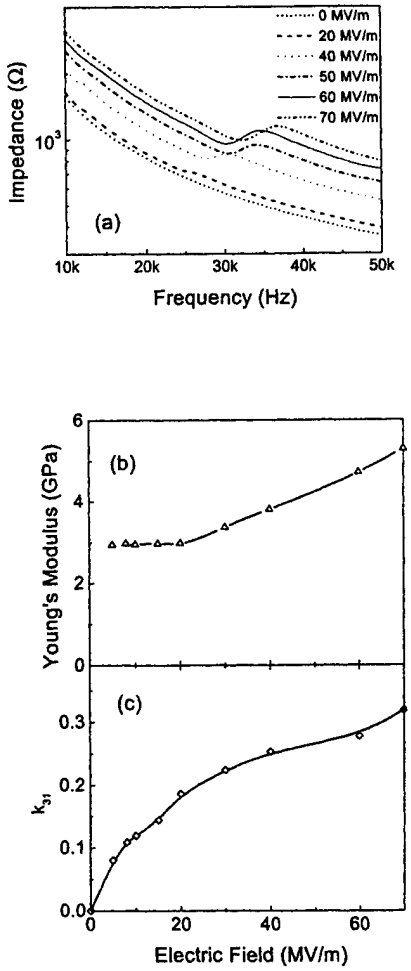

Fig. 11. (a) Frequency dependence of the impedance at room temperature for the stretched 68/32 mol% copolymer under different dc bias fields (from bottom to top, the dc bias is 0, 20, 40, 50, 60, 70 MV/m, respectively), the film was irradiated at 100°C with 70 Mrad of 1.2 MeV electrons; (b) and (c) are the Young's modulus and coupling factor k_{31} deduced from the data in (a).

electric fields. In addition, the electromechanical coupling factor, k_{31} shown in Fig. 11(c), determined from the resonance data is very close to and even higher than that obtained from Eq. (3) at near static limit, which again indicates that the copolymer can function well at high frequencies.

3.4. The mechanical load effect on the electrostrictive strains

Being a polymeric material, there is always a concern about the electromechanical response under high mechanical load, that is, whether the material can maintain the high strain level when subject to high external stresses. To address this concern, we carried out a series of measurement of the field induced strain under mechanical loads [16]. The data reported here are the transverse strain of stretched and irradiated 65/35 copolymer under tensile stress along the stretching direction and the longitudinal strain

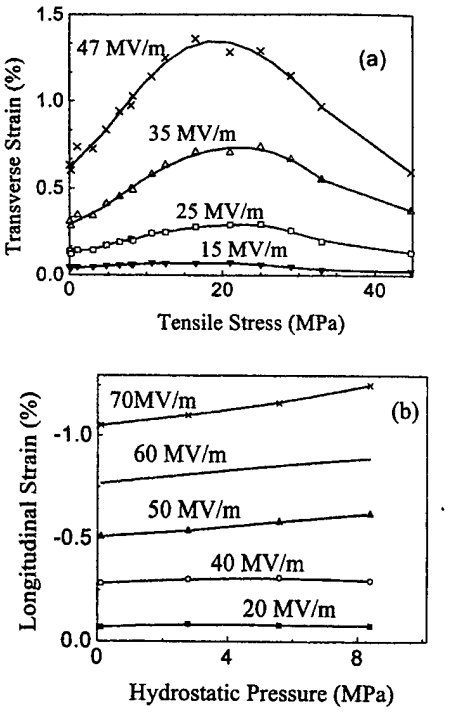

Fig. 12. (a) Transverse strain vs. tensile stress along the stretching direction for stretched 65/35 mol% copolymer film; (b) longitudinal strain vs. hydrostatic pressure for unstretched 65/35 mol% copolymer film. The strains were measured at room temperature. The films were irradiated at 95°C with 60 Mrad of 2.55 MeV electrons.

of unstretched and irradiated 65/35 copolymer under hydrostatic pressure [16,36].

The transverse strain at different tensile stresses along the stretching direction is presented in Fig. 12(a). As can be seen from the figure, under a constant electric field, the transverse strain increases with the load initially and reaches a maximum at the tensile stress of about 20 MPa. Upon further increase of the load, the field induced strain is reduced. One important feature revealed by the data is that even under a tensile stress of 45 MPa, the strain generated is still nearly the same as that without load, indicating that the material has a very high load capability.

The longitudinal strain for unstretched 65/35 films as a function of hydrostatic pressure was measured and the data is presented in Fig. 12(b). At low electric fields, the strain does not change much with pressure, while at high fields, it shows increase with pressure. Due to the limitation of the experimental set-up, we could not apply pressure higher than 8.2 MPa, which is the highest pressure level that the hydrostatic pressure system used can provide [36].

The results from both experiments demonstrate that the electrostrictive P(VDF-TrFE) copolymer has a high load capability and maintains its strain level even under very high load in contrast to many other EAPs. The observed change in the strain with load can be understood based on the consideration of the electrostrictive coupling in this relaxor ferroelectric material which has been analyzed in earlier publications [16,27].

3.5. *Performance of unimorph actuators fabricated from the electrostrictive P(VDF-TrFE) copolymers*

To demonstrate the device performance of the irradiated copolymers, several unimorph actuators were fabricated using the irradiated copolymer films. Shown in Fig. 13 is the field induced actuation of an unimorph made of an electrostrictive P(VDF-TrFE) 68/32 copolymer (active film) and an inactive polymeric substrate. The electrode area of the active film is 10 mm wide and 20 mm long. To prevent any possible edge discharge when operated under high voltage, there is ~1.5 mm wide unelectroded area at the edges of the active layer. The thickness of both the active and inactive films is 22 μm and the thickness of glue layer between two polymer films is about 1 μm. Fig. 13(a) shows the unimorph without electric field and Fig. 13(b) is under 65 MV/m field, where a transverse strain of about 1.7% was generated in the active film (68/32 copolymer, stretched and irradiated at 100°C with 65 Mrad dose of 1.2 MeV electrons). Clearly, there is a large actuation of the unimorph due to the high transverse strain.

For an unimorph, it has been derived that the tip displacement (δ) and blocking force (F), which are dependent on the

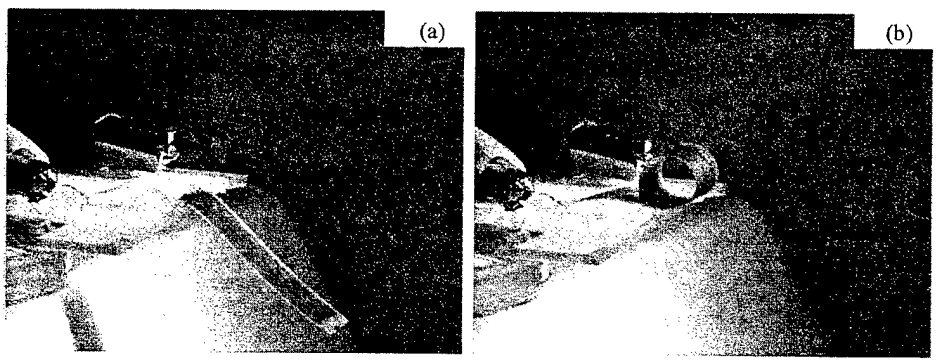

Fig. 13. The performance of an unimorph with one electrostrictive P(VDF-TrFE) copolymer layer of 22 μm bonded to an inactive polymer of the same thickness: (a) the picture shows the unimorph without electric field; (b) the picture shows the actuation of the unimorph under an electric field of 65 MV/m.

Table 1
Comparison of electromechanical properties

Materials		Y (GPa)	Typical S_m (%)	$YS_m^2/2$ (J/cm^3)	$YS_m^2/2\rho$ (J/kg)	Stress (MPa)
Piezoceramic		64	0.2	0.13	17	128
Magnetostrictor		100	0.2	0.2	21.6	200
Piezo P(VDF-TrFE)		4	0.15	0.0045	2.5	6
Electrostrictive P(VDF-TrFE)	S_3	0.4	5.0	0.5	267	20
	S_1	1.0	3.5	0.61	326	35

device geometric and material properties, can be expressed as [37]

$$\delta = \frac{3L^2}{2t}\frac{2AB(1+B)^2}{A^2B^4+2AB(2+3B+2B^2)+1}S_1 \quad (7)$$

$$F = \frac{2wt^2Y}{8L}\frac{2AB}{(AB+1)(1+B)}S_1 \quad (8)$$

where L, w and t are the length, width and thickness of the unimorph, S_1 and Y are the transverse strain and the Young's modulus along the length direction of the active film, respectively. In the equations, A and B are the ratio of Young's modulus and the thickness ratio of the substrate to active film, respectively. Because the unimorph tip in Fig. 13 has travelled more than one circle, Eq. (7) cannot be used to make the comparison.

For an unimorph with small t, the blocking force is small as indicated by Eq. (8). By increasing the thickness t of an unimorph, the blocking force can be increased. Here, in order to keep the driving voltage low, a multilayer configuration for the irradiated P(VDF-TrFE) copolymer is used [38]. The unimorph fabricated has eight active layers with each layer thickness of about 19 μm and bonded together by a polymer glue and the total thickness of the unimorph is 0.32 mm. The other dimensions and parameters are: $L = 22$ mm, $Y = 1$ GPa, $B = 3$ and $A = 1$. The actual unimorph width w is 13 mm, but the width of the electroded area is 10 mm. The blocking force measured for the unimorph was 3.3 g when a field of 40 MV/m was applied which results in a transverse strain of 0.33%. By substituting all the parameters into Eq. (8), a blocking force of 4.2 g is predicted (here $w = 10$ mm is used since it is the electroded area which generates the force). Considering the fact that there is a dead area (unelectroded part of the unimorph) of about 25% of the total unimorph and the inactive glue layers, the agreement between the prediction of Eq. (8) and measured blocking force is quite good. The result indicates that the field induced strain S_1 can be used to estimate the blocking force of an unimorph actuator and the copolymer films do have high load capability.

4. Summary

As a summary, the field induced strain, the elastic energy density, which is another important parameter for electromechanical actuator materials, and other related parameters for this new class of EAP are compiled in Table 1 [39,40]. For the comparison, we include the data for the conventional piezoelectric P(VDF-TrFE) copolymer, the piezoceramic and magnetostrictive materials. In the table, both the volumetric energy density, which is $YS_m^2/2$ and related to the device volume, and the gravimetric energy density, which is $YS_m^2/2\rho$ and related to the device weight, are included. Here S_m is the maximum strain level, ρ the density, and Y is the Young's modulus. In Table 1, we also include another parameter, the blocking stress, which is the stress level generated under a given electric field when the strain of the sample is zero. For the data in the table, the maximum blocking stress has been approximated as YS_m (neglecting the possible non-linear effect). Apparently, the irradiated copolymers exhibit a high elastic energy density, which is consistent with the results of high load capability as presented in the paper.

The results presented here represent a significant improvement in the electromechanical properties of P(VDF-TrFE) copolymers and also points to a new approach for improving the electromechanical responses in other related ferroelectric polymers, i.e. making using of modified electric field controlled phase transition. Using high energy electron irradiation is only one means to modify the phase transition. There exist other non-irradiation approaches to modify the transition which are currently under investigation.

Acknowledgements

This work was supported by DARPA (Contract no. N00173-99-C-2003) and ONR (Grant no. N00014-97-1-0667).

References

[1] P.M. Galletti, D.E. De Rossi, A.S. De Reggi (Eds.), Medical Applications of Piezoelectric Polymers, Gordon and Breach Science Publishers, NY, 1988).
[2] T.T. Wang, J.M. Herbert, A.M. Glass (Eds.), The Application of the Ferroelectric Polymers, Blackie, Chapman & Hall, New York, 1988.
[3] R.H. Baughman, Synth. Metals 78 (1996) 339.
[4] S.G. Wax, R.R. Sands, Proc. SPIE Smart Structured Mater. 3669 (1999) 1.
[5] B.K. Kaneto, M. Kaneko, W. Takeshima, Syo Buturi 65 (1996) 803.

[6] R.E. Pelrine, R.D. Kornbluh, J.P. Joseph, Sens. Actuators A 64 (1998) 77.
[7] Y. Bar-Cohen, T. Xue, B. Joffe, S.S. Lih, P. Willis, J. Simpson, J. Smith, M. Shahinpoor, P. Willis, Proc. SPIE Smart Structured Mater. 3041 (1997) 697.
[8] E. Smela, O. Inganas, I. Lundstrom, Science 268 (1995) 1735.
[9] S. Guo, T. Nakamura, T. Fukuda, K. Oguro, in: Proceedings of the IEEE International Conference on Robotics and Automation, 1997, p. 266.
[10] S. Tadokoro, T. Muramura, S. Fuji, R. Kanno, M. Hattori, T. Takamori, in: Proceedings of the IEEE International Conference on Robotics and Automation, 1996, p. 205.
[11] Q.M. Zhang, V. Bharti, X. Zhao, Science 280 (1998) 2101.
[12] M. Zhenyi, J. Scheinbeim, J.W. Lee, B. Newman, J. Polym. Sci. B: Poly. Phys. 32 (1994) 2721.
[13] K. Omote, H. Ohigashi, K. Koga, J. Appl. Phys. 81 (1997) 2760.
[14] X. Zhao, V. Bharti, Q.M. Zhang, T. Romotowski, F. Tito, R. Ting, Appl. Phys. Lett. 73 (1998) 2054.
[15] Z.-Y. Cheng, T.-B. Xu, V. Bharti, S. Wang, Q.M. Zhang, Appl. Phys. Lett. 74 (1999) 1901.
[16] V. Bharti, Z.-Y. Cheng, S. Gross, T.B. Xu, Q.M. Zhang, Appl. Phys. Lett. 75 (1999) 2653.
[17] K. Tashiro, K. Takano, M. Kobayashi, Y. Chatani, H. Tadokoro, Ferroelectrics 57 (1984) 297.
[18] K. Tashiro, S. Nishimura, M. Kobayashi, Macromolecules 23 (1990) 2802.
[19] Q.M. Zhang, J. Zhao, T. Shrout, N. Kim, L.E. Cross, A. Amin, B.M. Kulwicki, J. Appl. Phys. 77 (1995) 2549.
[20] T. Furukawa, Phase Transitions 18 (1989) 143.
[21] F. Jona, G. Shirane, Ferroelectric Crystals, Dover Publications, New York, 1993, p. 138.
[22] S. Ducharme, A.V. Bune, L.M. Blinov, V.M. Fridkin, S.P. Palto, A.V. Sorokin, S.G. Yudin, Phys. Rev. B 57 (1999) 25.
[23] A. Lovinger, Macromolecules 18 (1985) 190.
[24] F. Macchi, B. Daudin, J.F. Legrand, Nucl. Instr. Meth. B 46 (1990) 324.
[25] A. Odajima, Y. Takasa, T. Ishibashi, Y. Yuasa, Jpn. J. Appl. Phys. 24 (1985) 881.
[26] J. Su, P. Moses, Q.M. Zhang, Rev. Sci. Instrum. 69 (1998) 2480.
[27] Z.-Y. Cheng, V. Bharti, T.B. Xu, S. Wang, Q.M. Zhang, T. Ramotowski, F. Tito, R. Ting, J. Appl. Phys. 86 (1999) 2208.
[28] Z.-Y. Cheng, V. Baarti, T. Mai, T.-B. Xu, Q.M. Zhang, T. Ramotowski, K.A. Wright, R. Ting, IEEE Trans. Ultrason. Ferro. Freq. Contr. 47 (2000) 1296.
[29] F.J. Balta, A.G. Arche, T.A. Ezquerra, C.S. Cruz, F. Batallan, B. Frick, Prog. Polym. Sci. 18 (1993) 1.
[30] W. Kinase, H. Takahashi, J. Phys. Soc. Jpn 10 (1955) 942.
[31] Y.M. Shkel, D.J. Klingenberg, J. Appl. Phys. 83 (1998) 415.
[32] Q.M. Zhang, Z.-Y. Cheng, V. Bharti, Appl. Phys. A 70 (2000) 307.
[33] C. Hom, S. Pilgrim, N. Shankar, K. Bridger, M. Massuda, S. Winzer, IEEE Trans. Ultrason. Ferro. Freq. Contr. 41 (1994) 542.
[34] K. Tashiro, in: H.S. Nalwa (Ed.), Ferroelectric Polymers, Marcel Dekker, NY, 1995, p. 63.
[35] IEEE Standard on Piezoelectricity, ANSI/IEEE Standard 176-1987, 1988.
[36] S.J. Gross, Z.-Y. Cheng, V. Bharti, Q.M. Zhang, Proc. IEEE 1999 Inter. Symp. Ultrsonics 2 (1999) 1019.
[37] Q.M. Wang, PhD Thesis, The Pennsylvania State University, 1998.
[38] M. Toda, S. Osaka, Trans. IECE Jpn. E 61 (1978) 507.
[39] L.E. Cross, Ceram. Trans. 68 (1996) 15.
[40] K.B. Hathaway, A.E. Clark, Mater. Res. Bull. 18 (1993) 34.

Biographies

Zhong-Yang Cheng received his BS in physics, MS and PhD degrees in Electronic Materials and Engineering from Xian Jiaotong University, China in 1983, 1988 and 1995 respectively. His research interests are in characterization and fabrication of various functional materials (piezoelectric, ferroelectric, electroactive polymers, nonlinear optical polymers, single crystals, ceramics, thin films, et al.) and the application studies (actuators, sensors, transducers, MEMS, electro-optical modulation, et al.) of these materials. Dr. CHENG can be reached through e-mail: zxc7@psu.edu

Dr. Vivek Bharti received his BSc degree in science in 1989 from Meerut University, India, and masters in physics in 1992 and doctoral degree in polymer physics in 1997 from the University of Roorkee, Roorkee, India. His current research interests are in the area of characterization of structural and electromechanical properties of advanced materials for their applications as actuators, transducers, sensors, dielectrics and MEMS.

Tian-Bing Xu received the MSc degree in Electrical Engineering from the Pennsylvania State University in 1999. He is currently a candidate for the PhD degree in the Intercollege Graduate Program in Materials, The Penn State University. He is currently working on electroactive polymers and their application for actuators and transducers.

Haisheng Xu obtained his PhD degree in Department of Polymer Science and Engineering, Nanjing University, China. He is a faculty member of Nanjing University and became an associate professor since 1996. Currently, he works in Materials Research Laboratory, The Pennsylvania State University as a visiting scholar.

Tian Mai received the BS degree in Computer Science from the Shangdong University, China in 1988. He is currently working as a Visiting Research Assistant with the Material Research Laboratory, the Pennsylvania State University from Shangdong University. His research interest is the area of property characterization of electroactive materials.

Qiming Zhang is an associate professor of Electrical Engineering at the Materials Research Laboratory and Department of Electrical Engineering of Penn State University. He obtained his BS in 1981 from Nanjing University, China, and PhD degree in 1986 from Penn State University. He worked at the Brookhaven National Laboratory as a research scientist in the area of solid state thin films. He came back to Penn State University at 1991 as a faculty to conduct research in ferroelectric based materials and devices and electroactive polymer based materials and devices. The research activities in his research group include material development, modeling, and device development for transducers and actuators, dielectrics and capacitors, ferroelectric polymer thin film for memory devices, MEMS, photonic bandgap crystal, and electrooptic and acoustooptic materials and devices. He has delivered many invited presentations in those areas. There are 135 publications in those areas from his research group. He is a member of IEEE, Materials Research Society, and American Physical Society.

APPENDIX 26

Effect of High Energy Electron Irradiation on the Electromechanical Properties of Poly(vinylidene Fluoride-Trifluorethylene) 50/50 and 65/35 Copolymers

Zhong-Yang Cheng, Vivek Bharti, Tian Mai, Tian-Bing Xu, *Member, IEEE*, Qiming M. Zhang, *Senior Member, IEEE*, Thomas Ramotowski, Kenneth A. Wright, and Robert Ting

Abstract—**High energy electron irradiation with a broad range dosage was carried out on poly(vinylidene fluoride-trifluorethylene) copolymer 65/35 mol% and 50/50 mol% films at different temperatures from room temperature to a temperature close to the melt temperature. The effect of irradiation on the properties of the films, such as electric field-induced strain, dielectric and polarization behaviors, and mechanical modulus, is presented. The irradiated films can exhibit a very large electric field-induced strain, more than 4.5% longitudinal strain, and 3% transverse strain. The transverse strain of the stretched film can compare with the longitudinal strain; that of the unstretched film is much smaller than the longitudinal strain. With regard to the dielectric and polarization behaviors, we found that irradiation changes the copolymer from a typical ferroelectric to a relaxor ferroelectric in which the behavior of microregions under the electric field plays the key role. Between the two copolymers studied, we found that 65/35 copolymer is preferred for both longitudinal and transverse strain generation. A model is proposed to explain the experimental results that the amplitude of the charge electrostrictive coefficient (Q) increases with decreasing crystallinity.**

I. Introduction

From the application point of view, electroactive polymers (EAPs) offer many advantages over ceramics and crystals, such as flexibility, low weight, low cost, and easy processing, to form complicated shapes. Electroactive polymers have attracted much attention for many years [1], [2], which resulted in the discovery of ferroelectric (FE) polymers as a new type of functional material. These polymers have been recognized to have potential applications in a variety of devices, such as transducers, actuators, and sensors. However, in comparison with other existing functional materials, such as ceramics and single crystals [3], current FE polymers suffer low electroactivity, such as low electromechanical coupling coefficient and low strain energy density, which limit the applications of the materials.

To improve the material properties, there is interest in searching for new EAPs and modifying the existing materials. It was found that large strain response can be observed in some EAPs, such as heavily plasticized poly(vinylidene fluoride-trifluoroethylene) [P(VDF-TrFE)] and polyurethane [4]–[6]. However, the elastic modulus of these materials is low. In FE, it is well known that the defects have strong influence on the material properties. Recently, in an effort to study the effects of defects on, and to improve the material properties of, FE polymer, we showed that by making use of high energy electron irradiation, the P(VDF-TrFE) copolymers at a certain composition range exhibit a very large electrostrictive strain response (~5%) [7]–[9]. In addition to the large strain response, the irradiated P(VDF-TrFE) copolymers are of very high strain energy density (~0.5 J/cm^3 or ~240 J/kg) because the elastic modulus is relatively high [7], [9]. In addition, in the DC electric field biased state, high piezoelectric coefficients ($d_{33} \sim -350$ pm/V and $d_{31} \sim 260$ pm/V, which are comparable with those in ceramics) can be achieved [10]. More importantly from a material science point of view, the irradiated copolymer exhibits the features of typical relaxor FE [7], [11], [12]. Although inorganic relaxor FE have been widely studied in the last half century [13], no organic relaxor FE was reported before.

This paper presents the results of a detailed investigation on how the electromechanical properties (such as strain responses, polarization, and dielectric behavior) of the newly developed electrostrictive P(VDF-TrFE) copolymers with 50 mol% and 65 mol% VDF content [P(VDF-TrFE) 50/50 and 65/35] vary with different sample processing conditions prior to the irradiation, different electron treatment conditions, electric field driving conditions, and temperature. To elucidate what is responsible for these changes, data on microstructures and evolutions of the transitional phenomena will also be presented and analyzed. These results will be useful in guiding future work on improving the electroactive properties of the ma-

Manuscript received July 1, 1999; accepted January 10, 2000. This work was supported by the Office of Naval Research through Grant No. N00014-97-1-0900, the National Science Foundation through Grant No. ECS-9710459, and DARPA through Grant No. N00173-99-C-2003.

Z.-Y. Cheng, V. Bharti, T. Mai, T.-B. Xu, and Q. M. Zhang are with the Materials Research Laboratory, The Pennsylvania State University, University Park, PA 16802 (e-mail: zxc7@psu.edu).

T. Ramotowski is with the Naval Undersea Warfare Center, Newport, RI 02841.

K. A. Wright is with the Laboratory of Electromagnetic and Electronic Systems, Massachusetts Institute of Technology, Cambridge, MA 02139.

R. Ting is with the Department of Chemistry, University of Central Florida, Orlando, FL 32816.

terials and in designing the materials for different applications.

It is worthwhile to point out that in this study, P(VDF-TrFE) copolymers with VDF content at 70 mol% or higher were also investigated, and the results revealed that copolymers at those compositions cannot be converted to electrostrictive polymers with the 2.55-MeV electron source employed in this investigation. Therefore, only the results from the investigation on P(VDF-TrFE) 65/35 and 50/50 copolymers are presented.

II. Experiments

P(VDF-TrFE) copolymer powders with a mean molecular weight of 200,000 were purchased from Solvay and Cie (Bruxelles, Belgium). Two approaches were used here to prepare the copolymer films, i.e., melt press and solution cast. In the melt press process, the P(VDF-TrFE) copolymer 50/50 and 65/35 powders were pressed between two pieces of aluminum foil at 215 and 225°C, respectively. The films were then either slowly cooled to room temperature, resulting in high crystallinity in the films, or quenched in ice cold water, to keep the crystallinity of the films low. In the solution cast method, the copolymer was dissolved in dimethylformanide (DMF) first and then the solution was cast on a flat glass plate and dried in an oven at 70°C. Two types of films were used in this investigation: the stretched and unstretched. In unstretched films, the prepared films were annealed at 140°C for a period between 12 to 14 h to improve the crystallinity. In stretched films, films made from solution cast or quenched from melt press were uniaxially stretched by a factor of 5 at a temperature between 25 and 50°C. Afterward, these films were also annealed at 140°C for 12 to 14 h to increase the crystallinity. To prevent shrinkage during the annealing for the stretched films, the two ends of the films were mechanically fixed during annealing. The thickness of both stretched and unstretched films was in the range of 15 to 30 μm. The irradiation was carried out in a nitrogen or argon atmosphere at different temperatures (from room temperature to 120°C) with 2.55-MeV electrons.

For the characterization of the dielectric properties, polarization, and electric field-induced strain behavior of the films, gold electrodes of thickness about 400 Å were sputtered on both surfaces of a film. The dielectric constant of the films under a weak electric field (~1 V) at frequencies from 30 to 100 kHz was measured by a dielectric analyzer (model no. 2970; TA Instruments, New Castle, DE) at temperatures from -60 to 120°C with a heating/cooling rate of 2°C/min. Because of the FE nature of the films, it is expected that the dielectric properties are strongly dependent on the driving field amplitude. In this investigation, the effective dielectric constant of films under high electric field was measured. In the measurement, the induced polarization in the film was computed from the current flowing through a resistor, which is in series with the film and whose electric impedance is much smaller (more than 10,000 times smaller) than that of the film. The polarization hysteresis loop was measured by a computer-controlled automatic system based on the Sawyer-Tower circuit. The longitudinal strain, the strain response along the thickness direction, was characterized by a strain sensor, which was designed specifically for the polymer film strain measurements, based on the piezoelectric bimorph sensor [14]. The transverse strain, the strain response along the film surface, was measured using a cantilever-based dilatometer that was newly developed for characterizing transverse strain response of polymer film under external electric fields [12].

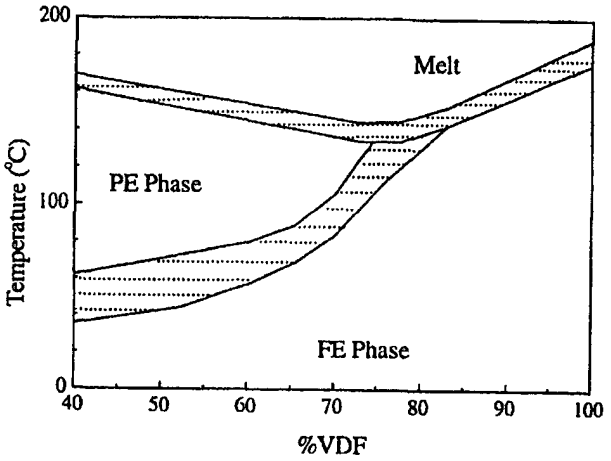

Fig. 1. Phase diagram of P(VDF-TrFE) copolymer. The exact phase transition temperature depends on sample fabrication, sample thermal treatment, and processing history. The dashed areas correspond to the phase transition temperature region.

Differential scanning calorimeter (DSC) measurements were performed to monitor the change of crystallinity with different irradiation conditions and were carried out at a scanning rate of 10°C/min under a nitrogen atmosphere using a DSC (model no. 2010; TA Instruments) from -60 to 200°C. The elastic modulus of the films was characterized along the film direction (perpendicular to the film thickness) using a dynamic mechanical analyzer (DMA) (model no. 2980; TA Instruments) in the temperature range from -60 to 100°C at different frequencies.

III. Results and Discussion

A. Polarization, Dielectric Properties, and DSC Data

At room temperature, P(VDF-TrFE) copolymer is a normal ferroelectric whose phase diagram is shown in Fig. 1. There is a melting transition at temperatures above 150°C and a clear FE to paraelectric (PE) phase transition for most of the copolymer compositions (at compositions below 85 mol% VDF) [1], [15]. A typical polarization hysteresis loop taken from P(VDF-TrFE) 65/35 copolymer is shown in Fig. 2(a). In most of the electromechanical applications, the material is operated near the

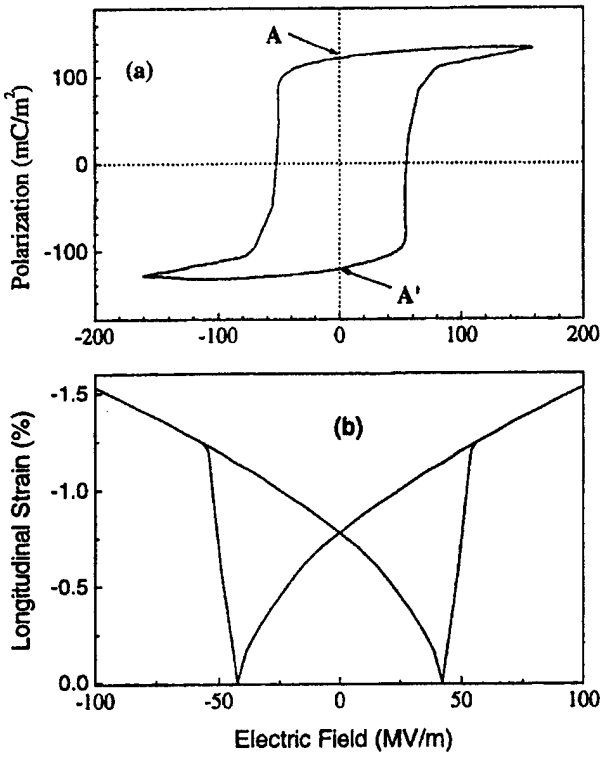

Fig. 2. Typical polarization and strain responses in P(VDF-TrFE) 65/35 copolymer at ferroelectric phase: a) polarization vs. electric field and b) longitudinal strain vs. electric field.

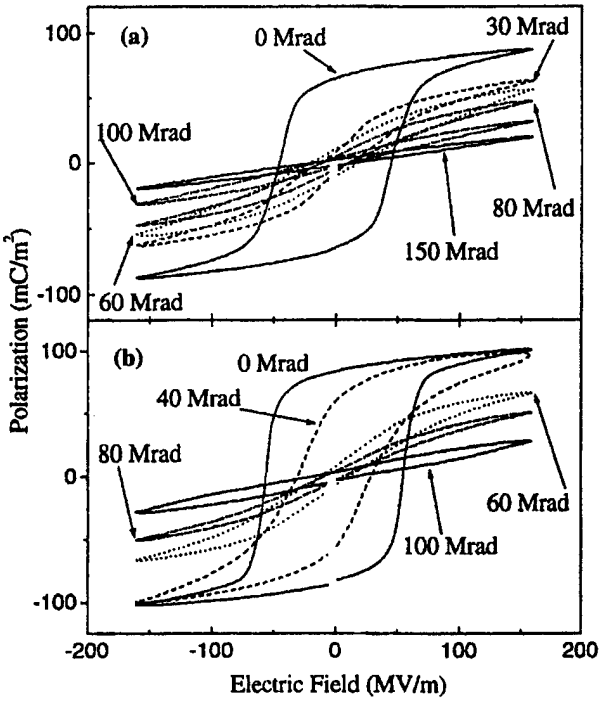

Fig. 3. Polarization hysteresis loops at 10 Hz of P(VDF-TrFE) copolymer films measured at room temperature for a) unstretched 50/50 films irradiated at 120°C and b) unstretched 65/35 films irradiated at 120°C with different irradiation dosages.

point A or A′, and the strain response (S) is linearly proportional to the applied electric field (E in V/m) (piezoelectric response) [2]:

$$S_{ij} = d_{ijk}E_k \tag{1}$$

where d_{ijk} (in m/V) is the piezoelectric strain coefficient. By switching the polarization through the polarization hysteresis, a larger strain response can be obtained as shown in Fig. 2(b), where a strain of about −1.5%, which is much higher than the strain level in the piezoelectric state, can be achieved for the P(VDF-TrFE) 65/35 copolymer. However, the strain response of Fig. 2(b) type is not desirable and may not be used in practical devices because it involves a high hysteresis and also because the large polarization hysteresis will cause severe dielectric loss, resulting in sample heating.

The large hysteresis observed in a normal ferroelectric P(VDF-TrFE) copolymer is due to the high nucleation barrier when switching polarization from coherent macroscopic polar domains [1], [2]. By breaking this macroscopic coherent polar domain, one can reduce or eliminate the polarization hysteresis. This is the reason behind the observed evolution from the large hysteresis polarization loop to a slim polarization loop when a P(VDF-TrFE) copolymer is irradiated with proper doses of high energy electrons [7], [10], [11]. That is, the electron irradiation breaks up the coherent polarization domains in the crystalline region into nanopolar regions. The data shown in Fig. 3 is the change of the polarization hysteresis loop with electron dosage for the unstretched copolymer films irradiated at 120°C, where Fig. 3(a) is for 50/50 films and Fig. 3(b) is for 65/35 films. With increasing dosage, the polarization loop becomes slim with little hysteresis. For the copolymers with a slim hysteresis loop, the dielectric constant measured at a weak electric field (~0.04 MV/m) exhibits a broad peak at a temperature near room temperature as shown in Fig. 4. In addition, the peak position shifts with frequency, and the relationship between the peak temperature (T_m) and frequency can be described by the Vogel-Fulcher law quite well [7], [11]. Therefore, these experiment results suggest that the irradiated copolymer obtained here belongs to a special class of ferroelectrics, i.e., relaxor ferroelectrics [13], [16]. That is, the high energy irradiation transforms the crystalline phase from a normal FE into a relaxor FE.

Fig. 3 also reveals that as the dosage increases, the induced polarization level under a given applied field reduces, and, at a high dosage, the polarization level becomes much smaller than that in an unirradiated sample. This is a result of the reduction of the crystallinity in the polymer with irradiation. Presented in Fig. 5 is the DSC data for both 65/35 and 50/50 copolymers under different doses. For unirradiated films, there are two well-defined peaks. The one at temperatures above 150°C is associated with the melting of the crystallites, and the low temperature one

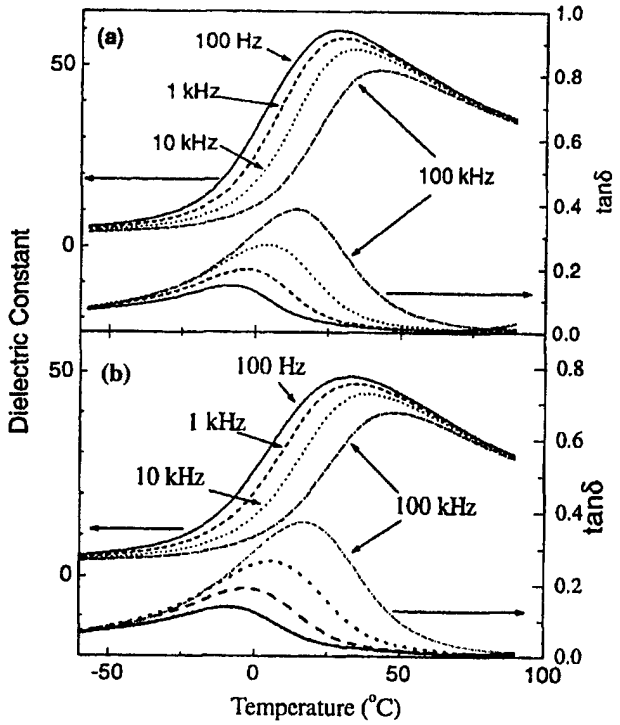

Fig. 4. Temperature dependence of the dielectric constant and loss at different frequencies (100 Hz, 1 k, 10 k, and 100 kHz) for irradiated P(VDF-TrFE) copolymer films: a) stretched 65/35 mol% irradiated at 95°C with 60 Mrad dosage, b) stretched 50/50 mol% irradiated at 95°C with 40 Mrad dosage.

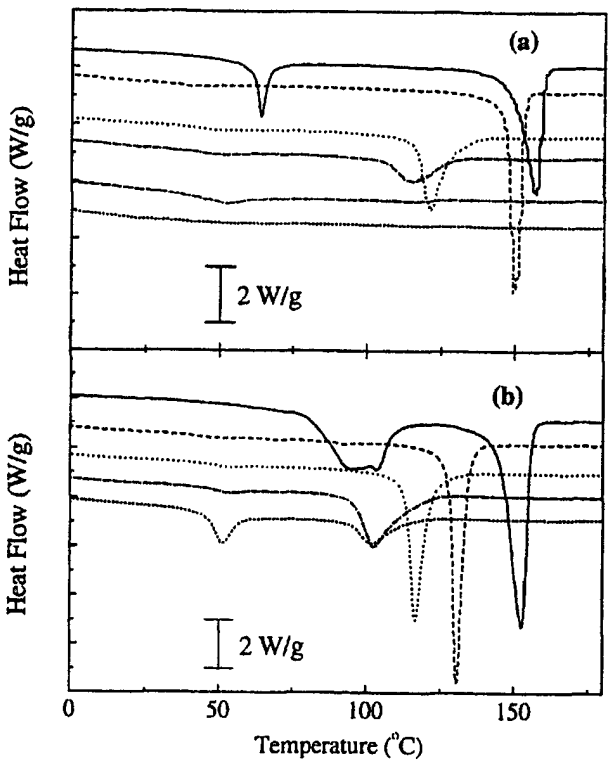

Fig. 5. Enthalpy change of the melting point of crystallites in a) unstretched P(VDF-TrFE) 50/50 irradiated at 120°C (from top to bottom curve, dosage is 0, 30, 60, 80, 100, and 150 Mrad, respectively) with the irradiation dosage and b) unstretched P(VDF-TrFE) 65/35 irradiated at 95°C (from top to bottom curve, dosage is 0, 60, 80, 100, and 120 Mrad, respectively).

is from the FE-PE transition. The enthalpy of the melting can be used as a measure of the crystallinity of the film. It is found that the crystallinity of both stretched and unstretched copolymer films before irradiation is about 75%. The data in Fig. 5 show that with increased dosage, the area under the melting peak (enthalpy of the melting) decreases, and, for the 50/50 copolymer at the 150-Mrad dosage, this peak disappears, indicating that the polymer is more or less amorphous. Therefore, in addition to transforming the crystalline region of the polymer from a normal FE with large polarization hysteresis to a relaxor FE with slim polarization loop, high energy electron irradiation also converts the crystalline phase into amorphous phase, and, as a result, the field induced polarization level is reduced. These are two competing processes, and how to increase one process (transformation in the crystalline region) and reduce the reduction of the crystallinity with dose is still a challenge. Because the electric field-induced strain in the material is proportional to the polarization level, a high crystallinity is clearly highly desirable to achieve a high strain and high elastic energy density. A way to increase the electric field-induced strain response of the irradiated material is varying irradiation condition, such as the electron energy, irradiation temperature, and dosage. The effect of the irradiation temperature, and dosage on the strain response of the copolymer will be presented in the following section. With regard to the irradiation energy, we recently found that using the electron beam with a low energy of (1.0~1.2 MeV) for irradiation seems better than using that 2.55 MeV. Further detailed studies of the electron energy effect will be carried out. To transform the crystalline region from normal FE to relaxor FE, besides irradiation, other possible approaches are introducing chemical defects in the polymer chain or using different thermal treatment processes, such as quenching, to treat the material to introduce defects.

B. Field-Induced Strain Responses in Irradiated Copolymers

Presented in Fig. 6 is the relationship between the electric field-induced longitudinal strain and electric field from P(VDF-TrFE) 65/35 copolymer irradiated at 120°C with a 80-Mrad dosage. The film was made from a solution cast with DMF and stretched. The data shows that, in irradiated films, an ultrahigh field-induced strain can be induced. From a recent x-ray diffraction experiment, it was observed that the field-induced strain in the relaxor FE P(VDF-TrFE) copolymer is mainly due to the field-induced local phase, transformation between the non-polar

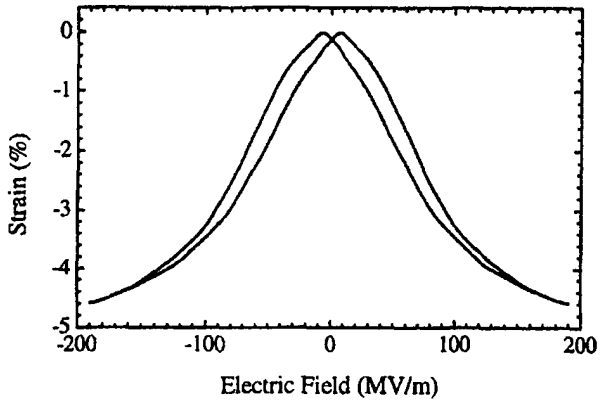

Fig. 6. Longitudinal strain vs. electric field in P(VDF-TrFE) 65/35 copolymer irradiated at 120°C with 80 Mrad dosage.

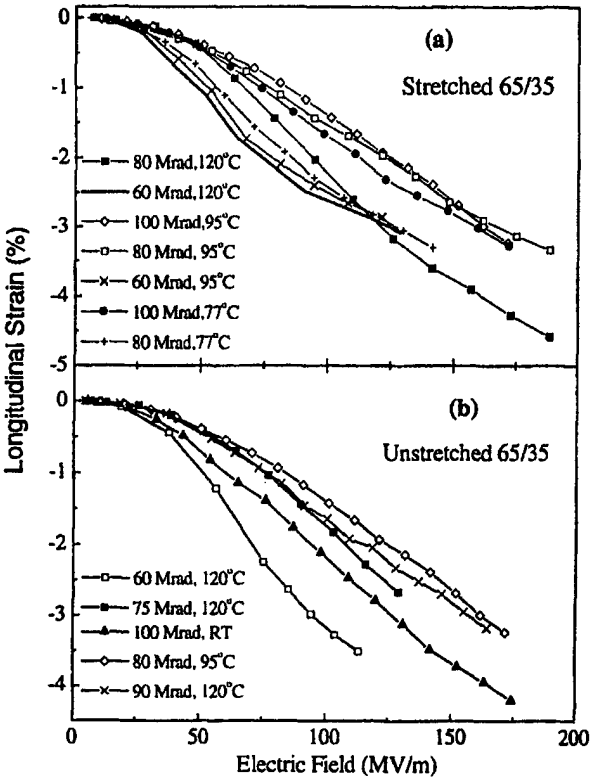

Fig. 7. Longitudinal strain amplitude vs. electric field amplitude in P(VDF-TrFE) 65/35 mol% copolymer films obtained at 1 Hz at room temperature: a) stretched films and b) unstretched ones.

phase and polar phase, which involves a very high lattice strain [17]. This is different from the strain observed in polarization switching in a normal FE P(VDF-TrFE) copolymer [Fig. 2(b)], where the strain is mainly due to the polarization reorientation between different domain states.

In an FE polymer, the electric field-induced strain response is closely related to the polarization in the material. Being a semicrystalline polymer, this response is affected by the crystallinity. Because the high energy electron irradiation influences both the crystallite polarization and crystallinity, as shown in the proceeding section, it is expected that the electric field-induced strain will be sensitive to the electron irradiation conditions such as dosage, irradiation temperature, and electron energy. Presented in Fig. 7 is the amplitude of the longitudinal strain S_3 vs. the amplitude of the applied field measured at 1 Hz at room temperature for the irradiated 65/35 copolymers, which exhibit slim polarization loops. In the figures, the results from both stretched and unstretched films are shown. Similar results for the irradiated 50/50 copolymers are presented in Fig. 8.

Because the copolymer film studied here is a semicrystalline polymer, effective electrostrictive coefficients Q_{ij} (effective charge-related electrostrictive coefficients) are introduced to describe phenomentally this polarization dependence behavior [18]:

$$S_3 = Q_{33}P^2 \tag{2a}$$

$$S_1 = Q_{13}P^2 \tag{2b}$$

where P is the polarization, S_3 is the longitudinal strain, and S_1 is the transverse strain. For stretched film, S_1 is the transverse strain along the stretch direction. For the irradiated copolymer exhibiting a slim polarization loop, it has been shown that in the entire polarization range, the electric field-induced strain (S) is proportional to the square of polarization (P) [8]. That is, as will be presented subsequently, the value of Q is independent of the electric field. For a linear dielectric material, (2) can be converted to the applied electric field (E),

$$S_3 = M_{33}E^2 \tag{3a}$$

$$S_1 = M_{13}E^2 \tag{3b}$$

where M_{ij} is the effective electric field-related electrostrictive coefficient and M_{ij} and Q_{ij} are related by the dielectric constant. In the following discussion, Q_{ij} and M_{ij} are termed as charge and field electrostrictive coefficients, respectively, for simplicity. For the copolymers investigated here, as shown in Fig. 3, the polarization is not a linear function of field, and (3) may not describe the $S \sim E$ relationship precisely. For comparison of different materials, we will still use M_{ij} to measure the effectiveness of the material in generating strain under a given field. M_{ij} presented in the following is defined as

$$S_{ap} = M_{ij}E_{ap}^2 \tag{4}$$

where S_{ap} and E_{ap} are the amplitude of the strain and the corresponding applied electric field amplitude, respectively. In Table I, M_{33} calculated for the longitudinal strain of the copolymers examined are presented for both 65/35

TABLE I
ELECTROSTRICTIVE COEFFICIENT ($-M_{33} \times 10^{18} m^2/V^2$) AT DIFFERENT ELECTRIC FIELDS AND Q_{33} FOR DIFFERENT SAMPLES.

Stretched 65/35	$-M_{33}$ 50 MV/m	100 MV/m	150 MV/m	$-Q_{33}$ (m^4/C^2)
60 Mrad, 120°C	4.20	2.25	1.6*	5.4 (±0.3)
80 Mrad, 120°C	1.75	2.23	1.68	9.0 (±0.3)
100 Mrad, 95°C	1.50	1.39	1.16	6.0 (±0.4)
80 Mrad, 95°C	1.63	1.54	1.1	7.2 (±0.2)
60 Mrad, 95°C	3.58	2.53	1.4*	4.5 (±0.4)
120 Mrad, 77°C	1.92	1.46	1.10	10.0 (±0.3)
100 Mrad, 77°C	1.76	1.69	1.25	8.6 (±0.3)
80 Mrad, 77°C	3.00	2.43	1.57	4.6 (±0.2)
160 Mrad, RT	0.47	1.04	0.80	
120 Mrad, RT	0.37	1.17	0.94	
Unstretched 65/35				
60 Mrad, 120°C	3.57	3.17	1.7*	12.0 (±0.5)
75 Mrad, 120°C	1.52	1.74	1.5*	
90 Mrad, 120°C	1.65	1.63	1.24	7.14 (±0.3)
80 Mrad, 95°C	1.49	1.39	1.17	7.5 (±0.3)
100 Mrad, RT	2.70	2.19	1.63	9.0 (±0.3)
140 Mrad, RT	1.54	1.31	1.06	5.7 (±0.2)
180 Mrad, RT	0.64	1.12		
Unstretched 50/50				
80 Mrad, RT	1.85			
100 Mrad, RT	2.01	1.97	1.58	8.0 (±0.7)
120 Mrad, RT	0.56	0.57	0.53	5.7 (±0.2)
35 Mrad, 120°C	4.50	2.00		
40 Mrad, 120°C	5.10	2.10	1.20	9.9 (±0.2)
70 Mrad, 120°C	1.30	1.17	0.97	10.6 (±0.3)
Stretched 50/50				
40 Mrad, 95°C	1.15	0.91	0.73*	4.2 (±0.2)
60 Mrad, 77°C	2.23	2.11	1.56	11.8 (±0.3)
35 Mrad, 120°C	4.04	2.20	1.50	13.0 (±0.5)
40 Mrad, 120°C	3.74	1.65*		
80 Mrad, RT	1.45	1.31	1.0*	12.8 (±0.5)
70 Mrad, RT	1.55	1.28		

*The data were extrapolated to the electric field.

and 50/50 compositions under different irradiation conditions for three driving field amplitudes, 50, 100, and 150 MV/m. Because of the nonlinear relationship between P and E, M_{33} varies with the field amplitude. The data in Table I reveal that, in most cases, for the slim loop copolymers, M_{33} decreases with dosage, which is consistent with the result in Fig. 3, where the induced polarization decreases with dosage. Because of the nonlinear relationship between P and E and the saturation of P at high fields, there are deviations from this general rule. To illustrate these features more clearly, M_{33} as a function of dosage under different applied field amplitude is presented in Fig. 9 for selected copolymers.

The copolymers in Table I can be divided into four groups: stretched films of 65/35, stretched films of 50/50, unstretched films of 65/35, and unstretched films of 50/50. Among the irradiation conditions investigated for each group, there is one irradiation condition that yields the highest M_{33} and, hence, the highest longitudinal strain. Based on the DSC data, it is found that the crystallinity of the samples exhibiting high strain response is about 60%. In Fig. 10, M_{33} from the best performed samples of each group is plotted as a function of applied field amplitude. The data in the figure indicate the following interesting features. 1) At low fields, stretched films yield better strain response than unstretched films; at high fields, this difference is not significant. 2) 65/35 copolymer generates higher strain response than 50/50 copolymer. Therefore, considering the reduced manufacturing cost and increased reliability of unstretched films, 65/35 unstretched films should

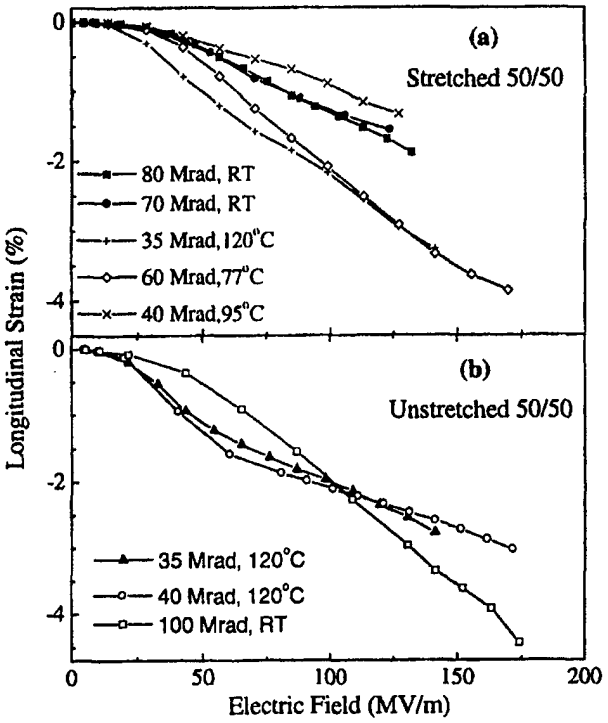

Fig. 8. Longitudinal strain amplitude vs. electric field amplitude in P(VDF-TrFE) 50/50 mol% copolymer films obtained at 1 Hz at room temperature: a) stretched ones and b) unstretched ones.

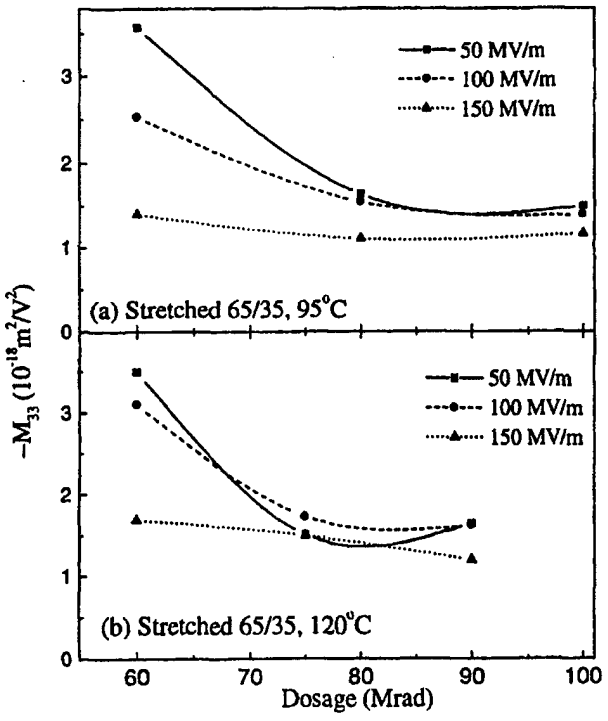

Fig. 9. Value of M_{33} vs. dosage for the different samples: a) stretched 65/35 irradiated at 95°C and b) unstretched 65/35 irradiated at 120°C.

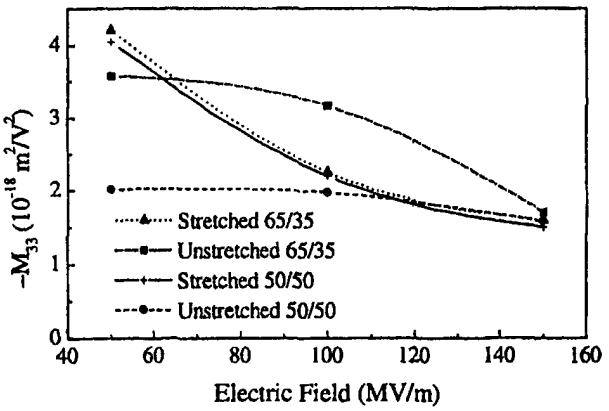

Fig. 10. Values of M_{33} vs. electric field for the sample with the best performance in each group from Table I.

be preferred for the longitudinal strain electromechanical transducer applications. As will be discussed, one additional reason for choosing unstretched films for longitudinal electromechanical transducer application is the very low transverse strain response in unstretched films.

Now we discuss the results from the transverse strain responses of the irradiated copolymers with slim polarization loop. For unstretched films, the transverse strain is quite small, and, in most of the films examined, the amplitude ratio between the transverse strain (S_1) and longitudinal strain is less than 0.33. This feature is attractive for many devices utilizing the longitudinal strain, such as ultrasonic transducers in the thickness mode and actuators and sensors making use of the longitudinal electromechanical responses of the material. For example, a very weak transverse electromechanical response in comparison with the longitudinal one can significantly reduce the influence of lateral modes on the thickness resonance and improve the performance of the transducer.

On the other hand, for stretched films, a large transverse strain can be achieved as shown in Fig. 11, which is taken from the strain measured along the stretch direction for 65/35 and 50/50 copolymers. The M_{13} coefficient from the transverse strain (S_1) along the stretch direction for both 65/35 and 50/50 copolymer films under different irradiation conditions is summarized in Table II. Comparison between Table I and Table II indicates that $|S_1|$ can reach as high as $|S_3|$ (e.g., 65/35 irradiated at 95°C). In addition, S_1 from the 65/35 copolymer is much higher than that from 50/50 copolymer, as shown in Fig. 12, which is different from the longitudinal strain where the difference is not so large. Hence, for transverse strain actuation applications, stretched 65/35 copolymer is the clear choice.

C. Effective Charge Related Electrostrictive Coefficients

Although M_{ij} varies with the applied field amplitude as discussed previously, it is found that the charge electrostrictive coefficient (Q) remains constant in the same electric field range. The experimental results for the

TABLE II
ELECTROSTRICTIVE COEFFICIENT ($M_{13} \times 10^{18} m^2/V^2$) AT DIFFERENT ELECTRIC FIELDS AND Q_{13} FOR DIFFERENT SAMPLES.

Stretched 50/50	M_{13} 50 MV/m	100 MV/m	150 MV/m	Q_{13} (m^4/C^2)
60 Mrad, 77°C	1.22	0.95	0.6*	4.3 (±0.2)
40 Mrad, 95°C	1.59	0.91	0.46*	2.6 (±0.2)
60 Mrad, 95°C	1.14	1.03	0.80*	6.4 (±0.3)
80 Mrad, 95°C	0.635	0.627		
100 Mrad, 95°C	0.53	0.57	0.50	11.0 (±0.4)
Stretched 65/35				
80 Mrad, 77°C	2.30	1.95		
100 Mrad, 77°C	1.01			
120 Mrad, 77°C	1.18	1.21	1.14*	10.3 (±0.4)
60 Mrad, 95°C	3.27	2.75*		4.6 (±0.2)
80 Mrad, 95°C	1.41	1.53*		6.9 (±0.3)
100 Mrad, 95°C	1.32	1.37	1.02	6.5 (±0.3)

*The data were extrapolated to the electric field.

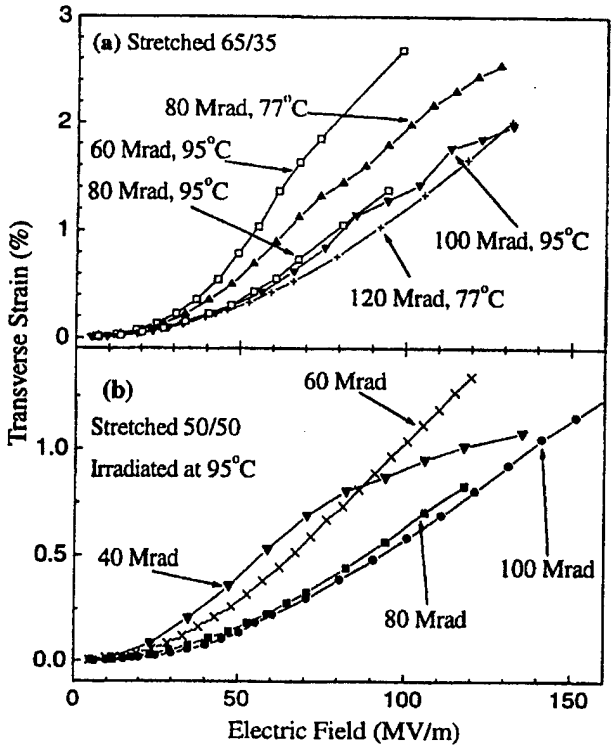

Fig. 11. Transverse strain amplitude vs. electric field amplitude in stretched P(VDF-TrFE) copolymer films obtained at 1 Hz at room temperature: a) 65/35 and b) 50/50. The transverse strain is the strain response along the stretching direction.

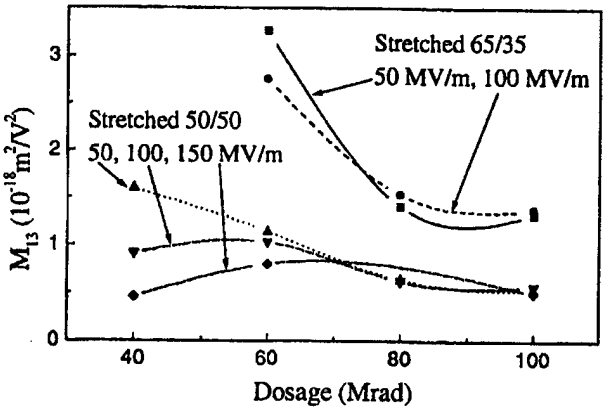

Fig. 12. Value of M_{13} vs. dosage for samples with the best performance in the stretched 50/50 and 65/35, respectively.

stretched 65/35 copolymer film irradiated at 95°C with 60 Mrad are shown in Fig. 13(a) and (b) for the electric field dependence of M_{13} and Q_{13}, respectively. The constant of Q indicates that the relationship between strain response and the polarization square is indeed linear as described by (2). This indicates that the change in M_{ij} with field is indeed caused by the nonlinear $P \sim E$ relationship. To illustrate this, in Fig. 13(c), the change of the effective dielectric constant with driving field amplitude for the same copolymer is presented.

The values of Q_{ij} determined using (2) are also listed in Table I and Table II. It appears that there is no significant difference in Q_{ij} between 50/50 copolymer and 65/35 copolymer. However, there seems to be a trend that the amplitude of Q_{ij} in films with higher induced polarization (hence, higher crystallinity) is smaller than that in films with lower induced polarization. This is shown in Fig. 14, where the polarization level (P_m) for the samples under an

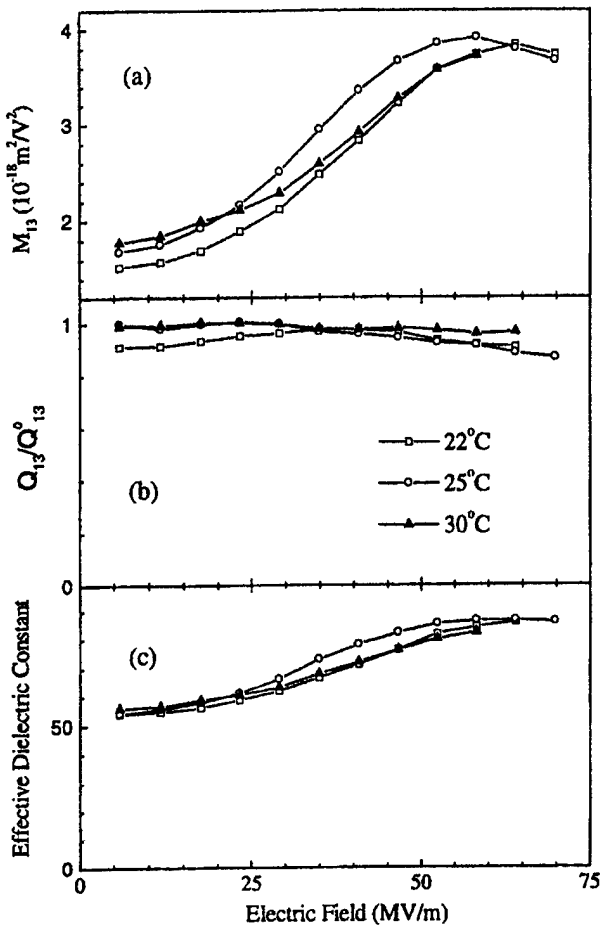

Fig. 13. Electric field dependence of some physical constants at room temperature in stretched 65/35 copolymer film irradiated at 95°C with 60 Mrad: a) M_{13} vs. electric field, b) Q_{13} vs. electric field, and c) effective dielectric constant vs. electric field.

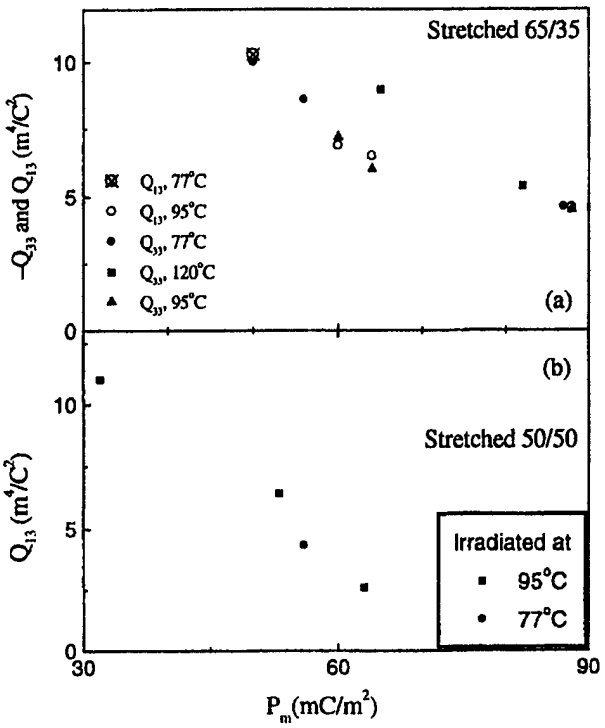

Fig. 14. Q_{33} and Q_{13} vs. polarization level of the samples under an external electric field of 150 MV/m: a) stretched 65/35 films and b) stretched 50/50 films.

external electric field of 150 MV/m is used. In other words, under the same irradiation temperature, $|\ Q_{ij}\ |$ increases with dosage (except for those irradiated at room temperature). Furthermore, the $|\ Q_{ij}\ |$ obtained here seems higher than those predicted for the intrinsic single crystal values of P(VDF-TrFE) copolymers [19]. The behaviors observed here can be qualitatively understood by the morphology of the copolymer, which is a semicrystalline polymer.

To illustrate this, consider the hydrostatic electrostrictive coefficient (Q_h) as an example where $S_v = Q_h P^2$ and S_v is the volume strain. For a polymer with a composite morphology, the total volume strain S_v will be the summation of that from the crystalline phase S_{Cv} and the amorphous phase S_{Av}:

$$S_v = v_C S_{Cv} + v_A S_{Av} \tag{5}$$

where v_C and v_A $(= 1 - v_C)$ are the volume fraction of the crystalline and amorphous phases. From an early study, it was found that in the irradiated P(VDF-TrFE) copolymer, the total polarization P measured from a film can be related to the polarization in the crystalline phase P_C and amorphous phase P_A by the logarithmic law of mixing observed for many diphase 0-3 composites [20]:

$$Log(P) = v_C log(P_C) + v_A log(P_A)\ . \tag{6}$$

In the crystalline region and amorphous, we will have

$$S_{Cv} = Q_{hC} P_C^2 \tag{7a}$$

$$S_{Av} = Q_{hA} P_A^2 \tag{7b}$$

where Q_{hC} and Q_{hA} are the effective hydrostatic electrostrictive coefficients in the crystalline and amorphous regions, respectively. Combining (5) to (7) yields

$$Q_h = Q_{hC} \left\{ v_C n^{2(1-v_C)} + \frac{Q_{hA}}{Q_{hC}} \frac{1 - v_C}{n^{2v_C}} \right\} \tag{8}$$

where $n = P_C/P_A$. From the pyroelectric study of the uniaxially stretched PVDF, it was found that the value of n is about 7.5 [21]. For the irradiated P(VDF-TrFE) 50/50 copolymer, it was found that the value of n is about 9.0 [20]. Using $n = 8$ as an example here, the ratio of Q_h/Q_{hC} as a function of the crystallinity v_c in the polymer is presented in Fig. 15 using (8), where the ratios of Q_{hA}/Q_{hC} with 0.5, 1, and 2 were used. The figure shows that over most of the crystallinity range, the ratio of Q_h/Q_{hC} is larger than 1, and it seems that this result is not very sensitive to the Q_{hA} value of the amorphous phase. That is,

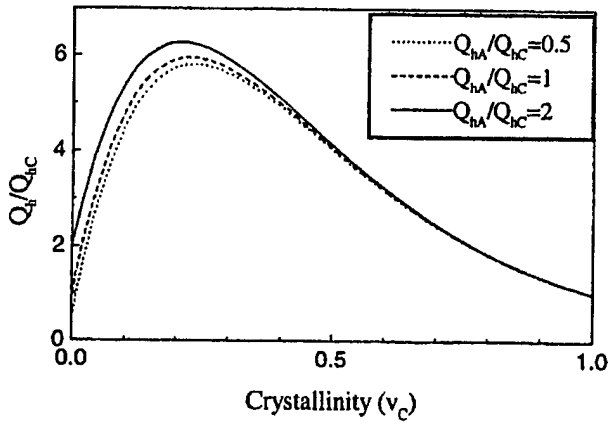

Fig. 15. Crystallinity (v_C) dependence of calculated Q_h through (7) where $n = 8$ is used and Q_{hA}/Q_{hC} is 0.5, 1, and 2, respectively.

the measured electrostrictive coefficient from the composite is higher than that of the crystallite when $P_C/P_A >> 1$, which may be consistent with the observation here that the measured electrostrictive coefficients increase with irradiation doses.

In (7b), Q_{hA} is used as an effective electrostrictive coefficient to describe the $S \sim P$ relationship in the amorphous region. In reality, the Maxwell stress-induced strain response, which is due to the Coulombic force between the free changes in the electrodes, can be quite significant in an amorphous polymer [6], [22], [23]. Therefore, the effective coefficient Q_{hA} also includes the contribution from this part, and, in the measured total electrostrictive coefficient Q, there will be contributions from the Maxwell stress. In the samples with very high irradiation dosages, which result in a low crystallinity, the contribution from the Maxwell stress effect can be significant. However, as has been discussed in an early publication and also revealed by a recent X-ray study of irradiated films under different electric fields [7], [12], [17], in the irradiated copolymers with very high strain responses, the main contribution is due to the local FE transformation and hence, the field-induced strain is electrostrictive in nature.

The temperature dependence of the electric field-induced strain in the irradiated copolymers was also studied. Presented in Fig. 16(a) is the transverse strain along the stretching direction for 65/35 copolymer irradiated at 95°C with 60 Mrad. The electric field induced strain increases with reduced temperature and reaches a broad peak at just below room temperature. For comparison, the elastic modulus along the stretching direction is also shown in Fig. 16(b). The increase of the field-induced strain with reduced temperature and the existence of a broad peak are typical signatures of relaxor FE associated with the increase of the local polarization in the material and increased normal FE behavior as the temperature is lowered [24]. This is clear experimental evidence that in the copolymers studied here, the strain response is from the local polarization and hence, electrostrictive. If the strain

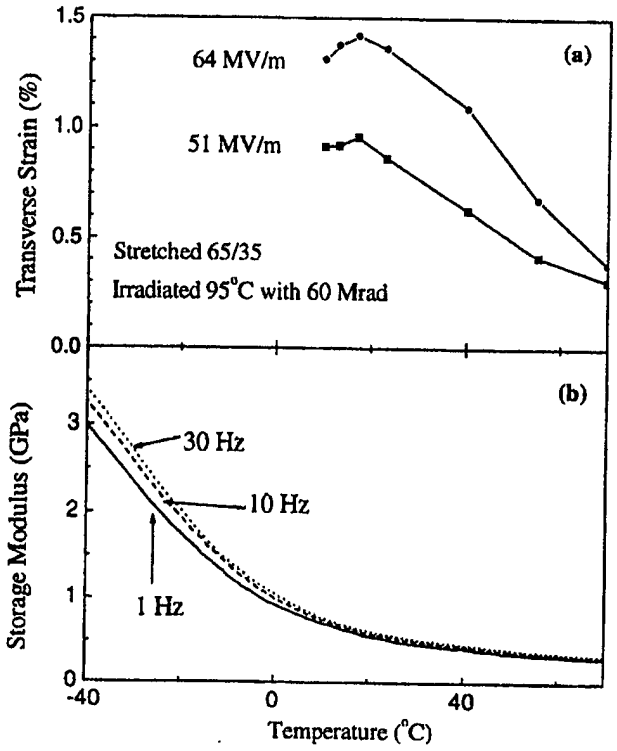

Fig. 16. For the stretched 65/35 film irradiated at 95°C with 60 Mrad: a) temperature dependence of the transverse strain along the stretch direction at different electric fields and b) temperature dependence of the elastic modulus along the stretching direction at different frequencies.

response is mainly from the Maxwell stress effect, as has been observed in the field-induced strain response in a polyurethane elastomer [23], [25], one would expect a decrease of the field-induced strain as the temperature is reduced because the elastic modulus increases as the temperature is lowered.

IV. Summary

The effect of high energy electron (2.55 MeV) irradiation on the polarization and dielectric behaviors and the electromechanical properties of P(VDF-TrFE) 50/50 and 65/35 copolymer films is reported. The results show that the electron irradiation transforms the normal FE P(VDF-TrFE) copolymer into a relaxor FE with ultrahigh electrostrictive strain. It also shows that in addition to this transformation, the irradiation also converts the crystalline phase into amorphous phase, causing a reduction in the polarization level of the polymer. To further increase the strain response and elastic energy density, it is necessary to reduce this latter process.

Among the two copolymers investigated, we found that the 65/35 copolymer is preferred for both longitudinal and transverse strain generation. Although the difference in the longitudinal strains generated by 65/35 and 50/50 copoly-

mers is not very large, the transverse strain along the stretching direction from 65/35 is much larger than that from 50/50 copolymer. Among the copolymers exhibiting slim polarization hysteresis loop and electrostrictive strain, we found that, in general, the electric field-induced strain decreases as the irradiation dosage increases, caused by the reduction of the crystallinity in the polymer by the irradiation. This, plus the temperature dependence of the field-induced strain, indicates that the electric field-induced strain is due to the responses of local polar regions in the relaxor P(VDF-TrFE) copolymer and, hence, confirms the electrostrictive nature of the strain response. As a result of this and the semicrystalline morphology of the copolymers, the effective charge-related electrostrictive coefficient (Q) measured from irradiated copolymers is higher than those from the intrinsic crystalline phase and shows an increase with the irradiation dosages. A simple model is presented to support this observation.

References

[1] H. S. Nalwa, *Ferroelectric Polymers*. New York: Dekker, 1995.

[2] T. T. Wang, J. M. Herbert, and A. M. Glass, *Applications of Ferroelectric Polymers*. New York: Chapman and Hall, 1988.

[3] L. E. Cross, "Ferroelectric ceramics: Materials and application issues," *Ceramic Trans.*, vol. 68, pp. 15–55, 1996.

[4] Z. Ma, J. I. Scheinbein, and B. A. Newman, "Electrostrictive response of elastomeric polymers," *Polymer Reprints*, vol. 33, pp. 385–386, 1992.

[5] Z. Ma, J. I. Scheinbein, and B. A. Newman, "High field electrostrictive response of polymers," *J. Polym. Sci. Part B, Polym. Phys.*, vol. 32, pp. 2721–2731, 1994.

[6] R. E. Pelrine, R. D. Kornbluh, and J. P. Joseph, "Electrostriction of polymer dielectrics with compliant electrodes as a mean of actuation," *Sens. Actuators A*, vol. 64, pp. 77–85, 1998.

[7] Q. M. Zhang, V. Bharti, and X. Zhao, "Giant electrostriction and relaxor ferroelectric behavior in electron-irradiated poly(vinylidene fluoride-trifluoroethylene) copolymer," *Science*, vol. 280, pp. 2101–2104, 1998.

[8] X. Zhao, V. Bharti, Q. M. Zhang, T. Romotowski, F. Tito, and R. Ting, "Electromechanical properties of electrostrictive poly(vinylidene fluoride-trifluoroethylene) copolymer," *Appl. Phys. Lett.*, vol. 73, pp. 2054–2056, 1998.

[9] Z.-Y. Cheng, T.-B. Xu, V. Bharti, S. Wang, and Q. M. Zhang, "Transverse strain responses in the electrostrictive poly(vinylidene fluoride-trifluoroethylene) copolymer," *Appl. Phys. Lett.*, vol. 74, pp. 1901–1903, 1999.

[10] Z.-Y. Cheng, V. Bharti, X. Zhao, S. Wang, T.-B. Xu, and Q. M. Zhang, "Relaxor ferroelectric polymers for actuators and transducers," *Proc. IEEE Ultrason. Symp.*, Miyagi, Japan, 1998, pp. 581–584.

[11] V. Bharti, X. Zhao, Q. M. Zhang, T. Ramotowski, F. Tito, and R. Ting, "Ultrahigh field induced strain and polarization response in electron irradiated poly(vinylidene fluoride-trifluoroethylene) copolymer," *Mater. Res. Innovat.*, vol. 2, pp. 57–63, 1998.

[12] Z.-Y. Cheng, V. Bharti, T.-B. Xu, S. Wang, Q. M. Zhang, T. Ramotowski, F. Tito, and R. Ting, "Transverse strain response in electrostrictive poly(vinylidene fluoride-trifluoroethylene) films and development of a dilatometer for the measurement," *J. Appl. Phys.*, vol. 86, pp. 2208–2214, 1999.

[13] L. E. Cross, "Relaxor ferroelectrics: an overview," *Ferroelectrics*, vol. 151, pp. 305–320, 1994.

[14] J. Su, P. Mouse, and Q. M. Zhang, "A bimorph based dilatometer for field induced strain measurement in soft and thin free standing polymer films," *Rev. Sci. Instrum.*, vol. 69, pp. 2480–2483, 1998.

[15] F. J. Balta, A. G. Arche, T. A. Ezquerra, C. S. Cruz, F. Batallan, B. Frick, and E. L. Cabarcos, "Structure and properties of ferroelectric copolymer poly(vinylidene fluoride)," *Prog. Polym. Sci.*, vol. 18, pp. 1–48, 1993.

[16] Z.-Y. Cheng, R. S. Katiyar, X. Yao, and A. Guo, "Dielectric behavior of lead magnesium niobate relaxors," *Phys. Rev. B.*, vol. 55, pp. 8165–8174, 1997.

[17] Q. M. Zhang, Z.-Y. Cheng, and V. Bharti, "Relaxor ferroelectric behavior in high energy electron irradiated poly(vinylidene fluoride-trifluoroethylene) copolymers," *Appl. Phys. A.*, vol. 70, pp. 307–312, 2000.

[18] F. Jona and G. Shirane, *Ferroelectric Crystals*. New York: Dover Publications, 1993.

[19] T. Furukawa, "Ferroelectric properties of vinylidene fluoride copolymers," *Phase, Transit.*, vol. 18, pp. 143–211, 1989.

[20] V. Bharti, H. S. Xu, G. Shanthi, Q. M. Zhang, and K. Liang, "Polarization and structural properties of high energy electron irradiated poly(vinylidene fluoride-trifluoroethylene) copolymer films," *J. Appl. Phys.*, vol. 87, pp. 452–461, 2000.

[21] D. Rollik, S. Bauer, and R. Gerhard-Multhaut, "Separate contributions to the pyroelectricity in poly(vinylidene fluoride) from the amorphous and crystalline phases, as well as from their interface," *J. Appl. Phys.*, vol. 85, pp. 3282–3288, 1999.

[22] Y. M. Shkel and D. J. Klingenberg, "Material parameters for electrostriction," *J. Appl. Phys.*, vol. 80, pp. 4566–4572, 1996.

[23] Q. M. Zhang, J. Su, C. H. Kim, R. Ting, and R. Capps, "An experimental investigation of electromechanical responses in a polyurethane elastomer," *J. Appl. Phys.*, vol. 81, pp. 2770–2776, 1997.

[24] Z.-Y. Cheng, R. S. Katiyar, X. Yao, and A. S. Bhalla, "Temperature dependence of the dielectric constant of relaxor ferroelectrics," *Phys. Rev. B.*, vol. 57, pp. 8166–8177, 1998.

[25] J. Su, Q. M. Zhang, C. H. Kim, R. Y. Ting, and R. Capps, "Effects of transitional phenomena on the electric field induced strain-electrostrictive response of a segmented polyurethane elastomer," *J. Appl. Polym. Sci.*, vol. 65, pp. 1363–1370, 1997.

Zhong-Yang Cheng was born in Shaanxi, China in December 1962. He received his B.S. in physics and his M.S. and Ph.D. degrees in Electronic Materials and Engineering from Xian Jiaotong University, China in 1983, 1988, and 1995, respectively. He is currently a research associate with Materials Research Laboratory, The Pennsylvania State University. Before joining Penn State in 1998, he worked at the Heinrich-Hertz-Institute in Berlin, Germany for one year and in the Department of Physics at the University of Puerto Rico for one and half years. His research interests are in structure-property studies of various functional materials and the application studies of these materials. He has published more than 50 articles. He is a member of the American Physical Society and Materials Research Society. Dr. Cheng can be reached through email at zxc7@psu.edu.

Vivek Bharti received his B.Sc. degree in science in 1989 from Meerut University, India and his Masters in physics in 1992. He earned the doctoral degree in polymer physics in 1997 from the University of Roorkee, Roorkee, India. During his doctoral program, he received research scholarship awards from Council of Scientific and Industrial Research (CSIR) India. He is currently working as a research associate at Materials Research Laboratory, The Pennsylvania State University. He has published many research articles in international scientific journals and has two patents to his credit. He is one of the researchers who discovered the Relaxor ferroelectric behavior in ferroelectric polymers. His current research interests are in the area of characterization of structural and electromechanical properties of advanced materials for their applications as actuators, transducers, sensors, dielectrics, and MEMS. He is a member of Materials Research Society.

Tian Mai was born in Shandong, China in 1966. He received the B.S. degree in Computer Science from the Shangdong University, China in 1988. He is currently working as a visiting research assistant with the Materials Research Laboratory, The Pennsylvania State University from Shangdong University. His research interest is in the area of property characterization of electroactive materials.

Tian-Bing Xu (M'98) received the M. Sc. degree in Electrical Engineering from The Pennsylvania State University in 1999. He is currently a candidate for the Ph.D. degree in the Intercollege Graduate Program in Materials, The Penn State University. Before he came to the USA, he had been working as an engineer and associate director with Ion Beam Laboratory, Institute of Physics, Chinese Academy of Science, China for 9 yr. He has a very strong background in the areas of ion implantation and ion beam analyses for semiconductors and other materials. He is currently working on electroactive polymers and their application for actuators and transducers. He has published about 35 papers in international journals. He is a member of IEEE and Materials Research Society.

Qiming M. Zhang (M'97–SM'99) is an associate professor of Electrical Engineering at the Materials Research Laboratory and Department of Electrical Engineering of The Penn State University. He obtained his B.S. in 1981 from Nanjing University, China and his Ph.D. degree in 1986 from The Penn State University. He worked at the Brookhaven National Laboratory as a research scientist in the area of solid state thin films. He came back to The Penn State University in 1991 as a faculty member to conduct research in ferroelectric-based materials and devices and electroactive polymer-based materials and devices. The research activities in his research group include material development, modeling, and device development for transducers and actuators, dielectrics and capacitors, ferroelectric polymer thin film for memory devices, MEMS, photonic bandgap crystal, and electrooptic and acoustooptic materials and devices. He has delivered many invited presentations in those areas. There are 135 publications in those areas from his research group. He is a member of IEEE, Materials Research Society, and American Physical Society.

Thomas Ramotowski has been employed from 1987 to the present as a chemist by the Naval Undersea Warfare Center, Division Newport and its predecessor organizations. He has over 10 yr of experience in materials analysis, characterization, and chemistry, with a special emphasis on polymeric materials and their associated adhesive systems. His research interests include polymer analysis and characterization by thermal analysis techniques, development and characterization of active and passive polymeric materials for use in undersea sensors and cables, accelerated life testing as a means for predicating/verifying long-term polymer performance in various environments, adhesive bonding and test methods for evaluating adhesives, thermal analysis test methods and standards, and the analysis of materials by SPM/AFM techniques. Mr. Ramotowski is a graduate of Brown University and a member of Sigma Xi, NATAS, and ASTM.

Kenneth A. Wright was born in Washington, DC, January 29, 1919. Haverford College awarded him a B.A. degree in physics in 1941. He was an army draftee in 1941 and ended military service in 1945 as a major after serving as a ground radar staff officer in the Headquarters, Allied Air Forces, Mediterranean Theater of Operations. The Massachusetts Institute of Technology awarded him the B.S and M.S. degrees in physics. He has been a staff member of the M.I.T. High Voltage Research Laboratory since 1947 and has been associated with the Lahey Clinic in radiation oncology physics since 1949. His principal research interests have been in the application of electron beams and x-rays to physical, chemical, and biological system.

Robert Ting was born in China and received his B.S. degree from the National Taiwan University in 1964. Later, he received graduate training at MIT (M.S., 1967) and University of California at San Diego (Ph.D., 1971). He began his Naval Research career in 1971 at the Naval Research Laboratory in Washington, DC, working in the areas of polymer drag reduction, polymer rheology, composite materials, and adhesion science. In 1980, he was promoted to be in charge of the Navy's basic and applied research in underwater acoustical materials at NRL's Underwater Sound Reference Division in Orlando, Florida. In addition to polymeric materials, his group was involved in the research of a wide range of new piezoelectric materials for the Navy's sonar transducer applications. Dr. Ting retired from the U.S. Navy in 1997 and is now Professor of Chemistry and Materials Engineering at the University of Central Florida in Orlando. He has published extensively and is a Fellow of the Acoustic Society of American.

APPENDIX 27

Jpn. J. Appl. Phys. Vol. 40 (2001) pp. 672–675
Part 1, No. 2A, February 2001

High Electromechanical Coupling Factor and Electrostrictive Strain over Broad Frequency Range in Electrostrictive Poly(vinylidene fluoride-trifluoroethylene) Copolymer Films

Vivek BHARTI, T.-B. XU, Z.-Y. CHENG, T. MAI, Q. M. ZHANG*, Tom RAMOTOWSKI[1] and K. A. WRIGHT[2]

Materials Research Laboratory, The Pennsylvania State University, University Park, PA 16802, USA
[1]*Naval Undersea Warfare Center, Newport, Rhode Island 02841, USA*
[2]*Laboratory of Electromagnetic and Electronic Systems, Massachusetts Institute of Technology, Cambridge, MA 02139, USA*

(Received July 27, 2000; accepted for publication November 8, 2000)

Electromechanical coupling factor is one of the most important parameters for measuring the performance of materials for electromechanical transduction applications. In this paper, we will show that a transverse electromechanical coupling factor k_{31} of more than 0.45 can be achieved in poly(vinylidene fluoride-trifluoroethylene) [P(VDF-TrFE)] copolymer under certain electron irradiation treatment conditions. In addition, the effective piezoelectric coefficients of the irradiated copolymer have been found to increase markedly in comparison to non-irradiated copolymers. Experimental evidences also indicate that the improved electrostrictive strains in irradiated copolymer films can be maintained over a broad frequency and temperature range.

KEYWORDS: electrostriction, P(VDF-TrFE), piezoelectric, coupling coefficient

1. Introduction

As the best known electromechanical polymers, polyvinylidene fluoride (PVDF) and its copolymers with trifluoroethylene (TrFE) have been extensively investigated in the past thirty years for a wide range of applications such as artificial muscles, electromechanical transducers, and electric energy generation from ocean powers.[1–4] Although the P(VDF-TrFE) copolymers possess the highest piezoelectric coefficients and electromechanical coupling factors among all the known polymers, they are still far below those from the piezoceramics. For example, the longitudinal coupling factor k_{33} for single crystal P(VDF-TrFE) 75/25 mol% copolymer is below 0.3, and other coupling factors have even lower values. The piezoelectric coefficients of these polymers at room temperature are also below 40 pm/V.[5–7] Therefore, continuous efforts are being made to improve the electromechanical properties of these copolymers by using different approaches.[8–12]

We have reported recently that by using high-energy electron irradiation, the electromechanical properties of P(VDF-TrFE) copolymers such as field-induced electrostrictive strains along both longitudinal and transverse directions can be improved significantly.[13,14] In the present study, we report that under a proper electron irradiation condition, an electromechanical coupling factor $k_{31} = 0.45$ (transverse coupling factor) can be reached in the irradiated copolymers, which is much higher than those in the non-irradiated copolymers ($k_{33} < 0.3$ and $k_{31} < 0.15$) and even higher than the k_{31} value in most of the piezoceramics.[5–7,15] Since the energy conversion efficiency is proportional to the square of the coupling factor, this improvement is significant.[16] In addition, we will present the results showing that the irradiated copolymer can maintain their high strain level to higher frequencies and over a relative broad temperature range.

2. Experimental

The data reported in this article are taken from the P(VDF-TrFE) 68/32 mol% copolymer films, which exhibit the best electromechanical properties among the copolymers investigated.[13,14,17] The copolymer powder was purchased from Solvay and Cie, Belgium. The non-stretched and stretched (4.5×) films of thickness ~20–25 μm were prepared by extrusion and casting from *N*,*N*-dimethyl formamide (DMF) solvent, respectively. The non-stretched films were used to investigate the longitudinal strain response (the strain along the thickness direction). As has been shown earlier, in order to obtain a high transverse strain, a stretched copolymer film should be used.[17] In order to improve the crystallinity and also to remove the residual solvent from the solution cast films, the films were annealed at 140°C for 16 h before the irradiation. The electron irradiation was carried out using 1 MeV electrons at National Institute of Standards and Technology, and 1.2 MeV electrons at the Massachusetts Institute of Technology. In both the cases the irradiation was carried out in a nitrogen atmosphere at temperatures near 100°C for the irradiation doses ranging from 60 to 75 Mrad.

The strains along the thickness direction (longitudinal strain, S_3) and the stretching direction (transverse strain, S_1) were measured using a piezo-bimorph-based sensor and a cantilever-based dilatometer, respectively.[17,18] Both set-ups were designed and developed specifically for strain measurement in polymer thin films. In the piezo-bimorph set-up, the strain in the polymer films generates a deflection in the piezo-bimorph, which in turn, produces an electric signal output due to the piezoelectric effect. In the cantilever-based dilatometer set-up, one end of the polymer is fixed and the other end is attached to a plastic cantilever. The transverse strain in the films causes the deflection of the tip of the cantilever, which is measured by a photonic sensor. A laser interferometer set-up was used to measure the electrostrictive strain at higher frequencies (up to 5 kHz which was the limit of the voltage amplifier used).[19] The Sawyer-Tower technique was used to measure the polarization response in the films at 10 Hz frequency.

3. Results and Discussion

Figure 1(a) presents the amplitude of electric field-induced transverse strain at 1 Hz near room temperature obtained from the stretched copolymer films irradiated at 100°C using 1.2 MeV electrons with 70 Mrad dose. The transverse strain $S_1 \sim 3.3\%$ under the electric field of 105 MV/m is observed,

*E-mail address: qxz1@psu.edu

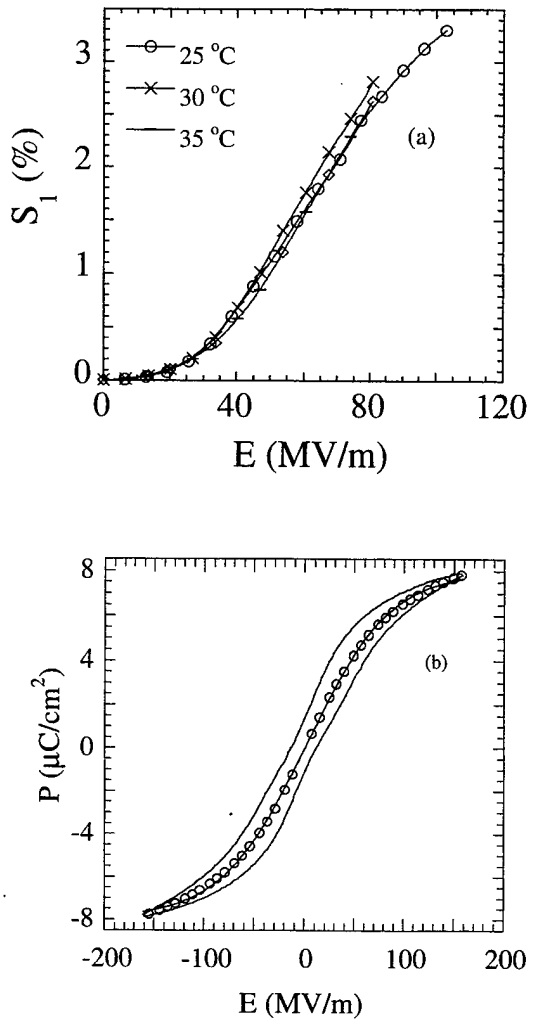

Fig. 1. (a) The dependence of electric field induced transverse strain (S_1) on electric field strengths at different temperatures, the solid curves are drawn to guide eyes; (b) the polarization hysteresis loop (solid curve) measured at 30°C, where the circles (O) are the average polarization of the observed polarization loop, while the solid line passes the circles is the fitted result using eq. (2). The material is stretched 68/32 mol% P(VDF-TrFE) copolymer films irradiated at 100°C with 1.2 MeV electrons for 70 Mrad dose.

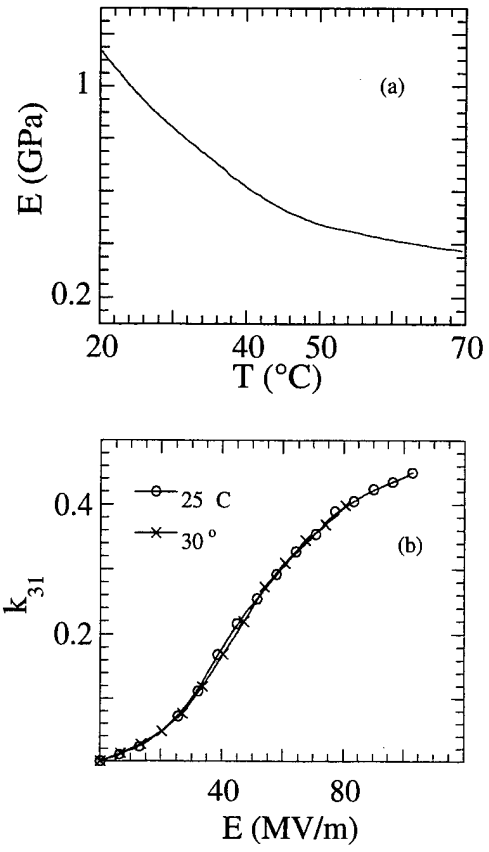

Fig. 2. The change in the (a) elastic modulus with temperature; (b) electromechanical coupling factor (k_{31}) with applied electric field at different temperatures (here the solid curves are drawn to guide eyes); measured for stretched 68/32 mol% P(VDF-TrFE) copolymer films irradiated at 100°C with 1.2 MeV electrons for 70 Mrad dose.

which is higher than the transverse strain obtained at a similar field for copolymers irradiated with 2.55 MeV electrons, as reported earlier.[14,17]

The quasi-static electromechanical coupling factor for electrostrictive materials has been derived by Hom *et al.*,[20] where the coupling factor depends on the induced polarization level P_B and strain S_i under a given electrical field, i.e.,

$$k_{3i}^2 = \frac{kS_i^2}{s_{ii}^P \left[P_B \ln\left(\frac{P_S + P_B}{P_S - P_B}\right) + P_S \ln\left(1 - \left(\frac{|P_B|}{P_S}\right)^2\right)\right]} \quad (1)$$

where $i = 1$ or 3, corresponding to the transverse or longitudinal direction (for example, k_{31}, is the transverse coupling factor) and s_{ii}^P is the elastic compliance under constant polarization. The polarization–field (P–E) relation is assumed to be

$$|P_B| = P_S \tanh(k|E|) \quad (2)$$

where P_S is the saturation polarization and k is a constant. As can be seen from Fig. 1(b), the averaged polarization loop can be quite well fitted by eq. (2). Using these data along with the elastic modulus shown in Fig. 2(a), the quasi-static transverse coupling factor k_{31} is calculated and presented in Fig. 2(b). As can be seen, at near room temperature, k_{31} is more than 0.45, which is much higher than that of non-irradiated P(VDF-TrFE) copolymers and even higher than k_{31}

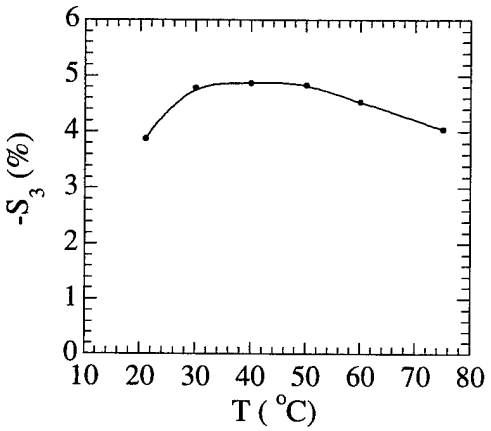

Fig. 3. The longitudinal strain (S_3) as a function of temperature measured under 147 MV/m and 1 Hz driving electric field for unstretched 68/32 mol% P(VDF-TrFE) copolymer films irradiated at 100°C with 1.0 MeV electrons for 70 Mrad dose. Data points are shown and the solid curve is drawn to guide eyes.

from most of the piezoceramics.[15] Since in many applications such as mico-electro-mechanical-systems (MEMS), electrical power generation from ocean waves, and artificial muscles, it is the transverse strain that is often used, a high transverse coupling factor, therefore, is highly desirable.[4,21–23]

The variation in longitudinal strain (S_3) at 1 Hz with temperature is presented in Fig. 3, where S_3 of near -5% can be induced by an electric field of 147 MV/m for unstretched copolymer films irradiated at 105°C with 70 Mrad dose of 1 MeV electrons. As can be observed that the induced strain is almost constant up to 80°C. Furthermore, the frequency effect on the field-induced strain, which is important for many actuator and transducer applications, was also characterized at near room temperature. The bimorph based set-up was used to measure the strain response in the frequency range from 1 Hz to near 100 Hz and a laser interferometer was utilized to measure strain at higher frequencies (up to 5 kHz).. The S_3 data obtained from both set-ups are presented in Figs. 4(a) and 4(b). At lower frequencies (<50 Hz), the laser interferometer has relatively large error in the strain measurement due to the environment noise. In the overlapped frequency range, the data measured from the bimorph sensor and from the laser interferometer is consistent with each other within the error bar. The result shows that the electrostrictive strain extrapolated to 10 kHz remains to be more than 50% of the value at 1 Hz (over 4 frequency decades). For the comparison, the polarization level was also measured in the same frequency range using the Sawyer-Tower circuit. Since the electrostrictive strain S is proportional to the square of the polarization P ($S = QP^2$, where Q is the electrostrctive coefficient), the change in the square of the polarization with frequency is also presented in Fig. 4. Apparently, the dispersion of the square of the polarization is smaller than that of the strain. Making use of the strain and polarization data, the electrostrctive coefficient Q is determined and is shown in Fig. 4(c). As indicated by the data, there is a small decrease of Q with frequency which suggests that there is a change of the polarization response with frequency and the low frequency component of the polarization is more effective in generating the strain response. This behavior is analogous to the one observed in the relaxor ferroelectric ceramic, $PbMg_{1/3}Nb_{2/3}O_3$, where due to the change in the polarization response with temperature, Q exhibits a large variation.[24] In the irradiated copolymer, the polarization response can be from several different sources such as the rotation of dipoles and the local phase transformation due

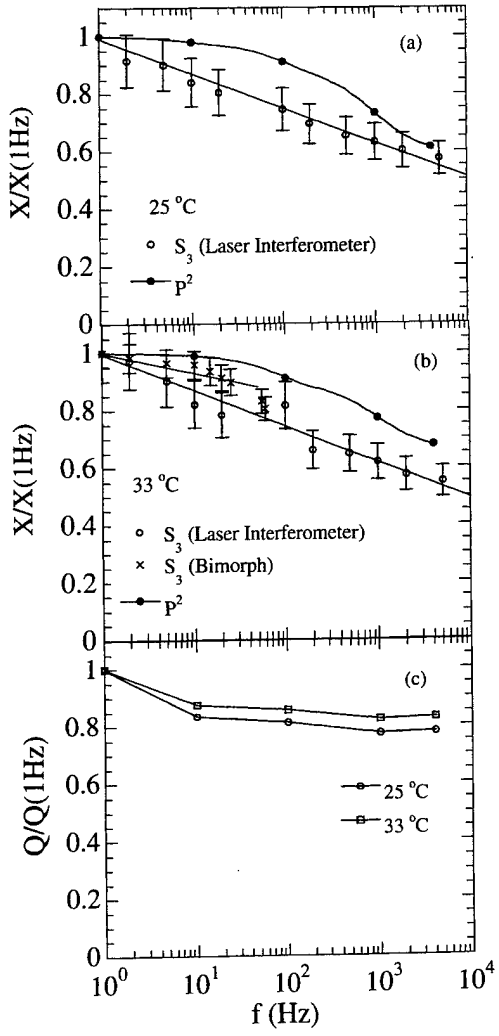

Fig. 4. The ratio of longitudinal strain (S_3) at higher frequencies to the strain at 1 Hz (open circles) as a function of frequency measured using laser interferometer at temperatures of (a) 25°C, and (b) 33°C; for unstretched 68/32 mol% P(VDF-TrFE) copolymer films irradiated at 105°C with 1.0 MeV electrons for 70 Mrad dose. For the comparison, the change in the square of the ratio of the polarization at higher frequencies to polarization at 1 Hz as a function of frequency is also shown (solid dots). The strain data (cross dots) measured using the bimorph based sensor is also presented. (c) The normalized electrostrictive coefficient Q_{11} ($Q = S/P^2$) as a function of frequency for the two temperatures measured. The symbols here are the data points and the curves are drawn to guide eyes.

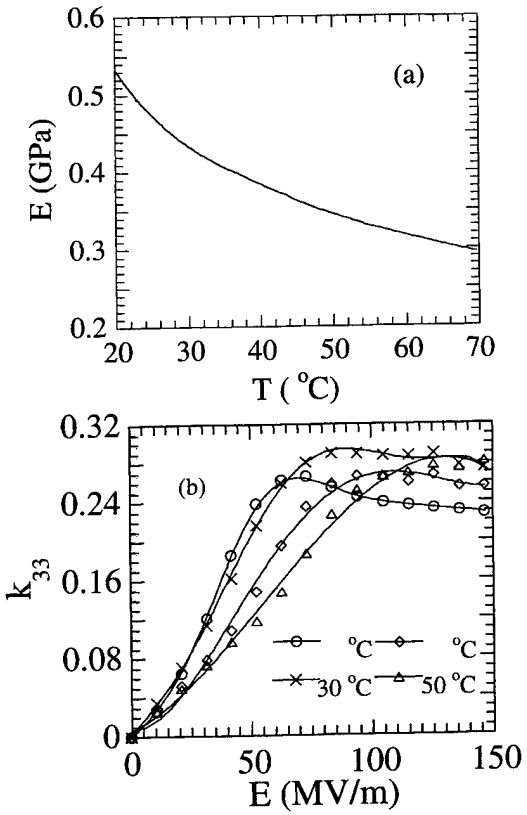

Fig. 5. (a) The elastic modulus as a function of temperature; (b) the electromechanical coupling factor (k_{33}) as a function of driving electric field at different temperatures (data points are presented and solid curves are drawn to guide eyes); for unstretched 68/32 mol% P(VDF-TrFE) copolymer films irradiated at 105°C with 1.0 MeV electrons for 70 Mrad dose.

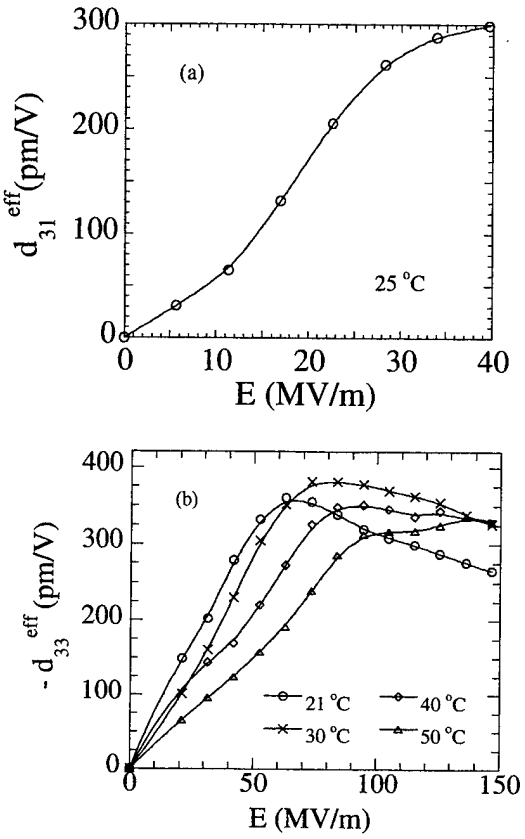

Fig. 6. Effective piezoelectric coefficients; (a) d_{31}^{eff} measured for stretched P(VDF-TrFE) copolymer films irradiated at 100°C with 70 Mrad using the 1.2 MeV electrons, and (b) d_{33}^{eff} measured for unstretched P(VDF-TrFE) copolymer films irradiated at 100°C with 70 Mrad using the 1.0 MeV electrons. The symbols here are the data points and the curves are drawn to guide eyes.

to the expansion and contraction of the local polar-regions.

Making use of eq. (1) with the elastic modulus [Fig. 5(a)] and polarization data, the longitudinal coupling factor (k_{33}) at 1 Hz is determined and presented in Fig. 5(b). At near room temperature and under 80 MV/m electric field, k_{33} of more than 0.3 is achieved.

Although after irradiation at temperatures near and above room temperature the copolymer behaves as an electrostrictive material, to compare it with other electromechanical actuator materials, an effective piezoelectric coefficient is defined here as the ratio of the induced strain versus applied unipolar ac electric field [S_i/E_3, where $i = 1$ is for the effective transverse piezoelectric coefficient (d_{31}^{eff}) and $i = 3$ for the effective longitudinal coefficient (d_{31}^{eff})].[17] As seen in Fig. 6, relatively large effective piezoelectric coefficients are obtained, and $d_{31}^{\text{eff}} = 300$ pm/V and $d_{33}^{\text{eff}} = -383$ pm/V are observed under 40 MV/m and 75 MV/m field for irradiated stretched and unstretched films, respectively. These values are comparable to the piezoelectric coefficient of conventional piezoceramic materials, for example PZT-5H ($d_{31} \sim -274$ pm/V and $d_{33} \sim 593$ pm/V).[15] It should be pointed out here that in many soft polymer elastomers, a high ratio of strain/applied field can be achieved due to the electrostatic force.[17,25,26] But because of the low elastic modulus of these polymer elastomers, the strain energy density, which is an important parameter for choosing a material as an actuator, is lower than irradiated copolymer films.[13,14,25,26]

Acknowledgements

This work was supported by DARPA (grant no. N00173-99-C-2003), NSF (grant no. ECS-9710459), and ONR (grant no. N00014-97-1-0667). The authors also wish to thank A. Glazonov for stimulating discussions and assisting in the experiments.

1) T. T. Wang, J. M. Herbert and A. M. Glass: *The Application of the Ferroelectric Polymers* (Blackie, Chapman and Hall, New York, 1988).
2) M. A. Marcus: Ferroelectrics **40** (1982) 29.
3) J. A. Chilton and M. T. Goosey: *Special Polymers for Electronics and Optoelectronics* (Chapman & Hall, New York, 1995) Chap. 5.
4) I. Amato: Sci. News **136** (1989) 305.
5) K. Omote, H. Ohigashi and K. Koga: J. Appl. Phys. **81** (1997) 2760.
6) K. Omote and H. Ohigashi: Appl. Phys. Lett. **66** (1995) 2215.
7) H. Wang, Q. M. Zhang, L. E. Cross and A. O. Sykes: J. Appl. Phys. **74** (1993) 3394.
8) A. J. Lovinger: Science **220** (1983) 1115.
9) H. Ohigashi and T. Hattori: Ferroelectrics **171** (1995) 11.
10) V. Bharti, T. Kaura and R. Nath: IEEE Dielectr. Electr. Insul. **2** (1995) 1106.
11) J. Su, Y. Ma, J. Scheinbeim and B. A. Newman: J. Polym. Sci. B **33** (1995) 85.
12) G. M. Sessler and J. Hillenbrand: Appl. Phys. Lett. **75** (1999) 3405.
13) Q. M. Zhang, V. Bharti and X. Zhao: Science **280** (1998) 2101.
14) Z.-Y. Cheng, T.-B. Xu, V. Bharti, S. Wang and Q. M. Zhang: Appl. Phys. Lett. **74** (1999) 1901.
15) B. Jaffe, W. R. Cook and H. Jaffe, Jr.: *Piezoelectric Ceramics* (Academic Press, London, 1971).
16) IEEE Standard on Piezoelectricity, ANSI/IEEE Std 176–1987 (IEEE, New York, 1987).
17) Z.-Y. Cheng, V. Bharti, T. Mai, T.-B. Xu, Q. M. Zhang, T. Ramotowski, K. A. Wright and R. Ting: IEEE Trans. Ultrason. Ferroelectr. Freq. Control. **47** (2000) 1296.
18) J. Su, P. Moses and Q. M. Zhang: Rev. Sci. Instrum. **69** (1998) 2480.
19) Q. M. Zhang, W. Y. Pan and L. E. Cross: J. Appl. Phys. **63** (1988) 2492.
20) C. Hom, S. Pilgrim, N. Shankar, K. Bridger, M. Massuda and S. Winzer: IEEE Trans. Ultrason. Ferroelectr. Freq. Control. **41** (1994) 542.
21) D. L. Polla and L. F. Francis: MRS Bull (1996) July, 59.
22) L. E. Cross: Jpn. J. Appl. Phys. **34** (1995) 2525.
23) R. H. Baughman, C. X. Cui, A. A. Zakhidov, Z. Iqbal, J. N. Barisci, G. M. Spinks, G. G. Wallace, A. Mazzoldi, D. De Rossi, A. G. Rinzler, O. Jaschinski, S. Roth and M. Kertesz: Science **284** (1999) 1340.
24) A. E. Glazonov, J. Zhao and Q. M. Zhang: *Fifth Williamsburg Workshop: First-Principles Calculations for Ferroelectrics*, AIP Conf. Proc. **436** (1998) 118.
25) R. Kornbluh, R. Pelrine, J. Joseph, R. Heydt, Q. Pei and S. Chiba: Proc. SPIE **3669** (1999) 149.
26) M. Zhenyi, J. I. Scheinbeim, J. W. Lee and B. A. Newman: J. Polym. Sci. B **32** (1994) 2721.

APPENDIX 28

ELSEVIER

January 2001

Materials Letters 47 (2001) 107–111

MATERIALS LETTERS

www.elsevier.com/locate/matlet

Evolution of transitional behavior and structure of electron-irradiated poly(vinylidene fluoride–trifluoroethylene) copolymer films

Vivek Bharti [a], G. Shanthi [a], H. Xu [a], Q.M Zhang [a,*], Kuiming Liang [b]

[a] *Materials Research Laboratory, The Pennsylvania State University, University Park, PA 16802, USA*
[b] *ATL Echo Ultrasound, Reedsville, PA 17084, USA*

Accepted 21 June 2000

Abstract

The effect of high-energy electron irradiation on poly(vinylidene fluoride– trifluoroethylene) (PVDF–TrFE) copolymer is investigated in a broad range of electron doses in light of a recent finding of the relaxor ferroelectric behavior and large electrostriction in the material. It is shown that although irradiation reduces both the crystalline and polar ordering, the two are not directly related to each other. In contrast to differential scanning calorimetery (DSC) and X-ray results which show that the copolymer becomes amorphous for higher irradiation dose, the dielectric data still exhibit relaxation peak which follows the Vogel–Fulcher law, indicating the presence of local polar ordering. © 2001 Published by Elsevier Science B.V.

Keywords: P(VDF–TrFE); Ferroelectricity; DSC; X-ray; Structure; Relaxor; Polymer

1. Introduction

Ferroelectric polymers have attracted much attention for the last few decades as they revealed a new aspect of polymers as functional materials. Among them, poly(vinylidene fluoride–trifluoroethylene) (P(VDF–TrFE)) copolymers have been investigated extensively because the material exhibits the highest ferroelectric polarization and electromechanical responses among the known polymers [1,2]. However, the electromechanical properties of P(VDF–TrFE) copolymers are still one order of magnitude smaller than those from piezoceramic materials, which severely limit their applications for electromechanical devices [3]. Recently, we reported [4,5] that under a proper high-energy electron irradiation, P(VDF–TrFE) copolymers exhibited a massive electrostrictive strain ($>4\%$) with high elastic energy density. It was also observed that a piezoelectric state can be induced in these polymers under a DC electric bias field with piezoelectric constants approaching those of the best piezoceramic materials [6]. In addition, the dielectric peak of irradiated films exhibited a strong frequency dispersion that followed the Vogel–Fulcher (V–F) law [7,8], an empirical law which was observed in many glass systems [9] and in relaxor ferroelectric ceramics [10,11], suggesting that

* Corresponding author. Tel.: +1-814-863-7846; fax: +1-814-863-7846.
E-mail address: qxz1@psu.edu (Q.M. Zhang).

00167-577X/01/$ - see front matter © 2001 Published by Elsevier Science B.V.
PII: S0167-577X(00)00219-6

the material may belong to the relaxor ferroelectric family. In this letter, we report the experimental results on the structural evolution and transitional behavior as revealed by X-ray diffraction, dielectric, polarization and differential scanning calorimetery (DSC) data of irradiated films of P(VDF–TrFE) at 50/50 mol% composition over a broad electron irradiation dose range.

2. Experimental

The P(VDF–TrFE) (50/50 mol%) was supplied by Solvay and Cie, Belgium and the molecular weight of the polymer is determined to be 200,000. The films were prepared by hot pressing the powder sandwiched between two aluminum foils at 215°C with a consequent slow cooling to room temperature. All the experiments were performed on 25-μm thick films. The irradiation was carried out using 3-MeV electrons under a nitrogen atmosphere at different temperatures. The dielectric data were taken in the frequency range from 30 Hz to 100 kHz, using a dielectric analyzer (TA Instruments, model 2970) in the temperature interval −60°C to 125°C for a heating and cooling rate of 2°C/min. The DSC measurements were carried out using a differential scanning calorimeter (TA Instruments, model 2010) at a scanning rate of 10°C/min under a nitrogen atmosphere. The X-ray pattern was taken at room temperature (20°C) using a diffractrometer (Scintag model Pad-V) with Ni-filtered CuKα radiation.

3. Results and discussion

Fig. 1 presented the dielectric constant data of unirradiated and irradiated (from 30 to 150 Mrad) copolymer films. Consistent with the early observations [4,5], the effect of irradiation is to broaden the dielectric peak and move it to near room temperature. More interestingly, although the dielectric peak height drops monotonically with dosage, all the dielectric data presented from irradiated films follow the V–F law. The V–F law is an empirical law that holds for the disorder dipolar systems, which undergo freezing of the relaxation time spectrum below a certain temperature (T_f), such as glassy and relaxor

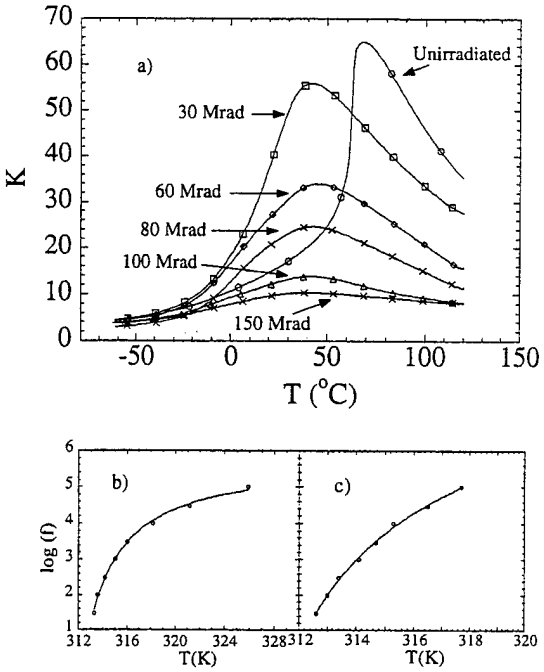

Fig. 1. (a) The dielectric constant measured at 1 kHz as a function of temperature for P(VDF–TrFE) 50/50 mol% copolymer films, unirradiated and irradiated at 120°C for different doses. Relationship between the measurement frequency and the temperature of the dielectric constant maximum for two irradiaton doses; (b) 30 and (c) 150 Mrad, points show experimental data, and the lines are fits to the Vogel–Fulcher law.

ferroelectric materials [10], and can be defined as: $f = f_0 \exp[-U/(k(T - T_f))]$ where T is the dielectric constant peak temperature, f is the frequency, and k is the Boltzman constant. It was found that the freezing temperature T_f does not significantly change with the irradiation dosage. For instance, for films irradiated at 30 Mrad, $T_f = 310$ K while at 150 Mrad, $T_f = 307$ K.

In contrast, both the DSC data (Fig. 2) and X-ray data (Fig. 3) show a large change in structure and transitional behavior in the polymer as the dosage increases from 30 to 150 Mrad. In unirradiated films (Fig. 2a), DSC data show two well-defined peaks, one at 160°C and the other at 65°C, corresponding to the melting and ferroelectric–paraelectric (F–P) transitions in the crystalline region, respectively [12]. At 30 Mrad irradiation (Fig. 2b), although there is no marked change in the melting peak (except a slight drop in the temperature), the peak associated with

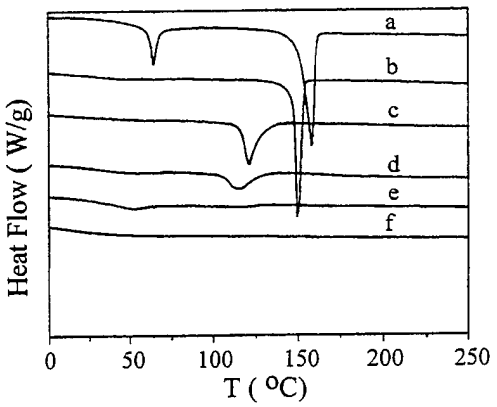

Fig. 2. DSC thermogram of P(VDF-TrFE) 50/50 mol% copolymer (a) unirradiated, and irradiated at 120°C for (b) 30, (c) 60, (d) 80, (e) 100, and (f) 150 Mrad doses.

the original F–P transition nearly disappears. Careful inspection of the data reveals that F–P transition peak becomes very broad and diffuse. When the dose is further increased to 60 Mrad, the melting peak shows a significant broadening as well as a large drop in transition temperature and transition enthalpy. At 100 Mrad, the melting peak could not be detected, indicating the disappearance of the crystalline phase in the films due to irradiation. The apparent lowering and broadening of the melting peak indicate a broad distribution in the crystallite sizes and reduction in the crystal ordering in irradiated films caused by the lattice defects, cross-linking within the crystallites and at the crystalline–amorphous interface.

It should also be noted that there is an important difference between the lattice ordering and the ferroelectric ordering. The lattice ordering is associated with the positional ordering of the monomer units while the ferroelectric ordering is from the dipolar alignment and their coupling. Hence, the ferroelectric ordering can be destroyed in a perfect lattice by the random introduction of *trans*-gauche bonds in polymer chains (such as a paraelectric phase), while the decrease of the crystal ordering in irradiated films is caused by the lattice defects and reduction of the crystallinity due to the conversion of the crystallites to amorphous. Furthermore, local polar ordering can persist even though there is not much crystalline ordering as observed in liquid crystals [13]. It is interesting to note here that although the enthalpy of the melting peak becomes zero at 100 Mrad, the enthalpy of the broad peak associated with the original P–F transition increases slightly at 100 Mrad, suggesting a slight increase of the local polar ordering in the copolymer. For films irradiated with 150 Mrad, the DSC data do not show any detectable features associated with the melting and polar order–disorder process.

We now analyze the evolution of the X-ray diffraction data with electron dose. These measurements were taken at 20°C, just below the temperature of the dielectric constant maximum (about 40°C) of irradiated films (Fig. 3). As expected, the unirradiated film (Fig. 3a) exhibits two closely-spaced peaks at 18.79° and 19.28°, corresponding to *d* spacings 4.72 and 4.59 Å, respectively. The one at 18.79° appears due to the presence of ferroelectric β-phase, which has an orthorhombic structure with (110) and (200) reflections nearly at the same position (pseudo-hexagonal at the plane perpendicular to the polymer chain direction). The one at 18.79° is from the 60° domain structure, which can be reduced or eliminated by drawing or high voltage poling [14]. Upon 30 Mrad irradiation, only one peak is observed at the lower angle, indicating the expansion of the crystal lattice due to the introduction of *trans*-gauche bonds as observed in FTIR data and hence, a reduction of ferroelectric ordering [15]. The finding here is

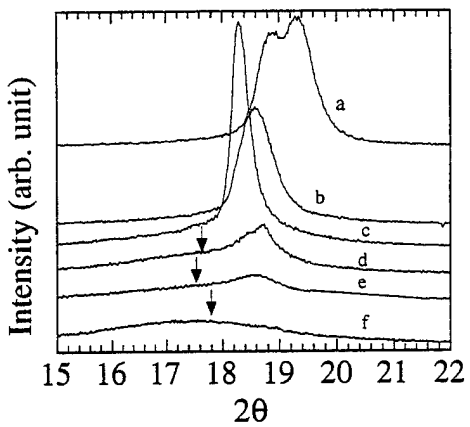

Fig. 3. The X-ray diffraction pattern of P(VDF–TrFE) 50/50 mol% copolymer films, (a) unirradiated, and irradiated at 120°C using (b) 30, (c) 60, (d) 80, (e) 100 and (f) 150 Mrad doses. The arrows indicate the position of the broad peak corresponding to the amorphous phase in the copolymer.

consistent with the polarization hysteresis measurement presented in Fig. 4 where the 30-Mrad-irradiated films exhibit hysteresis with a reduced remanent polarization and coercive field in comparison to unirradiated film.

Interestingly, after irradiation with 60 Mrad, the X-ray diffraction peak becomes sharper and more intense in comparison with unirradiated and 30-Mrad-irradiated films. The corresponding lattice spacing is equal to 4.84 Å, which is close to the d spacing of the paraelectric phase of this copolymer determined from the X-ray above the Curie temperature [16]. Correspondingly, a slim polarization hysteresis is observed (Fig. 4). The FTIR measurements conducted on the same films also do not show any change in structure even when the sample was cooled down to −25°C [15]. The results suggest that after the irradiation the broad dielectric constant peak temperature (T) does not correspond to the P–F phase change and macroscopically, the material is paraelectric-like even at temperatures below T. These results are very similar to those observed in relaxor ferroelectric ceramic and by drawing the analogy with those materials, the microstructure of irradiated P(VDF–TrFE) copolymer would consist of local micro-polar regions embedded in a non-polar matrix. The increased coupling among these micro-polar regions as the temperature is reduced results in the observed broad dielectric constant peak and freezing of the polar regions of V–F type. It should also be

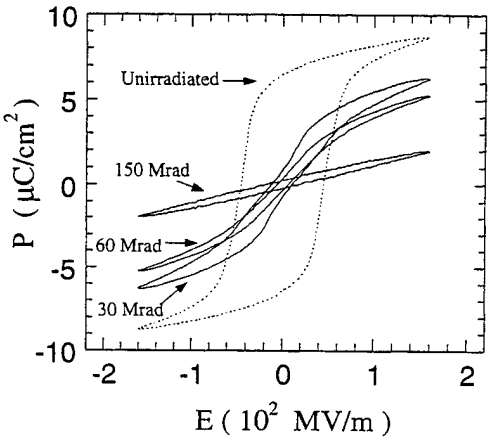

Fig. 4. Change in the polarization hysteresis loop with irradiation dose for P(VDF-TrFE) 50/50 mol% copolymer films irradiated at 120°C.

pointed out that although the sharpening of the X-ray peak implies that there is an increase in the coherent length for the X-ray diffraction, which is due to the disappearance of the ferroelectric ordering and hence, domain structure, the ordering of the crystal lattice is reduced and there is a significant conversion of the crystalline phase into amorphous phase as revealed by the broad melting peak and significant reduction in the enthalpy of the melting (reduced by half in the enthalpy at this dose).

As the dose is increased further, we observed a broadening of the X-ray peak as well as a significant contribution of the intensity from a very broad peak centered at $2\theta = 17.5°$, due to the amorphous phase. These results are consistent with the DSC and polarization data. However, in spite of significant broadening, the X-ray peak from the crystalline phase moves back towards the position of the original β-phase. This can be interpreted as a partial recovering to local trans bonds (polar ordering) from *trans-gauche* bonds at these dose levels. The same feature was also observed in the DSC data, where the entropy of F–P transition peak shows a slight increase after 100 Mrad irradiation. Above 100 Mrad irradiation, the diffraction data become totally diffuse, which indicates the disappearing of the crystalline phase. However, in contrast to X-ray and DSC results, the 150-Mrad-irradiated film still exhibits a V–F type dielectric constant maximum, indicating the existence of local polar-order regions and their coupling in an otherwise amorphous matrix.

All these results taken together give strong evidence that under high-energy electron irradiation, P(VDF–TrFE) 50/50 copolymer is transformed from a normal ferroelectric to a relaxor ferroelectric with the existence of local polar regions. From the fitting to the V–F law, it was found that f_0, which can be regarded as the relaxation frequency of local polar regions without much coupling with each other, increases with electron dose. At 30 Mrad, f_0 is at about 1 MHz while at 150 Mrad, it almost reaches 1 GHz. Such kind of increase of f_0 is consistent with the decrease of the micro-polar region size with electron dose. Assuming that f_0 is inversely proportional to the volume of micro-polar region, the result suggests that there is one order of magnitude reduction in the linear dimension of the micro-polar region when the dose is increased from 30 to 150 Mrad.

Acknowledgements

The authors are thankful to the Office of Naval Research (Grant no. N00014-97-1-0900) and National Science Foundation (Grant no. ECS-9710459) for providing the financial support to carry out this work.

References

[1] T.T. Wang, J.M. Herbert, A.M. Glass, The Applications of Piezoelectric Polymers, Blackie, London, 1988.
[2] T. Furukawa, Adv. Colloid Interface Sci. 71–72 (1997) 183.
[3] H. Wang, M. Zhang, L.E. Cross, O. Sykes, J. Appl. Phys. 74 (1993) 3394.
[4] Q.M. Zhang, V. Bharti, X. Zhao, Science 280 (1998) 2101.
[5] V. Bharti, X.-Z. Zhao, Q.M. Zhang, Mater. Res. Innovations 2 (1998) 57.
[6] Z.-Y. Cheng, V. Bharti, X. Zhao, S. Wang, T.-B. Xu, Q.M. Zhang, Intern. Symp. on Appl. of Ferroelectrics, Aug., Montreux, Switzerland, 1998.
[7] H. Vogel, Z. Phys. 22 (1921) 645.
[8] S. Fulcher, J. Am. Ceram. Soc. 8 (1925) 339.
[9] Richert, Blumen, Disorder Effects on Relaxational Processes, Springer-Verlag, Berlin, 1994.
[10] D. Viehland, S.J. Jang, E. Cross, J. Appl. Phys. 68 (1990) 2916.
[11] L.E. Cross, Ferroelectrics 151 (1994) 305.
[12] T. Yamade, T. Ueda, T. Kitayama, J. Appl. Phys. 52 (1981) 948.
[13] H. Poths, E. Wischerhuff, R. Zentel, A. Schonfeld, G. Honn, F. Kremer, Liq. Cryst. 18 (1995) 811.
[14] T. Davis, T. Furukawa, J. Lovinger, G. Broadhurst, Macromolecules 15 (1982) 329.
[15] T. Ramotowski, F. Tito, ONR Transducer Materials and Transducer Workshop, State College, USA, May 12–14, 1998.
[16] J. Lovinger, D. Davis, E. Cais, M. Kometani, Macromolecules 21 (1988) 78.

APPENDIX 29

Thickness dependence of ferroelectric polarization switching in poly(vinylidene fluoride–trifluoroethylene) spin cast films

Feng Xia, Haisheng Xu, Fei Fang, B. Razavi, Z.-Y. Cheng, Yu Lu, Baomin Xu, and Q. M. Zhang[a)]
Materials Research Laboratory, The Pennsylvania State University, University Park, Pennsylvania 16802

(Received 21 September 2000; accepted for publication 2 January 2001)

In poly(vinylidene fluoride–trifluoroethylene) copolymer spin cast films, it has been observed that the polarization switching time increases as the film thickness is reduced to below 1 μm. We will show that this change with film thickness can be divided into two thickness regimes, i.e., those above 120–150 nm and those below that thickness. For films thicker than 120–150 nm, the change in the switching behavior is due to interface effects that can be modeled by an effective interface layer with lower dielectric constant that is in series with the film. For films below 120–150 nm thickness, there is an additional and very large increase of the switching time with reduced film thickness. This additional effect is caused by the precipitous drop of the crystallinity in films at this thickness range. © *2001 American Institute of Physics.* [DOI: 10.1063/1.1351848]

Ferroelectric polymer films are attractive for a broad range of applications.[1–4] In these applications, the issues of how the functional properties change as the film thickness is reduced and what is responsible for these changes are of great interest and concern. In this letter, we investigate the ferroelectric switching behavior in poly(vinylidene fluoride-trifluoroethylene) [P(VDF–TrFE)] spin cast films. We will show that the variation in the polarization switching behavior with film thickness can be divided into two thickness regions, those above 120–150 nm and those below that thickness. For films thicker than 120–150 nm (referred to here as thin films), the change in the switching behavior can be understood by assuming an effective interface layer with lower dielectric constant, which is in series with the film. While for thinner films (referred to as ultrathin films), there exists an additional effect, i.e., the large reduction of the crystallinity in the film that causes a large increase in the switching time of the film.

Thin films of P(VDF–TrFE) 75/25 mol% copolymer were prepared by spin cast on platinum coated silicon substrate using dimethylformide (DMF) as the solvent. The films after spin cast were annealed at 135 °C to remove the residual solvent and to raise the crystallinity. The top electrode is thermally evaporated aluminum. Early experiment results have shown that for spin cast films thicker than 0.5 μm the ferroelectric behavior does not change with film thickness.[5,6] Therefore, we choose films at a thickness below about 0.5 μm for this study. The polarization switching experiment was carried out by applying a step voltage to the film and the induced current response of the film was measured. The difference in the induced currents between the positive step voltage and negative step voltage yields the current due to the polarization switching.[4,7] Integration of the current with time yields the switching polarization as shown in Fig. 1(a), where P_r is the remanent polarization. The switching time t_s is determined from the peak position of the derivative $dD/d\log(t)$ [Fig. 1(b)], where D is the surface charge density of the film.[7]

Figure 2(a) presents the switching time t_s versus the applied electric field E for films at different thicknesses. The data reveal that under a given field, the switching time increases as the film thickness is reduced. In contrast, the remanent polarization P_r (measured under 160 MV/m switching field) exhibits little change with thickness for thin film samples [Fig. 2(b)]. While for ultrathin films, a large drop in P_r is observed, which is caused by the large reduction in the crystallinity in the film, which will be discussed later. Figure 2(a) reveals several interesting features:

(1) t_s follows the relation:

$$t_s = t_\infty \exp(\alpha/E) \tag{1}$$

where α is the activation energy. This indicates that the polarization switching in the films studied is mainly controlled by the nucleation process, which is consistent with the early studies.[4,7–9]

(2) The activation energy α increases with reducing film thickness (i.e., the slope of $\ln(t_s)$ vs $1/E$ increases with reduced film thickness).

Following the approach by Merz, we plot α vs $1/d$, where d is the film thickness in Fig. 2(c) and it was found that for thin films studied, α can be written as,[4,10]

$$\alpha = \alpha_0(1+\beta/d), \tag{2}$$

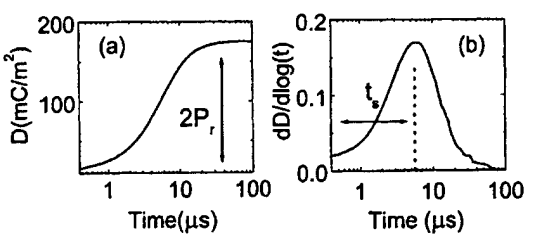

FIG. 1. (a) Switched polarization D and (b) the derivative of $dD/d\log(t)$ obtained from 200 nm thick film under a step field of 160 MV/m.

a)Author to whom correspondence should be addressed; electronic mail: qxzl@psu.edu

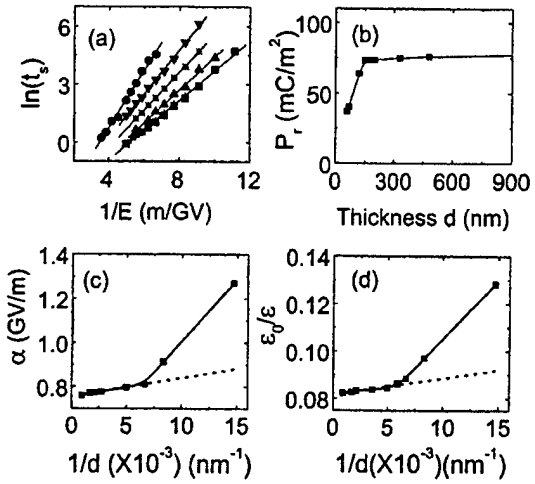

FIG. 2. (a) Switching time t_s vs electrical field E for the films with different thickness. From right to left; the thickness is: 600, 370, 200, 150, 120, and 68 nm, respectively. (b) P_r measured from the switching data under 160 MV/m step field vs film thickness. There is a precipitous drop of P_r at the film thickness about 100 nm. (c) Activation energy α vs $1/d$. Solid curves are drawn to guide eyes. The dashed line is the fitting of Eq. (2), which is extrapolated to the ultrathin film region. (d) The inverse of the measured dielectric permittivity $\varepsilon/\varepsilon_0$ vs $1/d$. The dashed line is the fitting to Eq. (5) and the solid curve is drawn to guide eyes.

where $\alpha_0 = 754\,\mathrm{MV/m}$ and $\beta = 1.126\times10^{-8}\,\mathrm{m}$. Here, α_0 corresponds to the activation energy of very thick films and the value obtained here is consistent with early experiment results.[10,11] The behavior observed in Eq. (2) can be interpreted as evidence of an interface layer which is electrically in series with the bulk of the film and thickness is directly proportional to β. On the other hand, for the ultrathin films α deviates from Eq. (2) and activation energy becomes very large as is evident from Fig. 2(c), which is due to the large reduction of the crystallinity in the film to be discussed later. Consequently, the switching time of ultrathin films becomes very high.

The effective thickness d_s and the effective dielectric constant ε_s of this interface layer at the thin film region can be estimated as the following. Because this interface layer is electrically in series with the bulk of the film, the total applied voltage V is divided between the two as, $V = V_f + V_s$, where V_f is the voltage drop across the bulk of the film which has a thickness d_f and dielectric permittivity ε_f, and V_s is the voltage drop across the interface layer. The charge continuity at the boundary between the two regions yields:

$$\frac{V}{V_f} = \frac{\varepsilon_f d_s}{\varepsilon_s d_f} + 1. \tag{3}$$

For the thin films, as will become evident later, there are two additional conditions: V_f is much larger than V_s, i.e., $(\varepsilon_f d_s/\varepsilon_s d_f) \ll 1$, and $d_f \gg d_s$. Therefore, Eq. (3) can be rewritten as

$$E_f = E\left(1 - \frac{\varepsilon_f d_s}{\varepsilon_s d}\right), \tag{4}$$

where E_f is the effective field on the bulk of the film. Comparing this with Eq. (2) leads to the relationship: $\beta = \varepsilon_f d_s/\varepsilon_s$

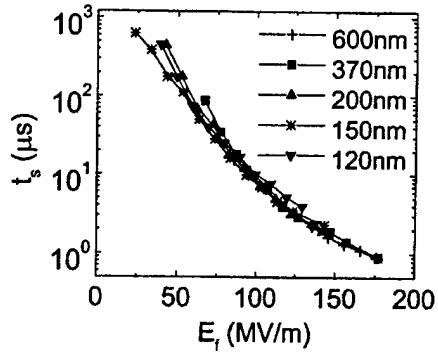

FIG. 3. t_s vs E_f for films of different thickness in the thin film region. Solid curves are drawn to guide eyes.

Making use of Eq. (4) and the β value obtained, the data in Fig. 2(a) can be replotted and indeed as presented in Fig. 3, t_s vs E_f does not vary with film thickness for the thin films studied, confirming that it is the interface effect that causes the change in the polarization switching behavior with film thickness in the thin film regime.

The existence of a low dielectric constant interface layer will also result in changes in the measured dielectric constant with film thickness d as

$$\frac{1}{\varepsilon} = \frac{1}{\varepsilon_f} + \frac{d_s}{d}\left(\frac{1}{\varepsilon_s} - \frac{1}{\varepsilon_f}\right). \tag{5}$$

As expected, for the thin films the measured dielectric constant fits Eq. (5) quite well as presented in Fig. 2(d), yielding $\varepsilon_f/\varepsilon_0 = 12.3$ and $d_s[(\varepsilon_0/\varepsilon_s - \varepsilon_0/\varepsilon_f)] = 6.9\times10^{-10}\,\mathrm{m}$, where ε_0 is the vacuum permittivity. For the ultrathin films there is an additional large drop of the dielectric constant with reduced film thickness, which, as has been pointed out, is caused by the large reduction of the crystallinity in the ultrathin films. Combining the results here with the β value obtained from the polarization switching, one can estimate both d_s and ε_s, which are $\varepsilon_s/\varepsilon_0 = 3$ and $d_s = 2.7\,\mathrm{nm}$.

The results presented indicate that there is an interface effect which causes the observed change of the switching behavior with thickness in the thin film region. The detailed mechanism responsible for the interface effect is not clear at present and the dielectric model presented is only a simplified picture. It should be mentioned that in recent studies in the switching behavior of ferroelectric thin films, a charge injection model was proposed to explain the observed interface effect.[12,13] The model may also be used here to explain the change of the switching behavior with thickness.

Two more experiments have been carried out to examine whether there are any significant changes in the ferroelectric and other properties in the bulk of the films, i.e., the interchain spacing, crystallinity and the ferroelectric transition temperature, which could also be responsible for the observed change in the polarization switching behavior. In bulk P(VDF–TrFE) copolymers, it has been observed that the switching time becomes longer with reduced TrFE content.[14] In the copolymer, the reduction in TrFE mol% raises the ferroelectric transition temperature and reduces the interchain spacing (increase the packing of the molecular chain).[7,15] Presented in Fig. 4(a) is the x-ray data taken from films in thickness from 50 to 470 nm, where the (110, 200)

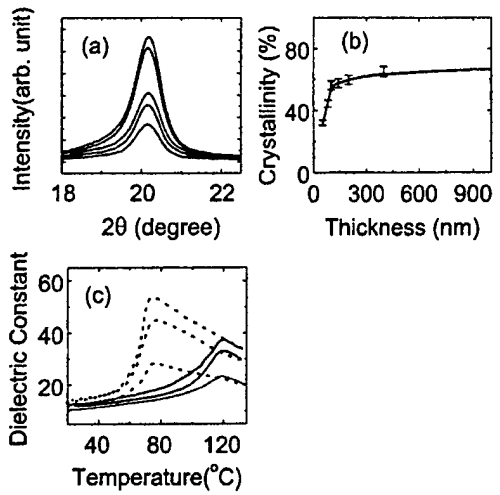

FIG. 4. (a) X-ray diffraction data measured near (110, 200) reflection from the copolymer films at different thickness. From top to bottom, the thickness is: 470, 310, 160, 80, and 50 nm. (b) The crystallinity deduced from the x-ray data (data are shown and solid line is drawn to guide eyes). (c) The measured dielectric constant at 1 kHz as a function of temperature for films with different thicknesses. Data taken from both heating (solid curves) and cooling (dashed curved) cycles are shown. From top to bottom, the thickness is: 2300, 250, and 100 nm.

reflection was measured and clearly, the (110, 200) peak remains at nearly the same position for all the films measured, indicating that the interchain spacing does not change with the film thickness. On the other hand, the fitting of the data (after subtracting the x-ray background from the substrate) shows that there is a large drop of crystallinity as the thickness of the film is reduced to the ultrathin film region [Fig. 4(b)].[16] This is consistent with the observed large drop of P_r in the ultrathin films [Fig. 2(b)]. The result suggests that the large increase of the switching time in the ultrathin film region is due to the loss of crystallinity in the films.

The dielectric constant versus temperature was also measured for these films to examine how the ferroelectric transition temperature changes with the film thickness. Figure 4(c) presents the typical data for films with several different thicknesses, where the data taken from both the heating and cooling cycles are shown, which provides information on the thermal hysteresis of the ferroelectric transition, which is an additional parameter reflecting the stability of the ferroelectric phase with respect to the paraelectric phase. As revealed by the data, for the films studied there is no significant variation of the ferroelectric transition peak with thickness. The thermal hysteresis is also nearly the same for the films measured. The results are consistent with early dielectric studies by Glatz-Reichenbach *et al.* and Tajits.[5,9]

In summary, these results suggest that the ferroelectric property does not change very much with thickness for the P(VDF–TrFE) films investigated here. The observed increase in the ferroelectric switching time with reducing film thickness in the thin film region is caused by the interface effect which can be modeled by a low dielectric layer in series with the bulk of the film, and for films investigated here, this layer has a thickness of about 2.7 nm and an effective dielectric constant of 3. For the ultrathin films, there is an additional effect that causes the further increase of the switching time, i.e., the large drop of the crystallinity in these films.

This work was supported in part by the NSF under Grant No. ECS-9710459.

[1] S. Bauer, J. Appl. Phys. **80**, 5531 (1996).
[2] R. Schellin, G. Hess, W. Kuehkel, G. M. Sessler, and E. Fukada, IEEE Trans. Electr. Insul. **27**, 867 (1992).
[3] N. Neumann, R. Kohler, and G. Hofmann, Ferroelectrics **171**, 225 (1995).
[4] M. E. Lines and A. M. Glass, *Principles and Applications of Ferroelectric and Related Materials* (Clarendon, Oxford, 1997).
[5] J. Glatz-Reichenbach, L. Jie, D. Schilling, E. Schreck, and K. Dransfeld, Ferroelectrics **109**, 309 (1990).
[6] K. Kimura and H. Ohigashi, Appl. Phys. Lett. **43**, 834 (1983).
[7] T. Furukawa, Phase Transitions **18**, 143 (1989).
[8] T. Furukawa and G. E. Johnson, Appl. Phys. Lett. **38**, 1027 (1981).
[9] Y. Tajitsu, Jpn. J. Appl. Phys., Part 1 **34**, 5419 (1995).
[10] W. J. Mertz, J. Appl. Phys. **27**, 938 (1956).
[11] K. Kimura and H. Ohigashi, Jpn. J. Appl. Phys., Part 1 **26**, 383 (1986).
[12] A. K. Tagantsev and I. A. Stolichnov, Appl. Phys. Lett. **74**, 1326 (1999).
[13] J. F. M. Cillessen, M. W. J. Prins, and R. M. Wolf, J. Appl. Phys. **81**, 2777 (1997).
[14] Y. Tajitsu, H. Ogura, A. Chiba, and T. Furukawaa, Jpn. J. Appl. Phys., Part 1 **26**, 554 (1987).
[15] A. G. Lovinger, T. Furukawa, G. T. Davis, and M. G. Broadhurst, Polymer **24**, 1225 (1983).
[16] Q. M. Zhang, H. S. Xu, F. Fang, Z.-Y. Cheng, F. Xia, and H. You, J. Appl. Phys. **89** (to be published).

APPENDIX 30

Critical thickness of crystallization and discontinuous change in ferroelectric behavior with thickness in ferroelectric polymer thin films

Q. M. Zhang,[a] Haisheng Xu, Fei Fang, Z.-Y. Cheng, and Feng Xia
Materials Research Laboratory and Department of Electrical Engineering, The Pennsylvania State University, University Park, Pennsylvania 16802

H. You
Argonne National Laboratory, Materials Science Division, 9700 South Cass Avenue, Argonne, Illinois 60439

(Received 25 September 2000; accepted for publication 4 December 2000)

We report on the observation of the critical thickness of crystallization of ferroelectric poly(vinylidene fluoride-trifluoroethylene) copolymer thin films, which were solution spun cast on platinum coated silicon wafer. The effect occurs at about 100 nm thickness, which is significantly above any currently known spatial dimensions of the polymer, so that for films at thickness below about 100 nm, the crystallization process is strongly hindered, resulting in a low crystallinity in these films. This low crystallinity leads to a large and discontinuous change of the dielectric constant and ferroelectric polarization in the films below the critical thickness. © *2001 American Institute of Physics.* [DOI: 10.1063/1.1344585]

I. INTRODUCTION

Polymer thin films have attracted a great deal of attention in recent years due to their emerging applications in electronics, photonics, and microsensors and actuators.[1–4] As the polymer film thickness is reduced, finite size effect where the system dimension approaches one of the intrinsic dimensions of the polymer will influence the structures of these films. Furthermore, it is expected that the surface and interface will play a significant role in the development of morphology and chain conformation of the films.[5–11] All of these will have a profound effect on the functional behavior of the polymer films. One of the interesting and important issues in predicting and understanding film structure and functional behavior is whether the properties of polymer films evolve gradually from bulk and what determines this evolution behavior.

Recently we investigated the ferroelectric behavior of poly(vinylidene fluoride-trifluoroethylene) [P(VDF-TrFE)] copolymer spin cast thin films. P(VDF-TrFE) copolymer is the best known and most widely used ferroelectric polymer,[12,13] which exhibits a typical polarization-electric field relationship as shown in Fig. 1(a). As a semicrystalline polymer, in which small crystallites are surrounded by amorphous regions, it is well-known that the ferroelectric responses such as the polarization are mainly from the crystalline phase. In bulk forms, experimental evidence has established that depending on the polymer processing conditions such as annealing temperature and time duration, the crystallinity, which is the volume content of the crystalline phase in the polymer, can be varied from very low (below 30%) to more than 80% for copolymer at compositions near 70/30 mol %.[14] In the copolymer thin films we will show that the crystallinity can also reach a relatively high value (>70%). However, as the film thickness is reduced, we observed a discontinuous change in the crystallization process at about 100 nm below which the crystallization is severely hindered and the crystallinity becomes very low. Corresponding to this critical thickness for the crystallization, we also observed discontinuous and marked changes in the functional properties such as the dielectric constant and ferroelectric hysteresis loop for films at thicknesses below about 100 nm.

II. EXPERIMENTS

P(VDF-TrFE) copolymers in the composition range from 50/50 to 80/20 mol % (the mol % ratio of VDF/TrFE) were chosen for this study because copolymers at those compositions are in the ferroelectric phase at room temperature when prepared using solution casting. In addition, extensive literature exists and hence, information on the structures, morphology, and ferroelectric and dielectric properties in the bulk copolymers in this composition range.[12–16] The copolymers were supplied by MSI Sensor, PA. The average molecular weight is about 200 000. The solvent used is dimethylformide (DMF) and solution concentrations ranging from 4 wet% to 12 wet% were used to produce spin cast films with different thicknesses, from 30 nm to more than 1 μm. Spin cast films were deposited on a platinum coated silicon wafer. Except otherwise specified, all the films used in the investigations were annealed after spin cast at 140 °C for 2 h under vacuum to remove the residual solvent and also to improve the crystallinity. The results from early studies have indicated that such a thermal treatment yields a thin film with relatively high crystallinity and ferroelectric properties near those in the bulk materials.[17] For the electric property measurement, the platinum on the silicon substrate was used as

[a]Electronic mail: qxz1@psu.edu

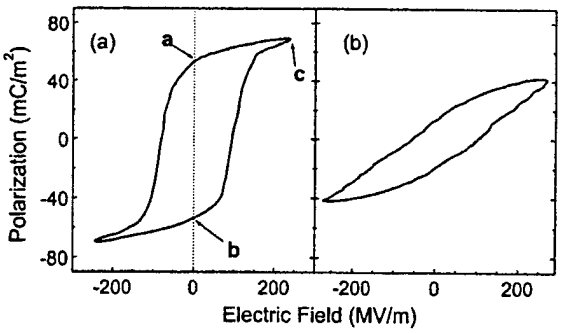

FIG. 1. The polarization hysteresis loops of P(VDF-TrFE) 75/25 mol% copolymer spin cast thin films on a platinum coated silicon wafer measured at 10 Hz: (a) 120 nm thick and (b) 75 nm thick.

the bottom electrode and aluminum electrodes of 2 mm diameter size, which were vacuum deposited on the top surface of the P(VDF-TrFE) copolymer films after the annealing treatment of the films, served as the top electrode.

III. RESULTS AND DISCUSSION

Figure 2(a) shows the dielectric constant measured at room temperature at 1 kHz as a function of film thickness for copolymer films of 50/50, 68/32, 75/25, and 80/20 mol%. The dielectric constants for films at a thickness near 1 μm (1000 nm) are nearly the same as those in the bulk. One

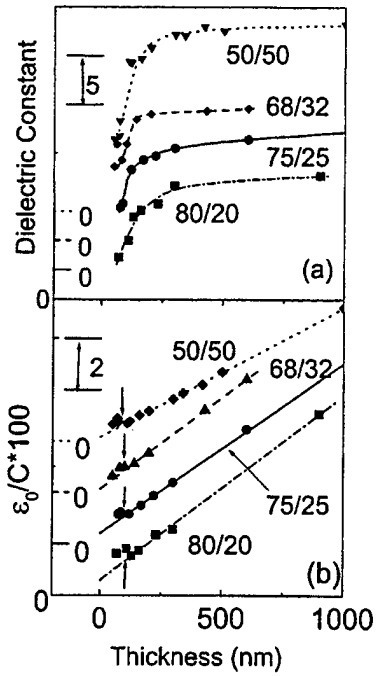

FIG. 2. (a) The dielectric constant measured at 1 kHz as a function of film thickness for copolymer films of 50/50, 68/32, 75/25, and 80/20. The zeros of the dielectric constant for films of 75/25, 68/32, and 50/50 copolymers are shifted as indicated in the figure. The curves are drawn to guide the eye. (b) The inverse of the capacitance of unit area ($1/C$) as a function of film thickness. The data points beyond thickness=1 μm are not shown in the figure. The solid and dashed lines are the fitting of Eq. (1) to the data points at the thickness above 100 nm. The arrows indicate the position of the discontinuous increase in $1/C$ which occurs near about 100 nm. The zeros for 75/25, 68/32, and 50/50 are shifted as indicated in the figure.

salient feature of the data is that as the film thickness is reduced, the dielectric constant exhibits a precipitous drop at a thickness near about 100 nm. The decrease of the dielectric constant in P(VDF-TrFE) copolymer thin films with reduced thickness has been observed in many earlier studies.[18,19] The phenomenon has been attributed in those studies to the existence of an equivalent interface layer of lower dielectric constant which is in series with the P(VDF-TrFE) dielectric film and has a dielectric constant of bulk material. From this model, the inverse of the capacitance of unit area ($1/C$) of the film can be expressed in terms of the dielectric constant of the interface layer K_s, the bulk K_b, and the thickness of the interface layer t_s,

$$\frac{\varepsilon_0}{C}=\frac{t}{K_b}+t_s\left(\frac{1}{K_s}-\frac{1}{K_b}\right), \tag{1}$$

where t is the total polymer film thickness and ε_0 is the vacuum dielectric permittivity ($=8.85\times10^{-12}$ F/m). By plotting ε_0/C versus t, Eq. (1) shows that there should be a nonzero interception point of ε_0/C at the zero film thickness, $t=0$, if there is a surface layer with a lower dielectric constant ($t_s\neq0$). Indeed, data from all four compositions shows such a nonzero interception point [Fig. 2(b)]. More interestingly, Fig. 2(b) also reveals that there is a discontinuous jump of the ε_0/C value at a thickness near 100 nm for all the films, indicating a large and discontinuous drop of the dielectric constant for films at thicknesses below 100 nm which is much beyond that accounted for by the surface layer effect.

In the P(VDF-TrFE) copolymer, the dielectric constant is closely related to the polymer structure such as the crystallinity in the polymer and crystalline orientation.[20–22] The data in Fig. 2 indicates that there exists a critical thickness near 100 nm in which large changes in structure or morphology in polymer thin films occur.

We first examined the scenario that a large reduction of the crystallinity in the films at thicknesses below 100 nm, is responsible for the observed dielectric behavior by carrying out an x-ray diffraction study on these films. The data for copolymer 68/32 mol% films is presented in Fig. 3(a) for selected thicknesses. The prominent x-ray peak observed in the figure is from the (200,110) reflection of the crystalline phase.[15] In addition to this sharp peak, there is a broad peak with a much lower intensity which is due to the amorphous phase in the films. In Fig. 3(a) we also illustrate the decomposition of the x-ray data into the crystalline peak and amorphous hola contribution.[14] The crystallinity can be estimated by comparing the area from the crystalline diffraction peak with the total diffraction area (crystalline plus amorphous phase) and the result is shown in Fig. 3(b). Indeed, we observed a large drop of crystallinity at the film thickness near 100 nm, suggesting that in films below 100 nm thickness, the crystallization process is strongly hindered.

In copolymer bulk single crystals, Ometo *et al.* have shown that the dielectric constant of the crystal also strongly depends on the crystal orientation.[20] Therefore a change in the average crystal orientation (with respect to the substrate) in the polymer films at thickness near 100 nm may also be a possible origin for the drop of the dielectric constant across

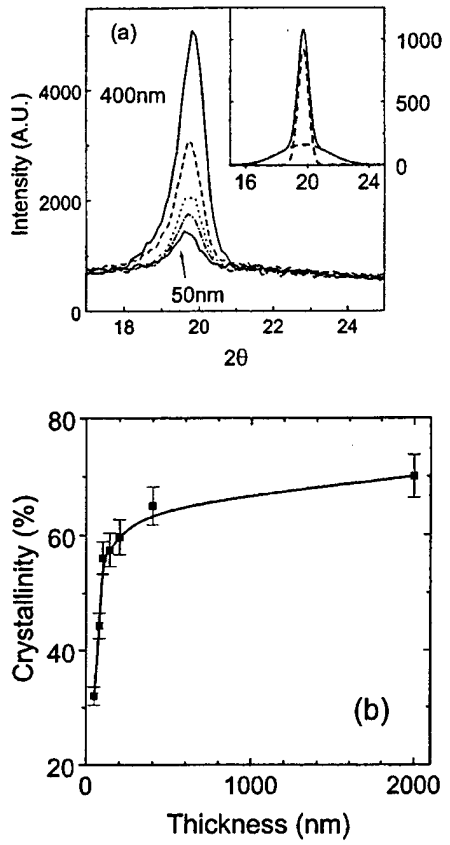

FIG. 3. (a) X-ray diffraction the copolymer films of 68/32 mol % at selected thickness: 400, 200, 140, 100, and 50 nm. The data was taken near the (200,110) reflection peak. The decomposition of the peak into the crystalline part and amorphous part is illustrated in the insert (from a 100 nm thick film). (b) The crystallinity as a function of the film thickness for 68/32 copolymer films. There is a large drop of the crystallinity at thickness near 100 nm. The curve is drawn to guide the eye.

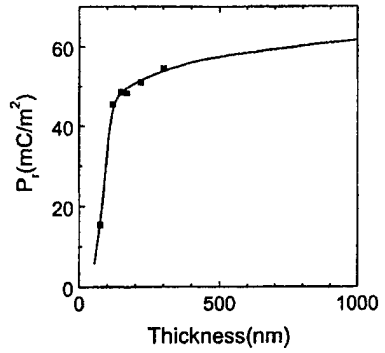

FIG. 4. The remanent polarization P_r as a function of the film thickness for 75/25 copolymer films. The curve is drawn to guide the eye and the data points at thickness larger than 1 μm are not shown.

that thickness. However, the measurement of the rocking curves of the (200,110) reflection which is sensitive to the change in the crystallite orientation in polymer films shows no change as the thickness is reduced from 200 to 50 nm (except the diffraction intensity),[23] indicating that there is no significant change in the average crystallite orientation with respect to the substrate in thin films when below 100 nm thickness.

To examine how the ferroelectric behavior changes across the critical thickness, we measured the remanent polarization P_r of these films as a function of film thickness since P_r is the most direct indicator of the ferroelectric properties and in bulk material it has been shown that there is a direct correlation between the crystallinity and P_r.[14,19] The data for thin films is shown in Fig. 4 for the copolymer of 75/25 mol %. The data was acquired using the polarization switching method which eliminates the contribution of conduction to the polarization measured and the maximum field of 160 MV/m was used in the measurement. In this method, two step voltages are applied, one changes the polarization from b to c and the other from a to c [Fig. 1(a)], and the difference in the polarization between the two yields is $2P_r$.[24] Apparently, the remanent polarization also exhibits a precipitous drop at the film thickness near 100 nm, a clear indication of a critical thickness below which the films exhibit a very weak ferroelectricity. In P(VDF-TrFE) thin films, the coercive field E_c increases as the film thickness is reduced. In order to take this into account, we also measured P_r for the 75 nm thick film under a field of 320 MV/m and found that P_r is still at about 17.5 mC/m^2. This marked change in the ferroelectric behavior of thin films near the critical thickness is illustrated in Fig. 1, where the polarization hysteresis loops measured for films of 120 nm (just above the critical thickness) and 75 nm (below the critical thickness) are compared.

All these results indicate that in spin cast P(VDF-TrFE) copolymer films on a platinum coated silicon substrate, there exists a threshold thickness below which the crystallization is hindered. Because of the close correlation between the crystallinity and the functional properties in copolymer films, there is a clear boundary in the film thickness below which the dielectric constant drops markedly and ferroelectric properties deteriorate. However, it is intriguing that this critical thickness occurs at 100 nm, which is far larger than any currently known relevant spatial dimensions of the polymer such as the radius of gyration R_g, which is about 15 nm, and the lamella thickness of crystallites in bulk P(VDF-TrFE) copolymer, which is about 20 nm. It is noted that in a recent study of the semicrystalline poly(di-n-hexyl silane) (PD6S), a critical thickness of 15 nm has been observed below which the crystallization is substantially hindered.[3] However, the critical thickness (~15 nm) is not far above the radius of gyration of the polymer chains (~10 nm) or the lamella thickness.

In several recent experiments, it has been observed that the chain diffusion rate in polymer thin films starts to deviate from the bulk value at about 100–150 nm, or about $10R_g$ from an interface.[7,25] This raises the issue of whether the observed phenomena here are caused by the kinetics of the crystallization process. In addition, it is also puzzling as to why the crystallites in ultrathin films do not grow to a higher crystallinity (for instance, the 50 nm film has a crystallinity of about 30%). We examined this by increasing the annealing time of the copolymer films and measured the change of the dielectric constant after a longer time annealing. In this experiment, copolymer films of 50/50 mol % were used because of their relatively high dielectric constant. The ratio of

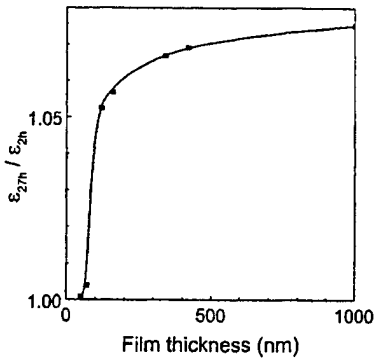

FIG. 5. The ratio of the dielectric constant of 55/50 copolymer films annealed at 140 °C for 27 h to that annealed for 2 h as a function of thickness. The curve is drawn to guide the eye.

the dielectric constant of thin films annealed at 140 °C for more than one day (27 h) to that after 2 h as a function of the film thickness is showing Fig. 5. Apparently, the prolonged annealing does not bring up the dielectric constant for films below 100 nm. In fact, for films at thicknesses below 100 nm, there is very little change in the dielectric constant with annealing time, while for films thicker than that, the dielectric constant increases with the annealing time, most probably caused by the increase of crystallinity. Again, the data indicates that the crystallization for films at thicknesses below 100 nm is strongly inhibited and that the critical thickness is not a consequence of kinetic effect.

One possible scenario for the low crystallinity in thin films below 100 nm could be due to the strain mismatch between neighboring crystallites which creates large amorphous regions in between them. In thin films, the crystallization process is controlled by the heterogeneous nucleation from the substrate which could lead to high nucleation density and also dictate the crystallite orientation, which could lead to orientation mismatch between neighboring crystallites and high elastic energy in thin films.[26] This may prevent the further growth of crystallites in very thin films.

ACKNOWLEDGMENTS

We thank S. Kumar, L. E. Cross, and R. Roy for stimulating discussions. The work at Penn State University was supported by the National Science Foundation under Grant No. ECS-97-10459. The work at Argonne National Laboratory was supported by the DOE under Contract No. W-31-109-ENG-38.

[1] S. Bauer, J. Appl. Phys. **80**, 5531 (1996).
[2] *Polymers for Electronic and Photonic Applications*, edited by C. P. Wong (Academic, 1993).
[3] C. W. Frank, V. Rao, M. M. Despotopoulou, R. F. W. Pease, W. D. Hinsberg, R. D. Miller, and J. F. Rabolt, Science **273**, 912 (1996).
[4] A. V. Bune, V. M. Fridkin, S. Ducharme, L. M. Blinov, S. P. Palto, A. V. Sorokin, S. G. Yudin, and A. Zlatkin, Nature (London) **391**, 874 (1998).
[5] R. L. Jones, S. Kumar, D. L. Ho, R. M. Briber, and T. P. Russell, Nature (London) **400**, 146 (1999).
[6] P. Calvert, Nature (London) **384**, 311 (1996).
[7] X. Zheng, M. H. Rafailovich, J. Sokolov, Y. Strzhemechny, S. A. Schwarz, B. B. Sauer, and M. Rubinstein, Phys. Rev. Lett. **79**, 241 (1997).
[8] W. L. Wu, J. H. van Zanten, and W. J. Orts, Macromolecules **28**, 771 (1995).
[9] S. K. Kumar, M. Vacatello, and D. Y. Yoon, J. Chem. Phys. **92**, 3827 (1990).
[10] G. ten Brinke, D. Ausserre, and G. Hadzlloannou, J. Chem. Phys. **89**, 4374 (1988).
[11] X. Q. Chen, H. Yamada, Y. Terai, T. Horiuchi, K. Matsushige, and P. Weiss, Thin Solid Films **353**, 259 (1999).
[12] A. J. Lovinger, Science **220**, 1115 (1983).
[13] T. Furukawa, Phase Transitions **18**, 143 (1989).
[14] Y. Tajitsu, H. Ogura, A. Chiba, and T. Furukawa, Jpn. J. Appl. Phys., Part 1 **26**, 554 (1987).
[15] A. J. Lovinger, T. Furukawa, G. T. Davis, and M. G. Broadhurst, Polymer **24**, 1225 (1983).
[16] M. C. Christie, J. Scheinbeim, and B. Newman, J. Polym. Sci., Part B: Polym. Phys. **35**, 2671 (1997).
[17] K. Kimura and H. Ohigashi, Appl. Phys. Lett. **43**, 834 (1983).
[18] J. Glatz-Reichenbach, L. Jie, D. Schilling, E. Schreck, and K. Dransfeld, Ferroelectrics **109**, 309 (1990).
[19] Y. Tajitsu, Jpn. J. Appl. Phys., Part 1 **34**, 5418 (1995).
[20] K. Omote, H. Ohigashi, and K. Koga, J. Appl. Phys. **81**, 2760 (1997).
[21] T. Furukawa, J. Aiba, and E. Fukada, J. Appl. Phys. **50**, 3615 (1979).
[22] S. Ikeda and M. Kutani, Jpn. J. Appl. Phys., Part 1 **30**, 3456 (1991).
[23] A. J. Bur, J. D. Barnes, and K. J. Wahistrand, J. Appl. Phys. **59**, 2345 (1986).
[24] Y. Tajitsu, M. Ishida, K. Ishida, H. Ohigashi, M. Date, and E. Fukada, Jpn. J. Appl. Phys., Part 2 **36**, L791 (1997).
[25] B. Frank, A. P. Gast, T. Russell, H. R. Brown, and C. Hawker, Macromolecules **29**, 6531 (1996).
[26] N. Bill, C. Magnet, J. M. Haudin, and D. Lefebvre, Colloid Polym. Sci. **272**, 633 (1994).

APPENDIX 31

Investigation of the electro-optic properties of electron-irradiated poly(vinylidene fluoride-trifluoroethylene) copolymer

Shizhuo Yin
Qiming Zhang
Kun-Wook Chung
Rui Yang
Zhongyang Cheng*
Yu Lu
Department of Electrical Engineering
The Pennsylvania State University
University Park, PA 16802

Abstract. The electro-optic property of electron-irradiated poly-(vinylidene fluoride-trifluoroethylene) (PVDF-TrFE) copolymer is presented. It is found that this special treated polymer not only has a giant electrostriction and relaxor ferroelectric behavior but also has a relatively good electro-optic effect. Thus, this copolymer may be a good candidate for making fast speed electro-optic modulators and switches, which are critical components for information optics. © *2000 Society of Photo-Optical Instrumentation Engineers.* [S0091-3286(00)01303-9]

Subject terms: electro-optic effect; electro-optic polymers; ferroelectric materials; electrostriction; wavelength-tunable filter; long period grating.

Paper IO-13 received Aug. 17, 1999; revised manuscript received Oct. 12, 1999; accepted for publication Oct. 13, 1999.

1 Introduction

Polymers have become widely used materials for information optics.[1,2] They can be used to store and modulate the light information. To reduce the required operating voltage, polymers with large electrostriction and electro-optic coefficients are expected. Recently, Zhang et al. reported giant electrostriction and relaxor ferroelectric behavior in electron-irradiated polymer(vinylidene fluoridetrifluoroethylene) (PVDF-TrFE) copolymer.[3] It was found that an electrostrictive response as large as 4% could be achieved. Note that, in general, ferroelectric materials that have large electrostrictive responses may also have good electro-optic effects. Since an electro-optic effect is very important for producing fast speed electro-optic modulators and switches, it is useful to investigate the electro-optic effect of this interesting electron-irradiated (PVDF-TrFE) copolymer. Our preliminary experiments show that this electron-irradiated (PVDF-TrFE) copolymer also has a good electro-optic coefficient with $r_{33} \approx 40$ pm/V.

Therefore, this electron-irradiated (PVDF-TrFE) copolymer may be a very good candidate for information optics.

2 Preparation of Electron-Irradiated (PVDF-TrFE) Copolymer

It is well known that PVDF consists of a repeat unit, CH_2CF_2, which carries a vacuum dipole moment (about 7×10^{-30} Cm) associated with positive hydrogen and negative fluorine atoms.[4] Since such dipoles are rigidly attached to main-chain carbons, their orientation (i.e., polarization direction) is directly controlled by the conformation and packing of molecules. Figure 1 shows the crystalline structure. An all-*trans* conformation induces the alignment of the CH_2CF_2 dipoles in the zigzag plane and perpendicular to the chain axis. Due to the existence of this dipole structure (i.e., dipoles are connected together), it is difficult to switch the polarization direction of the dipoles. Since the crystalline structure of PVDF copolymer can be substantially weakened by reducing the size of coherent polarization regions to a nanometer scale by high-energy radiation through introducing defects,[5] the (PVDF-TrFE) copolymer was radiated using high-energy electrons. It was found that under a proper high-energy electron irradiation, the large polarization hysteresis could be eliminated and a large electrostrictive strain (~4%) can be achieved.[3] To test the electro-optic properties of this polymer, an electron-irradiated (PVDF-TrFE) copolymer sample with following parameters were prepared:

1. composition of 70/30 ratio (70 mole % of VDF)
2. radiation dose of 7×10^5 J/Kg (= 70 Mrad) at 100°C.
3. thickness $t = 20\ \mu$m
4. length $L = 1$ mm
5. width $W = 5$ mm

3 Preliminary Experiments on the Electro-Optic Property of (PVDF-TrFE) Copolymer

Figure 2 shows the experimental setup used to measure the electro-optic coefficient r_{33} of this polymer, which is basi-

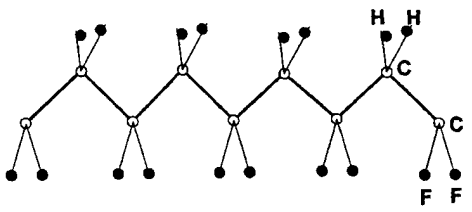

Fig. 1 Crystalline structure of PVDF.

*Material Research Lab.

 0091-3286/2000/$15.00

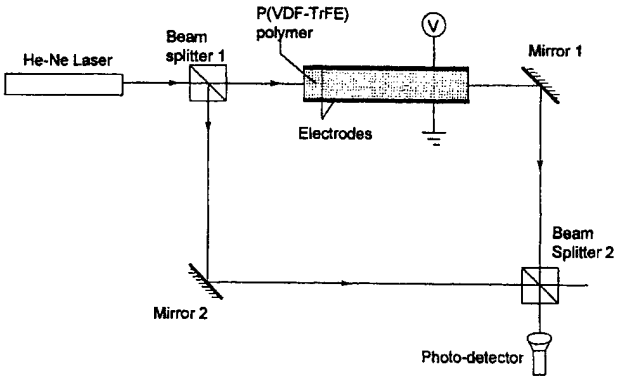

Fig. 2 Experimental setup used to measure the refractive index of P(VDF-TrFE) copolymer.

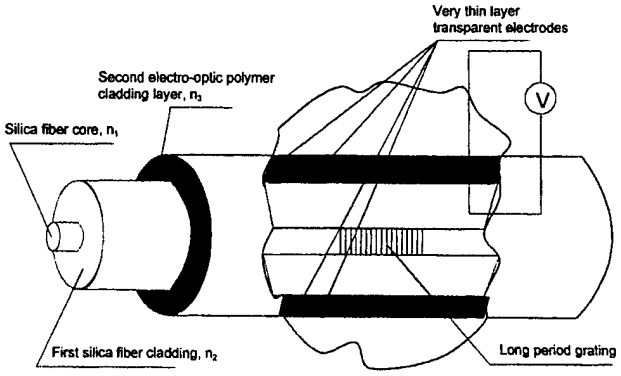

Fig. 3 Structure of fast-tuning-speed, wide-tuning-range filter using this P(VDF-TrFE) copolymer as the second cladding layer.

cally a Mach-Zehnder interferometer set-up. A He-Ne Laser with output wavelength $\lambda = 633$ nm was used as the light source. The prepared polymer sample, as described in Sec. 2, was inserted in one arm. To apply the electric field on the sample, two electrodes were formed by coating the silver conductive glue on the surfaces of the polymer, as shown in Fig. 2. The electric field is applied along the surface normal direction. The light is propagating along the surface direction. Since the polymer sample is very thin ($\sim 20\,\mu$m), a cylindrical lens is used to couple the light into the polymer sample from one side surface and another cylindrical lens of the same type is put on the other side of the sample so that a collimated output beam can be formed. This output beam interferes with the reference beam to form the interference pattern. A CCD camera connected to a computer is used to detect the interference pattern. When the voltage is applied on the polymer sample, the refractive index of the sample will be changed if the sample has the electro-optic effect. It was found that the interference fringe shifted one period (i.e., corresponding to one wavelength change in the optical path) when 300 V was applied to the sample. Substituting $n = 1.42$ (premeasured refractive index of the polymer), $v = 300$ V, wavelength $\lambda = 633$ nm, $t = 20\,\mu$m, and $L = 1$ mm into the following well-known equation,

$$r_{33} = \frac{2t\lambda}{n^3 vL}, \tag{1}$$

one can get $r_{33} = 40$ pm/V. Thus, the P(VDF-TrFE) copolymer also has a very good electro-optic effect. Note that, to ensure that the interference fringe shift is indeed caused by the refractive index change rather than by the geometric length change, the whole sample was clamped by sealing it with epoxy. After this sealing, no detectable geometric dimension change in the longitudinal direction (i.e., light passing through direction) was found. Another possible concern is that this refractive index change may come from the photoelastic effect rather than from the electro-optic effect. However, based on the previous investigation of the sample compression due to an electrostatic force,[6] the photoelastic effect will be much smaller than the electro-optic effect. Thus, the measured electro-optic coefficient is valid.

4 Potential Application of this Unique Electro-Optic Polymer to Fast Speed Wavelength-Tunable Filter

Long-period gratings (LPGs) were recently developed[7,8] that are photoinduced fiber devices that couple light from the core of a single-mode optical fiber into the fiber cladding at discrete wavelengths, producing one or more attenuation bands in the fiber transmission. The phase-matching condition of an LPG can be written as

$$\lambda_p = (n_{\text{core}}^{\text{eff}} - n_{\text{clad}}^{\text{eff}})\Lambda, \tag{2}$$

where λ_p is the wavelength of the pth-order resonance peak, Λ is the period of the grating, and $n_{\text{core}}^{\text{eff}}$ and $n_{\text{clad}}^{\text{eff}}$ are effective indices of core and cladding, respectively. Based on Eq. (2), the wavelength tuning range $\Delta\lambda$ for the LPG can be estimated as

$$\Delta\lambda = \frac{\Delta(n_{\text{core}}^{\text{eff}} - n_{\text{clad}}^{\text{eff}})}{n_{\text{core}}^{\text{eff}} - n_{\text{clad}}^{\text{eff}}}\lambda_p, \tag{3}$$

where $\Delta(n_{\text{core}}^{\text{eff}} - n_{\text{clad}}^{\text{eff}})$ is the difference of the effective refractive index change between the core and cladding. Since the effective refractive indices of core and cladding can be very close, i.e., $n_{\text{core}}^{\text{eff}} - n_{\text{clad}}^{\text{eff}} \ll 1$, a small change in the ambient refractive index can result in a large wavelength shift. Thus, a wide tuning range can be achieved. Most recently, a 50-nm tuning range filter was reported by thermally tuning the effective refractive index.[9] Although a wide tuning range was achieved, the tuning speed is still very limited due to the use of low-speed thermal tuning.

To substantially increase the tuning speed while maintaining the advantages of a wide tuning range and no medium transformation of the LPG, instead of using regular cladding and ambient materials, the tunable filter can consist of an LPG written inside the silica fiber core and this unique electro-optic polymer as cladding layer. Figure 3 shows the structure of the proposed filter. The filter consists of a fiber core and two cladding layers. The LPG is fabricated in the fiber core. The first cladding layer is a regular silica fiber cladding. The second cladding layer is the P(VDF-TrFE) electro-optic copolymer cladding layer. The refractive index of this layer can be tuned by applying the

voltage through the transparent electrodes, as marked in Fig. 3. Note that, this polymer is a very good candidate for this application due to the following reasons:

1. The electro-optic coefficient is relatively large so that relatively low driving voltage can be used.
2. The refractive index of this polymer is 1.42, which is very close to the silica cladding refractive index. Thus, a small change in the refractive index can result in a large change in the shift of wavelength response.

To minimize the influence of the electrodes, the thickness of the electrode layers will be very thin, $\ll 1$ μm. Thus, by controlling the voltage across the polymer cladding layer, the wavelength spectrum of the filter can be fast and widely tuned.

5 Conclusions

The electro-optic coefficient of electron-irradiated (PVDF-TrFE) copolymer was measured. We found that the electro-optic coefficient r_{33} is relatively good at about 40 pm/V. In particular, since this polymer also has a very large electrostrictive effect, the combination of two effects (i.e., electrostrictive and electro-optic effects) make it more flexible for producing electro-optic components such as fast-speed switching, tunable filters, which are critically needed in information optics.

References

1. L. A. Hornak, Ed., *Polymers for Lightwave and Integrated Optics*, Marcel Dekker, New York (1992).
2. H. S. Nalwa and S. Miyata, Eds., *Nonlinear Optics of Organic Molecules and Polymers*, CRC Press, New York (1997).
3. Q. M. Zhang, V. Bharti, and X. Zhao, "Giant electrostriction and relaxor ferroelectric behavior in electron-irradiated poly(vinylidene fluoride-trifluoroethylene) copolymer," *Science* **280**, 2101–2104 (1998).
4. T. Furukawa, "Ferroelectric properties of vinylidene fluoride copolymers," *Phase Transit.* **18**, 143–211 (1989).
5. S. J. Green, J. J. Stokes, M. J. Hostetler, J. J. Petron, and R. W. Murrey, "Three-dimensional monolayers: nanometer-sized electrodes of alkanethiolate-stabilized gold cluster molecules," *J. Phys. Chem. B* **101**, 2663–2668 (1997).
6. V. Bharti, X. Zhao, Q. Zhang, T. Romotowski, F. Tito, and R. Ting, "Ultrahigh field induced strain and polarization response in electron irradiated poly(vinylidene fluoride-trifluoroethylene) copolymer," *Mater. Res. Innovations* **2**, 57–63 (1998).
7. A. M. Vengsarkar, P. J. Lemaire, J. B. Judkins, B. Bhatia, T. Erdogan, and J. E. Sipe, "Long period fiber gratings as band-rejection filters," *J. Lightwave Technol.* **14**, 58–64 (1996).
8. H. J. Patrick, A. D. Kersey, and F. Bucholtz, "Analysis of the response of long period fiber gratings to external index of refraction," *J. Lightwave Technol.* **16**, 1601–1612 (1998).
9. A. Abramov, A. Hale, R. Windeler, and T. Strasser, "Widely tunable long-period fiber gratings," *Electron. Lett.* **35**, 81–82 (1999).

Shizhuo Yin is an assistant professor in the Electrical Engineering Department at The Pennsylvania State University, where he received his PhD degree in electrical engineering in 1993. His major research areas include optical material and optical instrumentation, electronic control and circuit design, optical metrology, analog and digital imaging processing, biomedical instrument development, and medical optics. He has published more than 50 refereed journal papers and was a co-chair of the SPIE international conference on Photorefractive Fibers. He has contributed chapters for six books. He was awarded the U.S. Army Young Investigator Award, and is a senior member of IEEE and a member of OSA and SPIE.

Biographies of the other authors not available.

APPENDIX 32

All-Polymer Electromechanical Systems Consisting of Electrostrictive Poly(vinylidene fluoride-trifluoroethylene) and Conductive Polyaniline

HAI-SHENG XU, Z.-Y. CHENG, VIVEK BHARTI, SHEXI WANG, Q. M. ZHANG

Materials Research Laboratory, The Pennsylvania State University, University Park, Pennsylvania 16802

Received 11 March 1999; accepted 17 July 1999

ABSTRACT: The low elastic modulus and the ability to withstand high strain without failure make the conducting polymer attractive for a wide range of acoustic applications based on high-strain electroactive polymers. In this article, we examine the electric and electromechanical performance of all-polymer electromechanical systems, fabricated by painting conductive polyaniline (PANI) doped with camphor sulfonic acid (HCSA) on both sides of electrostrictive Poly(vinylidene fluoride-trifluoroethylene) (P(VDF-TrFE)) copolymer films, and compare them with those from the same copolymers with gold electrodes. The all-polymer composite films are flexible, with strong coherent interfaces between the electrostrictive polymer layer and the conductive polymer layer. The electric performance such as dielectric properties and polarization hysteresis loops from P(VDF-TrFE)/PANI film is nearly identical to those of P(VDF-TrFE)/gold films in a wide temperature (from −50 to 120°C), and frequency range (from 1 Hz to 1 MHz). The all-polymer systems also show a similar or even larger electric field induced strain response than that of films with electrodes under identical measurement conditions. The results demonstrate that the polyaniline/HCSA is good candidate material as the electrodes for electroactive polymers. © 2000 John Wiley & Sons, Inc. J Appl Polym Sci 75: 945–951, 2000

Key words: electrostrictive polymer; conducting polymer; poly(vinylidene fluoride-trifluoroethylene) copolymer; polyaniline; all-polymer systems

INTRODUCTION

Polymers that exhibit a large strain response induced by electric fields have attracted a great deal of attention in recent years. These polymers include Polyvinylidene fluoride (PVDF) and its copolymer with trifluoroethylene, polyurethane, odd-numbered nylons, etc. Recently, we reported that electron-irradiated P(VDF-TrFE) copolymers exhibit an exceptionally high electrostrictive response,[1] which will have a great impact in transducer, sensor, and actuator technologies.[2] However, increased interest in using high strain electroactive polymeric materials for electroacoustic and electromechanical applications also raises the issue of new electrode materials to meet new requirements and to provide better performance. For instance, to achieve high acoustic transparency, very small acoustic impedance mismatching between the electrode and electrostrictive polymers is required. Because of a high elastic modulus compared with electrostrictive polymers, the commonly used metal electrodes, such as Au and Al, may impose mechanical clamping on the polymer, which can reduce the electric field induced strain level and the efficiency of the elec-

Correspondence to: H. S. Xu.

Contract grant sponsor: Office of Naval Research; contract grant number: N00014-98-1-0254.

Journal of Applied Polymer Science, Vol. 75, 945–951 (2000)

 CCC 0021-8995/00/070945-07

tromechanical transduction. In addition, in the newly developed electrostrictive P(VDF-TrFE) copolymer, a large transverse strain, more than 3%, can be achieved.[3] In general, at such a high strain level, thin metal electrodes will crack and cause failure in the devices. Hence, a new electrode material that can lower the clamping effect and withstand high strain is highly desirable. It is believed that a conducting polymer electrode will meet these requirements.[4,5] Due to the flexibility, low acoustic impedance, and elastic modulus of conductive polymer electrodes, such all-polymer electrostrictive systems may improve the performance of electromechanical polymer materials in acoustic and electromechanical applications.

For electroacoustic and electromechanical applications, in addition to the mechanical properties of the electrodes, the possible effect of conductive polymers on the electric and also electromechanical responses of the polymer systems should also be examined. For example, in many applications, a high electric power and high electric field will be delivered through polymer electrodes in electromechanical devices, and hence, the current density under high voltage of the conductive polymer electrode is of great concern. Furthermore, these polymer electrodes should be able to operate in a relatively wide temperature and frequency range.

As one of the most promising conductive polymers, Polyaniline (PANI) has been studied extensively in the past decade because of its many attractive features: the monomer is relatively inexpensive, the polymerization method is simple with high yield; and more importantly, PANI exhibits higher stability in air than other conducting polymers. After doping with functional protonic acid, such as camphor sulfonic acid (HCSA) and dodecylbenesulfonic acid (DBSA), the conductivity of polyaniline film can reach as high as 300 S/cm.[6,7] Moreover, functionally doped PANI can be dissolved in common solvents and processed in the conducting form directly, and therefore, requires no postprocessing chemical treatment. This is quite convenient for applications in electromechanical and microelectronic devices, especially in multilayer polymer devices. In addition, it has been shown that PANI doped with HCSA can carry a relatively high current density without failure.[8]

In this article, an all-polymer system, consisting of electrostrictive poly(vinylidene fluoride-trifluoroethylene) copolymer and polyaniline doped with HCSA and casting from *m*-cresol, was fabricated. In this system, a thin layer of about 1-μm thick soft conducting PANI/HCSA was coated onto opposing surfaces of P(VDF-TrFE) films to form a sandwich structure. The dielectric properties of this all-polymer system were characterized over a wide temperature and frequency range. The polarization and electric field induced strain were also evaluated. These results are compared with those of gold electroded films. The results demonstrate that the all-polymer films exhibit comparable dielectric properties to gold-electroded P(VDF-TrFE) films in a wide temperature (from -50 to 120°C) and frequency range (from 1 Hz to 1 MHz). In addition, the all-polymer films seem to show similar or even larger electric field induced strain responses than those from films with gold electrodes under identical measurement conditions.

EXPERIMENTAL

Sample Preparation

The P(VDF-TrFE) copolymer with different vinylidene content was from Solvay and Cie of Bruxelles, Belgium. In the present work, the content of vinylidene are 50 and 65% (mol percent), denoted as P(VDF-TrFE) 50/50 and P(VDF-TrFE) 65/35, respectively. The films were prepared by melt-pressing powder at 225°C and then slowly cooling it to room temperature. The final film thickness was about 30 μm. Two types of films were prepared for the investigation of irradiated films: unstretched and stretched films. For unstretched films, they were annealed at 140°C under vacuum for 24 h and then cooled down slowly to room temperature before the irradiation. For stretched films, films were uniaxially stretched at a temperature between 25–50°C with a stretching ratio of five times. The films were then annealed at 140°C under vacuum for 24 h and afterwards cooled down slowly to room temperature. The irradiation was carried out at either 95 or 120°C under nitrogen atmosphere by electrons at 3 MeV energy with different doses.

Polyaniline in salt form was prepared by chemical oxidation of aniline with ammonium persulphates oxidant in 1.5*M* HCl solution at about 0°C according to the ref. 9. An emeraldine base form (EB) of PANI was obtained by treating the salt form with 3% NH_4OH for 2 h. The EB powder was mixed with HCSA in the molar ratio of 0.5 HCSA per repeat unit of PANI. The mixture was ground

under a nitrogen atmosphere to a fine powder and then dissolve in *m*-cresol. The solution was treated in an ultrasonic bath and subsequently centrifuged. Minor insoluble solids were removed by decanting.

To prepare conductive polymer electrodes, the solution of PANI/HCSA was coated on both sides of the P(VDF-TrFE) film by either printing or stamping with a mask. The composite films were dried with an infrared lamp in the hood for 10 min to remove the solvent. The temperature was controlled below 50°C. The thickness of conductive polymer layer can be adjusted by varying the concentration of PANI/HCSA solution and coating times. The temperature must be controlled to below 50°C when the composite films are dried; otherwise, there will be some dissolving of P(VDF-TrFE) in the interface between the PANI layer and the P(VDF-TrFE) layer though the solvent, i.e., *m*-cresol, evaporates easily in the hood at a higher temperature. However, after irradiation at appropriate conditions, P(VDF-TrFE) copolymers become highly crosslinked, and will not be dissolved in any solvent. The composite films are soft and flexible.

Gold electroded P(VDF-TrFE) films were also prepared by sputting Au on opposing faces of the films. The thickness of the gold layer is about 500 Å. For conductivity measurement, freestanding PANI/HCSA films were obtained by casting the above-mentioned solution on a glass slide and dried on a hot plate at 50°C.

Measurement of Relevant Properties

The polarization hysteresis loops of these films were measured by a Sawyer Tower circuit[10] at the frequency of 1 and 10 Hz under different electric fields.

Dielectric properties of the P(VDF-TrFE) films with conductive polymer electrodes were characterized and compared with those of the P(VDF-TrFE) films with gold electrodes. The temperature dependence of dielectric properties was measured on DEA 2870 Dielectric Analyzer (TA Instruments Co., 30 Hz–100 kHz) in the temperature range from −50 to 130°C. The heating rate employed was 2°C/min. The frequency dependence of dielectric properties was measured using an HP 4192A Impedance Analyzer in the frequency range between 100 Hz and 13 MHz.

The electric field induced strain was characterized with bimorph-based strain sensors designed specially for polymer film strain measurement in our lab,[11] which consists of a piezoelectric bimorph-based cantilever dilatometer, a lock-in amplifier (Stanford Research System SR830 DSP), and a high voltage source (KEPCO-BOP 1000M).

RESULTS AND DISCUSSION

The so-prepared all-polymer systems have a sandwich structure of (PANI/HCSA)|P(VDF-TrFE)|(PANI/HCSA). The electrostrictive P(VDF-TrFE) copolymer acts as the functional layer and the green, semitransparent PANI/HCSA layer as electrodes. Different shapes of electrodes for different measurements can be prepared by coating conductive polymer with different masks.

The electrical conductivity was measured by the standard four-probe method on free-standing films casting from above-mentioned PANI/HCSA solution. The conductivity is about 250 S/cm. The current density was also measured on free-standing PANI/HCSA films, the limiting value is about 1500 A/cm^2. As will be shown in the following, the conductivity and current density of PANI/HCSA are appropriate for its intended use in the present research.

Polarization Hysteresis Loops and Field-Induced Strain Responses

The polarization hysteresis loop is one of the most important characteristics of ferroelectric materials, which reflects directly the microstructure of materials. The typical hysteresis loops for P(VDF-TrFE)/PANI and P(VDF-TrFE)/gold films are shown in Figure 1(a)–(b). Figure 1(a) is for P(VDF-TrFE) 65/35 unstretched films before any irradiation treatment, and the films have not been annealed at high temperature (hence, the polarization level is not very high). Figure 1(b) is for stretched 65/35 films irradiated at 120°C with 60 Mrad doses. The polarization loops measured from the conducting polymer electrode and gold electrode show a quite similar polarization loop. The coercive fields and the remnant polarization of P(VDF-TrFE) films with two different electrode systems measured at different electric fields also exhibit closed values. The similar results were observed for the polarization hysteresis loops measured at 10 Hz. The results indicate that electrically, the conductive polymer can sustain an electric field more than 120 MV/m (the voltage limit of the polarization measurement setup) with a similar performance as that of the gold elec-

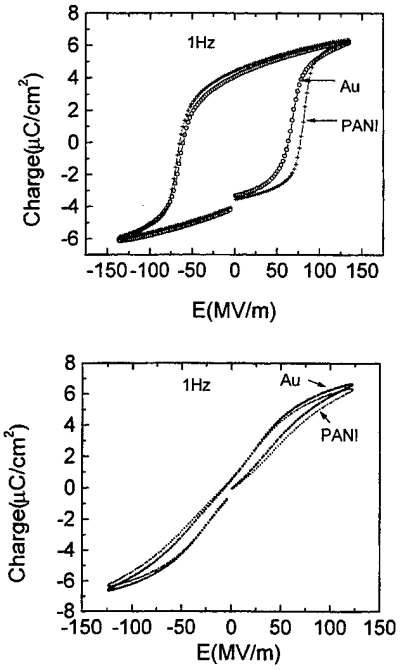

Figure 1 The polarization hysteresis loops of P(VDF-TrFE) 65/35 copolymer (a) unirradiated and unstretched films, (b) films of stretched and irradiated with 60 Mrad at 95°C.

trode. It is concluded that the all-polymer films show similar polarization properties as the gold electroded films under identical measurement condition.

The electrostrictive strains of the irradiated unstretched P(VDF-TrFE) 65/35 copolymers were measured and Figure 2 compares the longitudinal strain induced by external electric fields in the P(VDF-TrFE) films with conductive polymer electrodes and with gold electrodes, respectively. The data is presented as the amplitude of the induced strain vs. the amplitude of the applied field. Clearly, the two yield nearly identical results for applied electric fields up to 140 MV/m. Figure 2(b) shows the slim strain hysteresis loops measured from the two systems, which are also very similar to each other. It should be pointed out that although the data in Figure 2 shows that the longitudinal strains for the unstretched 65/35 films are nearly identical for films with different electrode materials; in some cases studied, the films with conducting polymer electrodes exhibit slightly higher strains than those from gold electroded films.

For electromechanical applications, in addition to the longitudinal response, the transverse strain response is also of great importance. Transverse strain responses are utilized in many areas, and because the applied electric field is perpendicular to the strain direction, it offers a convenient means in generating large actuation over large distances without the need to raise the driving voltage. Interestingly, for unstretched films, the transverse strains are quite small compared with longitudinal strains, and hence, they were not investigated here further. On the other hand, for stretched films, it was found that a large transverse strain can be achieved along the stretching direction. Figure 3 illustrates the electric field induced transverse strains of stretched (PVDF-TrFE) 65/35 films measured along the stretching direction and the comparison between the films with PANI and with gold electrodes. These films were irradiated with 60 and 70 Mrad doses at 95°C. The transverse strain measured from PANI electroded films is higher than that from gold electroded films. Part of the reasons for this difference could be due to the reduced mechanical clamping from the electrodes. In addition, due to the match of the acoustic impedance

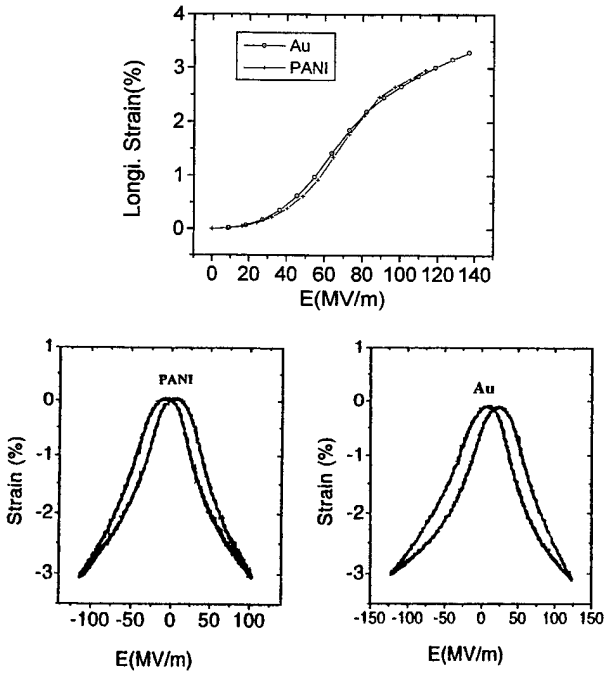

Figure 2 Comparison of the longitudinal electric field induced response of P(VDF-TrFE) films (65/35, unstretched and irradiated at 60 Mrad, 120°C) with a conductive polymer electrode and a gold electrode. (a) The amplitude of longitudinal strain as a function of the amplitude of applied electric field; (b) strain hysteresis loops.

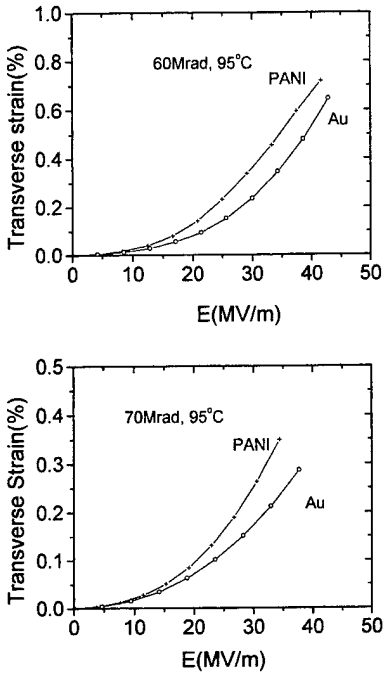

Figure 3 Transverse strain responses induced by electric fields of stretched irradiated P(VDF-TrFE) 65/35 films with a conductive polymer electrode and a gold electrode: (a) irradiated with 60 Mrad at 95°C, and (b) 70 Mrad at 95°C.

of the conductive polymer electrode with that of the electrostrictive polymers, all-polymer systems may improve the performance of electrostrictive polymer systems in acoustic and ultrasonic applications.

For the polymer films investigated, the transverse strain responses are smaller than longitudinal strain responses.

Dielectric Properties

The results presented show that the conductive polymer studied here is suitable for the electrodes on electroactive polymers. To probe the properties further, it is necessary to carry out a study over a broad temperature and frequency range. For example, in our early study of conductive polypyrrole electrode–polyurethane system, it was found that at temperatures above 40°C there is a large increase in the measured dielectric loss from the system due to the dehydration phenomena in the conductive polypyrrole.[12] Thus, the dielectric properties of the polymer systems are characterized in a broad temperature and frequency range.

Temperature dependence of the dielectric constant and dielectric loss measured at 100 kHz for the electron irradiated P(VDF-TrFE) 50/50 copolymer films (unstretched and irradiated with 30 Mrad at 120°C) with conductive polymer electrodes are shown in Figure 4, which are nearly the same as the dielectric properties of the same copolymer with gold electrodes shown in the same figure. This demonstrates that the polymer electrode developed here works well in the temperature range at least from −50 to +120°C, which is more than enough for most applications using the P(VDF-TrFE) copolymers. Although Figure 4 presents the data measured at 100 kHz, the data obtained at other frequencies also show the similar results (from 30 Hz to 100 kHz). The drop of the dielectric constant of gold electroded films at high temperatures (~ 125°C) is due to the melt of the sample. It is interesting to note that after the high-temperature dielectric measurement, the gold electroded films deformed while the films with conductive polymer electrodes were intact, which could be caused by a large difference in thermal expansion between the gold electrodes and P(VDF-TrFE) films.

The temperature range investigated covers the main transitions of irradiated P(VDF-TrFE) copolymers, i.e., the glass transition (at about −25°C) in the amorphous and the melting process (about 120°C) in the crystal phase. This indicates that the conductive PANI/HCSA electrodes function well, and do not have the problem as encountered in the conductive polypyrrole electrode.[11] In addition, the method of preparing polymer electrodes in the present work is simple and takes a little time.

The frequency dependence of the dielectric constant and loss of P(VDF-TrFE) 50/50 copolymer films with different electrodes and measured at room temperature is shown in Figure 5. It is

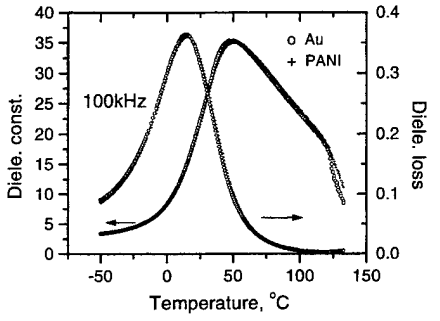

Figure 4 Temperature dependence of the dielectric constant and dielectric loss of PANI electroded and gold electroded irradiated P(VDF-TrFE) 50/50 copolymer unstretched film irradiated with 30 Mrad at 120°C.

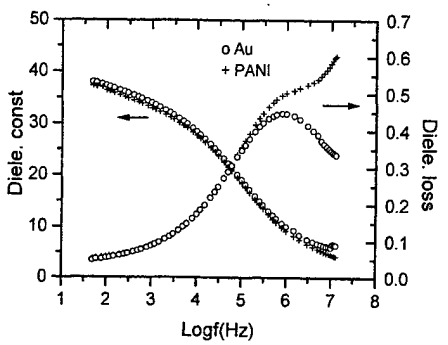

Figure 5 Comparison of frequency dependence of the dielectric constant and dielectric loss of conductive polymer electroded and gold electroded P(VDF-TrFE) 650/35 copolymer film (stretched and irradiated with 60 Mrad at 95°C).

observed that the two systems show very similar dielectric properties over a wide frequency range. The dielectric loss is nearly identical in frequencies from 100 Hz to 300 kHz, and the dielectric constant exhibits nearly the same value in frequencies from 100 Hz to 2 MHz. When the frequency is higher than 300 kHz, the dielectric loss of P(VDF-TrFE) film with conductive polymer electrodes starts increasing and becomes higher than that measured from the film with gold electrodes. The dielectric constant of PANI electroded film is lower than that of gold electroded film above 2 MHz.

The increase of the dielectric loss at high frequencies is due to the higher resistivity of the conductive polymer electrodes compared with gold electrodes. Using a model of a resistor in series with a P(VDF-TrFE) capacitor that has the complex dielectric constant as those from the P(VDF-TrFE)/gold electrode system, the loss data of the P(VDF-TrFE)/PANI system can be reproduced very well, as shown in Figure 6. Here, the resistor in the model has a frequency independent resistance of 1 kΩ, indicating that at weak fields, the resistivity of the conductive polymer used here is not frequency dependent in the frequency range examined (up to 10 MHz). In addition, the resistance value of 1 kΩ is very close to what is expected from that determined using the conductivity and dimensions of the conductive polymer electrodes. The consistence between the measured and model results indicate that the dielectric behaviors of P(VDF-TrFE) film itself with the conductive PANI electrode are the same as those with the gold electrode. That is, the conductive polymer electrode does not change the P(VDF-TrFE) films. Thus, there is no fundamental limitation in using the conductive polymer electrodes for P(VDF-TrFE) copolymers for electromechanical and electroacoustic applications. The main issue to be addressed is how to reduce the resistance of the conductive polymer electrodes, which may be solved by increasing the conductivity or the thickness of the conductive polymer electrode.

CONCLUSIONS

All-polymer electromechanical systems were fabricated with electrostrictive poly(vinylidene fluoride-trifluoroethylene) copolymer and conductive polyaniline doped with camphor sulfonic acid. The P(VDF-TrFE)/PANI composite films are soft and flexible with strong coherent interfaces between an electrostrictive polymer layer and a conductive polymer layer. These all-polymer systems exhibit similar dielectric properties as those from P(VDF-TrFE) films with the gold electrode in a wide temperature (from −50 to 120°) and frequency range (from 100 Hz to 1 MHz). The P(VDF-TrFE)/PANI and P(VDF-TrFE)/gold also exhibit similar polarization hysteresis loops. Moreover, in many cases, the all-polymer systems show a larger electric field-induced strain response than that of films with gold electrodes under identical measurement conditions. The experimental results suggest that as far as the P(VDF-TrFE) film itself is concerned, the conductive PANI electrodes function in a very similar manner as that of the gold electrodes. Most of the

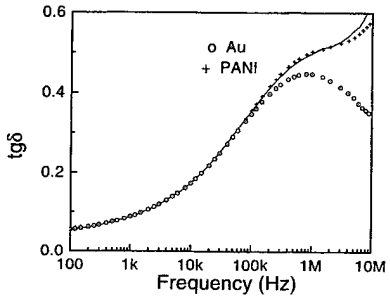

Figure 6 Simulation of frequency dependence of dielectric loss for the data from the film with a conductive polymer electrode. The solid curve is from the simulation and the pluses are the experimental data from the film with conductive polymer electrode. There is close agreement between the simulation and the data. The open circles are the data from the gold electroded film.

observed differences between the two systems can be accounted for by the difference in the electric resistance and elastic modulus between the two different electrodes.

This work was supported by the Office of Naval Research through Grant No: N00014-98-1-0254. The authors wish to thank Dr. K. Wynne of the Office of Naval Research and Prof. MacDiarmid at University of Pennsylvania for the stimulating discussions.

REFERENCES

1. Zhang, Q. M.; Bharti, V.; Zhao, X. Science 1998, 280, 2101.
2. Herbert, J. M. Ferroelectric Transducers and Sensors; Gordon and Breach Science Publishers: New York, 1982.
3. Cheng, Z.-Y.; Xu, T.-B.; Bharti, V.; Wang, S. X.; Zhang, Q. M. Appl Phys Lett 1998, 74, 1901.
4. Ueno, T.; Arntz, H.; Flesch, S.; Bargon, J. J Macromol Sci 1988, A25, 1557.
5. Tezuka, Y.; Aoki, K.; Shinozaki, K. Synth Met 1989, 30, 369.
6. Cao, Y.; Smith, P.; Heeger, A. J. Synth Met 1992, 48, 91.
7. Cao, Y.; Treacy, G. M.; Smith, P.; Heeger, A. J. Appl Lett 1992, 60, 2711.
8. Xu, H.; Cheng, Z.-Y.; Zhang, Q. M.; Wan, P. C.; MacDiarmid, A. G. J Polym Sci Part B Phys Ed, 1999, 37, 2845.
9. Cao, Y.; Andreatta, A.; Heeger, A. J.; Smith, P. Polymer 1989, 30, 2305.
10. Sinna, J. K. Rev Sci Instrum 1965, 42, 696.
11. Su, J.; Moses, P.; Zhang, Q. M. Rev Sci Instrum 1998, 69, 2480.
12. Su, J.; Zhang, Q. M.; Wang, P.-C.; MacDiarmid, A. G.; Wynne, K. J. Polym Adv Technol 1998, 9, 317.

APPENDIX 33

Ferroelectric and electromechanical properties of poly(vinylidene-fluoride–trifluoroethylene–chlorotrifluoroethylene) terpolymer

Haisheng Xu, Z.-Y. Cheng, Dana Olson, T. Mai, and Q. M. Zhang[a)]
Materials Research Laboratory, The Pennsylvania State University, University Park, Pennsylvania 16802

G. Kavarnos
EG&G, Inc., Groton, Connecticut 06340

(Received 6 December 2000; accepted for publication 31 January 2001)

This letter reports the ferroelectric and electromechanical properties of a class of ferroelectric polymer, poly(vinylidene-fluoride–trifluoroethylene–chlorotrifluoroethylene) terpolymer, which exhibits a slim polarization hysteresis loop and a high electrostrictive strain at room temperature. The dielectric and polarization behaviors of this terpolymer are typical of the ferroelectric relaxor. The x-ray and Fourier transform infrared results reveal that the random incorporation of bulky chlorotrifluoroethylene (CTFE) ter-monomers into polymer chains causes disordering of the ferroelectric phase. Furthermore, CTFE also acts as random defect fields which randomize the inter- and intrachain polar coupling, resulting in the observed ferroelectric relaxor behavior. © *2001 American Institute of Physics.* [DOI: 10.1063/1.1358847]

Polymers with large electromechanical responses are attractive for a broad range of applications. Among them, the poly(vinylidene-fluoride–trifluoroethylene) [P(VDF–TrFE)] copolymers are especially interesting because of their relatively high piezoelectric response and thermal and chemical stability.[1–3] Recently, it has been observed that with a proper high-energy electron irradiation treatment, P(VDF–TrFE) copolymers at compositions near 65/35 mol % exhibit a high electrostrictive strain and improved electromechanical coupling factors (electromechanical conversion efficiency).[4–7] In addition, the modified copolymers possess a relatively high-room-temperature dielectric constant and exhibit many features typical of ferroelectric relaxors.[4–7] These results demonstrate that the properties of P(VDF–TrFE)-based polymers can be modified and improved markedly by the introduction of "defect" structures. In this letter, we report on the electromechanical and ferroelectric properties of another polymer based on the concept of the defect structure modification of the P(VDF–TrFE) polymer system, poly(vinylidene-fluoride–trifluoroethylene–chlorotrifluoroethylene) terpolymer [P(VDF–TrFE–CTFE)]. It will be shown that the introduction of "bulky" CTFE into the P(VDF–TrFE) copolymer converts the normal ferroelectric P(VDF–TrFE) into a ferroelectric relaxor with high electrostrictive strain.

P(VDF–TrFE–CTFE) terpolymer was synthesized using the bulk polymerization method. The VDF/TrFE ratio was evaluated from the ^{19}F NMR spectrum; the CTFE mol % was determined by element analysis. To facilitate the discussion and comparison with the P(VDF–TrFE) copolymer, the composition of the terpolymer is labeled as VDF_x–$TrFE_{1-x}$–$CTFE_y$, where the mole ratio of VDF/TrFE is $x/1-x$ and the y is the mol % of CTFE in the terpolymer. In this investigation, terpolymers in the composition range from $x=60\%$ to 80% and $y=4\%$ to 13% were synthesized and evaluated. Among them, the terpolymer of 65/35/10 exhibits the highest electrostrictive strain with very little polarization hysteresis at room temperature. Accordingly, the properties of the terpolymer 65/35/10 are chosen to be the subject of this letter.

The polymer films were prepared using the solution cast method by first dissolving P(VDF–TrFE–CTFE) terpolymer in dimethyl formamide (DMF). The films were subsequently annealed at a temperature between 100 and 120 °C for 6 h to improve the crystallinity. Gold electrodes were sputtered on the two surfaces of the films for the electric measurement and the typical film thickness is about 20 μm. The thickness of films used in the Fourier transform infrared (FTIR) study is below 5 μm. The strain along the thickness direction (longitudinal strain S_3) was measured using a piezobimorph-based sensor.[8] The Sawyer–Tower technique was used to characterize the polarization response in the films.

As the bulky and less polar termonomer CTFE is randomly introduced into P(VDF–TrFE) normal ferroelectric crystals, it is expected that the ferroelectric transition will be broadened, and that the ferroelectric–paraelectric (FP) transition temperature will be lowered. Indeed, as shown in Figs. 1(a) and 1(b), those features have been observed in the dielectric data for the terpolymer 65/35/10. There are three main features in the dielectric data of the polymer due to the addition of CTFE: (1) the original FP transition peak of the 65/35 copolymer is moved to room temperature; (2) the peak becomes much broader and its position shifts progressively with frequency towards higher temperature; (3) there is no thermal hysteresis in the dielectric data, i.e., the broad dielectric peak stays at the same temperature when measured in the heating and cooling cycles [Fig. 1(b)]. In contrast, the copolymer shows thermal hysteresis in the dielectric data. In addition, the relationship between the measuring frequency f and the dielectric peak temperature T_m follows quite well the Vogel–Folcher (VF) law, as shown in the inset of Fig. 1(a),[9]

$$f=f_0 \exp\left[\frac{-U}{k(T_m-T_f)}\right],$$

where U is a constant and k is the Boltzmann constant, T_f

a)Electronic mail: qxz1@psu.edu

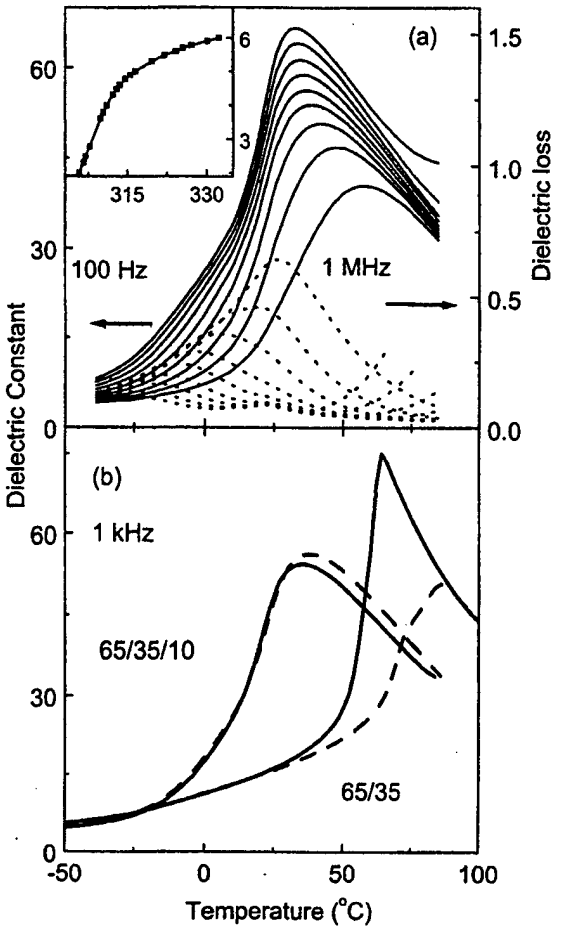

FIG. 1. Terpolymer P(VDF–TrFE–CTFE) 65/35/10. (a) Dielectric constant (solid curves) and dielectric loss (dashed curves) as a function of temperature at frequencies (from top to bottom for the dielectric constant and for the dielectric loss from bottom to top): 100, 300, 1, 3, 10, 30 kHz, 0.1, 0.3, and 1 MHz. (b) Dielectric constant at 1 kHz of the 65/35/10 terpolymer and 65/35 copolymer for both heating (dashed curves) and cooling (solid curves) cycles measured at room temperature.

can be regarded as the freezing temperature, corresponding to the peak temperature of the static dielectric constant (~0 Hz frequency), and the prefactor f_0 is the upper-frequency limit of the system, corresponding to the dipolar response when there is no coupling between the dipolar units in the system. The fitting yields $U=8.2$ meV, $f_0=15.4$ MHz, and $T_f=298.3$ K(25.15 °C). The results here are quite similar to those observed in the irradiated P(VDF–TrFE) copolymer.[4,6] It should also be noted that the terpolymer possesses a high-room-temperature dielectric constant (~60 at 1 kHz).

Figure 2(a) presents the polarization hysteresis loops measured at room temperature and −40 °C (233 K). Analogous to the irradiated copolymers, the terpolymer exhibits a slim polarization loop at room temperature, and as the temperature is lowered, both the remanent polarization and coercive field increase. All these features are remarkably reminiscent of ferroelectric relaxor behavior and the results suggest that the introduction of CTFE into P(VDF–TrFE) copolymers convert the normal ferroelectric P(VDF–TrFE) copolymer into a material closely resembling the ferroelectric relaxor.[10]

The terpolymer also exhibits a high-field-induced longitudinal strain S (~4% under 150 MV/m), as shown in Fig.

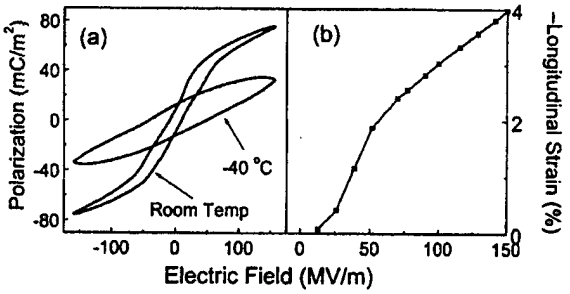

FIG. 2. Terpolymer P(VDF–TrFE–CTFE) 65/35/10. (a) Polarization hysteresis loops measured at room temperature (20 °C) and −40 °C and 10 Hz. (b) Longitudinal strain as a function of the driving field amplitude measured at room temperature and 10 Hz (dots are data and the solid line is drawn to guide the eyes).

2(b), which was measured at room temperature and 10 Hz. Combining the strain data with the measured elastic modulus $Y=0.4$ GPa yields a relatively high-elastic-energy density and the volumetric elastic-energy density $YS^2/2$ is 0.32 MJ/m^3.[4] For the copolymer, the corresponding strain is 0.15% and the volumetric elastic energy density is 0.0045 MJ/m^3.[5]

At this point, it is worthwhile to examine in more detail the effect of randomly introducing the termonomer CTFE or chlorine into the polymer chain and into the crystal. In comparison with the hydrogen and fluorine atoms, which have van der Waals (vdW) radii of 1.2 and 1.35 Å, respectively, chlorine has a much larger vdW radius of 1.8 Å. As a result, when considering the steric effects on the intrachain energies, the addition of chlorine to the polymer chain should favor the formation of transbond (T) rather than gauche (G) conformations. In the gauche conformation, substitution of chlorine in the polymer chain produces unfavorable 1, 4 steric repulsions between chlorine and fluorine atoms that can only be relieved by bond rotations to all-transconformations.[11] However, in order to accommodate the larger chlorine atom and relieve steric congestion, the interchain spacing in the crystalline phase in the terpolymers can expand and thereby favor energetically transgauche (TG) conformations in the neighboring chain segments. The delicate balance between those effects appears to leave room for incorporation of a certain number of gauche bonds. Indeed, computations on molecular models of terpolymers provide evidence of lattice expansion when CTFE termonomer units are substituted for TrFE monomers.[12] In addition, these calculations demonstrate that substitution of chlorine in the polymer chains raises the inter- and intrachain energies of $TGT\bar{G}$ forms to a greater extent than those of $T_3GT_3\bar{G}$ and all-trans forms because of steric repulsions. Consequently, the formation of the T_3G conformation appears more likely in the terpolymer.[12] Those features are supported by the x-ray and FTIR studies described below. Furthermore, the random incorporation of CTFE into the VDF–TrFE chain would be expected to produce random fields to frustrate the ferroelectric (polar) coupling, both inter- and intrachain, which will destabilize the polar ordering, resulting in relaxor ferroelectric behavior.

In Fig. 3(a), we present the room-temperature x-ray data collected near the angular position of the (200, 110) reflection of the P(VDF–TrFE) copolymer. The change of the

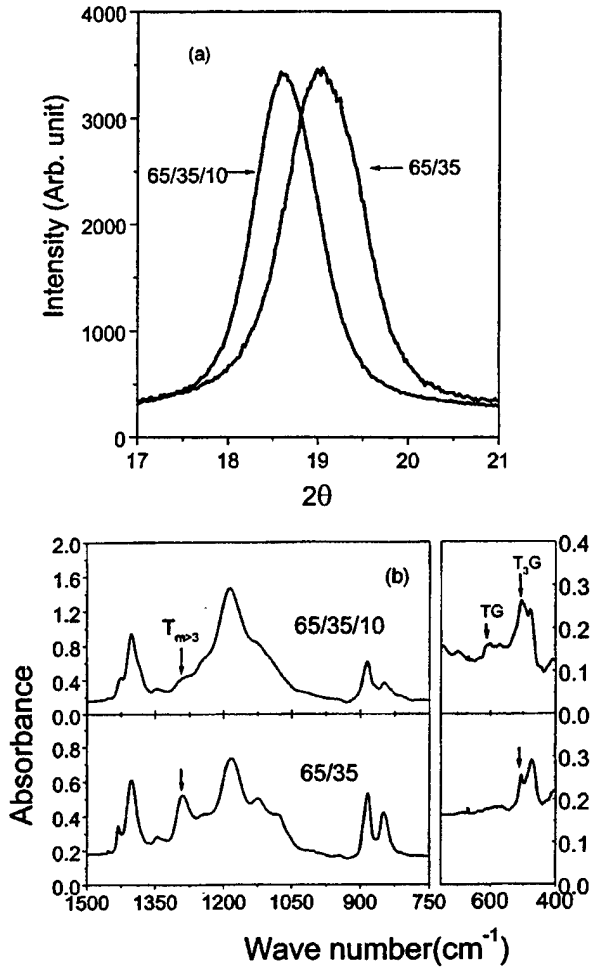

FIG. 3. (a) Comparison of the x-ray diffractions at 2θ angle near the (200, 110) reflection, which shows the expansion of the interchain spacing due to the incorporation of CTFE into the crystalline phase (the x-ray wavelength is 1.54 Å). (b) Comparison of the FTIR data between the terpolymer and copolymer which shows the reduction of the absorbance for $T_{m>3}$ and increase of the absorbance for the T_3G conformation in the terpolymer. Both x-ray and FTIR data were taken at room temperature.

crystallinity due to the introduction of CTFE can be estimated from the area of the crystalline diffraction peak and amorphous hola.[13] For the copolymer, the crystallinity is 75% while for the terpolymer here, it is reduced to 56%. For the 65/35 mol % copolymer, the interchain spacing from the (110, 200) reflection is 4.6 Å, while with 10 mol % CTFE, this spacing is increased to 4.8 Å, close to the interchain spacing of the paraelectric phase. Concomitantly with this shift in the x-ray peak position, the peak width is reduced, indicating an increase in the coherent x-ray diffraction length. This phenomenon is common to all the ferroelectric materials, where in the normal ferroelectric phase the x-ray peak width is limited by the ferroelectric domain size, which is normally much smaller than the crystallite size. The ferroelectric domains disappear in the nonferroelectric phase and the coherent x-ray diffraction length is mainly determined by the crystallite size.[14] This is consistent with the dielectric and polarization data presented in Figs. 1 and 2, indicating that there is no long-range polar ordering in the 65/35/10 terpolymer. However, unlike the paraelectric phase of copolymers, which is predominately all-transconformation,[15] the molecular conformation of 65/35/10 terpolymer is mainly $T_3GT_3\bar{G}$, as revealed by the FTIR data recorded at room temperature [Fig. 3(b)]. In this analysis, the method by Osaki and Ishida was used to calculate the fraction F_i of each chain conformation:

$$F_i=\frac{A_i}{A_{\mathrm{I}}+A_{\mathrm{II}}+A_{\mathrm{III}}},$$

where $i=$I, II, and III, and A_{I}, A_{II}, and A_{III} are the absorbencies of the chain conformations with all-trans ($T_{m>3}$, absorbance peak at 1285 cm^{-1}), $T_3GT_3\bar{G}$ (peak at 510 cm^{-1}), and $TGT\bar{G}$ (peak at 610 cm^{-1}), respectively.[16,17] For the copolymer, the fraction of three conformations are 75% ($T_{m>3}$), 18% ($T_3GT_3\bar{G}$), and 7% ($TGT\bar{G}$), while for the terpolymer the values change to 34% ($T_{m>3}$), 61% ($T_3GT_3\bar{G}$), and 5% ($TGT\bar{G}$).

This work was supported by DARPA under Contract No. N00173-99-C-2003 and ONR under Grant No. N00014-00-1-0623.

[1] *The Applications of the Ferroelectric Polymers*, edited by T. T. Wang, J. M. Herbert, and A. M. Glass (Blackie, Chapman and Hall, New York, 1988).
[2] *Medical Applications of Piezoelectric Polymers*, edited by P. M. Galletti, D. E. De Rossi, and A. S. De Reggi (Gorden and Breach Science, New York, 1988).
[3] *Ferroelectric Polymers*, edited by H. S. Nalwa (Dekker, New York, 1995).
[4] Q. M. Zhang, V. Bharti, and X. Zhao, Science **280**, 2101 (1998).
[5] Q. M. Zhang, Z. Cheng, V. Bharti, T. Xu, H. S. Xu, T. Mai, and S. Gross, Proc. SPIE **3987**, 34 (2000).
[6] Q. M. Zhang, Z. Y. Cheng, and V. Bharti, Appl. Phys. A: Mater. Sci. Process. **70**, 307 (2000).
[7] V. Bharti and Q. M. Zhang, Phys. Rev. B (in press).
[8] J. Su, P. Moses, and Q. M. Zhang, Rev. Sci. Instrum. **69**, 2480 (1998).
[9] H. Vogel, Z. Phys. **22**, 645 (1921); G. S. Fulcher, J. Am. Ceram. Soc. **8**, 339 (1925).
[10] L. E. Cross, Ferroelectrics **151**, 305 (1994).
[11] G. J. Kavarnos and R. W. Holman, Polymer **35**, 5586 (1994); R. W. Holman and G. J. Kavarnos, *ibid.* **37**, 1697 (1996).
[12] G. J. Kavarnos (unpublished).
[13] V. Bharti, H. S. Xu, G. Shanthi, Q. M. Zhang, and K. Liang, J. Appl. Phys. **87**, 452 (2000).
[14] G. T. Davis, T. Furukawa, A. J. Lovinger, and M. Broadhurst, Macromolecules **15**, 329 (1982).
[15] K. Tashiro, K. Takano, M. Kobayashi, Y. Chatani, and H. Tadokoro, Ferroelectrics **57**, 297 (1984).
[16] S. Osaki and Y. Ishida, J. Polym. Sci., Polym. Phys. Ed. **13**, 1071 (1975).
[17] H. S. Xu, G. Shanthi, V. Bharti, and Q. M. Zhang, Macromolecules **33**, 4125 (2000).

TRANSDUCER STUDIES

Composite Structures

APPENDIX 34

5.24
Piezoelectro Composites

KENJI UCHINO
Pennsylvania State University, University Park, PA, USA

5.24.1 INTRODUCTION 523

5.24.2 CONNECTIVITY 523

5.24.3 COMPOSITE EFFECTS 524
5.24.3.1 Sum Effects 524
5.24.3.2 Combination Effects 525
5.24.3.3 Product Effects 525

5.24.4 PZT–POLYMER COMPOSITES 526
5.24.4.1 Piezoelectric Composite Materials 526
5.24.4.2 Principle of PZT–Polymer Composites 527
5.24.4.3 Theoretical Models for 0-3 Composites 529
5.24.4.4 Advanced PZT–Polymer Composites 530

5.24.5 PZT COMPOSITE DAMPERS 531

5.24.6 REFERENCES 532

5.24.1 INTRODUCTION

Composite materials sometimes exhibit improved properties and/or new functions compared with single-phase materials. We will consider the principles of composite effects and their typical applications in this chapter, taking particularly piezocomposites as typical examples, which composed of a piezoelectric ceramic and polymer are promising materials because of their excellent tailorable properties. The geometry for two-phase composites can be classified according to the connectivity of each phase (1, 2, or 3 dimensionally) into 10 structures: 0-0, 0-1, 0-2, 0-3, 1-1, 1-2, 1-3, 2-2, 2-3, and 3-3. In particular, a 1-3 piezocomposite, or PZT(lead zirconate titanate)-rod/polymer-matrix composite, is considered most useful. The advantages of this composite are high coupling factors, low acoustic impedance, good matching to water or human tissue, mechanical flexibility, broad bandwidth in combination with a low mechanical quality factor, and the possibility of making undiced arrays by simply patterning the electrodes. The acoustic match to tissue or water (1.5 Mrayls) of the typical piezoceramics (20–30 Mrayls) is significantly improved when it is incorporated into such a composite structure, that is, by replacing some of the dense and stiff ceramic with a less dense, more pliant polymer. Piezoelectric composite materials are especially useful for underwater sonar and medical diagnostic ultrasonic transducer applications.

Another type of composite comprised of a magnetostrictive ceramic and a piezoelectric ceramic produces an intriguing product effect, the magnetoelectric effect, in which an electric field is produced in the material in response to an applied magnetic field.

5.24.2 CONNECTIVITY

Newnham *et al.* (1978) introduced the concept of "connectivity" for classifying the various PZT–polymer composite structures. When con-

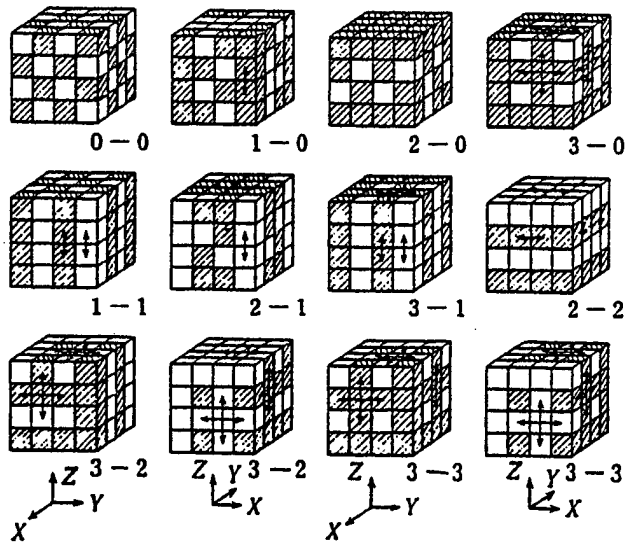

Figure 1 Classification of two-phase composites with respect to connectivity (after Newnham *et al.*, 1978).

sidering a two-phase composite, the connectivity of each phase is identified; e.g., if a phase is self-connected in all x, y, and z directions, it is called "3"; if a phase is self-connected only in the z direction, it is called "1." A diphasic composite is identified with this notation with two numbers m–n, where m stands for the connectivity of an active phase (such as PZT) and n for an inactive phase (such as a polymer). In general, there are 10 types of diphasic composites: 0-0, 1-0, 2-0, . . ., 3-2, 3-3, as illustrated in Figure 1.

A 0-0 composite, for example, is depicted as two alternating hatched and unhatched cubes, while a 1-0 composite has Phase 1 connected along the z direction. A 1-3 composite has a structure in which PZT rods (one-dimensionally connected) are arranged in a three-dimensionally connected polymer matrix, and in a 3-1 composite, a honeycomb-shaped PZT contains the one-dimensionally connected polymer phase. A 2-2 composite indicates a structure in which ceramic and polymer sheets are stacked alternately, and a 3-3 composite is composed of a jungle-gym-like PZT frame embedded in a three-dimensionally connecting polymer.

5.24.3 COMPOSITE EFFECTS

There are three types of composite effects (Figure 2): the *sum effect*, the *combination effect*, and the *product effect*.

5.24.3.1 Sum Effects

Let us discuss a composite function in a diphasic system to convert an input X to an output Y. Assuming Y_1 and Y_2 are the outputs from Phases 1 and 2, respectively, the output Y^* of a composite of Phases 1 and 2 could be an intermediate value between Y_1 and Y_2. Figure 2(a) shows the Y^* variation with volume fraction of Phase 2 for a case of $Y_1 > Y_2$. The variation may exhibit a concave or a convex shape, but the averaged value in a composite does not exceed Y_1 nor is it less than Y_2. This effect is called a *sum effect*.

An example is a fishing rod, i.e., a lightweight/tough material, where carbon fibers are mixed in a polymer matrix (between 3-1 and 3-0). The density of a composite should be an average value with respect to volume fraction, if no chemical reaction occurs at the interface between the carbon fibers and the polymer, following the linear trend depicted in Figure 2(a). A dramatic enhancement in the mechanical strength of the rod is achieved by adding carbon fibers in a special orientation, i.e., along a rod (showing a convex relation as depicted in Figure 2(a)).

Another interesting example is an NTC–PTC (negative temperature coefficient–positive temperature coefficient of resistivity) material (Uchino, 1986). V_2O_3 powders are mixed in epoxy with a relatively high packing rate (3-3), as illustrated in Figure 3. Since V_2O_3 exhibits a semiconductor–metal phase transition at 160 K, a drastic resistivity change is observed with increasing temperature. A further increase in temperature results in a larger thermal expansion for epoxy than for the ceramic, leading to a separation of each particle and the structure becomes a 0-3 composite. The V_2O_3 particle separation increases the resistivity significantly at around 100 °C. Thus, the conductivity of this composite is rather high only over

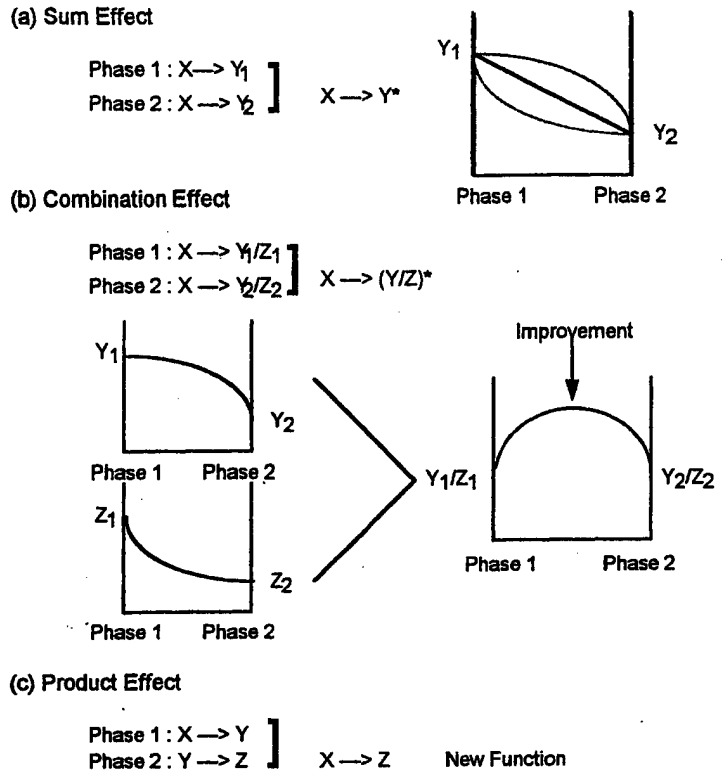

Figure 2 Composite effects: sum, combination, and product effect.

a limited temperature range (around -100 to 100 °C), which is sometimes called the *conductivity window*.

5.24.3.2 Combination Effects

In certain cases, the average value of the output, Y^*, of a composite does exceed Y_1 and Y_2. This enhanced output refers to an effect Y/Z which depends on two parameters Y and Z. Suppose that Y and Z follow convex and concave type sum effects, respectively, as illustrated in Figure 2(b), the combination value Y/Z will exhibit a maximum at an intermediate ratio of phases. This is called a *combination effect*.

Certain piezoelectric ceramic–polymer composites exhibit a combination property of g (the *piezoelectric voltage constant*) which is provided by d/ε (d = piezoelectric strain constant and ε = permittivity). The details of these materials will be described in the next section.

5.24.3.3 Product Effects

When Phase 1 exhibits an output Y with an input X, and Phase 2 exhibits an output Z with an input Y, we can expect for the composite an output Z with an input X. A completely new function is created for the composite structure, called a *product effect*.

Philips developed a *magnetoelectric material* based on this concept (Uchino, 1986). This material is composed of magnetostrictive $CoFe_2O_4$ and piezoelectric $BaTiO_3$ mixed and sintered together. Figure 4 shows a micrograph of a transverse section of a unidirectionally solidified rod of the materials with an excess of TiO_2 (1.5 wt.%). Four finned spinel dendrites are observed in cells (x100). Figure 5 shows the magnetic field dependence of the magnetoelectric effect in an arbitrary unit measured at room temperature. When a magnetic field is applied to this composite, cobalt ferrite generates magnetostriction, which is transferred to barium titanate as stress, finally leading to the generation of a charge/voltage via the piezoelectric effect in $BaTiO_3$.

Since the magnetoelectric effect in a single-phase material such as Cr_2O_3 can be observed only at a very low temperature (liquid helium temperature), observation of this effect at room temperature is really a breakthrough. Inexpensive sensors for monitoring magnetic field at room temperature or at elevated temperature can be produced from these composite materials.

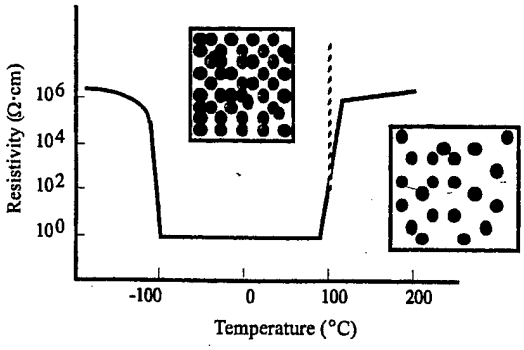

Figure 3 NTC–PTC effect observed in a V_2O_3–epoxy composite (after Uchino, 1986).

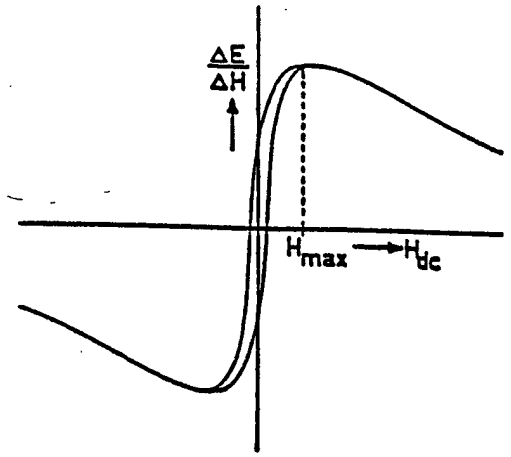

Figure 5 Magnetic field dependence of the magnetoelectric effect in a $CoFe_2O_4$–$BaTiO_3$ composite (arbitrary unit measured at room temperature).

5.24.4 PZT–POLYMER COMPOSITES

5.24.4.1 Piezoelectric Composite Materials

Polymer piezoelectric materials such as PVDF (polyvinylidene difluoride) are very suitable for sensor applications. However, because of its small piezoelectric *d* constants and very small elastic stiffness, PVDF cannot be used by itself in fabricating actuators or high-power transducers. PZT–polymer composites, however, play a key role in the design of transducers, for applications such as sonar, which have both actuator and sensor functions (Uchino *et al.*, 1982).

The representative data for several composite piezoelectric materials are listed in Table 1 (Uchino *et al.*, 1982), with data for some single-phase piezoelectric polymer and PZT materials. The piezoelectric *d* constant of PVDF, which indicates the strain per unit electric field (actuator applications!), is 1/10 smaller than that of PZT, however, because of its small dielectric constant, the piezoelectric *g* constant of PVDF, which indicates the voltage per unit stress (sensor applications!), is 10 times larger than that of PZT. PZT–polymer composites exhibit a wide range of piezoelectric response, but in general *d* is slightly smaller than PZT and *g* is slightly smaller than PVDF. Thus, particularly for underwater transducers, which

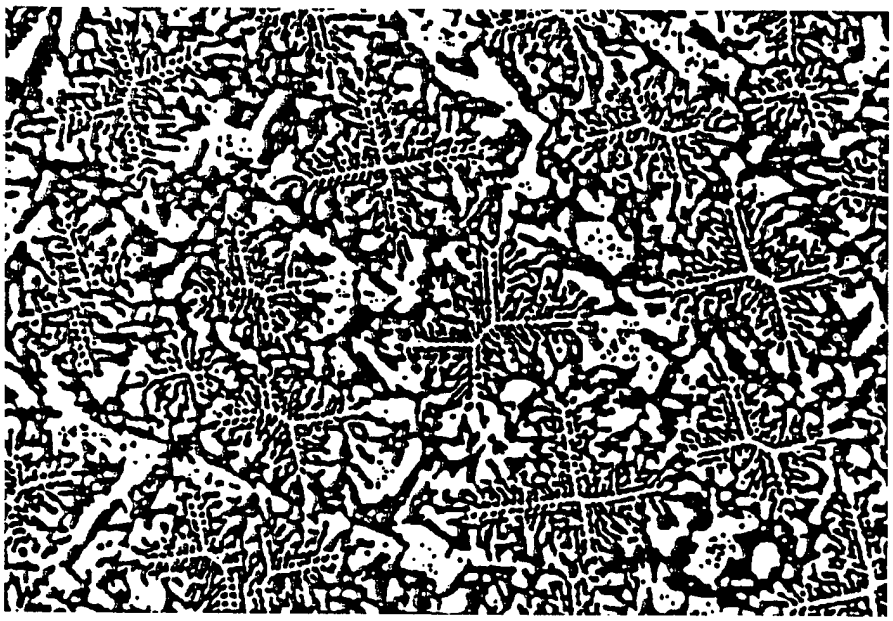

Figure 4 Micrograph of a transverse section of a unidirectionally solidified rod of mixture of magnetostrictive $CoFe_2O_4$ and piezoelectric $BaTiO_3$, with an excess of TiO_2 (1.5 wt.%) (after Uchino, 1986).

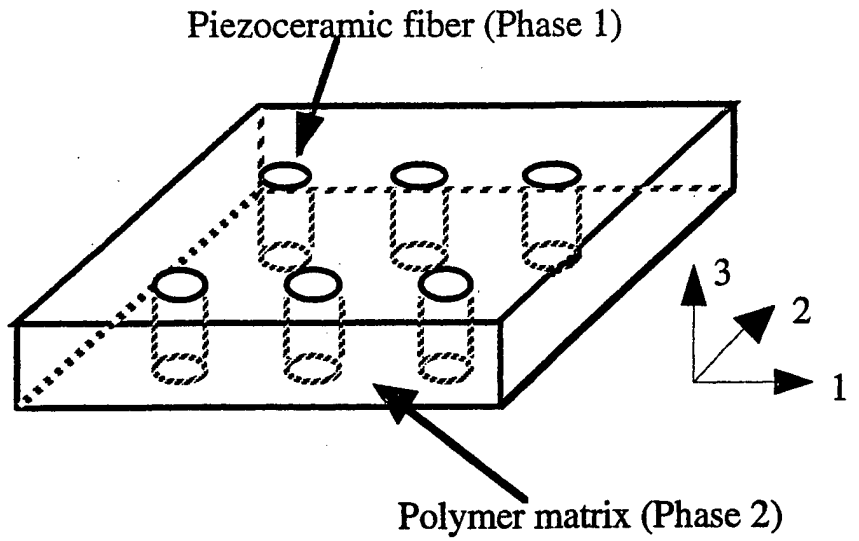

Figure 6 A 1-3 composite of PZT rods and polymer. The top and bottom planes are rigid electrodes.

perform both actuation and sensing and have a figure of merit of $d_h.g_h$, the composite materials are found to be far superior to single-phase materials like PZT or PVDF.

5.24.4.2 Principle of PZT–Polymer Composites

Here, in order to illustrate the principle, let us take a 1-3 composite which is composed of PZT fibers embedded in a polymer matrix as shown in Figure 6. The original fabrication process involves the injection of epoxy resin into an array of PZT fibers assembled with a special rack (Klicker *et al.*, 1981). After the epoxy is cured, the sample is cut, polished, electroded on the top and bottom, and finally electrically poled. The die casting technique has recently been employed to make rod arrays from a PZT slurry (Materials Systems Inc. Catalog, 1994).

The effective piezoelectric coefficients d^* and g^* of the composite can be interpreted as follows: when an electric field E_3 is applied to this composite, the piezoceramic rods extend easily because the polymer is elastically very soft (assuming that the electrode plates which are bonded to its top and bottom are rigid enough). Thus, d_{33}^* is almost the same as ${}^1d_{33}$ of the PZT itself:

$$d_{33}^* = {}^1d_{33} \tag{1}$$

Similarly,

$$d_{31}^* = {}^1V\,{}^1d_{31} \tag{2}$$

where ${}^1V$ is the volume fraction of Phase 1 (piezoelectric). On the other hand, when an external stress is applied to the composite, the elastically stiff piezoceramic rods will support most of the load, and the effective stress is drastically enhanced and inversely proportional to the volume fraction. Thus, larger induced electric fields and larger g^* constants are expected:

$$g_{33}^* = d_{33}^*/\varepsilon_0\varepsilon_3^* = {}^1d_{33}/{}^1V\varepsilon_0\,{}^1\varepsilon_3 = {}^1g_{33}/{}^1V \tag{3}$$

Figure 7 shows the piezoelectric coefficients for a PZT–Spurrs epoxy composite with 1-3 connectivity, measured with a Berlincourt d_{33} meter. As predicted by the model for this composite, the measured d_{33}^* values are independent of volume fraction, but are only about 75% of the d_{33} value of the PZT 501A ceramic. This discrepancy may be due to incomplete poling of the rods. A linear relation between the permittivity and the volume fraction ${}^1V$ is almost satisfied, resulting in a dramatic increase in g_{33}^* with decreasing fraction of PZT. The piezoelectric coefficients for the 1-3 composite are listed in Table 1, together with those of a PZT–silicone composite with 3-3 connectivity. In conclusion, for the composites, the piezoelectric g coefficient can be enhanced by two orders of magnitude with decreasing volume fraction of PZT, while the d coefficient remains constant.

The advantages of this composite are high coupling factors, low acoustic impedance, good matching to water or human tissue, mechanical flexibility, broad bandwidth in combination with a low mechanical quality factor, and the

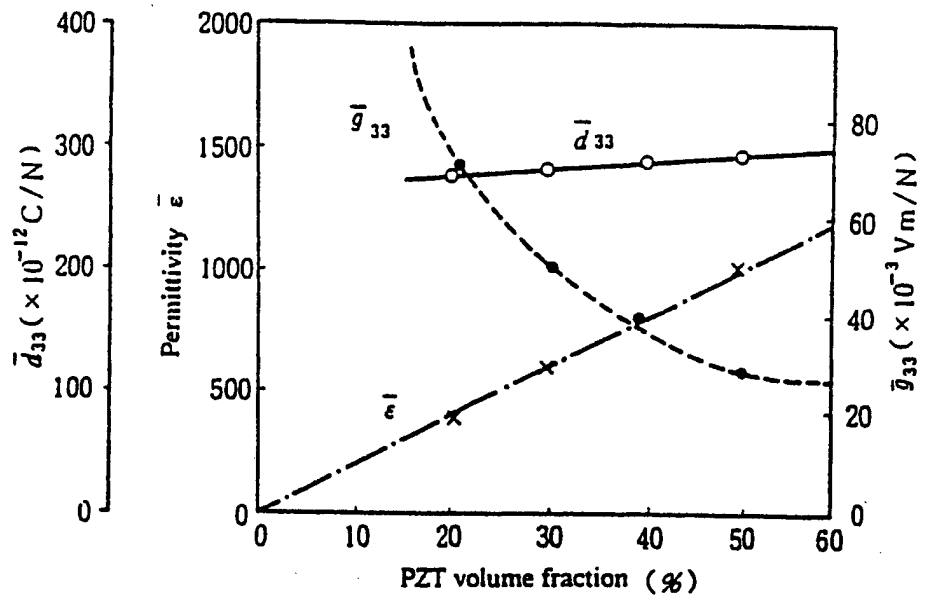

Figure 7 Volume fraction dependence of the permittivity ε and the piezoelectric constants d_{33} and g_{33} in a 1-3 PZT–polymer composite.

Table 1 Comparison of the piezoelectric response of PZT–polymer composites with the single-phase materials PVDF and PZT.

Connectivity	*Material*	*Density*	*Elastic constant*	*Dielectric constant*	*Piezoelectric constants*		
		ρ (10^3kg m^{-3})	c_{33} (GPa)	ε_3 (GPa)	d_{33} (10^{-12} CN^{-1})	g_{33} (10^{-3} m VN^{-1})	g_h (10^{-3} m VN^{-1})
	PZT(501A) Single phase	7.9	81	2000	400	20	3
3-1	PZT–Epoxy	3.0	19	400	300	75	40
3-3	PZT–Silicone rubber (Replica type)	3.3	3	40	110	280	80
	PZT–Silicone rubber (Ladder type)	4.5	19	400	250	60	
3-0	PZT–PVDF	5.5	2.6	120	90	85	
	PZT–Rubber	6.2	0.08	73	52	140	30
	PZT–Chloroprene rubber		40			90	
	Extended PVDF	1.8	3	13	20	160	80

possibility of making undiced arrays by simply patterning the electrodes. The thickness-mode electromechanical coupling of the composite can exceed the k_t (0.40–0.50) of the constituent ceramic, approaching almost the value of the rod-mode electromechanical coupling, k_{33} (0.70–0.80), of that ceramic (Smith, 1989). The acoustic match to tissue or water (1.5 Mrayls) of the typical piezoceramics (20–30 Mrayls) is significantly improved when they are incorporated in forming a composite structure, that is, by replacing the dense, stiff ceramic with a low density, soft polymer. Piezoelectric composite materials are especially useful for underwater sonar and medical diagnostic ultrasonic transducer applications.

Although the PZT composites are very useful for acoustic transducer applications, care must be taken when using them in actuator applications. Under an applied d.c. field, the field-induced strain exhibits large hysteresis and creep due to the viscoelastic property of the polymer matrix. More serious problems are found when they are driven under a high a.c. field, related to the generation of heat. The heat generated by ferroelectric hysteresis in the

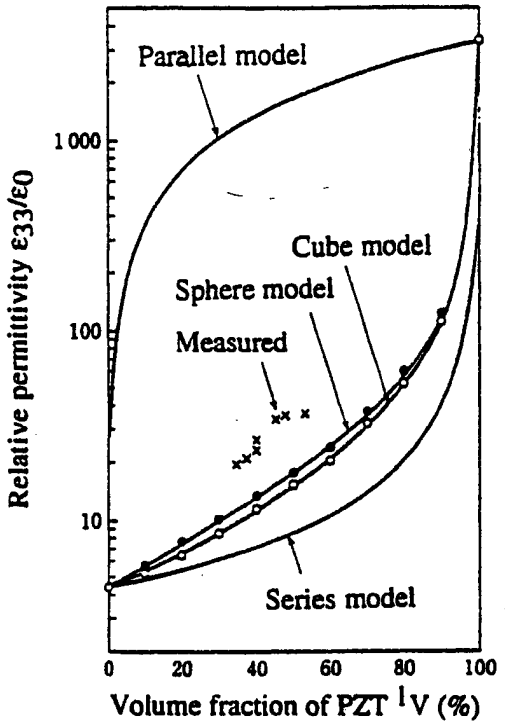

Figure 8 Relative permittivity plotted as a function of volume fraction of PZT in PZT powder–polyurethane rubber composites. Comparisons were made for the cube model, sphere model, parallel and series models.

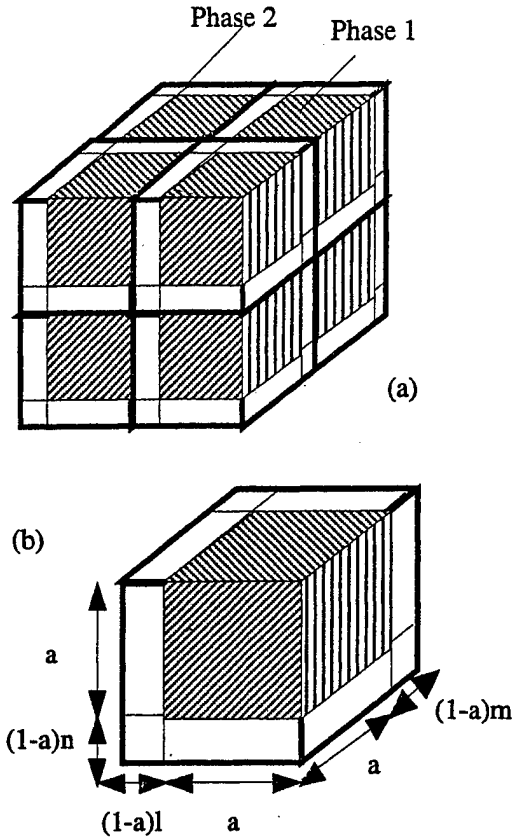

Figure 9 Unit cell configuration for a 0-3 composite according to Banno's modified cubes model.

piezoceramic cannot be dissipated easily due to the very low thermal conductivity of the polymer matrix, which results in rapid degradation of piezoelectricity.

5.24.4.3 Theoretical Models for 0-3 Composites

Various models have been proposed to predict the electromechanical properties of a composite material. Pauer (1973) developed a 0-3 composite material comprised of PZT powder and polyurethane rubber, and predicted its permittivity values by means of a cubes model. Figure 8 shows the relative permittivity plotted as a function of volume fraction of PZT powder, in comparison with theoretical values calculated on the basis of the cubes model (cubic PZT particles), the sphere model (spherical PZT particles), and the parallel and series models. None of the models provided a close fit to the experimental data.

Banno (1985) proposed a "modified cubes model," which took into account the anisotropic distribution of cubes in x, y, and z directions. The unit cell of this model is shown in Figure 9. The following formulas can be derived for a uniaxially anisotropic case (i.e., $l = m = 1, n \neq 1$):

$$\varepsilon_{33}^{*} = [a^2(a + (1-a)n)^2\,{}^1\varepsilon_{33}\,{}^2\varepsilon_{33}]/[a^2\,{}^2\varepsilon_{33} + (1-a)n\,{}^1\varepsilon_{33}] + [1 - a^2(a + (1-a)n)^2\,{}^2\varepsilon_{33}] \quad (4)$$

$$d_{33}^{*} = {}^1d_{33}\,[a^3(a + (1-a)n)]/[a + (1-a)n({}^1\varepsilon_{33}/{}^2\varepsilon_{33})]/[(1-a)n/(a + (1-a)n) + a^3] \quad (5)$$

$$d_{31}^{*} = {}^1d_{31}[a^2(a + (1-a)n)]/[a + (1-a)n({}^1\varepsilon_{33}/{}^2\varepsilon_{33})]a/[1-a(a + (1-a)n)^{1/2} + a^3] \quad (6)$$

The volume fraction of Phase 1 is given by

$${}^1V = a^3/(a + (1-a)n) \quad (7)$$

The case $n = 1$ corresponds to the cubes model, and a general case $0<n<1$ corresponds to a configuration more dense along the z direction. Figure 10 shows the experimentally determined permittivity and piezoelectric d_h^* ($= d_{33}^* + 2d_{31}^*$) coefficient for $PbTiO_3$–chloroprene rubber composites, with the theoretical curves (Banno and Tsunooka, 1987). When the volume fraction of $PbTiO_3$ (^1V) is small, n seems to be less than 1 (that is, the rubber thickness

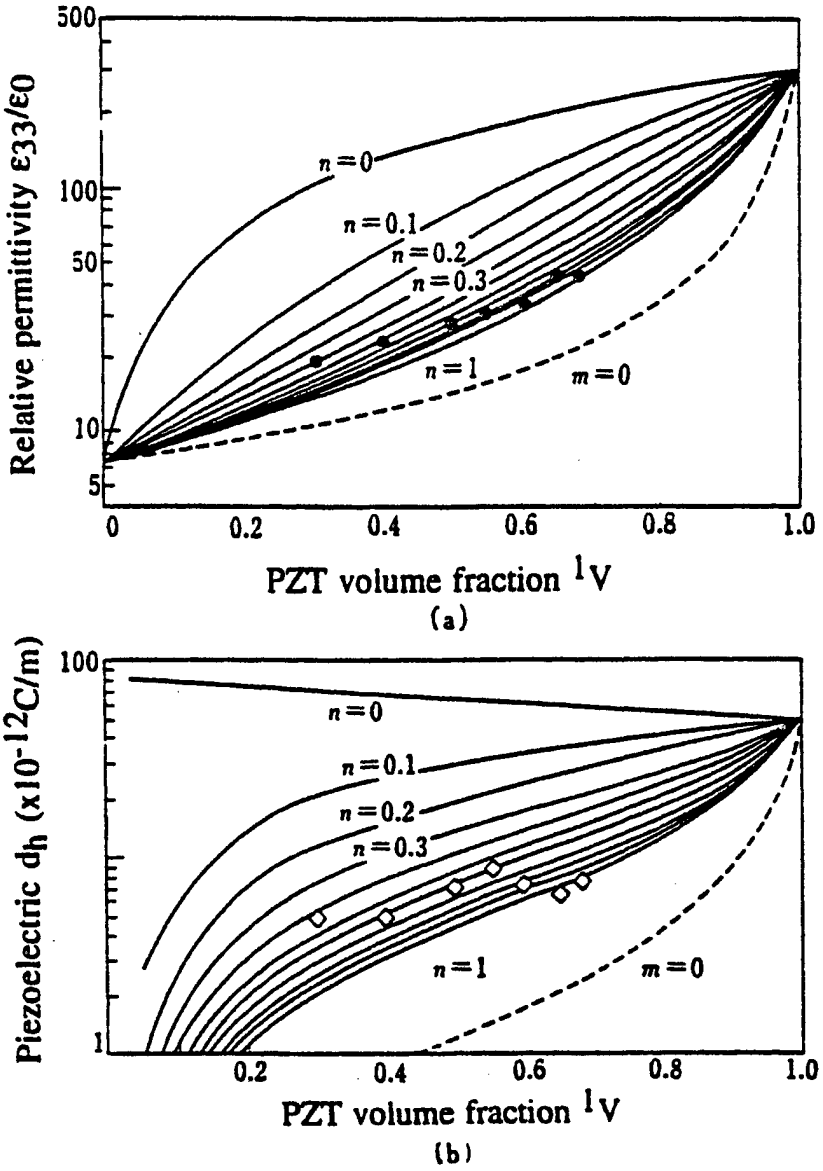

Figure 10 Experimental values of the permittivity (a) and the piezoelectric $d_h^*(= d_{33}^* + 2d_{31}^*)$ coefficient (b) for $PbTiO_3$–chloroprene rubber 0-3 composites, shown with theoretical curves based on the modified cubes model.

around a $PbTiO_3$ ceramic cube is thinner along the z direction and thicker along the x and y directions) and by increasing the volume fraction, n approaches 1 (that is, the rubber thickness becomes equal in all three dimensions). This configuration change may be caused by the method of fabrication, which typically involves rolling and calendering.

5.24.4.4 Advanced PZT–Polymer Composites

3-3 Composites were first fabricated by the replamine method. A negative replica of a natural coral structure with 3-3 connectivity was made of wax. Then a positive replica of the negative structure was prepared by introducing a PZT slurry into the porous network of the negative template, drying, burning out the wax, and finally sintering the PZT ceramic (Skinner *et al.*, 1978). In order to make highly porous PZT skeletons, the BURPS (BURned-out Plastic Spheres) method was proposed (Shrout *et al.*, 1979), where PZT powders and plastic spheres are mixed in a binder solution, and the mixture is sintered. Miyashita *et al.* (1980) reported an alternative method that involves piling up thin PZT rods in a three-dimensionally connected array.

3-1 and 3-2 composites can be fabricated by drilling holes in a PZT block and back-filling

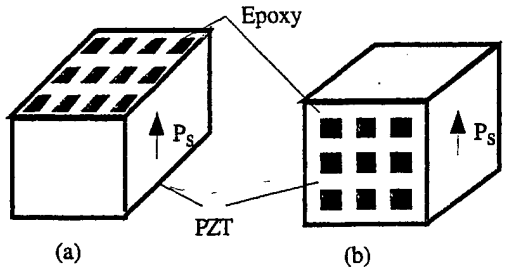

Figure 11 3-1 composites with (a) parallel and (b) series electrode configurations.

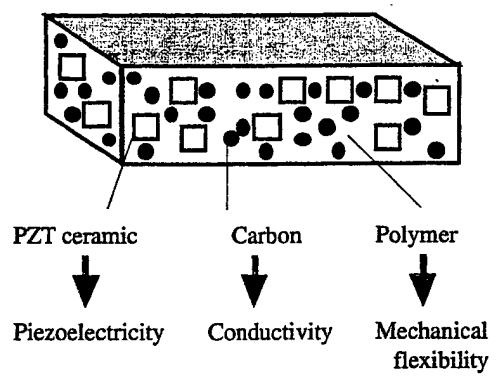

Figure 12 Piezoceramic–polymer–carbon black composite for vibration damping.

with epoxy. In addition to this drilling method, an extrusion method has also been used to fabricate a PZT honeycomb. The 3-1 and 3-2 composites show large d_h and g_h values (Safari *et al.*, 1982). As shown in Figure 11, there are two types of electrode configurations commonly applied to these composites: parallel [P] and series [S]. In general, S types exhibit larger d_h and g_h values than P types.

5.24.5 PZT COMPOSITE DAMPERS

Another intriguing application of PZT composites is a passive mechanical damper. Consider a piezoelectric material attached to an object whose vibration is to be damped. When vibration is transmitted to the piezoelectric material, the vibrational energy is converted into electrical energy by the piezoelectric effect, and an a.c. voltage is generated. If the piezoelectric material is in an open- or short-circuit condition, the generated electrical energy changes back into vibrational energy without loss. The repetition of this process provides continuous vibration. If a proper resistor is connected, however, the energy converted into electricity is consumed in joule heating of the resistor, and the amount of energy converted back into mechanical energy is reduced, so that the vibration can be rapidly damped. Taking the series resistance as R, the capacitance of the piezoelectric material as C, the vibration frequency as f, damping takes place most rapidly when the series resistor is selected in such a manner that the *impedance matching* condition, $R = 1/2\pi fC$, is satisfied (Uchino and Ishii, 1988). Using this technique, in collaboration with ACX Company, K2 developed ski blades with PZT patches to suppress unnecessary vibration during sliding (ACX Company Catalog).

The electric energy U_E generated can be expressed by using the electromechanical coupling factor k and the mechanical energy U_M:

$$U_E = U_M \times k^2 \tag{8}$$

The piezoelectric damper transforms electrical energy into heat energy when a resistor is connected, and the transforming efficiency of the damper can be raised to a level of up to 50%. Accordingly, the vibration energy is decreased at a rate of $(1-k^2/2)$ times for a vibration cycle, since $k^2/2$ multiplied by the amount of mechanical vibration energy is dissipated as heat energy. As the square of the amplitude is equivalent to the amount of vibrational energy, the amplitude decreases at a rate of $(1-k^2/2)^{1/2}$ times with every vibration cycle. If the resonance period is taken to be T_0, the number of vibrations for t seconds is $2t/T_0$. Consequently, the amplitude in t seconds is $(1-k^2/2)^{t/T_0}$. Thus, the damping in the amplitude of vibration in t seconds can be expressed as follows:

$$(1 - k^2/2)^{t/T_0} = \exp(-t/\tau) \tag{9}$$

or

$$\tau = -T_0 \ln(1 - k^2/2) \tag{10}$$

In conclusion, the higher the k value, the quicker the vibration suppression.

Being brittle and hard, ceramics are difficult to assemble directly into a mechanical system. Hence, flexible composites can be useful in practice. When a composite of polymer, piezoceramic powder, and carbon black is fabricated (Figure 12), the electrical conductivity of the composite is greatly changed by the addition of small amounts of carbon black (Suzuki *et al.*, 1991). Figure 13 illustrates the fabrication process. By properly selecting the electrical conductivity of the composite, the ceramic powder effectively forms a series circuit with the carbon black, so that the vibrational energy is dissipated. The conductivity changes by more than 10 orders of magnitude around a certain carbon

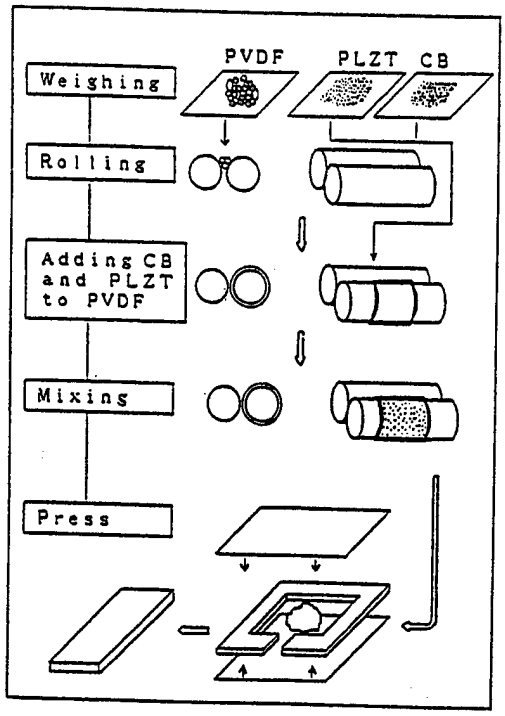

Figure 13 Fabrication process of carbon black containing PLZT–PVDF composies.

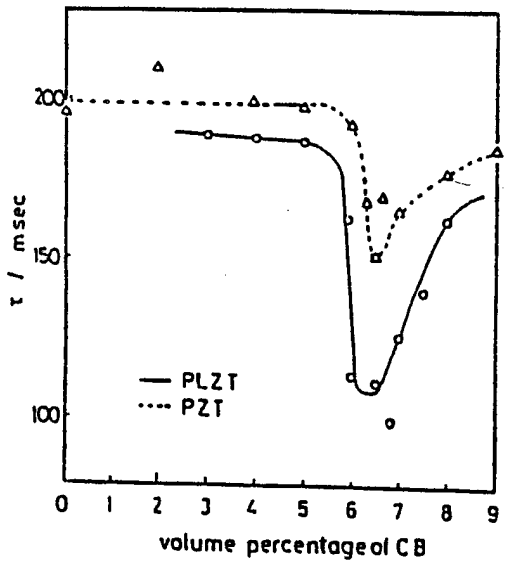

Figure 14 Damping time constant vs. volume percentage of carbon black in the PLZT–PVDF composite. The minimum time constant (quickest damping) is obtained at the percolation threshold.

fraction called the percolation threshold, where the carbon powder links start to be generated. This eliminates the use of external resistors.

Figure 14 shows the relation between the damping time constant and the volume percentage of carbon black in the PLZT–PVDF and PZT–PVDF composites. A volume percentage of about 7% carbon black exhibited the minimum damping time constant and therefore the most rapid vibrational damping. Note that the PLZT (lanthanum-doped PZT) with a higher electromechanical coupling k shows a larger dip (more effective) in the damping time constant curve.

5.24.6 REFERENCES

ACX Company Catalogue: Passive Damping Ski, Cambridge, MA.

H. Banno, in 'Proceedings of the 6th International Meeting on Ferroelectricity, IMF-6', Kobe and 1985, *Jpn. J. Appl. Phys.*, 1985, **24**(Suppl. 24-2), 445.

H. Banno and T. Tsunooka, in 'Ceramic Data Book 87', Industrial Product Technology Society, Chiyoda-Ku, Tokyo, 1987, p. 328.

K. A. Klicker, J. V. Biggers and R. E. Newnham, *J. Am. Ceram. Soc.*, 1981, **64**, 5–9.

Materials Systems Inc. Catalog, 1994, Concord, MA.

M. Miyashita *et al.*, *Ferroelectrics*, 1980, **27**, 397.

R. E. Newnham *et al.*, *Mater. Res. Bull.*, 1978, **13**, 525.

L. A. Pauer, IEEE International Convention Record, Piscataway, NJ, 1973, pp. 1–5.

A. Safari, R. E. Newnham, L. E. Cross and W. A. Schulze, *Ferroelectrics*, 1982, **41**, 197.

T. R. Shrout, W. A. Schulze and J. V. Biggers, *Mater. Res. Bull.*, 1979, **14**, 1553.

D. P. Skinner, R. E. Newnham and L. E. Cross, *Mater. Res. Bull.*, 1978, **13**, 599.

W. A. Smith, in 'Proceedings of the IEEE Ultrasonic Symposium 89', ed. B. R. McAvoy, IEEE Service Center, Long Beach, CA, 1989, pp. 755–766.

Y. Suzuki, K. Uchino, H. Gouda, M. Sumita, R. E. Newnham and A. R. Ramachandran, *J. Ceram. Soc. Jpn., Int. Edn.*, 1991, **99**, 1096.

K. Uchino, *Solid State Phys.*, 1986, **21**, 27.

K. Uchino and T. Ishii, *J. Ceram. Soc. Jpn.*, 1988, **96**, 863–867.

K. Uchino, S. Nomura and R. E. Newnham, *Sensor Technology*, 1982, **2**, 81.

APPENDIX 35

5.22
Piezoelectric Composite Sensors

JAMES F. TRESSLER
Consortium for Oceanographic Research and Education, Washington, DC, USA
and
KENJI UCHINO
Pennsylvania State University, University Park, PA, USA

5.22.1 INTRODUCTION 493
5.22.2 PIEZOELECTRICITY 493
5.22.3 PIEZOELECTRIC MATERIALS 494
5.22.4 SENSOR CHARACTERIZATION 495
5.22.5 COMPOSITES 496
5.22.5.1 Piezoelectric–Polymer Composites 496
5.22.5.2 Piezoelectric–Metal Composites 502
5.22.6 SUMMARY 503
5.22.7 REFERENCES 504

5.22.1 INTRODUCTION

Piezoelectric composite sensors consist of an electrically active piezoelectric phase combined with an electrically inert second phase. Typically, this second phase is a polymer, although in some cases it is a metal. This chapter will discuss the rationale behind this approach to sensor design. It will begin with a brief review of piezoelectricity, followed by the important commercial piezoelectric sensor materials and their relevant properties, and subsequently the need for incorporating them into composite form. The chapter will conclude by discussing the principle two-phase composite sensor configurations and their properties, the main commercial manufacturing techniques, and some practical applications.

5.22.2 PIEZOELECTRICITY

Piezoelectric materials develop an electrical charge on their electroded faces when subjected to stress. They also exhibit a shape change that is linearly proportional to an applied electric field. The latter, known as the converse piezoelectric effect, is used in actuation and acoustic source generation. The former, called the direct piezoelectric effect, is utilized in sensing changes in force, displacement, or velocity.

Physically, piezoelectricity describes the coupling between the elastic variables (stress and strain) of a material and its electrical parameters (electric field and dielectric displacement). There are four piezoelectric coefficients that are designated as d, e, g, and h by convention. These coefficients are not independent but

rather are inter-related through the material dielectric and elastic constants. The charge coefficient, d, relates (i) the applied electric field to induced strain and (ii) stress to dielectric displacement. The stress coefficient, e, relates (i) applied electric field to stress and (ii) strain to dielectric displacement. The voltage coefficient, g, relates (i) the applied stress to generated electric field and (ii) the dielectric displacement to strain. The strain coefficient, h, relates (i) strain to electric field and (ii) dielectric displacement to stress. The constitutive equations and the relationships between the piezoelectric constants can be found in any quality text which covers piezoelectricity such as Moulson and Herbert (1992), Rosen *et al.* (1992), Ikeda (1990), Jaffe *et al.* (1971), and Berlincourt *et al.* in Mason's series on Physical Acoustics (1964).

The constitutive equations show that piezoelectric materials exhibit a linear relationship between their elastic and electrical variables. This is only true, however, at low levels of stress and small electric fields. The effects of high mechanical stress on nonlinearity depend primarily on the orientation and frequency of the applied stress with respect to the polar axis, as well as the electrical load conditions (Berlincourt *et al.*, 1964).

5.22.3 PIEZOELECTRIC MATERIALS

Piezoelectricity only occurs in materials whose crystal structure is noncentric. As such, it is exhibited in certain classes of crystals, ceramics, and polymers. In sensor applications where a variable has to be monitored over a long period of time, piezoelectric crystals are typically preferred over their piezoelectric ceramic counterparts (Maines, 1989). This is because crystals have much more stable piezoelectric properties compared to poled ceramics. Even though some piezoelectric crystals used in sensor applications occur abundantly in nature, they are more commonly grown synthetically. To be of practical use, however, they must be oriented and cut along specific crystallographic directions to obtain the best piezoelectric response. A number of important piezoelectric crystals and their properties are described in Ikeda (1990) and by Bhalla *et al.* (1993) in the Landolt–Börnstein tables. The most common ones used in sensor applications will be discussed here briefly.

Piezoelectric crystals are used most often in accelerometers and specialty hydrophones (underwater microphones). Quartz is the predominant material used for accelerometers (Maines, 1989). Lithium sulfate (because of its large g_h coefficient) and tourmaline are two piezoelectric crystals still used in commercial hydrophones. Tourmaline, along with Rochelle salt, are used in hydrophones designed for shock and blast measurements (Wilson, 1988). Lithium niobate and lithium tantalate are used as high-temperature acoustic sensors because they both maintain high sensitivity up to 400 °C (Turner *et al.*, 1994).

The piezoelectric materials found in many force and displacement sensors, however, are poled polycrystalline ferroelectric ceramics. Ceramic materials in general are characterized as having high mechanical strength and reproducible properties, possess a high resistance to severe ambient conditions such as temperature, pressure, and humidity, and perhaps most importantly can usually be made into complex shapes and large area pieces with little difficulty.

Bulk polycrystalline ceramics are typically synthesized via a high-temperature solid-state reaction of mixed oxides. In ferroelectric ceramics, like-polarized regions within each ceramic grain are formed as the ceramic cools through a specific temperature. This temperature, known as the Curie temperature, depends primarily on the chemical composition of the ceramic. On a macroscopic scale, these like-polarized regions (domains) are randomly oriented throughout the ceramic, resulting in no preferred polarization direction. The ferroelectric is therefore nonpiezoelectric.

Piezoelectricity is induced, however, by a process known as poling. During poling, a large static electric field is applied to the ceramic in a certain direction to switch the polarization axes of the domains to those directions (allowed by symmetry) which are nearest to that of the applied field (Gallego-Juárez, 1989). When the electric field is removed, some of the more highly strained domains revert to their original positions (depolarization), but a large majority remain aligned (remnant polarization).

When poled, polycrystalline ferroelectrics are often referred to as piezoelectric ceramics, or simply piezoceramics (Berlincourt *et al.*, 1964). The piezoceramic will remain in a poled state until it is either subjected to a mechanical stress or electric field (the coercive field) sufficiently large to reorient the domains or until it is heated above its Curie temperature, at which time its crystal structure will again become centric and piezoelectricity will be lost. Depolarization over a long period of time (i.e., months to years) due to internal stress relaxation is known as aging.

The lead zirconate titanate family of compositions, which are better known as PZTs (a

Table 1 Room temperature piezoelectric properties of common piezoceramic materials.

Military specification	*Commercial specification*	T_c	d_{33}	d_{31}	d_{15}	K_{33}^T	M^*
Type I	PZT-4	328	289	−123	496	1300	−229
Type II	PZT-5A	365	374	−171	584	1700	−234
Type III	PZT-8	300	218	−93	330	1000	−229
Type V	PZT-5J	250	500	−220	670	2600	−232
Type VI	PZT-5H	193	593	−274	741	3400	−236
	$(Pb,Ca)TiO_3$	255	68	−3	71	209	−209

Source: Gallego-Juárez, 1989; Jaffe and Berlincourt, 1965; Morgan Matroc; Vernitron Piezoelectric Division.

registered trademark of Clevite Corporation (Jaffe and Berlincourt, 1965)), are the piezoelectric ceramics of choice for many sensor applications. This is because of their easily tailorable, high piezoelectric properties as well as their high electromechanical coupling and relative ease of fabrication. In general, lead zirconate titanate compositions are modified by the addition of very small amounts (typically less than 2 mol.%) of either donor or acceptor dopants. The addition of dopants has a profound impact on both the physical and electrical properties of PZT. Donor dopants cause cation (metal) vacancies in the crystal structure which enhance domain reorientation and hence the extrinsic contribution to piezoelectric properties. These piezoelectrically "soft" PZTs are characterized by large piezoelectric coefficients, large dielectric constants, high dielectric losses, large electromechanical coupling factors, very high electrical resistance, low mechanical quality factors, a low coercive field and poor linearity (Jaffe and Berlincourt, 1965; Berlincourt, 1981).

Acceptor dopants cause anion (oxygen) vacancies in the crystal structure. This leads to piezoelectrically "hard" PZTs. Compared to soft PZTs, hard PZTs have lower piezoelectric coefficients, lower permittivity, lower dielectric losses, lower electrical resistivity, a higher mechanical quality factor, higher coercive field, are more difficult to pole and depole, and have better linearity (Ikeda, 1990; Berlincourt, 1981). Commercial PZT manufacturers have developed a general nomenclature based on US Military Standard specifications (1995) to differentiate the different PZT types, the physical and piezoelectric properties of which are listed in Table 1. Piezoelectric properties can show statistical and systematic fluctuations (up to 20%) from batch to batch or even within a batch due to slight chemical differences, variations in density, inhomogeneous chemical compositions, variations in grain size, and varying response to the poling treatment, etc. (Berlincourt *et al.*, 1964).

Other poled piezoceramic materials are used for specialty sensor applications. For instance, lead titanate is sometimes used as a hydrophone material or as a transceiver for use in medical diagnosis when it is doped with either calcium or strontium (Ikeda, 1990; Gallego-Juárez, 1989). This is due to its strong piezoelectric anisotropy. When doped with other elements, lead titanate is used as a knock sensor in automobiles. Its higher operating temperature range allows it to be mounted closer to the combustion chamber, giving it a faster response time than PZT (Turner *et al.*, 1994). Because of the difficulty in making and poling lead titanate, it is not used in more applications. Bismuth titanate, when doped with sodium, can be used for accelerometers at temperatures up to 400 °C (Turner *et al.*, 1994). Lead metaniobate, a member of the tungsten bronze family, is often used in nondestructive testing, medical diagnostic imaging, and for deep submergence hydrophones (Wilson, 1988). However, problems such as a high level of porosity and relatively low mechanical strength are often encountered in its use. Antimony sulfur iodide has a very high g_h coefficient, especially when it is modified with 4–8% oxygen, making it attractive for some hydrophone applications. It can only be used at temperatures below 34 °C though (Wilson, 1988).

5.22.4 SENSOR CHARACTERIZATION

For a poled ferroelectric ceramic, there are five nonzero piezoelectric coefficients. They are C_{31}, C_{32}, C_{33}, C_{24}, and C_{15}, where C can represent either d, e, g, or h. Because of crystal symmetry, $C_{31} = C_{32}$ and $C_{24} = C_{15}$. In the case of the g_{ij} coefficient, the first digit in the subscript, i, refers to the direction in which the voltage is measured and the second digit, j, refers to the direction of the applied stress. For a piezoceramic poled in the 3- (or thickness) direction, a voltage (V_3) will be generated

across the electrodes which is proportional to the voltage coefficient (g_{33}), thickness of the element (t), and magnitude of the applied stress (σ_3) as:

$$V_3 = g_{33} \cdot t\sigma_3 \tag{1}$$

The receiving sensitivity (M) of a piezoelectric is equal to the open circuit voltage (V_i) that it generates due to an applied stress (σ_j), or

$$M = V_i/\sigma_j = g_{ij} \cdot t \tag{2a}$$

Often, the sensitivity is reported in terms of decibels (dB) referenced to 1 volt per 10^{-6} Pascal (μPa) of pressure as

$$M(\text{dB}) = 20 \cdot \log\left(\frac{g_{ij} \cdot t}{10^6}\right) \quad (0\,\text{dB re}: 1\text{V}/\mu\text{Pa}) \tag{2b}$$

The sensitivity needs to be sufficiently high so that the generated signal can be detected above the background noise. In practice, the generated signal is small and has to be enhanced by an appropriate charge or voltage amplifier. The sensitivity is maximized when the g coefficient is maximized. The g coefficient is related to the d coefficient through the material's dielectric constant, K_{ij}^T, as:

$$g = d/K_{ij}^T\varepsilon_0 \tag{3}$$

where ε_0 is the permittivity of free space. Typically a large capacitance, which is directly proportional to dielectric constant, is also desirable for sensors in order to overcome the electrical losses associated with the cables. Unfortunately, an increase in dielectric constant results in a lower voltage coefficient, as seen in the aforementioned equation. A flat sensitivity response over the frequency band of interest is another desirable characteristic for a sensor.

For in-air applications, either the g_{33} (longitudinal mode) or the g_{15} (shear mode) coefficient of the piezoceramic is typically utilized. When operating in the hydrostatic mode (i.e., when the incident stress is equal on all sides), the tensor coefficients are represented as $d_h = d_{33} + 2d_{31}$ and $g_h = g_{33} + 2g_{31}$. Unfortunately, for poled piezoceramics (namely PZT), the d_{33} coefficient is approximately twice the magnitude and opposite in sign to the d_{31} coefficient (see Table 1). Since K_{ij}^T for most ferroelectric ceramics is very large (>1000), the g_h coefficient is also small (Equation (3)). As a consequence, the voltage generated by an incoming pressure wave is very low. In order to improve the sensitivity of the piezoceramic, it must be configured in such a way that the effect of the hydrostatic pressure is minimized. This usually takes the form of air backing one side of the ceramic element, encapsulating part of the ceramic in a soft polymer to absorb a portion of the hydrostatic stress, or incorporating air spaces into the sensor itself.

A figure-of-merit, the $d_h \cdot g_h$ product, is often reported as a measure of the quality of the sensing capability of the piezoelectric element or to compare different hydrophone materials (Bhalla and Ting, 1988). Quantitatively, it is used to ascertain the type of amplifier required in the electronic circuitry to overcome the self-noise of the system. In the case of piezocomposites, the $d_h \cdot g_h$ product should be normalized by the volume of the device in order to make accurate comparisons between the different configurations (Gabrielson, 1997).

5.22.5 COMPOSITES

The basic idea behind a composite structure is to maximize the desirable traits of each component in the composite while minimizing the effects of the less desirable features. In a two-phase composite, each individual phase can be connected to itself throughout the volume of the composite in either 0, 1, 2, or 3 directions. The connectivity of the individual phases is of utmost importance because it controls the electric flux pattern as well as the mechanical properties of the composite. Both, in turn, can be changed by orders of magnitude depending on how the individual phases are connected (Pilgrim *et al.*, 1987).

The notation used to denote the different connectivity patterns is known as the Newnham connectivity (or classification) system (Pilgrim *et al.*, 1987; Newnham *et al.*, 1978). The convention is for the connectivity of the active phase to appear first, followed by the connectivity of the passive phase (Pilgrim *et al.*, 1987). There are 16 possible two-phase piezocomposite structures. The configurations for which sensitivity measurements have been reported are shown schematically in Figure 1.

5.22.5.1 Piezoelectric–Polymer Composites

The two most common composite types used for sensor applications are those with 0-3 and 1-3 connectivity. The remainder of this chapter will focus on describing in more detail the manufacturing techniques, properties, and some practical applications for these two types of piezocomposite. Other configurations for which sensitivity results have been reported

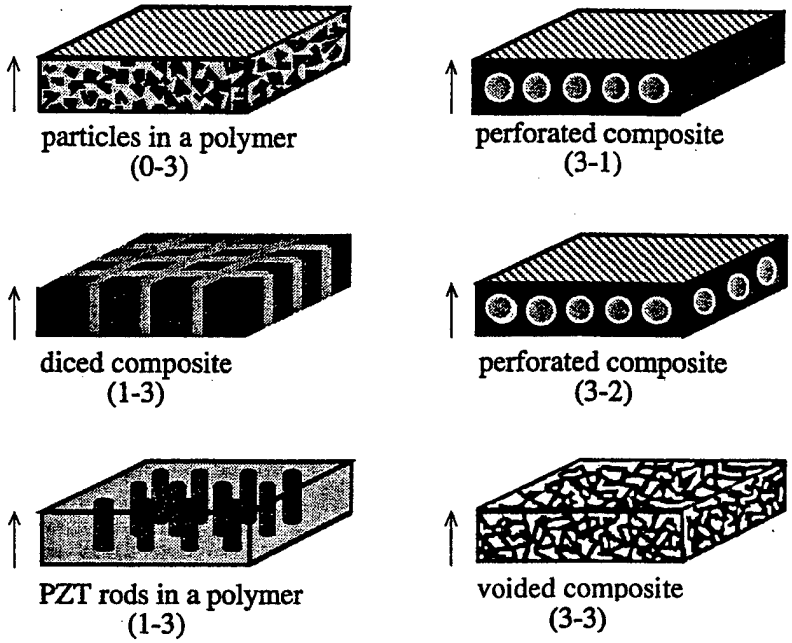

Figure 1 Diagram of the various composite connectivity schemes described in this chapter. The poling direction is noted by the arrows.

will also be briefly discussed for the sake of completeness.

Piezocomposites with 0-3 connectivity consist of tiny nontouching piezoelectric particulates randomly dispersed within a chloroprene rubber host matrix. These composites are characterized by their mechanical robustness, flexibility, and by their good acoustical impedance match to air and especially water. Currently, the primary commercial manufacturer of 0-3 type piezocomposites is the NTK Technical Ceramics Division of the NGK Spark Plugs Corporation in Japan. NTK markets their products under the tradename *Piezo Rubber* (usually abbreviated as PR or PZR). Although the PZT family predominates as the active phase in most other piezocomposite designs, lead titanates (PTs) are preferred in the 0-3s (Newnham *et al.*, 1984; Banno, 1983). The reason for this is the large piezoelectric anisotropy inherent in lead titanate and modified lead titanates, which ultimately results in a higher piezoelectric activity in the poled composite.

Piezo Rubbers are fabricated by rolling a well-dispersed ceramic–rubber mixture into thin ($\approx$5 mm) large surface area sheets using a hot roller, followed by an additional heat and pressure treatment (Banno, 1990). Finally, both the upper and lower surfaces are electroded using an elastomer-based silver coating. Because the individual ceramic particulates in the composite are all surrounded by a low permittivity dielectric polymer, poling requires a very large static electric field. Fields of the order of 100 kV cm^{-1} applied for 1 h are not unreasonable. Adequate poling can be accomplished at much lower fields (35–40 kV cm^{-1}) and for shorter poling times (a few minutes) if a small amount (about 1.5%) of carbon is added to the polymer matrix during the mixing stage (Newnham *et al.*, 1984). Unfortunately, the addition of carbon contributes to an increase in the dielectric dissipation loss (and subsequently Johnson noise) in the composite. As a consequence, the sensor signal-to-noise ratio is reduced. An alternative approach to reduce the poling field without introducing an electrically conducting material into the system is to deliberately select a polymer host matrix with a relatively high temperature coefficient of resistivity. By poling the composite at an elevated temperature, it becomes possible to use the improved ceramic/polymer resistivity balance to give saturation poling, while at the same time retaining the low resistivity and low loss at the temperatures of operation (Twiney, 1992).

In addition to sheet form, NTK also manufactures 0-3s in the form of long thin wires under the tradename *Piezo Wire*. NTK *Piezo Wire* is marketed primarily as a flexible acceleration sensor, although it can also be used as a pick up for an electric piano or electric guitar, stretched across a street to monitor traffic flow, or wrapped around the body to detect heart sound and blood pressure. Research has also included using 0-3s in smart systems to actively control acoustic noise (Salloway, 1996). In addition, it has been investigated as a potential thin-layer vibration detector which can be coated directly onto a structure due to its

Table 2 Properties of 0-3 *Piezo Rubber* composites.

NTK designation	ρ	ρc	K_{33}^T	*tan* δ	d_{33}	d_{31}	d_h	g_h	M^*
PR-303	5300	7.0	43	0.06	48	−15.5	17	45	−207
PR-304	5300	8.3	40	0.03	56	−18.5	19	55	−205
PR-305	5500	6.7	37	0.03	46	−2.5	41	124	−198
PR-306	5300	8.5	38	0.02	34	−7.0	20	58	−205
PR-307	5900	8.4	45	0.05	52	−4.0	44	111	−199
PR-308	6200	9.1	57	0.05	58	−5.0	48	95	−200

Source: NTK Technical Ceramics.

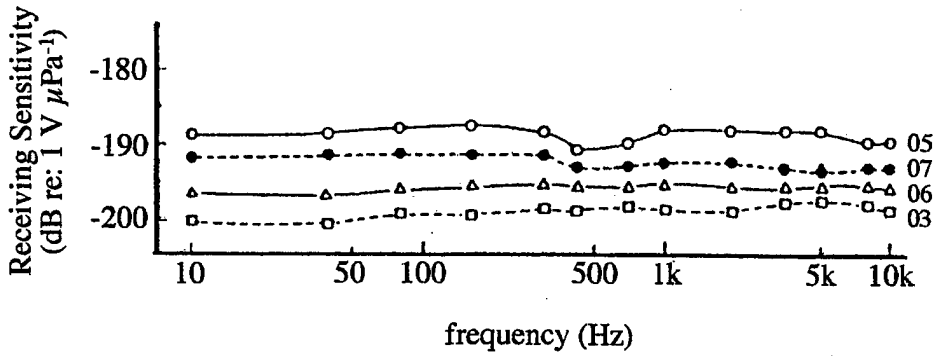

Figure 2 Frequency dependence of the receiving sensitivity for *Piezo Rubber* composites PR-303, PR-305, PR-306, and PR 307, which are designated by 03, 05, 06, and 07 in the figure. PR-303, PR-305, and PR-306 were each 3 mm thick, whereas PR-307 was 2 mm thick (reproduced by permission of the American Institute of Physics from *Jpn. J. Appl. Phys.*, 1987, **26 Suppl. 26-1**, 153–155).

paint-like texture in the initial stage of manufacture (Egusa and Iwasawa, 1994).

Table 2 shows the relevant low-frequency properties of various *Piezo Rubber* compositions. The various numerical designations are based on different ceramic powder volume fractions and/or different particle size distributions. The dielectric constant of each of the composites is much less than that of the lead titanate active phase (see Table 1) due to the presence of the polymer matrix. Nevertheless, the acoustic impedance, dielectric constant, and dielectric loss are approximately constant for all the PR types shown. The low characteristic impedance implies that the *Piezo Rubbers* have a better acoustic impedance match to either an air or water medium than does the ceramic alone. The reduction (compared to the monolithic ceramic) and the variation in the d_h coefficients are a result of the change in the volume fraction of ceramic present from one PR type to another. The large increase in the g_h coefficient is due to the associated decrease in dielectric constant.

Figure 2 shows the frequency dependence of the receiving sensitivity (as defined by Equation 2(b)) for four different types of *Piezo Rubbers* when used as a hydrophone. The nearly flat sensitivity response between 10 Hz and 10 kHz indicates that they can be used effectively over this entire frequency band. The pressure dependencies of the receiving sensitivity (measured at 160 Hz) for these same PR types (plus 06) are compared in Figure 3. As a rule of thumb, the pressure in MPa is equivalent to 100 m of water depth. The sensitivity of PR-305 is the most pressure dependent. This was attributed to the presence of porosity in the epoxy matrix (Banno *et al.*, 1987). The other compositions are approximately pressure independent up through 15 MPa. Taking into account the thickness of the various *Piezo Rubbers* in the figure, their receiving sensitivities are 20–40 dB better than bulk PZT and up to 10 dB better than pure lead titanate (see Table 1). The dielectric, piezoelectric, and elastic properties of 0-3 composites also vary as a function of temperature. These property variations are attributed to the transition of the polymer matrix from stiff glass-like to soft rubber-like behavior as the temperature is increased (Rittenmyer and Dubbelday, 1992).

Piezoelectric–polymer composites with 1-3 connectivity consist of parallel aligned piezoceramic (generally PZT) rods or fibers imbedded within a three-dimensional polymer host matrix (Figure 1). This composite design is intended to operate in its pure thickness mode. The 1-3 type composites have been

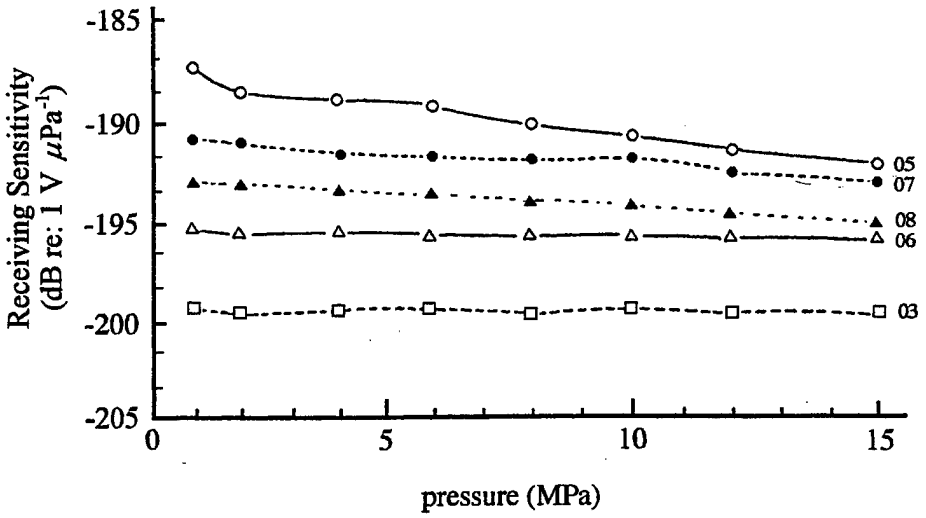

Figure 3 Pressure dependence of the receiving sensitivity (measured at 160 Hz) for *Piezo Rubbers* PR-303, PR-305, PR-306, PR-307, and PR-308 which are designated by 03, 05, 06, 07, and 08 in the figure. PR-303, PR-305, and PR-306 were each 3 mm thick, whereas PR-307 and PR-308 were both 2 mm thick (reproduced by permission of the American Institute of Physics from *Jpn. J. Appl. Phys.*, 1987, **26 Suppl. 26-1**, 153–155).

used effectively as sensors at frequencies spanning from Hz to MHz. When used solely as a sensor, the volume fraction of PZT in the composite is generally between 5 and 25%. When used for both transmit as well as receive, the optimum PZT volume fraction is between 30 and 50%. As such, 1-3 type piezocomposite sensors are generally much lighter in weight than their 0-3 counterparts.

The polymer phase in a 1-3 composite serves a dual purpose. First, it improves the mechanical compliance as well as the acoustic impedance match to either air or water compared to the monolithic ceramic. Second and most importantly, the polymer acts as a stress transfer mechanism to decouple the longitudinal and transverse contributions of the piezoceramic to a hydrostatic stress. When subject to a hydrostatic stress, there are three contributions to the hydrostatic piezoelectric voltage coefficient, g_h, of the composite (Smith, 1993). The first comes from the composite g_{33}, in which the longitudinal, or axial, stress is transferred directly to the piezoceramic rods. The second contribution comes from the composite g_{31}. In this case, the transverse stresses are transmitted to the sides of the piezoceramic elements via the polymer. The third contribution also arises from the composite g_{31}. When squeezed from all sides, the polymer bulges due to the Poisson ratio effect, pulling on the ceramic rods and lengthening them. This g_{31} contribution from the composite effectively counteracts the g_{33} contribution and consequently lowers the g_h of the structure. The effectiveness of the stress transfer is characterized by a stress amplification factor which depends on the individual rod diameters, the rod-to-rod spacing, the volume percent and arrangement of the rods, as well as the stiffness of the polymer. Under a hydrostatic pressure, the stress amplification factor is practically reduced by a factor of (1–2ν), where ν is the Poisson ratio of the polymer phase (Cao *et al.*, 1992). Since the applied stress incident on a 1-3 piezocomposite is designed to be carried mainly by the piezoceramic rods, a pressure-induced depolarization effect also occurs in the rods. This effect can become quite pronounced under large loads as well as for a low volume fraction of rods, which is often the preferred design choice for sensor applications. When used under these conditions, the performance of a 1-3 piezocomposite degrades, causing reliability problems in the device.

Various modifications to the 1-3 composite design have been investigated in an attempt to alleviate these problems. The preferred solution is to incorporate air pockets into the structure to absorb the lateral strain. This has been done by drilling air holes through the epoxy matrix in a direction parallel to the ceramic rods (Hossack and Bedi, 1994), eliminating the interface between the rods and polymer, instead allowing the stress transfer to be realized by armature plates located on the upper and lower surfaces of the composite (Eyraud *et al.*, 1994), and utilizing hollow, radially poled piezoceramic tubes which operate in the g_{31} rather than the g_{33} mode (Zhang *et al.*, 1993; Wang *et al.*, 1995). This latter design also has the advantage of not depoling under high pressures. Incorporating a softer polymer phase between the

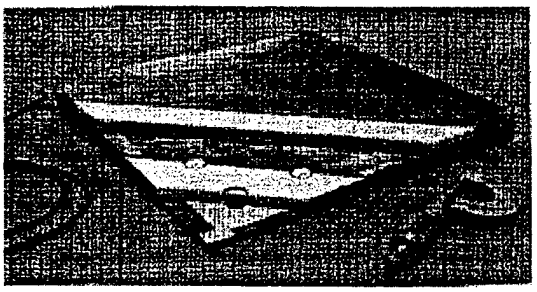

Figure 4 Piezocomposite SmartPanel™ from MSI used for active control of underwater vibration and noise (reproduced by permission of the SPIE from 'Proceedings of the SPIE: Smart Structures and Materials 1997—Industrial and Commercial Applications of Smart Structures Technologies', 1997, vol. 3044, pp. 391–396).

ceramic rods and the stiffer polymer matrix has also been tried (Kim *et al.*, 1994), as well as a glass fiber reinforcement phase in the lateral direction to support the transverse direction stress (Haun *et al.*, 1986). All these solutions, however, add complexity and manufacturing cost to the composite.

The two primary commercial methods used to manufacture 1-3 piezocomposites are the dice-and-fill technique and injection molding. The technology used typically depends on the desired properties of the end product. For the dice-and-fill technique (Savakus *et al.*, 1981), a diamond saw is used to cut perpendicular grooves nearly through a piezoceramic plate to form rows and columns of pillars. A suitable polymer is then vacuum cast into the grooves. After the polymer has cured, the ungrooved backplate is ground away and the composite is polished to the desired thickness. The composite assembly is completed by electroding both the upper and lower surfaces and poling. The dice-and-fill technique limits the shape of the pillars to be square or rectangular. Pillars 100 μm on edge and groove sizes down to 25 μm can be achieved (Janas and Safari, 1995; Smith, 1992). Both are limited by the machinability of the ceramic as well as the width of saw blade. The dice-and-fill technique is adequate for the production of small area samples, such as required in medical transducers. However, it is not cost effective and is too time consuming for applications requiring large area coverage.

Manufacturing 1-3 composites for large area coverage is better suited to injection molding. In order to perform the injection molding technique, the piezoceramic powder first has to be thoroughly mixed with a suitable organic binder which acts as a carrier during molding, allowing its transfer as a viscous fluid under heat and pressure (Bowen *et al.*, 1993). This hot thermoplastic mixture is then rammed, or injected, into a cold metal mold which is the negative of the desired end product. This gives a green (i.e., unfired) ceramic preform. When the preform has been ejected from the mold, it is slowly heated to burn out the organic binder before being sintered. The sintered preform is electroded, poled, encapsulated in a polymer, and has the backing plate ground off (in that order). Injection molding is a fast and simple net-shape process which can provide dense, large area pieces with different rod shapes, arrangements, and diameters. The most expensive feature of this technique is the production of the mold. The primary commercial manufacturer of injection molded 1-3 piezocomposites at the present time is Material Systems Incorporated (MSI) in the USA. Their composites, sold under the tradename SonoPanels, can have rod diameters between 70 μm and 5 mm with thicknesses upwards of 25 mm. In addition, ceramic volume fractions have ranged from 15 to 40% (Bowen *et al.*, 1993, 1996).

There has been a long-term interest by the US Navy in developing piezocomposites for underwater sensor applications because of their high hydrostatic sensitivity response. Over the years, this research effort has resulted in the development of the piezo-polymer PVDF as well as 0-3 piezocomposites. Advancement of the 1-3 type piezocomposites, however, was hindered due to the lack to manufacturing technology. With the advent of advanced processing methods, including the highly successful injection molding technique previously described, the advantages of the 1-3 piezocomposites are now being realized. For example, one application is a hull-mounted conformal array for acoustical detection. Other recent applications based on the advanced material processing capabilities include in-air and in-water active control applications which use 1-3s consisting of integrated pressure sensors, accelerometers, and actuators (Gentilman *et al.*, 1996; Fiore *et al.*, 1997a, 1997b; Corsaro *et al.*, 1997). A photograph of the cutaway of a panel used for vibration control applications is shown in Figure 4.

Additional interest in 1-3 piezocomposites include their use in medical pulse-echo ultrasonic transducers for acoustic imaging. The primary manufacturers of ultrasonic probes that feature 1-3 piezocomposite materials as the active component have been Phillips Medical Systems, Echo Ultrasound, Acuson, Acoustic Imaging, Precision Acoustic Devices, Hitachi, and Siemens AG (Smith, 1992; Oakley, 1991; Wersing, 1986; Takeuchi *et al.*, 1984). Medical ultrasonic transducers use the 1-3 design because of their lower acoustic impedance matching to the medium, higher bandwidth, and clean, mode-free operations.

Table 3 Comparison of typical low-frequency piezoelectric properties of various piezocomposite structures.

Type	ρ	K_{33}^T	d_{33}	d_h	g_h	$d_h.g_h$	M^*
0-3	5900	45	52	44	111	4884	−199
1-3	1800	460	550	268	66	17688	−204
3-1		760	350	230	34	7800	−209
3-2		320	300	322	113	36300	−199
3-3	3840	200	190	90	50	4500	−206

Source: NTK Technical Ceramics; Bowen *et al.*, 1996; Safari *et al.*, 1982; Gururaja *et al.*, 1988.

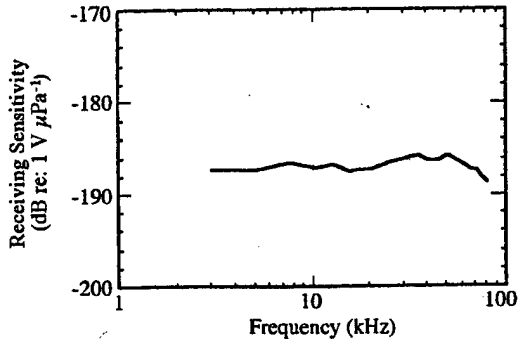

Figure 5 Frequency dependence of the receiving sensitivity of a 6.4 mm thick MSI injection molded 1-3 composite utilizing PZT-5H (reproduced by permission of the IEEE from 'Ultrasonics Symposium Proceedings', 1993, vol. 1, pp. 499–503).

The receiving sensitivity as a function of frequency for a 6.3 mm thick 1-3 piezocomposite (SonoPanel™) containing 15 vol.% PZT-5H rods each 1.15 mm in diameter is shown in Figure 5. The receive sensitivity is quite high at about −186 dB, re:1 V μPa^{-1}, and is nearly constant from 1 kHz to almost 100 kHz. The sensitivity of the composite is over 30 dB higher than monolithic PZT-5H of the same thickness and also compares well to a 0-3 *Piezo Rubber*.

The pressure dependence of the receive sensitivity (measured at both 4 °C and 29 °C at 1 kHz) of a 1-3 type piezocomposite is shown in Figure 6. The composite contains 30 vol.% PZT-4 rods each 1 mm on edge and 3 mm thick and is encapsulated in an epoxy resin. The response is flat up to at least 15 MPa of pressure. Compared to the 1-3 piezocomposite in Figure 5, the lower sensitivity response in this case is likely due to a combination of effects from different PZT type, different epoxy matrix, and thinner sample.

The low frequency properties of 1-3 piezocomposites are shown in Table 3. In comparison with 0-3 piezocomposites, the 1-3s exhibit higher d_{33} and d_h coefficients, indicating that they make better electromechanical actuators and acoustic transmitters. Conversely, the 1-3s have comparable or slightly lower g_h constants (due to their higher dielectric constants). This indicates that 1-3s and 0-3s are roughly equivalent in terms of receive, or sensor, capability. However, because of the lower dielectric dissipation of 1-3 piezocomposites compared to the 0-3s, the self-noise level is 3–6 dB less for 1-3 devices (Geil and Matteson, 1992; Geil *et al.*, 1996). Another advantage that the 1-3 configuration has over the 0-3 design is in design tailorability. The 1-3 design can be easily modified to change the mechanical resonance frequency and the mechanical Q, as well as other aspects.

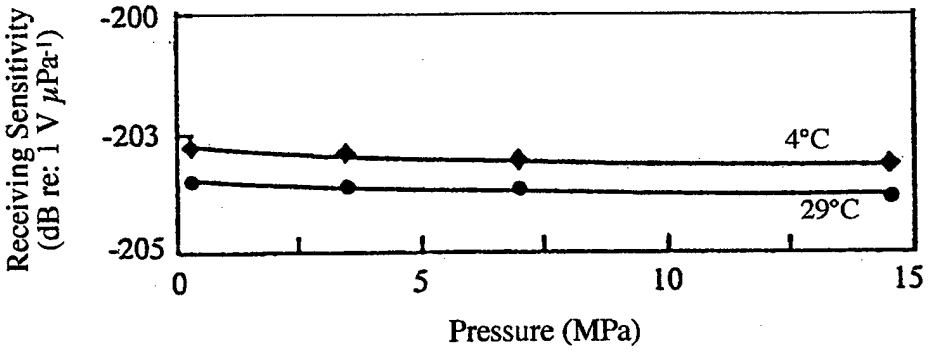

Figure 6 Pressure and temperature dependence of the low-frequency receiving sensitivity of a 1-3 composite utilizing PZT-4 (reproduced by permission of Gordon and Breach Publishers from *Ferroelectrics*, 1990, **102**, 215–224).

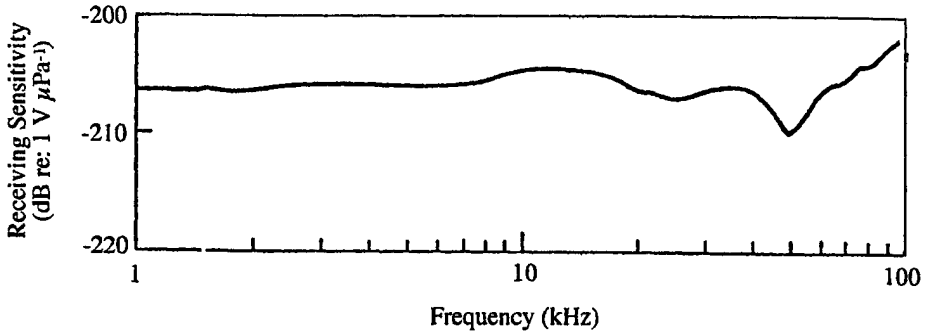

Figure 7 Frequency dependence of the receiving sensitivity of a porous (3-3) composite PZT-5 hydrophone (reproduced by permission of Gordon and Breach Publishers from *Ferroelectrics*, 1990, **102**, 215–224).

Other piezocomposite connectivity schemes are either in the developmental stage, such as the 3-3s, or essentially have been abandoned because they are too difficult/costly to manufacture or show no significant advantage over the 0-3 or 1-3 type piezocomposites (i.e., the 2-2s). Composites with 3-3 connectivity were initially fabricated by a technique known as the replamine process (Skinner *et al.*, 1978) which is the lost wax replication of a coral skeleton. Since then, additional technologies have been developed such as the fugitive phase, or BURPS (BURned out Polymer Spheres), process (Shrout *et al.*, 1979; Rittenmyer *et al.*, 1982) which produces a porous three-dimensionally interconnected ceramic structure by sintering a compacted mixture of volatilizable plastic spheres and PZT powder. A reticulated ceramic technology (Creedon and Schulze, 1996) and solid freeform fabrication (Bandyopadhyay *et al.*, 1997) are two recently developed potential manufacturing methods. In the latter technique, a honeycomb-like piezoceramic structure is built up layer by layer by computer-aided fused deposition technology. The ceramic lattice is then backfilled with polymer and electroded to complete the composite.

In some 3-3 composites, the passive phase is air rather than polymer. This kind of composite is called a porous piezoceramic composite. Mitsubishi Mining and Cement (now Mitsubishi Materials) has developed several techniques for introducing connected porosity into PZT ceramics: reactive sintering, foaming agents, organic additives, and careful control of particle size and firing conditions (Gururaja *et al.*, 1988). The receiving sensitivity of such a composite is shown in Figure 7. This composite exhibits a nearly constant receive sensitivity of -207 dB, re: $1\,V\,\mu Pa^{-1}$, from 1 kHz through 40 kHz. When the g_h constant of this composite was measured as a function of hydrostatic pressure, a nearly flat response was observed up through 60 MPa. At this pressure, the response had decreased by only 1 dB from its initial value (Ting, 1990).

Conventional composites exhibiting 3-1 and 3-2 connectivity consist of a PZT block with holes drilled through either one side (3-1) or both sides (3-2) in a direction perpendicular to the poled direction of the PZT. The holes are subsequently back-filled with polymer. In 3-1 and 3-2 composites manufactured in this way, the dielectric constant, as well as the d_h and g_h coefficients, are all functions of hole size, PZT thickness, poling technique, and center-to-center distance between adjacent holes (Safari *et al.*, 1982). The receiving sensitivity for a typical 3-1 piezocomposite at three different frequencies is shown in Figure 8. The response is relatively independent of frequency and pressure up through 6 MPa. A higher response is generated in the 3-2 composite because of its greater mechanical compliance. The primary drawbacks of these latter two configurations are in manufacturing, durability, and mechanical flexibility.

5.22.5.2 Piezoelectric–Metal Composites

In ceramic–metal composites, metal faceplates, shells, or caps are mechanically coupled to both the active ceramic as well as the surrounding medium and are the means by which the incident stress is transferred to the piezoceramic. The best ceramic–metal composite sensors are the flextensional-type transducers. In a flextensional sensor, the flexural vibration of the metal shell causes an extensional (or contractional) vibration in the piezoelectric element. Flextensional transducers are typically quite massive, in terms of both size and weight. The "moonie" and "cymbal" type transducers are miniaturized versions of flextensionals.

The moonie and cymbal transducers possess 2-(0)-2 connectivity. These transducers consist of a piezoceramic disk sandwiched between two

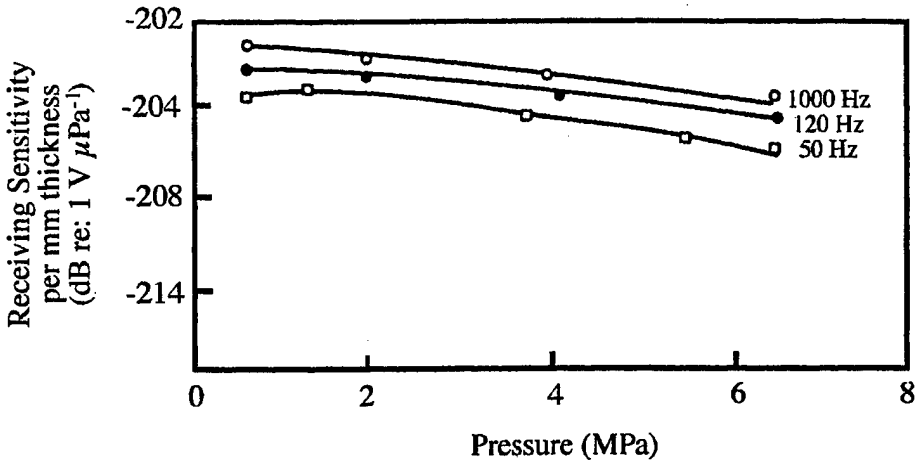

Figure 8 Pressure and frequency dependence of the receiving sensitivity of a 3-1 composite utilizing PZT-5 (reproduced by permission of Elsevier Applied Science Publishers Ltd. from *Applied Acoustics*, 1994, **41**, 325–335).

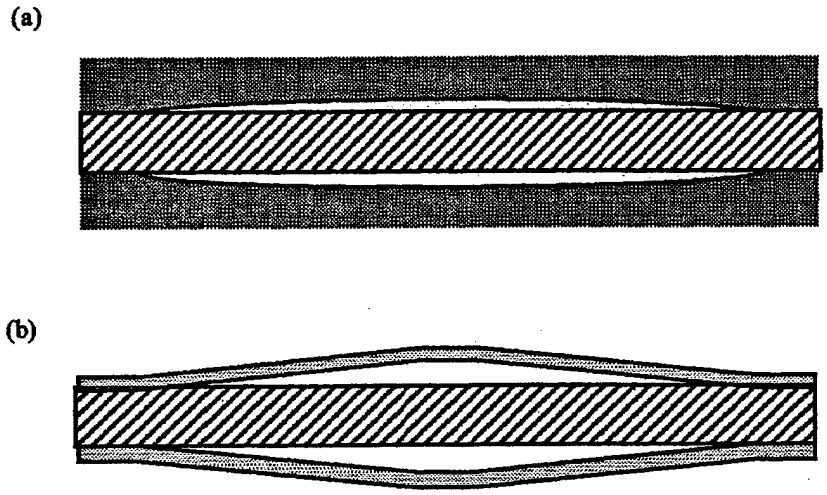

Figure 9 Cross-sectional views of the (a) moonie-type and (b) cymbal-type flextensional metal–ceramic composite sensors. The cross-hatched areas represent the piezoceramic disk and the gray areas designate the metal caps (after Tressler *et al.*, 1995).

metal caps, each of which contains a shallow air-filled cavity on its inner surface. In the case of the moonie, the cavities are in the shape of a half-moon, whereas the cymbal has a truncated cone-shaped cavity (Figure 9). The presence of these cavities allows the metal caps to serve as mechanical transformers for converting and amplifying a portion of the incident axial-direction stress into tangential and radial stresses of opposite sign. Thus, the g_{31} and g_{33} contributions of the PZT now add together (rather than subtracting) in the effective g_h of the device (Tressler *et al.*, 1995). For a moonie transducer, an effective $d_h \cdot g_h$ product exceeding $50\,000 \times 10^{-15}\,m^2N^{-1}$ is achievable (Xu *et al.*, 1991). A cymbal transducer, on the other hand, can exhibit an effective $d_h \cdot g_h$ product exceeding $100\,000 \times 10^{-15}\,m^2N^{-1}$ because of its more efficient stress-transfer mechanism (Tressler *et al.*, 1995). The higher sensitivity in the case of the cymbal compared to the moonie is at the expense of an increase in pressure dependence in its performance. Flextensional moonie-type transducers have seen extensive use as the sensor component in towed arrays used for underwater oil exploration.

5.22.6 SUMMARY

The sensitivity (M) of a piezoelectric is a function of its voltage coefficient (g_{ij}) and its thickness (t) as $M = g_{ij} \cdot t$. A poled piezoelectric ceramic such as PZT has five nonzero coeffi-

cients: $g_{31} = g_{32}$, g_{33}, and $g_{15} = g_{24}$. For in-air applications, either the g_{33} (longitudinal mode) or g_{15} (shear mode) coefficients are typically used. When used in a hydrostatic mode, such as when fully immersed in water, the sensitivity is proportional to the hydrostatic g-coefficient (g_h) which is equal to $g_{33} + 2g_{31}$. For a poled piezoelectric ceramic, $g_{33} \approx -2g_{31}$ due to crystallographic symmetry arguments. Thus, the sensitivity of a monolithic piezoelectric ceramic under hydrostatic conditions is rather low. This is the main reason why piezoelectric ceramics are incorporated into composite configurations.

Piezoceramic–polymer composites are designed to eliminate either the g_{31} or g_{33} contribution to g_h. The manner in which the ceramic and polymer are self-connected throughout the composite volume has a marked effect on its properties. Composites with 0-3 connectivity are typically in the form of flexible rubber sheets. They are characterized by high sensitivity, high-pressure tolerance, a broad operating bandwidth, as well as a good acoustical impedance match to air or water. Piezocomposites with 1-3 connectivity have roughly the same performance characteristics as 0-3s. Physically, though, they are more rigid, lighter in weight, and can be more easily tailored to application-specific needs. As seen in Table 3, other piezocomposite designs have not shown any marked advantage over the 0-3 or 1-3 composite designs. Piezoceramic–metal composites (flextensional devices) exhibit very high sensitivity because they are engineered such that the g_{33} and g_{31} coefficients of the piezoceramic constructively contribute to the g_h of the device (i.e., they effectively add together rather than subtract). Compared to the aforementioned piezoceramic–polymer composites, metal ceramic composites have a much narrower operating bandwidth and show more highly pressure-dependent performance characteristics.

5.22.7 REFERENCES

A. Bandyopadhyay, R. K. Panda, V. F. Janas, M. K. Agarwala, S. C. Danforth and A. Safari, *J. Am. Ceram. Soc.*, 1997, **80**, 1366–1372.

H. Banno, *Ferroelectrics*, 1983, **50**, 3–12.

H. Banno, in 'Proceedings of the 7th IEEE International Symposium on Applications of Ferroelectrics', University of Illinois at Urbana-Champaign, eds. S. B. Krupanidhi and S. K. Kurtz, IEEE, Piscataway, NJ, 1990, pp. 67–72.

H. Banno, K. Ogura, H. Sobue and K. Ohya, *Jpn. J. Appl. Phys.*, 1987, **26 Suppl. 26-1**, 153–155.

D. Berlincourt, *J. Acoust. Soc. Am.*, 1981, **70**, 1586–1595.

D. A. Berlincourt, D. R. Curran and H. Jaffe, in 'Physical Acoustics', ed. W. P. Mason, Academic Press, New York, 1964, vol. 1, Part A, pp. 169–270.

A. S. Bhalla, W. R. Cook, Jr., S. T. Liu, in 'Landolt–Börnstein Numerical Data and Functional Relationships in Science and Technology New Series: Low Frequency Properties of Dielectric Crystals—Piezoelectric, Pyroelectric, and Related Constants', ed. D. F. Nelson, Springer, New York, Berlin, Heidelberg, 1993, vol. III/29b.

A. S. Bhalla and R. Y. Ting, *Sensors and Materials*, 1988, **4**, 181–185.

L. Bowen, R. Gentilman, D. Fiore, H. Pham, W. Serwatka, C. Near and B. Pazol, *Ferroelectrics*, 1996, **187**, 109–120.

L. J. Bowen, R. L. Gentilman, H. T. Pham, D. F. Fiore and K. W. French, in 'Ultrasonics Symposium Proceedings, Baltimore', eds. M. Levy and B. R. McAvoy, IEEE, Piscataway, NJ, 1993, vol. 1, pp. 499–503.

W. W. Cao, Q. M. Zhang and L. E. Cross, *J. Appl. Phys.*, 1992, **72**, 5814–5821.

R. D. Corsaro, B. Houston and J. A. Bucaro, *J. Acoust. Soc. Am.*, 1997, **102**, 1573–1581.

M. J. Creedon and W. A. Schulze, in 'Proceedings of the 10th IEEE International Symposium on Applications of Ferroelectrics', New Brunswick, NJ, 1996, eds. B. M. Kulwicki, A. Amin, and A. Safari, IEEE, Piscataway, NJ, 1996, vol. 1, pp. 527–530.

S. Egusa and N. Iwasawa, *J. Intell. Mater. Sys. Struct.*, 1994, **5**, 140–144.

L. Eyraud, C. Richard and D. Guyomar, in 'Ultrasonics Symposium Proceedings', Cannes, 1994, eds. M. Levy, S. C. Schneider and B. R. McAvoy, IEEE, Piscataway, NJ, 1994, vol. 2, pp. 929–934.

D. Fiore, R. Gentilman, H. Pham, W. Serwatka, P. McGuire, C. Near and L. Bowen, in 'Proceedings of the SPIE: Smart Structures and Materials 1997—Industrial and Commercial Applications of Smart Structures Technologies', San Diego, CA, ed. J. M. Sater, SPIE, Bellingham, WA, 1997a, pp. 391–396.

D. Fiore, R. Torri and R. Gentilman, in 'Proceedings of the 8th US–Japan Seminar on Dielectric and Piezoelectric Ceramics', Plymouth, MA, 1997, eds. R. Guruaja and T. R. Shrout, Internal Publication, 1997b, pp. 344–347.

T.B. Gabrielson, Presented at the 1997 ONR Transducer Materials and Transducers Workshop, The Pennsylvania State University, University Park, PA, April 1997.

J. A. Gallego-Juárez, *J. Phys. E. Sci. Instrum.*, 1989, **22**, 804–816.

F. Geil and L. Matteson, in 'Proceedings of the ADPA/AIAA/ASME/SPIE Conference on Active Materials and Adaptive Structures', Alexandria, VA, 1992, ed. G. J. Knowles, Institute of Physics Publishing, Philadelphia, PA, 1992, pp. 135–138.

F. G. Geil, R. Gentilman, W. Serwatka and K. Webman, *J. Acoust. Soc. Am*, 1996, **100**, 2583.

R. Gentilman, D. Fiore, H. Pham-Nguyen, W. Serwatka, B. Pazol, C. Near, P. McGuire and L. Bowen, in 'Proceedings of the SPIE: Smart Structures and Materials 1996—Industrial and Commercial Applications of Smart Structures Technologies', San Diego, CA, ed. C. R. Crowe, SPIE, Bellingham, WA, 1996, pp. 234–239.

T. R. Gururaja, A. Safari, R. E. Newnham and L. E. Cross, in 'Electronic Ceramics: Properties, Devices, and Applications', ed. L. M. Levinson, Marcel Dekker, New York, 1988, pp. 92–145.

M. J. Haun, R. E. Newnham and W. A. Schulze, *Adv. Ceram. Mater.*, 1986, **1**, 361–365.

J. A. Hossack and R. L. Bedi, *Key Eng. Mater.*, 1994, **92–93**, 92–93.

T. Ikeda, 'Fundamentals of Piezoelectricity', Oxford University Press, New York, 1990, pp. 16, 210–226.

H. Jaffe and D. A. Berlincourt, *Proc. IEEE*, 1965, **53**, 1372–1386.

B. Jaffe, W. R. Cook and H. Jaffe, 'Piezoelectric Cera-

mics', Academic Press, New York, 1971.
V. F. Janas and A. Safari, *J. Am. Ceram. Soc.*, 1995, **78**, 2945–2955.
C. Kim, K. M. Rittenmyer and M. Kahn, *Ferroelectrics*, 1994, **156**, 19–24.
R. Maines, *Sensors*, 1989, **6**, 26–27.
Military Standard, *Piezoelectric Ceramic Material and Measurements Guidelines for Sonar Transducers*, MIL-STD-1376B (SH), 24 February 1995.
Morgan Matroc, Product literature.
A. J. Moulson and J. M. Herbert, 'Electroceramics', Chapman & Hall, New York, 1992, pp. 265–317.
R. E. Newnham, A. Safari, G. Sa-gong and J. Giniewicz, in 'Ultrasonics Symposium Proceedings', Dallas, TX, ed. B. McAvoy, IEEE, Piscataway, NJ, 1984, pp. 501–506.
R. E. Newnham, D. P. Skinner and L. E. Cross, *Mat. Res. Bull.*, 1978, **13**, 525–536.
NTK Technical Ceramics, NTK *Piezo Rubber* product information.
C.G. Oakley, Ph.D. Thesis, The Pennsylvania State University, 1991, pp. 3–4.
S. M. Pilgrim, R. E. Newnham and L. L. Rohlfing, *Mat. Res. Bull.*, 1987, **22**, 677–684.
K. M. Rittenmyer and P. S. Dubbelday, *J. Acoust. Soc. Am.*, 1992, **91**, 2254–2260.
K. Rittenmyer, T. Shrout, W. A. Schulze and R. E. Newnham, *Ferroelectrics*, 1982, **41**, 189–195.
C. Z. Rosen, B. V. Hiremath and R. E. Newnham (eds.), 'Piezoelectricity', American Institute of Physics, New York, 1992.
A. Safari, R. E. Newnham, L. E. Cross and W. A. Schulze, *Ferroelectrics*, 1982, **41**, 197–205.
A. J. Salloway, *Ferroelectrics*, 1996, **187**, 219–226.
H. P. Savakus, K. A. Klicker and R. E. Newnham, *Mat. Res. Bull.*, 1981, **16**, 677–680.
T. R. Shrout, W. A. Schulze and J. V. Biggers, *Mat. Res. Bull*, 1979, **14**, 1553–1559.
D. P. Skinner, R. E. Newnham and L. E. Cross, *Mat. Res. Bull.*, 1978, **13**, 599–607.
W. A. Smith, in 'Proceedings of the SPIE: New Developments in Ultrasonic Transducers and Transducer Systems', San Diego, CA, ed. F. L. Lizzi, SPIE, Bellingham, WA, 1992, pp. 3–26.
W. A. Smith, *IEEE Trans. Ultrason., Ferroelect., Freq. Contr.*, 1993, **40**, 41–49.
H. Takeuchi, C. Nakaya and K. Katakura, in 'Ultrasonics Symposium Proceedings', Dallas, TX, ed. B. R. McAvoy, IEEE, Piscataway, NJ, 1984, pp. 507–510.
R. Y. Ting, *Ferroelectrics*, 1990, **102**, 215–224.
R. Y. Ting, *Applied Acoustics*, 1994, **41**, 325–335.
J. F. Tressler, A. Dogan, J. F. Fernandez, J. T. Fielding, Jr., K. Uchino, R. E. Newnham, in 'Ultrasonics Symposium Proceedings', Seattle, WA, 1995, eds. M. Levy, S. C. Schneider and B. R. McAvoy, IEEE, Piscataway, NJ, 1995, pp. 897–900.
R. C. Turner, P. A. Fuierer, R. E. Newnham and T. R. Shrout, *Applied Acoustics*, 1994, **41**, 299–324.
R. C. Twiney, *Adv. Mater.*, 1992, **4**, 819–822.
Vernitron Piezoelectric Division, *Piezoelectric Technology—Data for Designers.*
H. Wang, Q. M. Zhang, L. E. Cross and C. M. Trottier, *Ferroelectrics*, 1995, **173**, 181–189.
W. Wersing, in 'Proceedings of the 6th IEEE International Symposium on the Application of Ferroelectrics', Lehigh University, Bethlehem, PA, 1986, ed. W. A. Smith, IEEE, Piscataway, NJ, 1986, pp. 212–223.
O. B. Wilson, 'Introduction to Theory and Design of Sonar Transducers', Peninsula Publishing, Los Altos, CA, 1988.
Q. C. Xu, S. Yoshikawa, J. R. Belsick and R. E. Newnham, *IEEE Trans. Ultrason., Ferroelect., Freq. Contr.*, 1991, **38**, 634–639.
Q. M. Zhang, H. Wang and L. E. Cross, *J. Mater. Sci.*, 1993, **28**, 3962–3968.